Modelling shoreline evolution in the vicinity of shore normal structures

Implementation and validation of ShorelineS model using the case study of Constanta, Romania

T.S.F. (Tim) Overgaauw

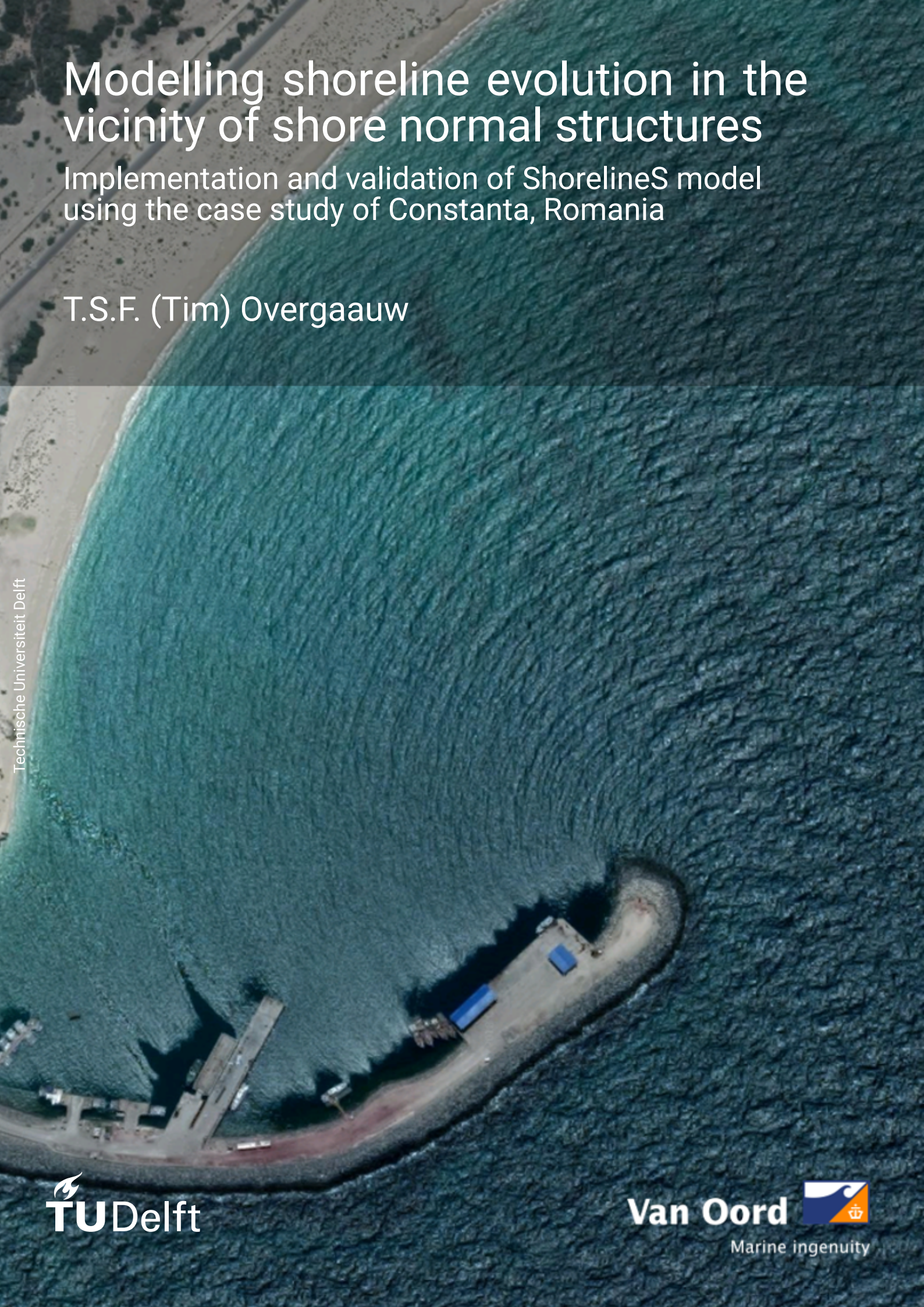

Technische Universiteit Delft

TU Delft

Van Oord

Marine ingenuity

Modelling shoreline evolution in the vicinity of shore normal structures

Implementation and validation of ShorelineS model using the case study of Constanta, Romania

by

T.S.F. (Tim) Overgaauw

to obtain the degree of

Master of Science

in

Hydraulic Engineering

at the

Delft University of Technology

to be defended publicly on 16-02-2021

Student number:	4262360	
Project duration:	February 10, 2020 – February 16, 2021	
Thesis committee:	Dr. ir. M. A. de Schipper,	TU Delft
	Dr. ir. A. P. Luijendijk,	TU Delft
	Dr. J. E. A. Storms,	TU Delft
	Ir. P. G. F. Brandenburg,	Van Oord
	Dr. ir. B. J. A. Huisman,	Deltares
	Ir. A. M. Elghandour,	IHE Delft

An electronic version of this thesis is available at `http://repository.tudelft.nl/`.

TU Delft

Preface

This report is written to fulfil the graduation requirements of my Master of Science degree in Hydraulic Engineering with specialization Coastal Engineering at the faculty of Civil Engineering and Geoscience at the Delft University of Technology. I am grateful that I had the opportunity to perform my research in collaboration with the great company Van Oord. Despite the situation surrounding Covid-19, they offered me the chance to experience what it is like to be *a real coastal engineer*. I would like to take this opportunity to show my gratitude to some people, not only for guidance in this project but also in every day life, without who this endeavour would have been much harder.

Firstly, I would like to thank my committee: Matthieu de Schipper, Arjen Luijendijk, Joep Storms, Peter Brandenburg, Bas Huisman and Ahmed Elghandour. Their guidance and input throughout the research helped me to develop my skills in scientific research, reporting and programming. Thanks for all of the helpful meetings, they were really beneficial in finishing my thesis.

Ahmed, your knowledge of the ShorelineS model was instrumental for my work. During long online-meetings we solved multiple modelling problems that came to my path, I really appreciate that. Good luck with the remainder of your PhD study.

A special thanks to my daily supervisor at Van Oord, Peter, who helped me in finding a balance between the academic level and a more practical engineering point of view in my thesis. The weekly meetings were really enjoyable and productive at the same time. When I ran into a modelling issue you always helped me to look at the problem from a broader perspective, this contributed significantly to the progress of my study. I hope we work together in the future!

Lastly, and most importantly, I want to thank my family, Mariska, Jelle, Nienke and girlfriend Pauline for their unconditional love and trust they placed in me. You have stimulated me to get the best out of my abilities and cheered me up when necessary. Many thanks also go out to my roommates and close friends for the amazing period I have had being a student in Delft. All of the great memories put a smile on my face. Sorry for being very busy the last couple of months, I will make up to you guys!

T.S.F. (Tim) Overgaauw
Delft, February 2021

Summary

Because of an increasing pressure on the coastal zones, the urge to perform long-term analysis of the coastline evolution exists. Nowadays, multiple types of models are available to simulate the dynamic behaviour of coastlines for engineering purposes. Each type has its characteristics and contains specific pros and cons. Aims of the modelling effort, associated time and spatial scales, and the site specific characteristics are some of the most important aspects while considering the model type to be used in a particular case. Recently, a new one-line model is developed to deal with complex sandy coasts, but still being computational effective for short and larger time scales. This new model, named ShorelineS, is suitable for geometric complex coastlines and allows for the interaction between different coastline sections. Therefore, being capable of modelling spit formation, merging of islands, and the formation of tombolo's and salients.

However, Elghandour (2018), Ghonim (2019) and Mudde (2019), which contain recent ShorelineS model developments, recommended separately to include the effect of wave diffraction behind shore normal structures to improve the model performance. Furthermore, applying the model to a study area situated at Constanta, lying at the coast of Romania, initially did not lead to a numerical result matching the survey data. Based on the site specific characteristics, it was suggested to include the effect of wave diffraction while modelling the shoreline evolution to retrieve a more representative shoreline shape. Therefore, the core of this thesis is focused on incorporating the effect of wave diffraction onto the shoreline evolution in the vicinity of shore normal structures. This study demonstrates that while accounting for wave diffraction effects, the numerical result of the Constanta case study is matching the observed coastline shape. The improved model succeeded in simulating an anti-clockwise rotation of the coastal cell.

While waves are propagating towards the shore and are interrupted by an obstacle like a groyne, they will turn around the tip into the sheltered region of the groyne. This sheltered region is called the shadow zone and contains a reduced wave climate. The turning of the waves is based on the lateral transfer of wave energy along the wave crest, caused by a gradient in wave height. This process is called diffraction. Breaking wave heights and angles inside the shadow zone will be influenced significantly because of wave diffraction. Since variations in breaking wave height and/or angle are responsible for gradients in the alongshore sediment transport, the process of wave diffraction should be taken into account while simulating the shoreline evolution in the vicinity of a groyne. Different methods were found to incorporate the effects of wave diffraction inside a numerical model. This study applies the methods described by Kraus (1984), Kamphuis (1992), Leont'Yev (1999), Hurst et al. (2015), and Elghandour et al. (2020). A new function is implemented inside ShorelineS so that the effects of wave diffraction can be incorporated. The structure of this function and multiple parameters are based on the method established by Elghandour et al. (2020) to model wave diffraction in the case of an offshore breakwater. First, the breaking parameters without the effect of diffraction are calculated. Subsequently, the influence area of diffraction is determined based on the wave characteristics at the groyne tip. In the influence zone, a distinction is made between the shadow zone and transition zone. By definition, the breaking parameters at the edge of the transition zone are not subjected to diffraction effects anymore. Next, for each point of breaking inside the shadow or transition zone, the diffracted breaking wave height and angle are calculated following one of the methods listed earlier. Some of these methods needed to be modified to be applicable in this study. Finally, the alongshore sediment transport is determined using the diffracted breaking parameters. Based on gradients in this alongshore sediment transport, the new coastline position is determined by the model. Additional to developing this function, a new approach regarding the boundary condition of the groyne is suggested to retrieve a better coastline response very close to the groyne. The key aspect of this approach is dividing the shoreline into two sections, containing the total updrift and downdrift area respectively.

The performance of the improved model, applied to a simplified coastline situation, is examined in three different ways. First, it is shown that the breaking wave height, wave angle, and alongshore sediment transport properly evolve while simulating. Secondly, the conservation of sediment mass regarding the numerical results is demonstrated to remain valid while incorporating diffraction effects. Therefore, satisfying that the updrift sedimentation is equal to the total downdrift erosion. This means that no mass is lost out of the control volume. Finally, a comparison between the numerical results and analytical solutions of the shoreline evolution incorporating the effects of wave diffraction is made. The numerical results indicated to be in line with the analytical solution that assumes a linear varying diffracted breaking wave angle, as is described by Larson et al. (1987).

The improved model performance regarding a real-world case study is addressed by using the shoreline of Constanta, Romania. The consequence of incorporating wave diffraction effects onto the shoreline evolution of Constanta is demonstrated in detail. The accretion close to the Southern groyne and erosion near the Northern groyne are visible in the numerical result of the improved model. Therefore, matching the observed anti-clockwise rotation of the coastal cell. Without accounting for diffraction effects, this matching result was not achievable. The transition zone width is found to be an important factor in determining the coastline shape affected by diffraction. After calibration of this parameter, the numerical result demonstrated to be in almost perfect agreement with the observed coastline shape. The bias of the modelled and observed coastline change decreased from 28.11 m to 5.19 m after incorporating wave diffraction effects. Additionally, the root mean square error reduced from 14.24 m to 2.89 m. The scaling down of these two parameters indicates that the survey data is modelled more precisely while using the improved model.

The findings in this study imply that effects of wave diffraction onto the shoreline evolution in the vicinity of shore normal structures can be incorporated inside ShorelineS. Accounting for these effects is needed to retrieve a representative shoreline response as is demonstrated for the Constanta case study. Model developments are suggested to improve the reliability of future research concerning the transition zone width definition which is concluded to be an important parameter inside the diffraction calculations.

Contents

Nomenclature

Variables

$\alpha_{s,corr}$	Diffracted wave angle relative to x-axis used Elghandour et al. (2020)	°
α_s	Undiffracted wave angle relative to x-axis used Elghandour et al. (2020)	°
β	Bed slope	°
δ	Angle between shadow zone edge and transition zone edge	°
γ	Breaker index	–
λ	Wavelength in analytical solution of Bakker et al. (1970)	m
ω	Wave frequency	s^{-1}
ϕ	Incident wave angle direction	°
ϕ_c	Local coastline orientation	°
ϕ_{loc}	Relative angle of incoming wave to local coastline orientation	°
ϕ_{tip}	Wave angle at groyne tip	°
ρ_s	Density of sediment	kgm^{-3}
ρ_w	Density of water	kgm^{-3}
Θ	Wave propagation direction relative to x-axis	°
θ	Angle between shadow zone line and the line between groyne tip and random point X	° or rad
B	Width of the shadow zone at the breakerline in analytical solution of Larson et al. (1987)	m
b	Width of certain volume inside the wave energy balance	m
b_{CERC}	Calibration factor simplified CERC	–
c	Wave phase velocity	ms^{-1}
c_f	Friction coefficient	–
c_g	Wave group velocity	ms^{-1}
D	Total active profile height	m
D_b	Berm height	m
D_c	Depth of closure	m
D_{50}	Median grain size diameter	m
E	Wave energy	kgm^2s^{-2}
F_x	Cross shore directed force	N
F_y	Alongshore directed force	N

g	Gravitational acceleration	ms^{-2}
h	Water depth	m
H_s	Significant wave height	m
k	Calibration factor CERC formula	–
k_2	Calibration factor CERC adapted formula	–
K_d	Diffraction coefficient	–
K_r	Refraction coefficient	–
K_s	Shoaling coefficient	–
K_{swell}	Swell factor in van Rijn transport formula	–
L	Wavelength	m
L_s	Coastline section situated inside the shadow zone	m
n	Ratio wave group velocity over wave velocity	–
P_E	Cumulative relative wave energy	%
q	Derivative of alongshore sediment transport to incident wave angle	m^2s^{-1}
Q_0	Alongshore sediment transport rate amplitude	m^3s^{-1}
Q_s	Alongshore sediment transport rate	m^3s^{-1}
S	Radiation stress	Nm^{-1}
s	Coastal constant used in analytical solution	–
S_{max}	Directional spreading parameter	–
T	Wave period	s
$t_{b,y}$	Bed shear stress	Nm^{-2}
V_{total}	Alongshore current factor in van Rijn transport formula	–

Sub- and superscripts

x_0	Location 0
x_1	Location 1
x_∞	Offshore location
x_{br}	Breaking value
x_{diff}	Diffracted value
x_{undiff}	Undiffracted value

List of Figures

List of Tables

1 Introduction

1.1. Background

Creel (2003) stated that approximately half of the world's population lives near the coast. During the past decades, the coastal zone development and utilisation have been increasing. This increase is expected to proceed in the future years. Consequently, the pressure on coastal areas will keep growing significantly (Neumann et al., 2015). Another aspect that generates pressure on coastal zones is the expected sea-level rise as a result of climate change. To deal with this increasing pressure, natural circumstances are being altered by humans. Coastal structures are built to make sure that human properties are protected against the sea. Changing these natural circumstances could lead to unexpected (and unwanted) effects like erosion and/or accretion of the coast. According to Gracia et al. (2018) a large part of the world coastlines are facing issues because of erosion. This erosion can be part of natural processes, however is in most cases triggered by human interventions. On the contrary, these interventions were in the first place built to prevent erosion. Therefore, the urge to perform a long-term analysis of the coastline evolution to get a better understanding of its mechanisms arose (Ghonim, 2019).

Long-term analysis of coastline evolution is mainly performed using (a) data of historical shoreline position, (b) physical model tests or (c) numerical models (Dean and Dalrymple, 2001). Nowadays, multiple types of numerical models are available to model the dynamic behaviour of coastlines. Each type has its characteristics and contains specific pros and cons. Aims of the modelling effort, associated time and spatial scales, and the site-specific characteristics are some of the most important aspects while considering the model type to be used in a particular case. Roelvink and Reiniers (2011) distinguished three types of numerical models used by engineers for modelling the shoreline evolution. Firstly the coastal profile models, they are mainly used for modelling the impact of individual storms and sand bar migration in the cross-shore direction. They schematize the coastal area into a two-dimensional system and assume alongshore uniformity. A commonly used coastal profile model is described in Ruessink et al. (2007). Secondly, coastline models are models in which the shape of the coastal profile itself does not change over the considered period. The profile is simplified to a single line that only may move seaward in the case of accretion or landward if erosion takes place. These models are often also called one-line models and are used in situations where alongshore processes play a dominant role. Applications are for example modelling the reorientation of coastlines due to variations in the wave climate and describing the alongshore spreading of large beach nourishments (Roelvink and Reiniers, 2011). UNIBEST-CL+ (Deltares, 2011), LITPACK (DHI, 2011) and Genesis (Hanson, 1989) are well-known examples of coastline models. Huisman (2014) described that besides the one-line coastline models there are also multi-line coastal models. In those models, different depth layers can be defined. Therefore, allowing for different rates of coastline changes for each depth layer. Finally, there are coastal area models, Delft3D (Deltares, 2020) for instance. Such models can provide highly detailed results. For example, they are applied to study the details of the waves and wave-driven flow patterns and resulting morphology changes around small structures (Roelvink and Reiniers, 2011). Coastal area models are very computational extensive compared to the other two types of models. Therefore, they are not applicable to perform long-term calculations.

Despite the earlier mentioned different kinds of models, Roelvink et al. (2020) stated that there is a lack of reliable and widely usable models to manage complex sandy coasts. Thomas and Frey (2013) compared the traditional coastline models and elaborated on the limitations. ShorelineS is a new coastline model introduced by Roelvink et al. (2020), to overcome these limitations. This model aims to predict coastline evolution for short and for long time scales, suitable for geometrical complex coastlines. The shoreline is represented by a freely moving string of points, allowing for multiple coastline sections which can interact with each other. Therefore, capable of modelling spit formation, merging of islands, and the formation of tombolo's and salients (Roelvink et al., 2020).

After development of the preliminary version of ShorelineS, multiple tests have been performed to investigate the accuracy and potential of the model. Principal tests were executed to examine the model performance related to merging and splitting of different coastal sections. Roelvink et al. (2020) stated that the test results were quite realistic, thereby forming an illustration of the capability of ShorelineS to simulate not just simple coastline changes, but radical transformations of the coast over long timescales. Furthermore, the analytical Pelnard-Considerè groyne test (Pelnard-Considere, 1956) and linear diffusion test (Vitousek and Barnard, 2015) were performed. Based on these tests, it was concluded that the basic equations and applied numerical scheme have been implemented correctly inside ShorelineS (Roelvink et al., 2020). An extensive elaboration of those analytical tests can be found in Elghandour (2018). Succeeding the principal and analytical tests, the first application to a real-world case was performed. Both the Sand Engine case (figure 1.1) and Ijmuiden Port case showed the great potential of the ShorelineS model regarding engineering purposes (Roelvink et al., 2020).

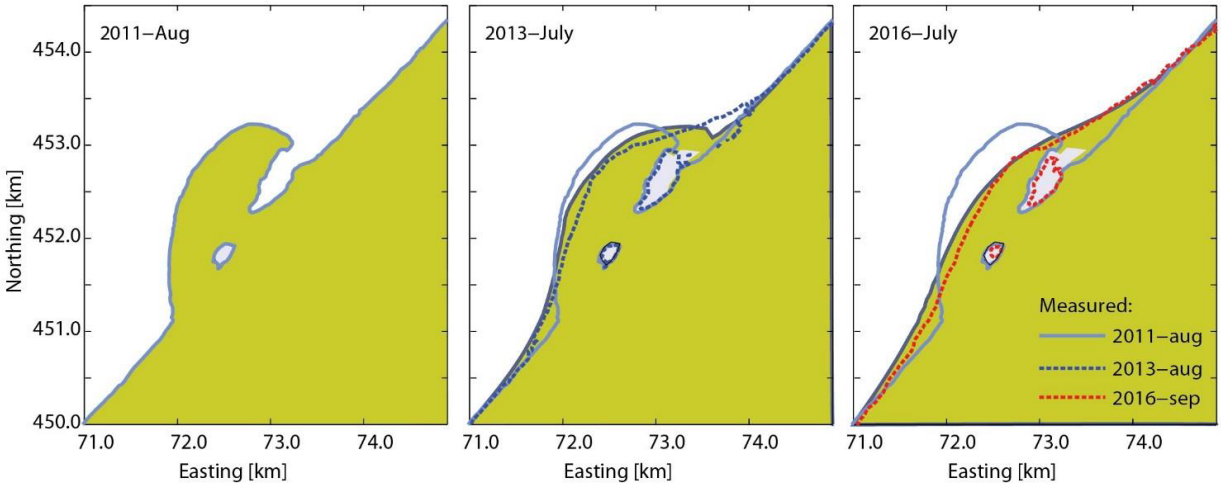

Figure 1.1: Observed and simulated evolution of the Sand Engine using ShorelineS. Filled contours: snapshots of simulation at start (left), after two years (middle), and four years (right). Colour-coded lines are data from field observations. (Roelvink et al., 2020)

1.2. Problem description

The urge in understanding the effects of human interventions on the evolution of the coastline is described in section 1.1. Numerical models like ShorelineS could be used for that purpose. Despite all the promising test results, further investigation is needed to improve the applicability of the ShorelineS model (Mudde, 2019). Roelvink et al. (2020) addressed that the model is continuously under development. Currently, a large number of aspects remain on the to-do list regarding these improvements. Since the first version of ShorelineS was established, multiple studies contributed to the development of certain model parts. Elghandour (2018), Ghonim (2019) and Mudde (2019) independently examined ShorelineS and established a variety of model implementations. Furthermore, they all recommended to include wave diffraction behind shore normal structures and headlands to retrieve a better response of the coastline at such places.

Applying the model to a study area situated at the coast of Romania, initially led to a mismatch between the numerical result and the observed coastline shape. It is expected that accounting for wave diffraction effects is required to retrieve the correct coastline evolution. The relative long groynes will provide a large sheltered area regarding the incoming waves (figure 1.2). Diffraction will be one of the governing processes in this area and therefore affecting the coastline evolution significantly.

To conclude, the urge in accounting for wave diffraction effects onto the shoreline evolution in the vicinity of a groyne field derived from the two different perspectives mentioned above.

Figure 1.2: Coastline of Constanta, Romania (Google Earth, 11/2020). Highlighted coastal cell: study area

1.3. Objective and research questions

The core of this thesis is focused on incorporating the effect of wave diffraction onto the shoreline evolution in the vicinity of shore normal structures. This is expected to improve the model performance when applying it to the Constanta case study. Hence, the research objective is as follows:

Developing the existing wave diffraction routine in ShorelineS to incorporate the diffraction effect in the vicinity of a groyne field, to simulate the coastline evolution of the Constanta case study.

To achieve the above mentioned objective, the following research questions will be addressed:

1. How to account for wave diffraction inside coastline modelling?
2. How to correctly implement the boundary condition belonging to a groyne into the freely moving coastline model ShorelineS?
3. To what extent are certain model parameters, involved in the diffraction calculations, influencing the resulting coastline shape?
4. How does the model perform in modelling the shoreline evolution of a simplified diffraction scenario?
5. How does the model perform in modelling the shoreline evolution of the Constanta case study?

1.4. Approach

This section contains the approach that will be applied to provide answers to the research questions. Simultaneously to this study, A.M. Elghandour is improving the model part in which the effects of wave diffraction concerning an offshore breakwater are accounted for. Cooperation between his work and this study will enhance both model improvements.

1.Literature study
The literature study will contain the following components. First, retrieve insight into the processes responsible for coastline evolution. Subsequently, examine the details of wave diffraction to understand all the ins and outs concerning this topic. Focus on how to implement wave diffraction effects inside numerical modelling. Next, investigate the ShorelineS model and the recently established improvements. Finally, perform an extensive model walk-through to get familiar with ShorelineS.

2.Model development
First of all, examine in which way the boundary condition of a groyne is currently incorporated inside the model. If necessary, suggest a new method regarding this boundary condition to retrieve a more representative coastline response. After that, develop the model in such a way that it accounts for wave diffraction effects in the lee of a groyne.

3.Model validation
Validate the improved model according to the following steps. To begin with, investigate the development of the breaking wave height, wave angle, and alongshore sediment transport while simulating. Subsequently, verify the conservation of sediment mass. In the end, compare the numerical results with analytical solutions.

4.Model application
Apply the improved model to the Constanta case study. Investigate if the numerical result is in line with the observed coastline shape.

1.5. Readers Guide

Chapter 2 provides a summary of the literature study performed to gain knowledge about the relevant coastal processes in the vicinity of a shore normal groyne. Furthermore, this chapter contains the important characteristics of the ShorelineS model including the recently made model improvements. In chapter 3, the process of wave diffraction is examined in detail. Analytical solutions regarding the coastline evolution in which the effects of wave diffraction have been taken into account are investigated extensively. At the end of this chapter, methods to incorporate wave diffraction effects inside numerical modelling are provided. Chapter 4 elaborates on the model development regarding the established function to account for wave diffraction effects near shore normal structures A new approach for taking into account the boundary condition of such a structure is suggested. Furthermore, a detailed description of the implemented function is provided. At the end of this chapter, the resulting shorelines corresponding to different model runs are provided. In chapter 5, a model validation is performed by firstly examining the trend of breaking wave height, wave angle, and alongshore sediment transport while simulating the coastline evolution. Subsequently, the conservation of mass is investigated. Furthermore, the numerical results are compared to the analytical solutions regarding the coastline evolution including diffraction effects. Chapter 6 provides the application of the improved model to a real-world case. Finally, chapter 7 contains the key findings of this thesis as well as a discussion of recommendations for future development and research.

2

Literature review

First, by the means of a literature study, insight is gained into the relevant coastal processes in the vicinity of a groyne regarding coastline modelling for engineering purposes. Subsequently, literature concerning the ShorelineS model is examined. The important characteristics of this model are provided in section 2.2. Furthermore, the most recent model improvements are briefly addressed (section 2.3). More details of these improvements are stated in Appendix A. To get familiar with ShorelineS, an extensive model walk-through is performed. While doing this, it is examined if the governing nearshore processes, found by means of the above mentioned literature study, are incorporated inside the model. A schematization of the model loop is made for convenience and provided in figure 2.7.

2.1. Relevant nearshore processes in the vicinity of a groyne field

Coastline evolution is caused by gradients in the alongshore sediment transport. These gradients are depending on nearshore hydrodynamics. Many different kinds of processes are influencing the hydrodynamics in the coastal area, therefore playing a role in the coastline evolution. The following processes could all affect this evolution:

- Linear wave propagation (shoaling and refraction)
- Non-linear wave propagation effects (asymmetry, skewness and Stokes Drift)
- Wave breaking and dissipation
- Wave driven alongshore transport
- Wave set-up and set-down
- Reflection of waves
- Presence of wave groups and bound-long waves
- Undertow in the case of breaking waves
- Bottom effects: wave boundary layer including Longuet Higgins streaming
- Wave diffraction nearby coastal structures or headlands
- Alongshore and local nearshore currents
- Sediment bypassing and transmission in the presence of a structure.

Taking into account all of the processes cannot be done efficiently while modelling the shoreline evolution near a groyne. Aims of the modelling effort, associated time and spatial scales, and the site-specific characteristics are the most important aspects regarding the considerations for a model set up (Huisman, 2014). Therefore, they are determining the relevance of each nearshore process in modelling the dynamic behaviour of coastlines. Time and spatial scales are responsible for the required level of detail regarding the computations.

Aim	Spatial scale	Time scale
Long-term strategy development	O (100km)	Century
Indicative studies (landscape designers)	O (kilometres)	Yearly
Budget studies	O (10 km)	Years - Decades
Nourishment evaluation	O (kilometres)	Years - Decades
Impact of harbour moles / jetties	O (kilometres)	Years - Decades
Beach schemes with groynes / breakwaters	O (100 m)	Months - Decades
Long-term trends for safety assessment *	O (kilometres)	Years - Decades
Initial response of nourishments **	O (100 m)	Months

* additional to modelling of the impact of episodic events

** indicative studies on the initial development of nourishments

Figure 2.1: Time and spatial scales regarding typical coastline modelling studies (Huisman, 2014)

Modelling the coastline evolution of beaches influenced by groynes has associated time and spatial scales varying from months to decades and a couple of 100 meters to kilometers respectively (figure 2.1). Those scales implicitly assume the dominance of alongshore transport processes rather than cross-shore processes. Furthermore, groynes are typically constructed to solve erosion problems of coastal areas that are dominated by alongshore processes which cause gradients in the alongshore sediment transport (Kristensen et al., 2016). Cross-shore transport becomes dominant when studying individual storm events and the subsequent dune overtopping or the movement of sand bars for example. Therefore, cross-shore processes are not in the scope of this thesis. Besides the alongshore wave-driven transport, which generally has a dominant role in shaping a beach influenced by groynes, also local effects caused by the groyne itself should be taken into account while modelling the coastline evolution. Wave diffraction and sheltering downdrift of the groyne, local currents caused by water level setup differences and the blockage of alongshore sediment transport are all processes that will influence the local coastline shape significantly (Huisman, 2012).

The subsequent sections provide insight into the governing physical processes regarding modelling the coastal evolution near a groyne for engineering purposes. Those processes are visualized in figure 2.2.

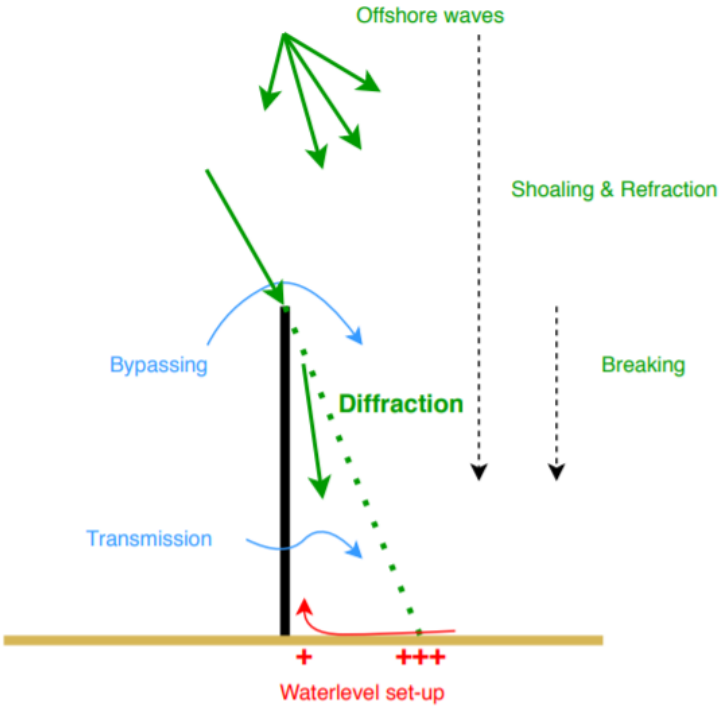

Figure 2.2: Relevant coastal processes

2.1.1. Linear wave propagation; shoaling and refraction

While waves propagate towards the shore, multiple processes are responsible for altering the wave parameters. Shoaling and refraction of waves are one of these processes. They are the result of wave energy convergence or divergence, caused by a changing sea bottom profile while traveling in the direction of the coastline. Any harmonic wave at the water surface propagating towards the shore can be described using the dispersion relation. It relates the wavelength or wavenumber to the wave frequency.

$$\omega^2 = gk\tanh(kh) \tag{2.1}$$

The above equation is valid for any arbitrary water depth. Consequently, a wave propagating towards the nearshore will experience a decrease in wavelength L because the water depth h is decreasing but the wave frequency w remains constant. Since the wavelength L decreases, also the speed at which an individual wave travels, the phase speed c, decreases. The group velocity c_g is related to the phase velocity c (equation 2.2). This group velocity c_g is the speed at which the energy of the waves travels, variations in group velocity result in a changing wave energy E. Subsequently, leading to variations in wave height. This process is called shoaling.

$$c_g = cn = c * \frac{1}{2}\left(1 + \frac{2kh}{\sinh(2kh)}\right) \tag{2.2}$$

Summarizing, shoaling leads generally to an increase in wave height while waves propagate into shallow water because of the decreasing group velocity leading to energy convergence. Holthuijsen (2010) interpreted this as energy bunching; the horizontal compacting of wave energy.

While propagating towards the coast, waves are also exposed to depth variations along the wave crest. This is contrary to shoaling, where depth variations in the propagation direction cause a change in wave height. Following the dispersion relation again, a depth variation along the wave crest causes a changing phase speed in the same direction. Subsequently, the part of the wave crest that is situated in deeper water will propagate with a larger velocity. This means that for a particular time interval, that part of the wave crest will propagate over a larger distance compared to the part of the wave crest situated in shallower water. As a result, the total wave crest will bend towards the region of shallower water. In other words, the wave will align itself with the depth contours and eventually turn towards the coast.

The effect of shoaling and refraction is commonly expressed using a shoaling and refraction coefficient, K_s and K_r respectively. Holthuijsen (2010) described a wave energy balance that could be used to determine these coefficients. Assuming stationary conditions and neglecting source and dissipation terms like wind input and bottom friction, the energy balance is reduced to a simple statement (equation 2.3). Here s is the coordinate along a wave ray.

$$\frac{d}{ds}(Ec_g) = \text{constant} \tag{2.3}$$

Equation 2.3 is rewritten using two locations in the coastal area. A location with subscript 0 and the more nearshore location with subscript 1 (figure 2.3). Also, the distance b between two wave rays is included. While taking into account the above assumptions, the wave energy entering a volume over width b_0 should be equal to the wave energy leaving the same volume over width b_1.

$$(Ec_g)b = (Enc)b = (Encb)_0 = (Encb)_1 \tag{2.4}$$

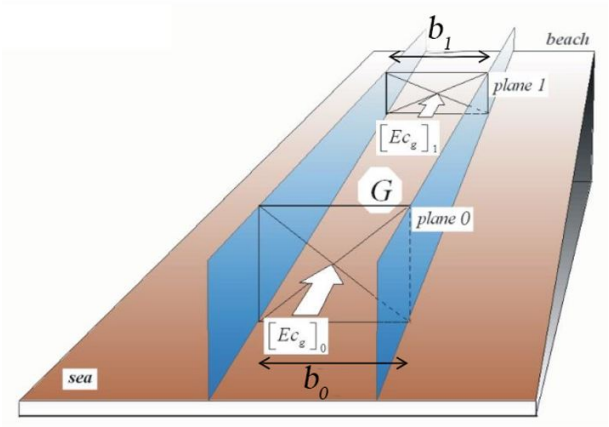

Figure 2.3: Wave energy balance (Bosboom and Stive, 2015)

The wave height $H_{s,0}$ can now be related to $H_{s,1}$ using $E = \frac{1}{8}\rho g H_s^2$. Subsequently, the shoaling and refraction coefficients can be calculated according to the equations below.

$$\begin{aligned} K_s &= \sqrt{\frac{n_0 c_0}{n_1 c_1}} \\ K_r &= \sqrt{\frac{b_0}{b_1}} = \sqrt{\frac{\cos(\phi_0)}{\cos(\phi_1)}} \end{aligned} \tag{2.5}$$

Snell's Law states that for uniform parallel depth contours the direction of the incoming wave rays varies proportionally to the wave celerity. In other words, along an incoming wave ray the term $\frac{\sin(\phi)}{c}$ is constant.

$$\frac{\sin(\phi_0)}{c_0} = \frac{\sin(\phi_1)}{c_1} = \text{constant} \tag{2.6}$$

The wave angle at different locations at the cross-shore profile can be determined using Snell's Law.

2.1.2. Wave breaking

The most clearly visible nearshore wave process is that of wave breaking. Walking along a certain beach, incoming waves that gradually grow until they collapse can be observed. Depending on the location of the beach, this collapsing could be quite intense. In the previous section, it is depicted that waves propagating into shallower water will experience an increase in wave height. This increase can not last forever. At a certain moment, the wave becomes unstable and starts to break. A distinction is made between two types of breaking, steepness-induced wave breaking and water depth-induced wave breaking. Miche (1944) studied the first type of breaking and came up with a limiting wave steepness ($\frac{H}{L}_{\max}$) while using the Stokes wave theory. Often, the term *white-capping* instead of steepness-induced breaking.

$$\left(\frac{H}{L}\right)_{\max} = 0.142 \tanh(kh) \tag{2.7}$$

Depth-induced wave breaking starts when the wave height relative to the local water depth becomes too large. In this case, it is the water depth that limits the wave height and not the steepness of the wave itself. In the nearshore area almost all wave breaking is depth-induced. Using the shallow water approximations equation 2.7 can be rewritten as follows:

$$\left(\frac{H}{L}\right)_{\max} = 0.142 \tanh\left(\frac{2\pi h}{L}\right) \approx 0.88 \frac{h}{L} \tag{2.8}$$

Equation 2.9 is equivalent to equation 2.8, only then written in terms of the so-called breaker index γ. The breaking wave height H_{br} relative to the breaking water depth h_{br} is assumed to be constant throughout the whole breaker zone, this aspect is often called the simple dissipation model.

$$\gamma = \left(\frac{H}{h}\right)_{\max} = \frac{H_{br}}{h_{br}} \approx 0.88 \tag{2.9}$$

Breaking waves play an important role in the alongshore sediment transport. They are the main driving factor of an alongshore current when they approach the coastline under an angle. Furthermore, breaking waves stir up sediment and bring particles into suspension, resulting in a higher sediment concentration. The highest concentration in the water column is found at the location where most of the waves break (Bosboom and Stive, 2015).

2.1.3. Wave driven alongshore current

When waves approach the shoreline under an angle, an alongshore current will be generated. Longuet-Higgins (1970) came up with a formulation that describes the alongshore current. The basic principle is that waves carry momentum and that the change in this momentum causes a force on the fluid. Longuet-Higgens used his earlier work about the radiation stress developed by waves to define the radiation stress as the depth-integrated and wave-averaged momentum flux caused by the presence of waves (Bosboom and Stive, 2015). The transport of x-momentum in the x-direction, S_{xx}, in equation form is written as follows:

$$S_{xx} = \overline{\int_{-h_0}^{\eta} (\rho u_x) u_x \, dz} + \overline{\int_{-h_0}^{\eta} p_{wave} \, dz} \tag{2.10}$$

The radiation stress S_{xx} can be divided into two parts (equation2.10). The first part originating from the transfer of momentum and the second part is caused by the wave-induced pressure. Integration of equation 2.10 leads to the general form of S_{xx} for waves propagating with a direction Θ relative to the positive x-direction (equation 2.11). Usually, the x-direction and y-direction represent the shore normal and alongshore direction respectively. The formulations of S_{yy}, S_{xy} and S_{yx} are retrieved in the same way as S_{xx}. Bosboom and Stive (2015) provided a complete derivation of those parameters.

$$\begin{aligned} S_{xx} &= \left(n - \frac{1}{2} + n\cos^2\Theta\right)E \\ S_{yy} &= \left(n - \frac{1}{2} + n\sin^2\Theta\right)E \\ S_{xy} &= S_{yx} = n\cos\theta\sin\Theta E \end{aligned} \tag{2.11}$$

As mentioned before, a gradient in the radiation stress will cause a force in the corresponding direction. Assuming an alongshore uniform coastline, the alongshore directed force is caused by a gradient in the x-direction of the radiation shear stress S_{yx}. The cross-shore directed force is the result of a gradient in the x-direction of the radiation stress S_{xx}.

$$\begin{aligned} F_y &= -\frac{\delta S_{yx}}{\delta x} \\ F_x &= -\frac{\delta S_{xx}}{\delta x} \end{aligned} \tag{2.12}$$

In case of an infinitely long uninterrupted coastline, the force F_y needs to be balanced in some way. The counteracting force making this balance is created by the bed shear stress $t_{b,y}$. Using this balance of forces, a formulation for the alongshore current velocity in case of a uniform coastline can be found. The whole derivation is left behind but is stated in Bosboom and Stive (2015), the final result is provided in equation 2.13. Here c_f is a friction coefficient and V(x) the current velocity.

$$V(x) = -\frac{5}{16}\pi\frac{\gamma}{c_f}g\frac{\sin(\phi_0)}{c_0}h\frac{dh}{dx} \tag{2.13}$$

The counteracting force in the cross-shore direction is caused by a water level set up. A further elaboration is provided in section 2.1.5.

2.1.4. Wave diffraction

Coastal structures will create a shadow zone for which a reduced wave climate is present. This wave climate is highly affected by the process of wave diffraction. Wave diffraction is defined as the lateral transfer of wave energy along the wave crest, caused by a gradient in wave height along the crest. When waves are propagating towards shore and are interrupted by an obstacle like a groyne, they will turn around the edge into the shadow zone and alter the (breaking) wave heights and angles in this zone. Since a variation in breaking wave height and/or angle will cause a gradient in the alongshore sediment transport, wave diffraction should be taken into account to determine the coastline evolution near structures. Literature distinguishes the diffraction of regular monochromatic waves and irregular wave diffraction. The process has been studied for a long time and different methods are available to account for wave diffraction effects while simulating the shoreline evolution. Chapter 3 provides a detailed description of the phenomenon of wave diffraction.

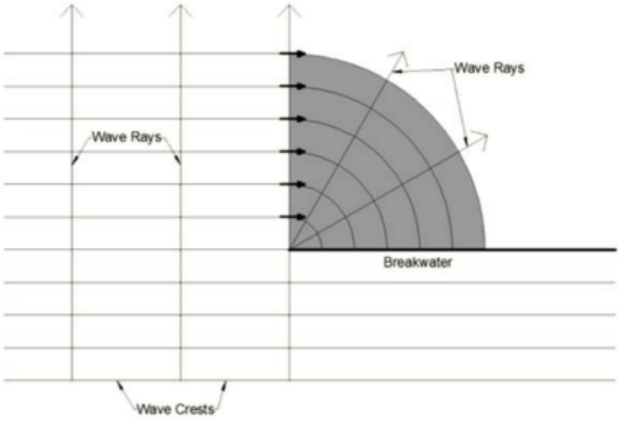

Figure 2.4: Schematised diffraction (Van der Salm, 2013)

2.1.5. Local nearshore currents due to water level setup differences

Section 2.1.4 describes that there will be a variation in breaking wave height inside the shadow zone of the groyne. An alongshore difference in breaking wave height will cause a variation in water level set-up inside this area. This could be demonstrated by assuming normally incident waves, applying the shallow water approximations and make use of the simple energy dissipation model together. In the case of normally incident waves propagating in shallow water, the radiation stress S_{xx} is equal to $\frac{3}{2}E$. Going from the breakerline towards the coast, S_{xx} is getting smaller because of a decreasing wave energy E. The resulting negative gradient in S_{xx} is responsible for a force directed towards the shoreline (equation 2.12). An offshore-directed force is needed to satisfy an equilibrium. This force will be caused by the raising of the water level in the direction of the coast, often called water level set-up. The resulting offshore-directed pressure force will balance the force caused by a gradient in the radiation stress. The water level set-up can be expressed using the following equation.

$$\Delta\eta = \frac{3}{8}\gamma H_{br} \tag{2.14}$$

Here $\Delta\eta$ is the water level difference between the breakerline and the point of maximum water level set-up. The maximum water level set-up compared to the still water level is equal to $\frac{5}{16}\gamma H_{br}$. A full derivation of the water level set-up calculation is provided by Bosboom and Stive (2015).

A groyne could cause a water level difference in the alongshore direction as follows. Just behind the groyne, where the lowest wave height will be present, the smallest wave set-up at the shoreline will occur. Moving downstream, the waves will hardly be affected by the groyne resulting in larger wave heights. Subsequently, a larger water level set-up will occur at the shoreline. The resulting alongshore water level set-up difference will generate a secondary current that is located towards the groyne and eventually will be directed in the seaward direction along the groyne. This current could transport a considerable amount of sediment towards the groyne, inducing local sedimentation (or less erosion).

2.1.6. Sediment bypassing and transmission

Depending on the characteristics of the groyne structure itself, bypassing and/or transmission of sediment could occur. In the case of transmission, sediment will pass through the structure. The main factor determining the amount of transmission is the permeability of the structure material. Bypassing is the process of sediment going past the seaward end of the groyne from updrift to downdrift. The water depth at the tip of the groyne compared to the maximum water depth of active transport D_{LT}, plays a dominant role concerning the amount of bypass. If the tip water depth is less than the maximum depth of active transport, the amount of bypass will be significant. Hanson (1989) defined the maximum water depth of active transport to be equal to the depth of breaking of the highest $\frac{1}{10}$ incoming waves. Bypass will also occur if the amount of sediment deposited updrift of the groyne exceeds the groyne tip.

2.2. ShorelineS

The urge of modeling the coastline evolution and the rise of the ShorelineS model are mentioned in chapter 1. In the following sections, different considerations and characteristic model features of ShorelineS are addressed. First, a comprehensive visualization of the morphodynamic loop applied in ShorelineS is provided. This visualization is made by the means of an extensive model walk-through. While performing this walk-through, it is examined if the governing coastal processes described in section 2.1 are incorporated inside ShorelineS.

2.2.1. Model set-up

Roelvink and Reiniers (2011) described that every numerical model for simulating the dynamic behaviour of coastlines consists of the same general set-up (figure 2.5).

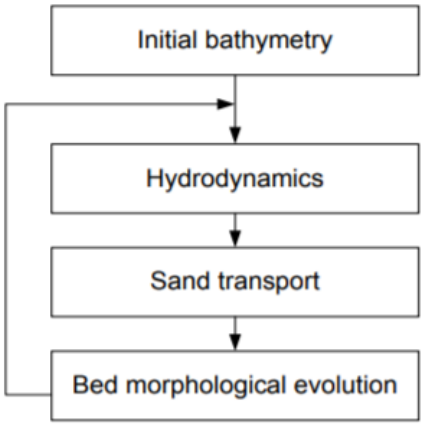

Figure 2.5: General set-up coastline evolution models

ShorelineS also follows such a kind of model set-up. After the initial bathymetry and boundary conditions are established, the wave characteristics are calculated. Subsequently, the alongshore sediment transport rates between every adjacent grid points are determined based on these wave characteristics. The effects of currents onto the alongshore sediment transport are not taken into account inside ShorelineS. The coastline changes are calculated using the gradient in the alongshore sediment transport. Finally, together with the initial coastline position, the new location of the coastline is determined after which the loop is repeated.

To retrieve a detailed model schematization, an extensive model walk-through has been performed. In doing so, all the ins and outs of the ShorelineS model are examined. This will enhance the model development and validation, which are described later on in this thesis. Just like any other numerical model, the user needs to provide input parameters. Some of these parameters are first prepared by the model so that they could be used in the real simulation (figure 2.6). The outcome of this model preparation is a data structure containing all the necessary parameters. A part of these are defined by the user but there are also some default parameters stored in this data structure.

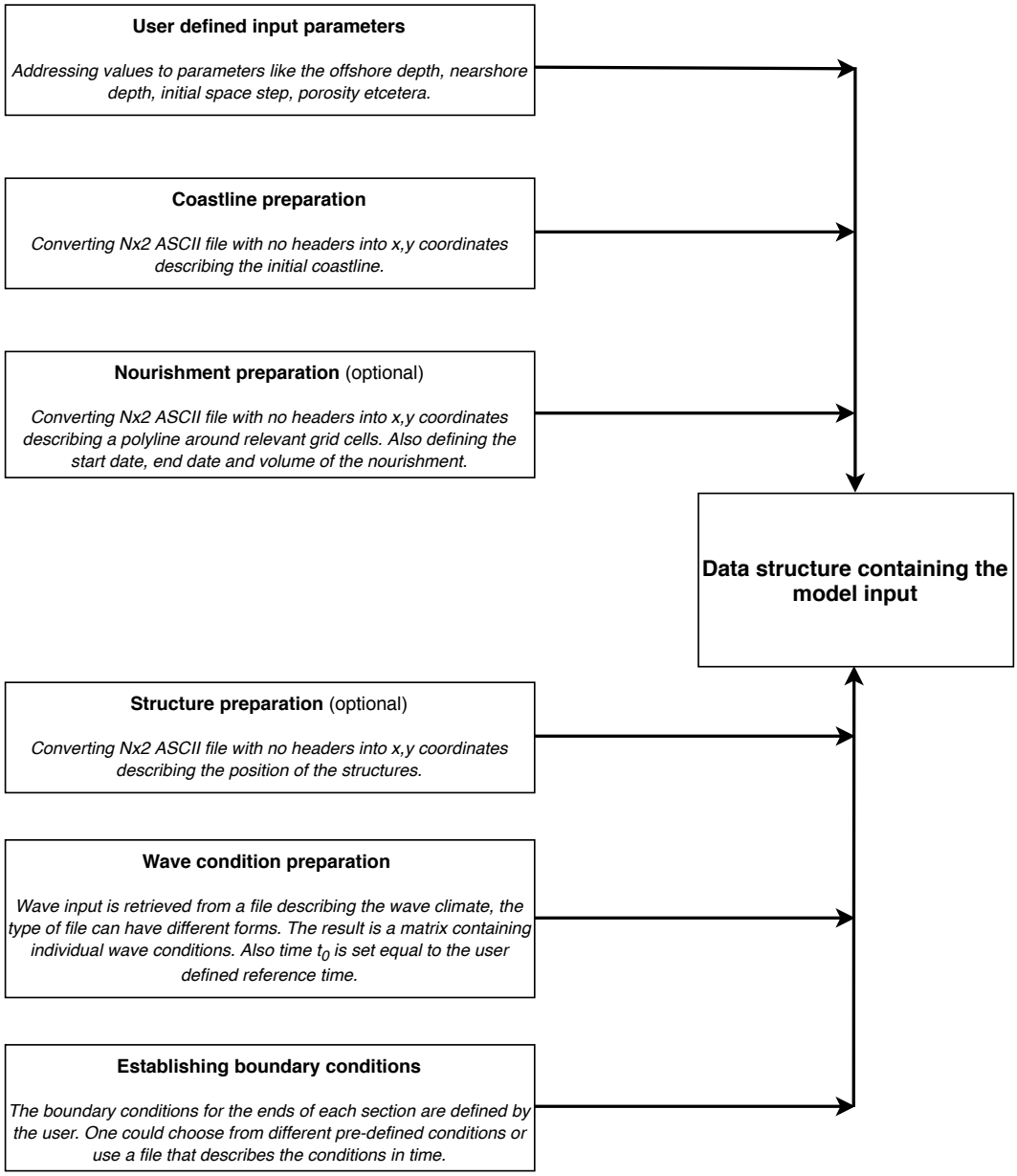

Figure 2.6: Overview ShorelineS model input preparation

Once the model preparations are finished, different coastal sections are identified. Subsequently, initializing and smoothing the grid for each section takes place. Hereafter, the real simulation starts with the first time step Δt_1. The first wave condition is retrieved and forced upon the different coastal sections. Those sections are all looped individually for each time step Δt. Figure 2.7 visualizes the model loop that is performed inside ShorelineS while simulating the shoreline evolution. The required parameters are all retrieved from the data structure containing the model input.

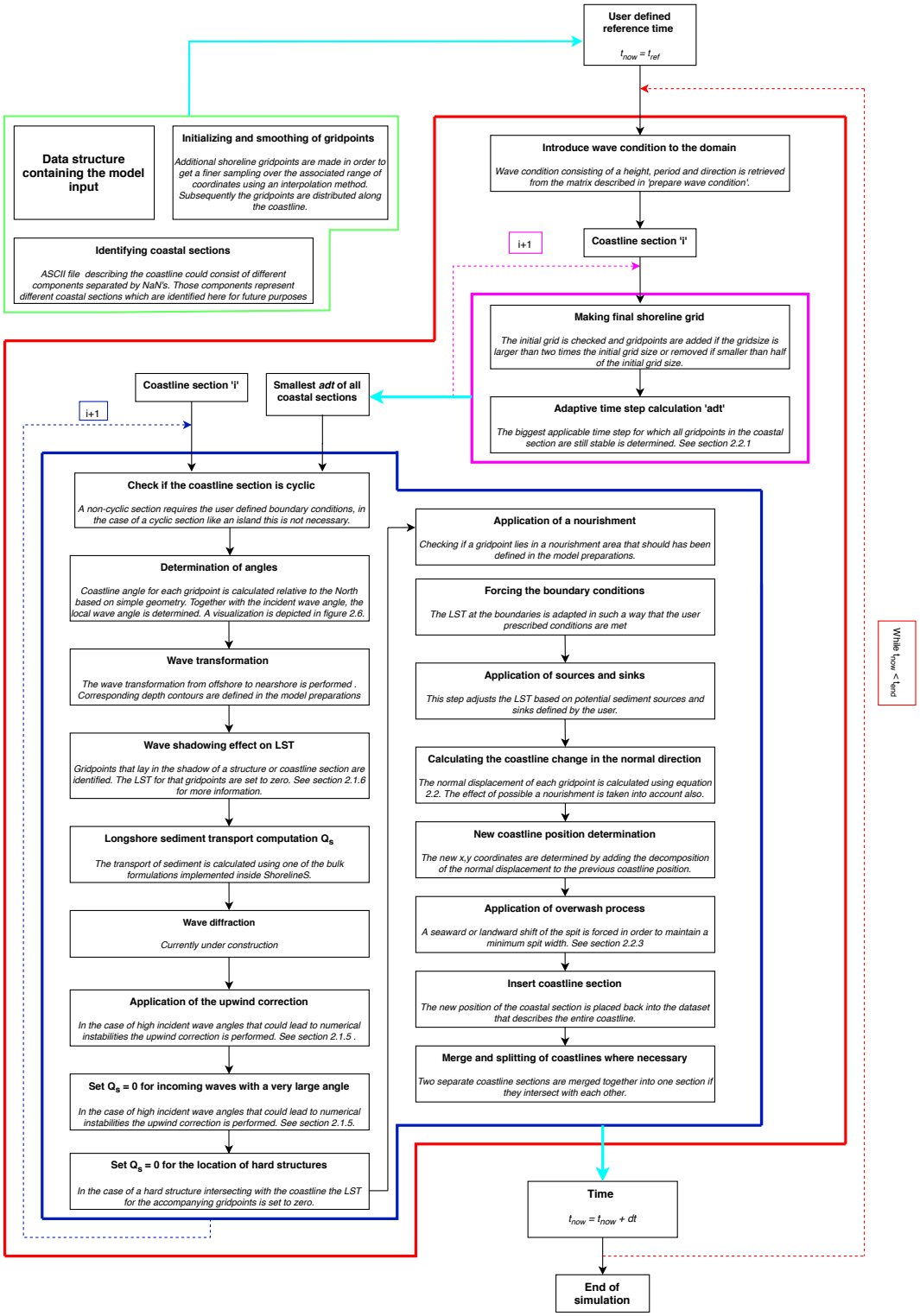

Figure 2.7: Model loop ShorelineS

2.2.2. One-line model

ShorelineS is a coastline type of model, applicable to coastline systems for which the alongshore sediment transport dominates the shoreline evolution. This evolution is caused by gradients in the alongshore sediment transport and calculated based on the considerations made by Pelnard-Considere (1956). Pelnard-Considere (1956) developed the first practical method to calculate coastline evolution caused by wave-driven sediment transport. In doing so, an analytical solution for the coastline change under the assumption that the cross-shore profile had a fixed shape was established. The foundation behind his assumption was that extreme storms only temporarily change the cross-shore profile. In the long-term, the slope will be in equilibrium with a characteristic slope for that particular coast. If the profile slope is constant, only one point on the slope is needed to define the entire shape of the cross-shore coastal profile relative to a baseline (Baykal, 2006). Consequently, movement of the coastline only takes place parallel to itself. This movement is seaward in the case of accretion and shoreward in the case of erosion. The actual profile slope used in the calculations could consist of any kind of shape, as long as this shape stays constant while moving in the cross-shore direction. Consequently, all contours lines will move at the same rate.

Another assumption made by Pelnard-Consideré is that only up to a certain seaward extend the coastal shoreface is morphodynamically active. This seaward limit is called the depth of closure, behind this limit no significant depth changes will occur. In literature, there is a great variety of the definition of this closure depth. A well-known description is made by Kraus et al. (1998) and is as follows: 'the depth of closure for a given or characteristic time interval is the most landward depth seaward of which there is no significant change in bottom elevation and no significant net sediment transport between the nearshore and the offshore. Hallermeier (1980) stated that if no relevant measurements are available, the closure depth D_c can be estimated based on the significant wave height $H_{s,12}$ (equation 2.15). $H_{s,12}$ is the significant wave height that occurs 12 hours per year on average.

$$D_c = 1.6 H_{s,12} \tag{2.15}$$

Based on the above mentioned assumptions, Pelnard-Considere (1956) came up with the sediment continuity equation which originates from the conservation of mass.

$$\frac{\delta y}{\delta t} + \left(\frac{\delta Q_s}{\delta x} + sink/source \right) \frac{1}{D} = 0 \tag{2.16}$$

This equation describes the cross-shore shift δy over time as a function of the gradient in alongshore sediment transport $\frac{\delta Q_s}{\delta x}$, a possible source or sink term, and the active profile height D. This active profile height is divided into the depth of closure D_c and the berm height D_b, measured from the mean sea level (figure 2.8).

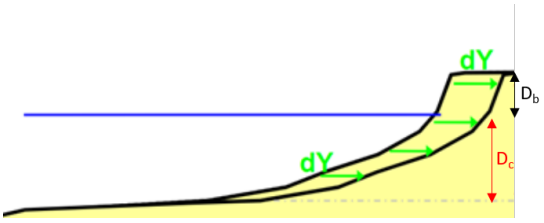

(a) Shoreline shift in the cross shore direction only (Huisman, 2012)

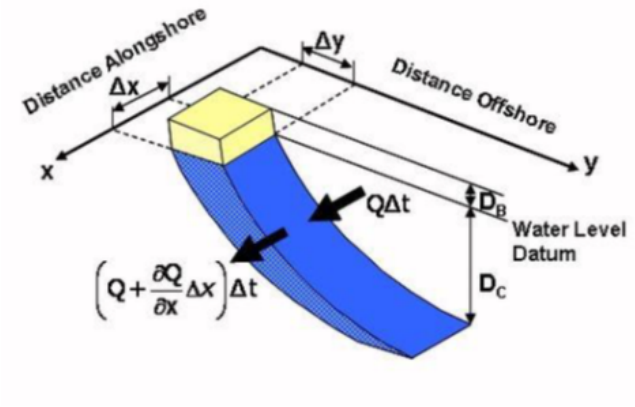

(b) Sketch of sand continuity equation (Hanson and Kraus, 2011)

Figure 2.8: One-line model

2.2.3. Coastline description

Hurst et al. (2015) proposed a method to model the shoreline evolution of highly curved and crenulate-shaped coasts. However, only allowing for one coastal section. As in Hurst et al. (2015), the coastline inside Shorelines is described by grid points that can freely move around, together they form a polyline (figure 2.9). In doing so, ShorelineS accounts for multiple coastline sections. The model allows for a rich behaviour like the migration of islands, merging and splitting of coastal sections, and formation of tombolo's and salient (Roelvink et al., 2020).

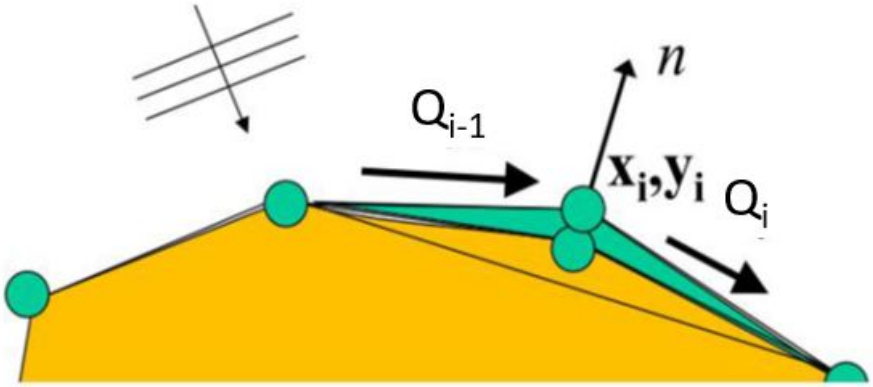

Figure 2.9: Polyline describing the coastline in ShorelineS (Roelvink et al., 2020)

The initial coastline is usually specified with grid points described by x and y coordinates. As mentioned in section 2.2.2, the coastline change is caused by a gradient in alongshore sediment transport. To determine the new x and y coordinates, after each time step the mass conservation is solved. Rewriting equation 2.16, applying alongshore coordinate s and using a forward in time and central in space explicit scheme for discretization purposes leads to the following statement, incorporated inside the model (Roelvink et al., 2020):

$$\frac{n_i^{j+1} - n_i^j}{\Delta t} = -\frac{1}{D}\frac{2\left(Q_{s,i}^j - Q_{s,i-1}^j\right)}{L_i} \tag{2.17}$$

The normal displacement of gridpoint n_i, moving seaward or landward, is determined by the gradient in alongshore sediment transport over the section between grid points n_i and n_{i-1}. This gradient is calculated by dividing the difference of sediment transport between n_i and n_{i-1} by the length L_i. This is the length of the segment between the two adjacent grid points n_{i-1} and n_{i+1}.

$$L_i = \sqrt{(x_{i+1} - x_{i-1})^2 + (y_{i+1} - y_{i-1})^2} \tag{2.18}$$

The new x and y coordinates of gridpoint n_i can now be calculated based on geometry. Figure 2.10 is made to clarify this process. In this example, the coastline displacement of gridpoint i_3 is calculated. i_3 has representative x_3 and y_3 coordinates which define the position of the gridpoint. The displacement dn is normal to the red dotted line L.

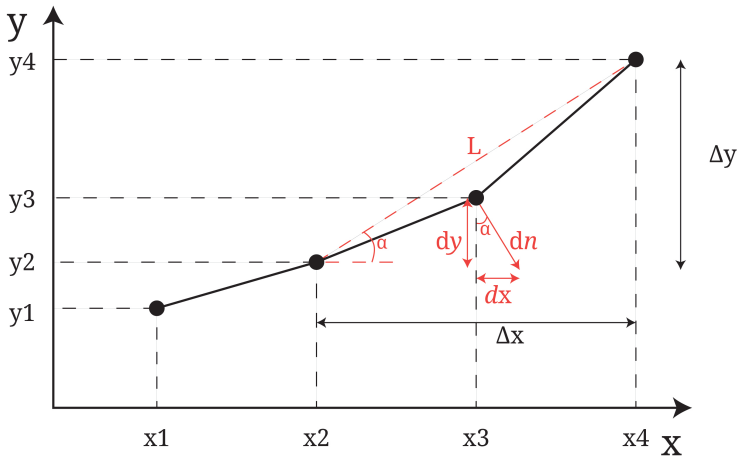

Figure 2.10: Calculating new coastline position)

Because of similarity, the angle α in the bigger triangle and smaller triangle are equal. The value of α can be determined using the following relations:

$$\sin(\alpha) = \frac{\Delta y}{L} \qquad \cos(\alpha) = \frac{\Delta x}{L}$$
$$\sin(\alpha) = \frac{dx}{dn} \qquad \cos(\alpha) = \frac{dy}{dn}$$

The new position of gridpoint i_3 can now be calculated as follows:

$$\begin{aligned} x_{3,new} &= x_3 + dx = x_3 + \frac{\Delta y}{L} dn \\ y_{3,new} &= y_3 + dy = y_3 + \frac{\Delta x}{L} dn \end{aligned} \tag{2.19}$$

After the next time step, equation 2.17 is solved again and eventually resulting in the new coordinates of the shoreline. This procedure is repeated until the end of the simulation.

2.2.4. Wave transformation

The previous section describes how the new coastline position is calculated based on gradients in the alongshore sediment transport. An elaboration on the different alongshore sediment transport formulations that are currently implemented inside the ShorelineS model is provided in section 2.2.5. Most of these formulations require the breaking wave parameters $H_{s,br}$ and ϕ_{br} as input. Generally, these parameters are not available since they are hard to measure. Furthermore, the breaking wave parameters are strongly dependent on the local nearshore properties like bed slope and bottom depth. Consequently, the breaking wave parameters will vary along the coastline. Sometimes breaking wave measurements are available, they should be carefully used because the morphological change over time will alter these parameters. Therefore, the determination of breaking wave parameters should be inside the morphological model loop (Mudde, 2019). This means that the wave parameters should be calculated after each time step based on the updated morphology.

Software tools are nowadays available to establish wave transformation from offshore to the nearshore. They are able to model the change in length, height and direction while a wave is travelling towards the shore. USACE (1984a) described that the following processes could play a role in this wave transformation: refraction, shoaling, diffraction, dissipation due to friction, dissipation due to percolation, breaking, growth due to wind input, wave-current interaction and wave-wave interaction. The first three processes result from wave energy convergence or divergence while propagating. The changing sea bottom profile, in the cross-shore and alongshore direction, while traveling towards shore causes this energy convergence or divergence. Wave diffraction is caused by structures that lay in the propagation path of waves.

The subsequent three processes from the above summation are all responsible for withdrawing energy, therefore called sink terms. Local wind effects could transfer energy into the waves causing additional growth, in doing so being a source term. Wave-wave interaction results in the transfer of energy from a wave to another wave, leading to a shift in the energy density spectrum.

ShorelineS uses simplified calculations to account for the effects of wave shoaling, refraction and eventually wave breaking. The other processes which are stated above are currently not implemented inside the model. Shoaling and refraction are strongly dependent on the coastal bathymetry. In coastline models, the bathymetry is represented using depth contours that are assumed to remain coastline parallel during the coastal evolution. Inside the ShorelineS model, offshore waves are transformed to such a depth contour, the breaker line, to determine the breaker parameters. This transformation takes place in two steps. In the first step, the nearshore wave angle and height are determined using the offshore local wave angle and height. In doing so, Snell's Law is applied and the dispersion relation is used. The second step consists of the transformation from the nearshore to the breaker line.

In section 2.3, the model adjustments provided by Mudde (2019) are described. Mudde (2019) introduced a third step in the wave transformation part. In doing so, more accurate breaking wave parameters are obtained. An elaboration of those steps can be found in appendix A which addresses the details of the recently made model improvements. The formulation which is used inside ShorelineS to calculate the breaking wave water depth is depicted in equation A.11.

2.2.5. Sediment transport calculation

In literature, different methods for calculating sediment transport can be found. Coastline models usually incorporate so-called bulk alongshore sediment transport formulations. These formulations are based on simplifications of physical processes. Usually, empirical parameters are involved to calibrate (Mil-Homens, 2016). These bulk formulations provide an easy way to calculate the alongshore sediment transport using a limited amount of input variables. Therefore, being suitable for long-term shoreline evolution calculations. However, bulk alongshore sediment transport equations do not provide information about the distribution over the depth profile. In ShorelineS, bulk transport formulations described by USACE (1984a), Kamphuis (1992), Ashton et al. (2001), Mil-Homens (2016) and van Rijn (2014) are currently incorporated. Each formulation is briefly addressed in the section below.

CERC

Ashton and Murray (2006b) and van Rijn (2002) stated that the most commonly used alongshore sediment transport bulk formulation is the CERC, developed by USACE (1984a). The most simple form of the CERC formulation relates the alongshore sediment transport Q_s to the alongshore wave energy flux per unit length P inside the surfzone multiplied by a calibration factor K (van Rijn, 2002). Only alongshore transport caused by waves approaching the coast under an angle is taken into account. Transport induced by tidal currents for instance, is not considered (Bosboom and Stive, 2015).

$$Q_s = P * K \tag{2.20}$$

The physical interpretation of this term P, being the alongshore component of the energy flux, has been argued extensively in the past decades (Bosboom and Stive, 2015). Longuet-Higgins and Stewart (1964) related P to the shear component of the radiation stress S_{xy} multiplied by the wave velocity c. This relation was established by using the small-amplitude wave theory and assuming that the total energy flux in shoaling waves propagating towards shore remains constant (USACE, 1984a).

$$P = S_{xy} * c = n\cos(\phi)\sin(\phi)E * c_g \tag{2.21}$$

The CERC formulation is often written down in terms of wave height parameters. In doing so, a relation between the wave energy E and breaking wave height H_{br} is applied.

$$E = \frac{1}{8}\rho g H_{br}^2 \tag{2.22}$$

Assuming that the waves break in shallow water, n (equation 2.21) could be replaced by the value of one. Furthermore, the wave speed c_g can be computed very easily when assuming shallow water conditions (equation 2.23).

$$c_g = c = \sqrt{g h_{br}} \tag{2.23}$$

The water depth at which breaking occurs can be replaced by the factor $\frac{H_{br}}{\gamma}$. For the breaker index γ, often a value of 0.78 satisfies (Bosboom and Stive, 2015). Using rules for geometry, the product of $\cos(\phi)\sin(\phi)$ (equation 2.21) can be rewritten as follows:

$$\cos(\phi)\sin(\phi) = \frac{1}{2}\sin(2\phi)) \tag{2.24}$$

Combining equations 2.20, 2.21,2.23 and 2.24 results in the so-called full CERC formulation as described in USACE (1984a):

$$Q_s = \frac{k\rho_w}{16(\rho_s - \rho_w)(1-p)}\sqrt{\frac{g}{\gamma}} H_{s,br}^{2.5}\sin(2\phi_{loc,br}) \tag{2.25}$$

In which k is a calibration coefficient, ρ_w and ρ_s represent the density of water and sediment respectively, p is the porosity, $H_{s,br}$ the significant breaking wave height and $\phi_{loc,br}$ is the local breaking wave angle. The term loc refers to the relative angle between the waves and the shoreline.

CERC - Adapted by A. Asthon

Another form of the CERC formulation, in which the breaking wave parameters are replaced by the offshore wave conditions, was suggested by Ashton et al. (2001). Breaking wave parameters are hard to measure compared to offshore wave conditions. The latter ones are often measured using a wave buoy. Besides that, Ashton and Murray (2006a) stated that the breaking wave parameters are far from constant along a coast because of the changes in local bathymetry. They proposed to account for the variations in breaking parameters or to come up with an alongshore sediment transport formulation in terms of offshore wave parameters. Those parameters are not influenced by processes like refraction and shoaling, therefore being constant along a coastline. The second option was chosen, resulting in an adapted form of the CERC equation which uses deep water wave conditions (equation 2.26).

$$Q_s = k_2 H_{s,0}^{12/5} T^{\frac{1}{5}} \sin(\phi_{loc,0})\cos^{\frac{6}{5}}(\phi_{loc,0}) \tag{2.26}$$

The subscript 0 refers to the deep water values of the wave parameters. The factor k_2 is implemented to account for the process of refraction when waves travel from offshore to the coastal area. Assuming parallel depth contours and depth limited breaking, an expression for k_2 was found (equation 2.27).

$$k_2 = \frac{\sqrt{g\gamma}}{2\pi}^{\frac{1}{5}} * 0.4 \tag{2.27}$$

Simplified CERC

The simplified CERC is also implemented inside the ShorelineS model. Actually, this expression is similar to the full CERC (equation 2.25). However, now using $H_{s,0}$ and $\phi_{loc,0}$ instead of the breaking wave parameters. All the parameters stated in front of $H_{s,br}$ inside equation 2.25 are summarized in a calibration factor b_{CERC}.

$$Q_s = b_{CERC} H_{s,0}^{2.5}\sin(2\phi_{loc,0}) \tag{2.28}$$

J.W. Kamphuis

A limitation of the earlier described CERC formulation is that the sediment transport only depends on wave parameters. Sediment characteristics, like grain size, are not included. However, larger transport rates are expected for smaller sediment grains since they will mobilize more easily. Kamphuis (1992) presented a bulk alongshore sediment transport formulation that is based on dimensional analysis and calibration of data from laboratory and field experiments. Besides the same wave parameters used in the CERC formulation,

Kamphuis (1992) included the bed slope and grain diameter. The wave angle has less influence on the transport rate compared to CERC, however, the wave period has a larger contribution (equation 2.29).

$$Q_s = \frac{1}{(\rho_s - \rho_w)(1-p)} 2.27 H_{s,br}^2 T_p^{1.5} \big(\tan(\beta)\big)^{0.75} D_{50}^{-0.25} \big(\sin(2\phi_{loc,br})\big)^{0.6} \tag{2.29}$$

Here T_p is the peak period, $\tan(\beta)$ the bed slope at the breaker point and D_{50} the median grain size diameter. The sediment transport is proportional to the bed slope and inversely proportional to the grain size diameter. However, one should realize that those two parameters are interdependent. For the same hydraulic conditions, coarser sediment will result in a steeper bed slope.

J. Mil-Homens

Mil-Homens et al. (2013) provided an evaluation of the most commonly used alongshore sediment transport formulations. An extensive data set was used to test the predictive skills of the CERC and Kamphuis equations. Both being significantly improved after calibration of the empirical coefficients. In doing this, a least-squares optimization algorithm was used. Thereafter, the improved formulations were compared to each other. Mil-Homens (2016) concluded that the adjusted-Kamphuis relation (equation 2.30) showed the best results.

$$Q_s = \frac{1}{(\rho_s - \rho_w)(1-p)} 0.149 H_{s,br}^{2.75} T_p^{0.89} \big(\tan(\beta)\big)^{0.86} D_{50}^{-0.69} \big(\sin(2\phi_{loc,b})\big)^{0.5} \tag{2.30}$$

L.C. van Rijn

The above stated alongshore sediment transport formulations are strictly spoken only valid for sandy beaches. Therefore, van Rijn (2014) tried to establish a formulation being applicable to gravel and shingle beaches. He presented an easy formulation that can be applied to grain sizes within the range of 0.1 - 100 millimeters.

$$Q_s = \frac{1}{(\rho_s - \rho_w)(1-p)} 0.006 K_{swell} \rho_s H_{s,br}^{2.6} \big(\tan(\beta)\big)^{0.4} D_{50}^{-0.6} V_{total} \tag{2.31}$$

Compared to the other formulations, there are two new parameters: K_{swell} and V_{total}. The first one is included to account for the influence of the wave period. Sensitivity computations were performed to asses this influence. van Rijn (2014) concluded that in the case of wind waves, the period does not have a large impact on the transport rate. However, swell waves with a height of 1 to 2 meters seemed to produce significantly larger transport rates compared to wind waves with the same heights. This effect is taken into account by applying the $swell$ factor K_{swell}.

$$K_{swell} = 0.015 \rho_{swell} + (1 - 0.01 \rho_{swell}) \tag{2.32}$$

In which ρ_{swell} is the percentage of low-period swell wave heights compared to the total wave height record. If this relative amount of swell waves increases, the sediment transport rate will increase. ρ_{swell} varies between 1 (no swell waves) and 1.5 (only swell waves). The second new parameter, V_{total}, is implemented to account for additional velocities caused by the tide and wind (equation 2.33). The previously stated transport formulations only incorporate wave induced sediment transport.

$$V_{total} = V_{wave} + 0.01 p_1 V_1 + 0.01 p_2 V_2 \tag{2.33}$$

In which V_1 is the representative velocity in positive alongshore direction due to the combined action of wind and tide. V_2 is in the negative alongshore direction. p_1 and p_2 are the percentages of time in which positive and negative flow are present. The wave induced alongshore current velocity V_{wave} is calculated according to equation 2.34.

$$V_{wave} = 0.3 (g H_{s,br})^{0.5} \sin(2\phi_{loc,br}) \tag{2.34}$$

2.2.6. High wave angle instability

Different coastline models have been developed since the 1980's. Examples are UNIBEST-CL+ (Deltares, 2011), LITPACK (DHI, 2011) and Genesis (Hanson, 1989), each being a powerful numerical tool to model long-term coastline evolution. Inside those models is the alongshore sediment transport rate calculated as a function of the (local) incident wave angle (figure 2.11), described by a sine function (Roelvink et al., 2020).

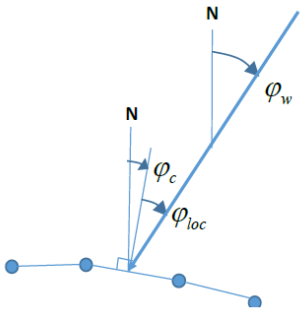

Figure 2.11: Definition of the coastline angle ϕ_c, incident wave angle ϕ_w and local wave angle ϕ_{loc} (Roelvink et al., 2020).

The transport rate will be maximum when the local incident wave angle approaches 45°. Ashton et al. (2001) stated that for larger angles the transport rate will decrease, leading to unstable behaviour of the coastline evolution. High angle incident waves, waves with a higher angle than the maximum transport angle, will enhance small perturbations leading to instabilities like spit formation. Wang and Mehaute (1980) studied the shoreline stability in different mathematical models and already concluded that when waves have a large breaking angle, instabilities in the shoreline evolution could arise. For low angle waves, the alongshore sediment transport increases for larger relative wave angles (figure 2.12). The definition of relative wave angles is the same as for local wave angles. Controversially, the increase in wave angle for high angle waves results in a decrease of sediment transport, leading to shoreline instabilities that increase over time (figure 2.12). This growth of perturbations is a positive feedback mechanism that eventually leads to self-organized coastline patterns (Bosboom and Stive, 2015).

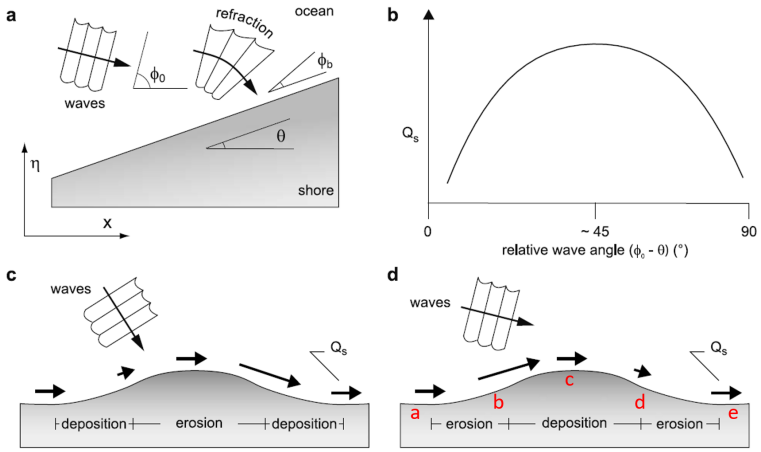

Figure 2.12: High angle wave instability (Ashton and Murray, 2006a).(a) Definition of terms and axes. (b) Relationship between alongshore sediment transport and relative wave angle. (c) Shoreline response to low angle waves. (d) Shoreline response to high angle waves.

Panel (d) of figure 2.12 represents the case of high-angle incoming waves. Going along the coast from a to b, the relative wave angle decreases. Consequently, increasing the alongshore sediment transport. Because of the positive alongshore sediment transport gradient, this section of the coast will be subjected to erosion. The same situation takes place in the coastline section between d and e. Going from b to c and from c to d, the relative wave angle increases resulting in accretion for this coastline section. Therefore, simulating the growth of the perturbation. The coastline models mentioned at the beginning of this section can not deal with high angle wave instabilities (Roelvink et al., 2020). Ashton et al. (2001) introduced a method to account for high angle incoming waves using an upwind approach. Inside ShorelineS, the same kind of upwind correction is applied (Roelvink et al., 2020). A numerical scheme being a combination of upwind and central-difference techniques is incorporated to overcome the instabilities caused by high angle waves. Elghandour (2018) provided details of this method. Here, the method is briefly addressed.

When a certain grid point i is subjected to a high wave angle and its updrift neighbour $i+1$ to a low wave angle, the alongshore sediment transport will be calculated using the angle that leads to a maximum transport of sediment. Also for the case when gridpoint i is subjected to low wave angles and $i+1$ to high wave angles, the maximizing transport angle is used. In this way, sediment is transformed from the upwind grindpoint to the more downdrift gridpoint, allowing a smooth spit evolution (figure 2.13). The angle causing the maximum transport is called the critical angle and is different for each alongshore sediment transport formulation.

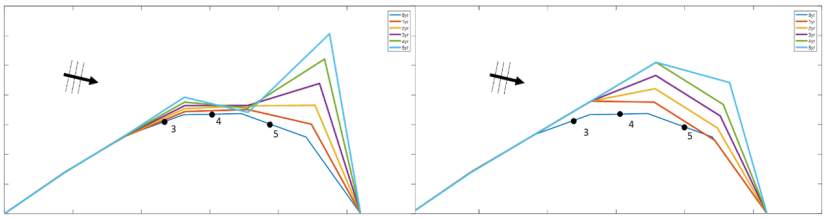

Figure 2.13: Difference between coastline evolution without (left) and with (right) implementation of the high angle wave correction (Elghandour, 2018).

2.2.7. Wave shadowing

Another feature of the ShorelineS model is that it takes into account the effect of wave shadowing. For example, human coastal structures or natural headlands could provide shelter for incoming waves. The area which is sheltered is often called the shadow area. A procedure is implemented in which for every time step a line is drawn in the direction of the incoming wave. If this line crosses a hard structure or a part of the coast itself, the shadowing effect is activated and the sediment transport is set to zero in this area. This simple method neglects the amount of energy that is transferred into the shadow zone by the diffraction of waves. Also, the effect of possible wind input inside this area is not taken into account in ShorelineS. Hence, local wind generated waves are neglected.

Figure 2.14: Wave shadowing effect inside ShorelineS (Roelvink et al., 2020).

2.2.8. Spit overwash

As stated before, one of the advantages of ShorelineS is that it is suitable for modelling multiple sections of coastline that can interact with each other. Therefore, the merging of an island with the coast and the formation of spits can be simulated. According to Leatherman (1979), the process of overwash is essential in maintaining the width of a spit or barrier to a certain limit. If a spit keeps growing, breaching of the spit at the updrift side because of erosion is expected. However, from field observations, Leatherman (1979) concluded that barrier overwash is often maintaining the barrier itself. Overwash occurs during storm events and redistributes sediment over the considered area, therefore influencing the barrier width. Considering the expected sea level rise in the next decades, overwash becomes even more important since the increased rate of coastline erosion will increase the number of overwash events (Carruthers et al., 2013). Ashton and Murray (2006a) described an analytical solution for maintaining a minimum barrier width because of overwash. A similar approach is implemented inside ShorelineS (Roelvink et al., 2020). During the simulation, the barrier width at every gridpoint is determined at each time step. Subsequently, it is checked if the critical barrier width prevails at each gridpoint. If not, the landward point of the barrier is extended over such a distance that the barrier width becomes equal to the critical width. In doing so, the process of overwash is mimicked inside the ShorelineS model (Roelvink et al., 2020).

2.3. ShorelineS recent model improvements

Recently, multiple studies contributed to the improvement of the ShorelineS model. This section contains a brief elaboration on those improvements. Most of the numerical aspects are not depicted, the reader is referred to the associated studies of Elghandour (2018), Ghonim (2019) and Mudde (2019). Appendix A contains more details of the improvements stated in this section.

2.3.1. Adaptive time step, boundary conditions and wave diffraction

Elghandour (2018) described efforts to increase the robustness, efficiency and accuracy of ShorelineS to be capable of simulating any sandy beach all over the world. The most worth mentioning adjustments are the implementation of the adaptive time step approach, the addition of boundary conditions to deal with multiple coastal sections and accounting for wave diffraction around an offshore breakwater. The adaptive time step is a method to determine the biggest applicable time step for which all grid points in the model are still stable. Using this method, the computational time is being optimized. Elghandour (2018) also reorganized the method to deal with high wave angle instability in which the critical angle is used. After this adaptation, it was possible to apply the alongshore sediment transport formulations depicted in section 2.2.5, inside ShorelineS. Before, only the simplified CERC could be used while dealing with high angle wave instability. For each transport formulation, Elghandour (2018) provided the corresponding critical angle. All the values are close to the theoretical critical angle of 45°, belonging to the CERC formulation.

To mimic a variety of coastal environments, Elghandour (2018) implemented multiple boundary conditions inside the model. For example, the so-called Dirichlet boundary, which can be used to account for a sediment supply caused by a river. Appendix A contains an overview of all the implemented boundary conditions. Furthermore, Elghandour (2018) studied three different methods to account for wave diffraction concerning an offshore breakwater. It was concluded that ShorelineS was able to account for wave diffraction in the case of a single or multibeam breakwater system very well. The model was capable of simulating both tombolo's and salients (figure 2.15).

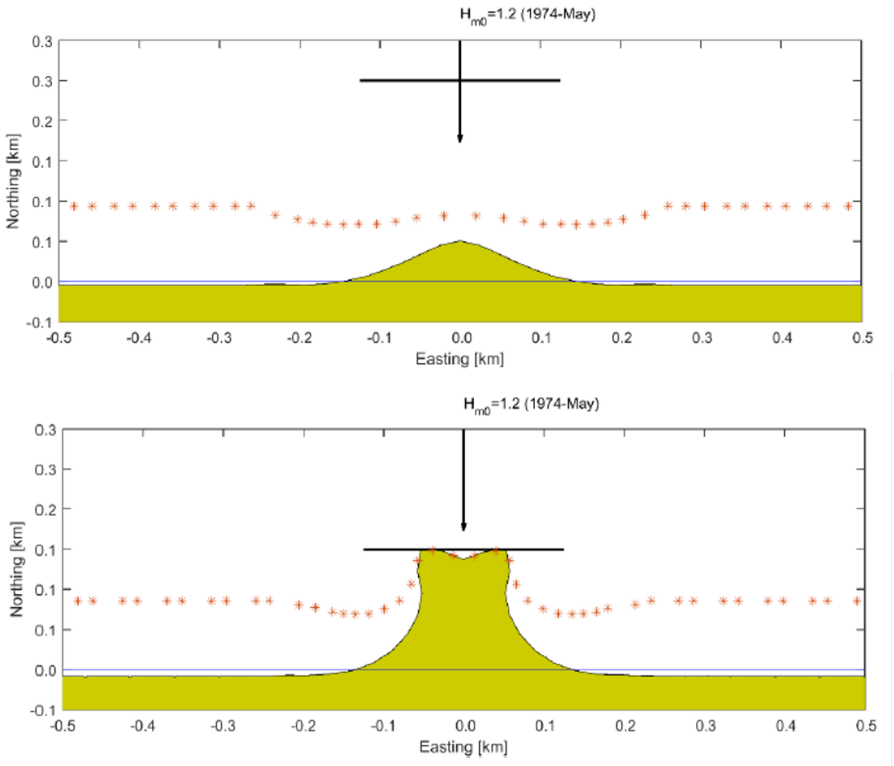

Figure 2.15: Tombolo and salient formation simulated with ShorelineS (Elghandour, 2018)

2.3.2. Sediment bypassing, transmission and dune foot evolution

The main goal of Ghonim (2019) was to enhance the model performance of ShorelineS and verify its application in more complex situations dealing with multiple coastal features. As a start, the model application close to shore normal structures was improved by implementing sand bypassing and transmission. In doing so, first the definition of structures inside the model domain was upgraded (figure 2.16.)

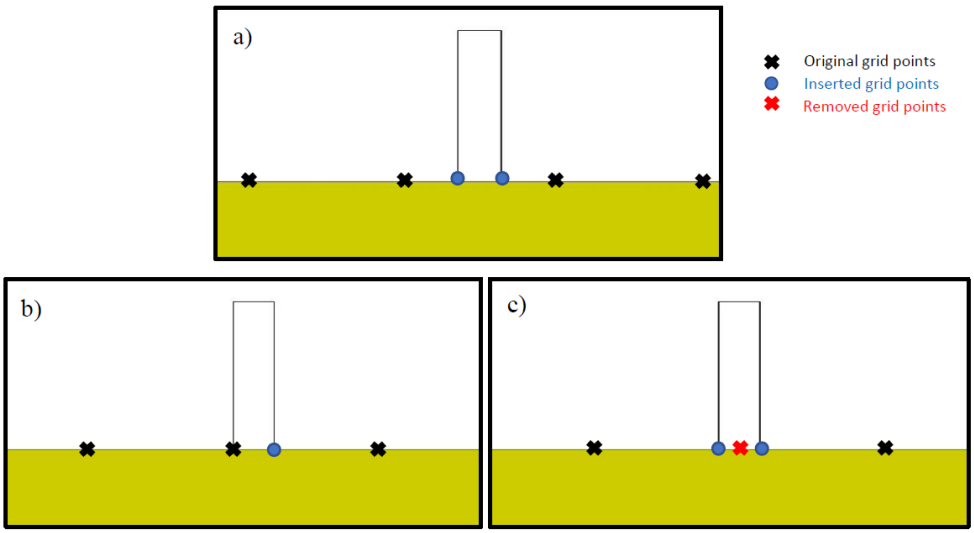

Figure 2.16: New groyne definition in ShorelineS (Ghonim, 2019). Initial locations of a groyne (a) in between two grid points, (b) on top of a grid point, (c) before and after a grid point.

A general method proposed by Hanson and Kraus (2011) is followed to include sand bypassing and transmission inside ShorelineS. In doing so, a bypassing factor BYP is introduced to quantify the amount of bypassing. Furthermore, Ghonim (2019) examined the capabilities of ShorelineS to simulate the consequences of extreme storms on the long-term dune foot evolution. A method that determines this evolution was implemented based on the schematised situation depicted in figure 2.17. More details concerning the suggested methods for implementing sediment bypassing, sediment transmission and dune foot evolution are stated in Appendix A.

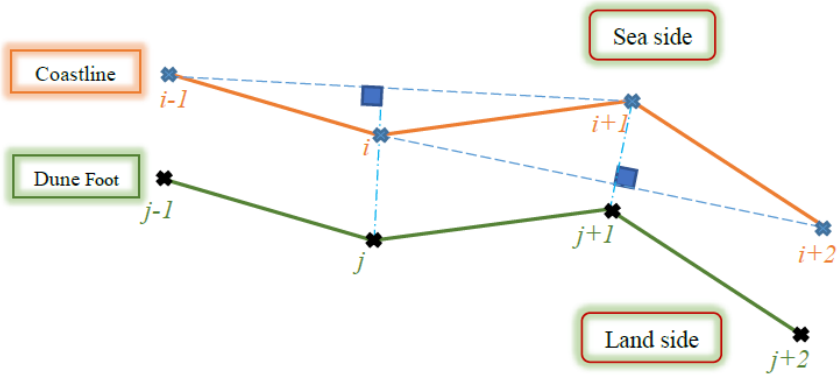

Figure 2.17: Polylines describing the dune foot location and shoreline location (Ghonim, 2019).

2.3.3. Dynamic boundary and spit formation

Mudde (2019) tested and validated different capabilities of the ShorelineS model. The focus of his study lay in the determination of the alongshore sediment transport and the behaviour of spit formation simulated by ShorelineS. During his research model difficulties were found. To overcome these difficulties, multiple model adjustments were made. The most important ones are the implementation of the so-called dynamic boundary and modifications to the procedure determining the spit width. The dynamic boundary divides the cross-shore profile into a dynamic and static part (figure 2.18). Depth contours lying in the active part could rotate. Contradictory, contours situated in the static part have a fixed orientation. Mudde (2019) showed by a model to model comparison that the implementation of a dynamic boundary resulted in more accurate wave transformation. Therefore, improving the subsequent sediment transport calculations.

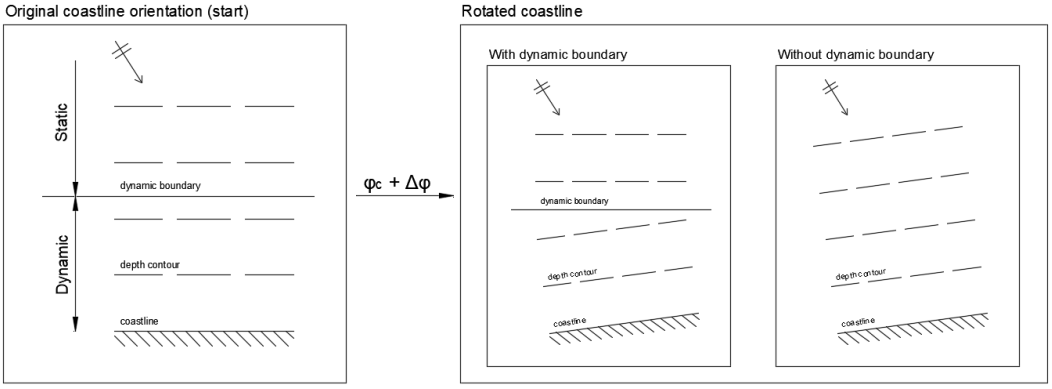

Figure 2.18: Evolution of depth contours with and without the dynamic boundary (Mudde, 2019).

Mudde (2019) applied the dynamic boundary concept also in the model part calculating the critical angle of a specific alongshore sediment transport formulation. A new method was proposed, relating the direction and width of the spit formation to this critical angle. This new method is activated when the critical angle belonging to the users specified alongshore sediment transport formulation is exceeded. Appendix A elaborates on the concept of the dynamic boundary and the improved method for calculating the spit width and orientation. An extensive elaboration can be found in Mudde (2019).

3

Wave diffraction theory

The main purpose of ShorelineS is to model the coastline evolution for short and larger time scales, suitable for geometrical complex coastlines. The hydrodynamics in the vicinity of coastal structures will be influenced by waves diffracting into the shadow zone of the structure. Since a variation in breaking wave height and/or angle will cause a gradient in the alongshore sediment transport, wave diffraction effects should be taken into account when modelling the coastline evolution near a structure. In section 2.1.4, the process of wave diffraction is briefly addressed. This chapter presents a literature review about wave diffraction. First, the development of the initial solution regarding the diffraction of monochromatic water waves is provided. Subsequently, the transition to irregular wave diffraction is made. Thereafter, analytical solutions of the coastline evolution including and excluding the effects of diffraction are examined. Lastly, methods to account for wave diffraction inside numerical modelling are discussed.

3.1. Monochromatic wave diffraction

The process of wave diffraction has been studied extensively. First, the diffraction of light passing the edge of a semi-infinite screen was examined. Sommerfeld (1896) found the solution for this general problem of diffraction. Soon after that, the relation with the diffraction of water waves was established. Penny and Price (1944) discovered that the solution provided by Sommerfeld (1896) was also applicable to linear surface waves diffracting around a structure while the water depth is constant. In literature, much can be found concerning the diffraction of waves around a breakwater. Because of design purposes, engineers have an interest in the effects of wave diffraction on the wave climate. In general, the following relation to quantify the amount of diffraction is applied:

$$K_d = \frac{H_{diff}}{H_i} \tag{3.1}$$

In which K_d is the diffraction coefficient, defined as the ratio between the diffracted wave height H_{diff} and the incident wave height at the source H_i. Penney et al. (1952) provided a solution for regular waves diffracting around an impermeable breakwater and trough a breakwater gap, both in the case of a constant water depth. Applying a uniform depth will make it possible to neglect refraction and shoaling effects. Penney et al. (1952) came up with a solution by first describing the motion of water with a velocity potential and applying the following assumptions:

- Water is incompressible and non-viscous
- The flow of water is irrotational and satisfying the Laplace equation
- Waves have a small amplitude and can be described using the linear wave theory

After establishing multiple boundary conditions and using the tables of Fresnel's integrals, a solution was found for the diffraction of waves under the mentioned circumstances. Penney et al. (1952) concluded that the diffraction coefficient for regular waves in the presence of a semi-infinite breakwater depends on (a) the ratio between the radial distance r from the breakwater tip to the point where K_d has to be determined and the incoming wavelength at the tip, (b) the angle β between the breakwater alignment and this radial distance, and (c) the incident wave angle at the tip θ_i (figure 3.1).

$$K_d = f(\frac{r}{L_{tip}}, \beta, \theta_i) \tag{3.2}$$

Figure 3.1 visualizes the case of a long-crested monochromatic wave approaching a semi-infinite breakwater in uniform depth. After diffracting at the tip, the waves will form circular arcs with a varying wave height along the crest (USACE, 1984b). The smallest wave height is located close to the breakwater, getting larger while increasing the distance from the breakwater. It is assumed that the region beyond the diffracted wave ray depicted with the dashed curved line, is not affected by diffraction.

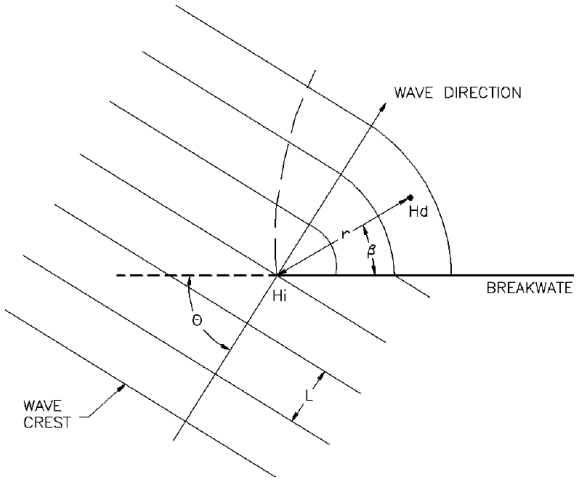

Figure 3.1: Definition of diffraction (USACE, 1984b)

Elaborating on the work of Penny and Price (1944) and Penney et al. (1952), several analyses have been performed to account for wave diffraction effects for coastal engineering purposes because a good breakwater design requires knowledge of the process of wave diffraction. Two general types of wave diffraction are distinguished in the field of engineering (Johnson, 1951); waves diffracting around the edge of an impermeable semi-infinite breakwater and waves propagating through a gap in a breakwater. Different experimental tests have been performed to validate the solution of Penney et al. (1952) for those two cases.

Putnam and Arthur (1948) made a comparison of the general wave diffraction solution and a simplified solution. The case of a semi-infinite impermeable breakwater, situated in a uniform water depth was used. Results obtained from laboratory tests were compared to the results of both solutions. The simplified solution was established by introducing a boundary condition caused by the impermeable breakwater. This condition requires that the normal component of the fluid velocity is zero along the entire breakwater. Two different wave periods and six varying incoming wave angles have been analyzed. Five carefully calibrated float-type recorders were used to measure the wave heights in the lee of the breakwater. Subsequently, wave diffraction coefficients along lines behind the breakwater have been calculated using the two different solutions. It was concluded that the simplified solution showed good agreement for most of the practical applications, especially in the lee of the breakwater. The wave period demonstrated to have little effect on the behaviour of diffracted waves. In the region directly behind the breakwater, results from the laboratory tests demonstrated to be almost exactly the same as the simplified solution. Sorensen (1993) highlighted that the solution of the diffraction problem was solved assuming small amplitude waves. Putnam and Arthur (1948) performed those laboratory experiments using waves with an average wave height to length ratio of 0.035. Therefore, satisfying the small amplitude assumption.

The diffraction coefficient of steeper waves, not satisfying this assumption, would differ significantly from the theoretical results. Considering the area outside the shadow zone, the wave heights from test results appeared to be considerably less than the ones determined by theory. Consequently, applying the theoretically derived solution for wave diffraction in the breakwater design process would lead in general to somewhat larger wave heights in the disturbed area than would occur in nature. As a result, the design of the breakwater would be a bit conservative, which is not a negative property.

Blue Jr and Johnson (1949) examined the diffraction of normal incoming waves through a breakwater gap in a uniform depth situation. The simplified equation provided by Putnam and Arthur (1948) was extended to be used in the case of a breakwater gap. Laboratory tests were performed for the deep-water and shallow-water cases. Penney et al. (1952) already stated that the proposed solution for wave diffraction through a breakwater gap is accurate enough in case the gap width is equal to two times the wavelength. The test results showed good agreement with the results obtained by using the theoretical solution up to a gap width to wavelength ratio of 1.41. Furthermore, Blue Jr and Johnson (1949) concluded that the solution of Penney et al. (1952) could also be applied in shallow water having a constant depth. The only parameter inside the equations that should be modified is the wavelength. The shallow water wavelength should be used instead of the deep water wavelength.

Johnson (1951) and Dunham (1951) provided wave diffraction diagrams to be used for the design of breakwaters. These diagrams are based on the results of the laboratory tests described by Putnam and Arthur (1948) and Blue Jr and Johnson (1949). The origin of the coordinate system is at the tip of the breakwater. Each curve represents a values of the diffraction coefficient. Wiegel (1962) extended and generalized the solution of Penney et al. (1952). Subsequently, diffraction coefficient diagrams applicable to different incoming wave angels were established. USACE (1984a) published those diagrams, suitable for a varying incoming wave angle θ_i by intervals of 15° going from 0° to 180°. Figure 3.2a visualizes the diagram that can be used to determine the K_d coefficients in the case of an incoming wave angle of 45°. When the diagrams are used to actual problems, the wavelength corresponding to a water depth equal to the depth at the toe of the breakwater should be calculated. The application of this diagram is shown in figure 3.2b. The diagram is turned in such a way that the origin is located at the diffraction source, which is in this case the tip of the groyne. Subsequently, the diagram is scaled to match the distance of the wavelength. The perpendicular distance between two wave crests, displayed using red lines, should be the same as the indicated wavelength distance on the diagram. The incoming wave ray is depicted using a green line. Furthermore, the coastline and groyne are represented by the horizontal and vertical black lines respectively. A horizontal blue line is used to depict the location of the breakerline. The transition zone edge is highlighted with the light blue line. More details about the transition zone are provided later on in this thesis. The K_d coefficient at the shadow zone edge (green line), is equal to 0.5. This is a characteristic property of the monochromatic wave diffraction theory.

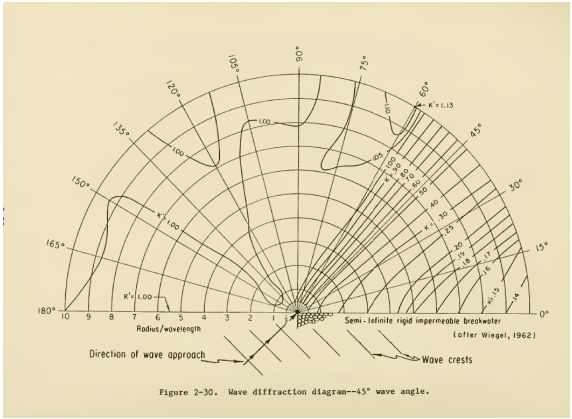

(a) Diffraction coefficient diagram (USACE, 1984a)

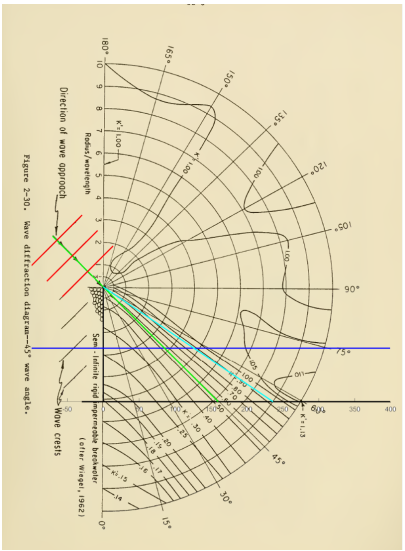

(b) Application of diffraction coefficient diagram

According to McCormick and Kraemer (2002), engineers are still using the diffraction diagrams published in USACE (1984b) to determine the wave heights in the lee of coastal structures. This is somewhat remarkable because nowadays newer and improved methods do exist to deal with the diffraction of surface waves in nearshore areas.

3.2. Irregular wave diffraction

Monochromatic waves diffracting around a semi-infinite impermeable breakwater and through the gap of a breakwater have been extensively analyzed in literature for incoming waves with different heights, frequencies and approach angles. Such a wave consists of a single frequency and wavelength. Sea waves are actually random waves, having a directional spreading. Those random waves consist of multiple wave components, each having an individual frequency. The diffraction coefficient depends amongst others on the incident wave frequency and direction (equation 3.2). Hence, each component of a directional wave spectrum will diffract according its own wave parameters. Goda et al. (1978) concluded that the pattern of wave diffraction for irregular sea waves is significantly different from the diffraction effects visualized in conventional diffraction diagrams made for monochromatic waves. Therefore, application of conventional diagrams to a real-world case could lead to disastrous errors.

Mobarek and Wiegel (1967) depicted with an experimental study that the knowledge of a directional wave spectrum is applicable to determine the energy wave spectra in the lee of a breakwater. First, a two-dimensional spectrum of wind waves for a specific wind speed and fetch was generated in the laboratory. The resulting wave heights at locations in the lee of a breakwater were measured and the corresponding one-dimensional spectra were calculated. Subsequently, the wave diffraction theory was used to establish the one-dimensional energy spectra at the same locations. A comparison was made between the two sets of determined energy spectra, showing high agreement.

A random sea wave is described by the superposition of an infinite number of individual wave components with a single frequency and direction. Goda et al. (1978) constructed a new set of diffraction diagrams for random waves, having a directional spectrum based on the directional wave spreading function described in (Mitsuyasu et al., 1975). First, the influence of frequency irregularity compared to directional spreading was examined. In doing so, the diffraction patterns behind a breakwater gap for monochromatic waves and waves with a frequency spectrum but at the same time a uniform direction were compared (figure 3.3a). The curves describing the diffraction coefficient for both cases are almost the same, indicating that frequency dispersion is not important. Subsequently, the diffraction coefficients for random waves with varying directions and waves with a single frequency but a direction spreading were compared (figure 3.3b). Again, the behaviour of both cases is quite similar. However, the curves in figure 3.3a and figure 3.3b visualize significant different diffraction patterns. Therefore, indicating the importance of directional spreading rather than the frequency related dependency regarding the behaviour of wave diffraction (Goda et al., 1978).

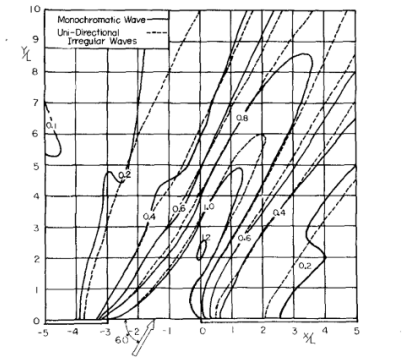

(a) Monochromatic waves and uni-directional irregular waves (Goda et al., 1978).

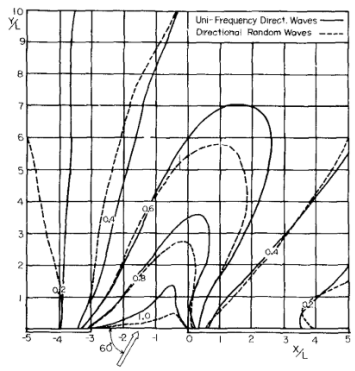

(b) uni-frequency directional waves and directional random waves (Goda et al., 1978).

Figure 3.3: Frequency spreading compared with directional spreading

The solution of the random wave diffraction problem provided by Goda et al. (1978) is stated in the equation below. Here $K_d(f,\theta)$ denotes the diffraction coefficient of an individual monochromatic wave with a certain frequency f and direction θ. m_0 is the zero order spectral moment and $S(f,\theta)$ represents the directional waves spectrum.

$$(K_d)_{eff} = \left[\frac{1}{m_0} \int_0^{\infty} \int_{\theta_{min}}^{\theta_{max}} S(f,\theta) K_d^2(f,\theta) d\theta df \right]^{\frac{1}{2}} \tag{3.3}$$

To come up with this solution, a modified form of the directional spreading function provided by Mitsuyasu et al. (1975) is used. Extensive attention is paid to the directional concentration parameter S. This parameter has a maximum value at the peak frequency of the spectrum and decreases from both sides. Originally, the deep water value of S_{max} was related to the wave speed U and peak frequency f_p (equation 3.4).

$$S_{max,0} = 11.5\left(2\pi f_p \frac{U}{g}^{\frac{-5}{2}}\right) \tag{3.4}$$

The deep water spreading parameter $S_{max,0}$ could also be determined by using the deep water wave steepness. Goda (1985) established a diagram that relates the deep water wave steepness H_0 / L_0 to the maximum spreading parameter in deep water.

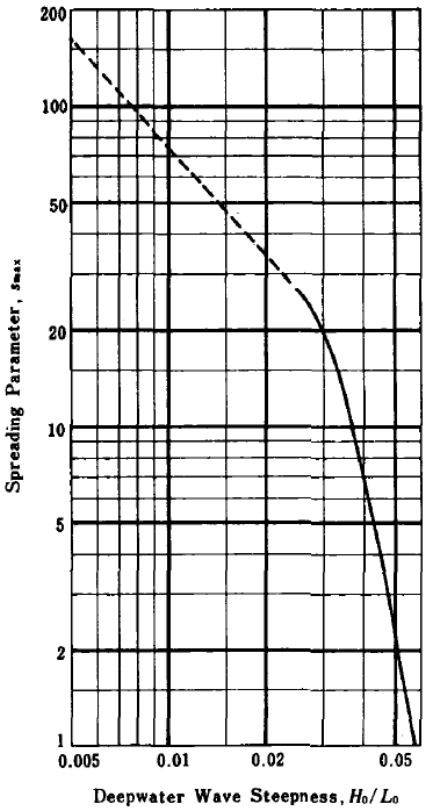

Figure 3.4: Relation between deep water wave steepness and the wave spreading (Goda, 1985).

However, in the field of engineering, the design of a coastal structure is generally related to the design wave height and period. Usually, those wave parameters are not determined while taking into account the wind speed. Goda et al. (1978) suggested the following values of S_{max} for engineering applications:

- $S_{max,0}$ = 10: For wind waves
- $S_{max,0}$ = 25: For swell waves with short to medium decay distance
- $S_{max,0}$ = 75: For swell with medium to long decay distance

When applying the solution of Goda et al. (1978) in the case of shallow water, correction to the value of S_{max} is necessary. Because of the refraction of waves in shallow water, the directional spreading decreases. Subsequently, the value of S_{max} should be larger compared to the same situation in the case of deep water. Goda et al. (1978) provided a diagram, displaying curves that are representing the values of S_{max} as a function of the ratio between the actual water depth and deep water wavelength. He assumed straight parallel depth contours while taking into account wave refraction.

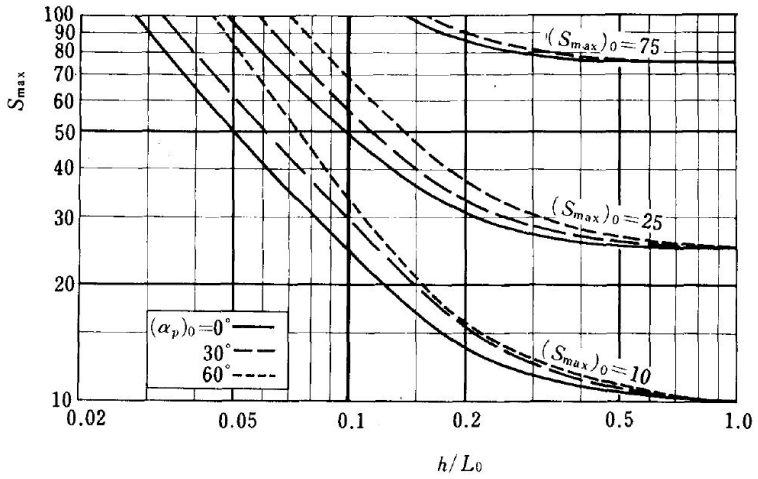

Figure 3.5: Change of maximum directional concentration parameter, due to wave refraction in shallow water (Goda, 1985).

The final products provided by Goda et al. (1978) are diffraction diagrams, applicable to a semi-infinite breakwater and breakwater gap situation in the case of the three different values of S_{max}. A characteristic property of those figures is that the diffraction coefficient at the edge of the shadow zone is equal to 0.7. According to the conventional diagrams, this value is 0.5. All diagrams depicted in Goda et al. (1978) assume normal incoming waves.

Goda (1985) provided an extensive elaboration of his work performed in 1978. Examples are given to deal with the diffraction of random waves in the field of engineering. The problem of obliquely incoming waves to a semi-infinite breakwater is solved by rotating the axis of the breakwater inside the diagram while keeping the coordinate system and wave direction the same. He concluded that the use of conventional diagrams in practical engineering applications could lead to disastrous errors in the design of a breakwater. However, in situations where the directional spreading is very limited, those diagrams could still have a purpose. This is the case for swell waves penetrating a well-protected harbour for example (Goda, 1985). Another method to determine the diffracted wave height is also described by (Goda, 1985). This method is called the Angular Spreading Method and is based on the directional distribution of the total wave energy. Pierson (1955) introduced a same kind of method to prescribe the attenuation of swell waves related to the angular spreading of waves. This attenuation is as a process that takes into account the travelling of waves in many different directions, away from the generation area. The total wave energy for a certain spectrum of waves $P_E(\theta)$ is calculated as follows:

$$P_E(\theta) = \frac{1}{m_0} \int_0^{\infty} \int_{\theta_{min}}^{\theta_{max}} S(f,\theta) df d\theta \tag{3.5}$$

The main assumption of this approach is that the individual wave diffraction coefficient of each wave component is equal to 0 inside the shadow zone and equal to 1 outside this zone. A graphical representation is provided in figure 3.6, showing the cumulative distribution of wave energy for varying directions relative to the principal wave motion in the case of a directional concentration parameter of 5, 10, 25 and 75.

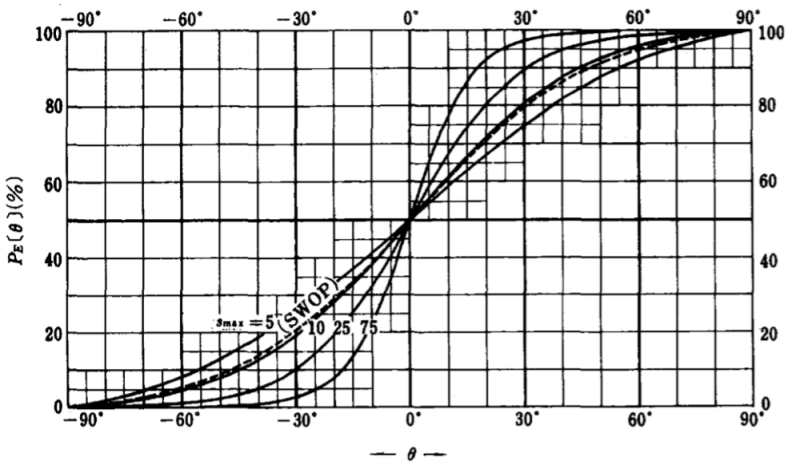

Figure 3.6: Cumulative distribution of wave energy (Goda, 1985).

The relative amount of energy arriving at the point of interest could be estimated using figure 3.6. Subsequently, the diffraction coefficient is approximated by taking the square root because the wave energy is related to the wave height squared. This angular spreading approach could only be used if the dimensions of the structure are very large, otherwise, the errors caused by simplifying the diffraction coefficient either to 0 or 1 are not negligible anymore. The dimensions should be in the order of several tens of wavelength (Goda, 1985).

3.3. Analytical solution coastline evolution

Pelnard-Considere (1956) provided the first analytical solution for the shoreline evolution around a coastal structure using the one-line theory. Nowadays, this solution is still the basis of many approaches that are used to determine the effects of coastal structures on the coastline. Especially, to come up with a quick and qualitative evaluation of the coastline response regarding a variety of different engineering conditions, this solution is still very useful (Larson et al., 1987). A detailed description of the analytical solution provided by Pelnard-Considere (1956) is given in this section. Larson et al. (1987) extended this solution to account for wave diffraction effects inside a groyne system. The solution of Larson et al. (1987) is addressed at the end of this section.

3.3.1. Analytical solution excluding diffraction

The equilibrium cross-shore coastline profile, described in section 2.2.2, is the key consideration of the solution provided by Pelnard-Considere (1956). Because of this assumption, he needed to provide a solution for one depth contour only; the coastline itself. Furthermore, Pelnard-Considere (1956) made the following assumptions to establish his solution:

- no currents
- constant wave direction
- small breaking wave angle
- linear relation between wave angle and the alongshore sediment transport

The x and y direction were chosen to align with the alongshore and cross-shore direction respectively. The local coastline orientation is equal to $\arctan\left(\frac{\delta y}{\delta x}\right)$ which can be approximated by $\frac{\delta y}{\delta x}$ because δy is often very small compared to δx. An incoming wave with a breaking angle ϕ_{br} relative to the North, has a local breaking angle $\phi_{loc,br}$ with respect to the coastline orientation.

$$\phi_{loc,br} = \phi_{br} - \frac{\delta_y}{\delta_x} \tag{3.6}$$

The alongshore sediment transport is expressed as a function of the incident wave angle using a Taylor series. The resulting linear approximation contains a variable Q_0, which can be interpreted as the amplitude of the transport rate formulation that is used (equation 3.7). Many different expressions do exist concerning this amplitude Q_0, most of them being established using the results of laboratory tests and being dependent on the breaking wave height (Larson et al., 1987).

$$Q = Q_0 + \frac{dQ}{d\phi_{loc,br}}\left(\phi_{loc,br} - \phi_{br}\right) \approx Q_0 - q\frac{\delta y}{\delta x} \tag{3.7}$$

Here q is equal to the derivative of the alongshore sediment transport to the incident breaking wave angle $\left(\frac{\delta Q}{\delta \phi_{loc,br}}\right)$. Pelnard-Considere (1956) found an expression describing the coastline evolution over time by substituting the expression for Q (equation 3.7), into the mass continuity equation 2.16.

$$\frac{\delta y}{\delta t} = \frac{1}{D}\frac{\delta Q}{\delta \phi_{loc,br}}\frac{\delta^2 y}{\delta x^2} \tag{3.8}$$

The above equation is a parabolic partial differential equation. It is the basis of any coastline model and should in general be solved numerically. The term $\left(\frac{\delta Q}{\delta \phi_{loc,br}}\right)$ could be retrieved from any alongshore sediment transport formulation by slightly varying the incoming breaking angle and subsequently calculating the corresponding transport rates. Pelnard-Considere (1956) provided analytical solutions to this equation while considering different coastal situations. In doing so, a simplification of equation 3.8 is needed. Pelnard-Considere (1956) used a general form of the alongshore sediment transport formulation which determines the transport as a function of $\sin(\phi_{loc,br})$ (equation 3.9). This formulation is established while assuming a small breaking angle and using the expression for the local breaking wave angle stated in equation 3.6.

$$Q = Q_0 \sin\left(2\phi_{loc,br}\right) = 2Q_0\phi_{loc,br} = 2Q_0\left(\phi_{br} - \frac{\delta y}{\delta x}\right) \tag{3.9}$$

After differentiating and substituting of this general formulation of alongshore sediment transport into equation 3.8, the governing equation reduces to a form of the well-known diffusion equation (equation 3.10). While doing this, a constant alongshore sediment transport amplitude Q_0 and breaking angle ϕ_{br}, constant in time and space, are assumed. A constant Q_0 implicitly assumes a constant alongshore breaking wave height as well.

$$\frac{\delta y}{\delta t} = \frac{2Q_0}{D}\frac{\delta^2 y}{\delta x^2} \tag{3.10}$$

The term $\frac{2Q_0}{D}$ is defined as a coastal constant s, which scales the curvature of the coastline (Bosboom and Stive, 2015). It has the dimension of $\frac{Length^2}{Time}$ and can be interpreted as the time scale of a shoreline change induced by a disturbance. Larson et al. (1987) concluded that a higher amplitude of the sediment transport will result in a fast shoreline response to achieve a new shape, being in equilibrium with the incoming waves. On the other hand, a larger depth of closure D means that a greater part of the cross-shore coastline profile requires sediment inflow or outflow to be in equilibrium with new conditions. Therefore, showing a slower shoreline response.

Larson et al. (1987) provided more than 25 solutions, corresponding to different scenarios, for the differential equation stated in 3.10. In general, one initial condition and two boundary conditions are needed to solve this equation. The position of the coastline at t=0 is usually chosen as the initial condition. The boundary conditions depend on the particular situation that is considered. In the case of a groyne, interrupting an initially straight coastline, Pelnard-Considere (1956) assumed that at a great distance away from the groyne the alongshore sediment transport remains constant. In other words, at that location is the alongshore sediment transport not influenced by the presence of the groyne. The second boundary condition imposed by Pelnard-Considere (1956) is an alongshore sediment transport equal to zero at the groyne. Thereby, assuming that the groyne is completely impermeable, meaning that there is no transmission of sediment. This condition is only valid as long as the water depth at the tip of the groyne is larger than the depth of closure. Substituting a zero sediment transport at the groyne location (x=0) into equation 3.9, leads to a requirement of the coastline orientation at the groyne (equation 3.11).

$$\left(\frac{\delta y}{\delta x}\right)_{x=0} = \phi_{br} \tag{3.11}$$

The coastline orientation must change to satisfy the condition of an incoming wave angle with respect to the coastline of zero. Hence, at the groyne the coastline will develop in such away that it becomes parallel to the incoming wave crests. Figure 3.7 visualizes the solution for the coastline evolution updrift of a groyne, established by Pelnard-Considere (1956). The boundary conditions are depicted in the same figure.

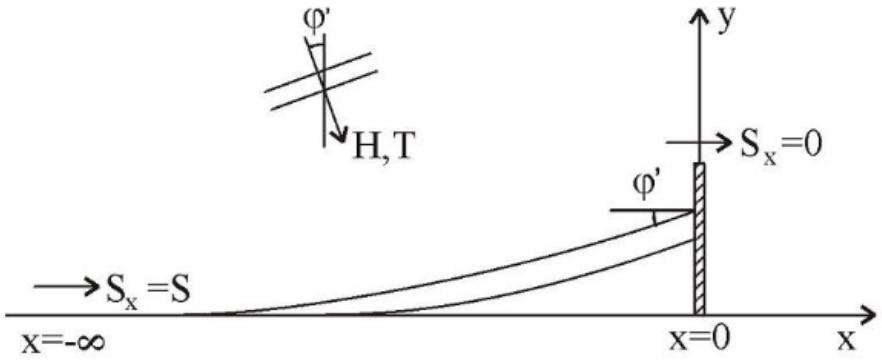

Figure 3.7: Coastline evolution according to Pelnard-Consideré (Bosboom and Stive, 2015)

Using the boundary conditions depicted in the above figure, Pelnard-Considere (1956) established the first analytical solution for the shoreline evolution in the vicinity of a groyne (equation 3.12).

$$y(x,t) = 2\tan(\phi_{loc,br})\sqrt{(st)}\,\text{ierfc}\Big(\frac{x}{2\sqrt{st}}\Big) \tag{3.12}$$

The term ierfc(u) stands for *the first integral of the complementary error function.* This is a well-kown function in the field of probability, statistics and partial differential equations. The following equations describe the relations between the *error function* (erf), the *complementary error function* (erfc) and the *the first integral of the complementary error function* ierfc(u).

$$\begin{aligned} \text{erf(x)} &= \frac{2}{\sqrt{\pi}}\int_x^0 \exp^{-t^2}\,dt \\ \text{erfc(x)} &= 1-\text{erf(x)} \\ \text{ierfc(x)} &= \frac{1}{\pi}\exp^{-x^2} - \text{erfc(x)} \end{aligned} \tag{3.13}$$

With the use of the above relations, equation 3.12 is rewritten. Resulting in a solution for the shoreline evolution updrift of the groyne (equation 3.14). The solution for the downstream area is exactly the same, only with an opposite sign.

$$y(x,t) = 2\tan\phi_{loc,br}\Big(\sqrt{\frac{st}{\pi}}\exp^{-x^2/4st} - \frac{x}{2}\text{erfc}\big(\frac{x}{2\sqrt{st}}\big)\Big) \tag{3.14}$$

This solution is valid until the shoreline has reached the tip of the groyne. At that moment, bypassing will occur. Therefore, not satisfying the condition of zero sediment transport at the groyne location anymore. Applying this solution to simulate the coastline evolution of an initial straight coastline results in a fully symmetrical result, meaning that the amount of sedimentation updrift is equal to the erosion downdrift of the groyne (figure 3.8).

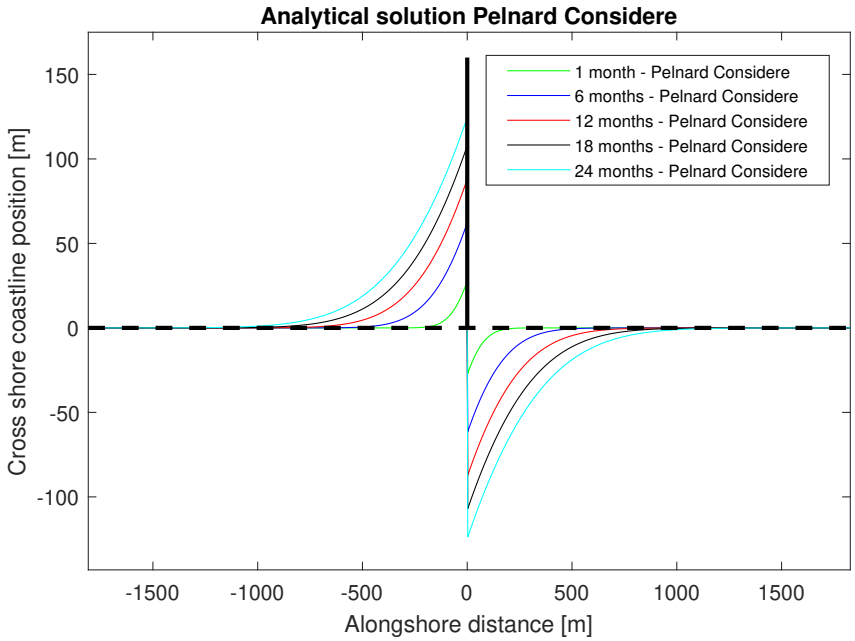

Figure 3.8: Analytical solution for the coastline evolution in the vicinity of a groyne

3.3.2. Analytical solution including wave diffraction

One of the major drawbacks of the solution provided by Pelnard-Considere (1956) is that the wave height and angle are assumed to be constant along the coast. Consequently, the solution will provide an adequate description of the shoreline evolution at some distance downdrift of the groyne. However, close to the groyne the solution does not agree with the shoreline shape that is commonly observed. The amount of erosion directly downdrift of the groyne is overestimated. As mentioned in section 2.1.4, the wave height and angle will vary in the vicinity of the structure because of diffraction. Therefore, accounting for the effect of diffraction will imply that assuming a constant wave height and angle is not applicable. In other words, $\frac{2Q_0}{D}$ being the coastal constant s in equation 3.10 is not a constant anymore but varies as a function of x instead. Bakker et al. (1970) extended the solution of Pelnard-Considere (1956) to account for the effect of diffraction at the lee side of the groyne. He included the effect of a varying wave angle and wave height along the coast. Larson et al. (1987) provided different ways to account for a changing alongshore sediment transport amplitude (caused by a varying wave height) and a varying breaking angle. However, the resulting coupled system of equations involves intensive calculations that can only be solved using extremely complex algebraic manipulations. A suggestion is made to choose between a varying amplitude of the alongshore transport or a varying breaking wave angle. This section contains the simplified analytical solution of Larson et al. (1987) and the more complete solution provided by Bakker et al. (1970).

Analytical solution (Larson et al., 1987)

Larson et al. (1987) stated that the analytical solution of the shoreline evolution in the lee side of a groyne can be simplified by assuming that only the wave angle or wave height is varying. The same general formulation describing the alongshore sediment transport as used in Pelnard-Considere (1956) is applied by Larson et al. (1987). After differentiating, this equation is substituted into the sediment continuity equation (equation 2.16). In contradiction to the solution of Pelnard-Considere (1956), the alongshore sediment transport and breaking angle are not assumed to be constant in space this time. Therefore, depending on alongshore location x (equation 3.15). However, the depth of closure (D) is defined to be a constant factor.

$$\frac{\delta y}{\delta t} + \frac{2}{D}\frac{\delta Q_0}{\delta x}\phi_{br} + \frac{2Q_0}{D}\frac{\delta \phi_{br}}{\delta x} = \frac{2}{D}\frac{\delta Q_0}{\delta x}\frac{\delta y}{\delta x} + \frac{2Q_0}{D}\frac{\delta^2 y}{\delta x^2} \tag{3.15}$$

Here, the complete description ($\frac{2Q_0}{D}$) of the coastal constant s is used, to stress the influence of all variables.

An analytical solution of equation 3.15 can be found by defining different solution areas inside the shadow zone. The diffracted breaking wave angle and amplitude of the alongshore sediment transport are constant within a certain solution area but could change from one area to another. Applying this method will result in a coupled system of equations which is not easy to solve analytically. In the case of only two defined solution areas, the amount of mathematical effort to retrieve an analytical solution is already quite complex. Larson et al. (1987) suggested to treat the varying breaking wave angle and amplitude of the alongshore sediment transport separately. In doing so, equation 3.15 is rewritten into two different forms. The first one belongs to a constant breaking wave angle. For retrieving the second formulation, a constant alongshore sediment transport amplitude is assumed.

$$\frac{\delta y}{\delta t} + \frac{2}{D}\frac{dQ_0}{dx}\phi_{br} = \frac{2}{D}\frac{dQ_0}{dx}\frac{\delta y}{\delta x} + \frac{2Q_0}{D}\frac{\delta^2 y}{\delta x^2} \tag{3.16a}$$

$$\frac{\delta y}{\delta t} + \frac{2Q_0}{D}\frac{d\phi_{br}}{dx} = \frac{2Q_0}{D}\frac{\delta^2 y}{\delta x^2} \tag{3.16b}$$

Larson et al. (1987) stated that an analytical solution for equation 3.16a is quite complex and not easy to find. Even if a simple relation is used to express the alongshore sediment transport as a function of x. The analytical solution of equation 3.16b is easier to establish. A linear variation of the breaking angle inside the shadow zone is used to obtain this analytical solution (equation 3.17).

$$\phi_{br} = \phi_{br,S} + \left(\phi_{br,H} - \phi_{br,S}\right)\frac{x}{B} \tag{3.17}$$

Here $\phi_{br,S}$ is the breaking angle at the structure and $\phi_{br,H}$ is the breaking angle outside the shadow zone, $\phi_{br,H}$ is therefore not being altered because of diffraction. According to Larson et al. (1987), the width of the shadow zone is equal to $B = L\tan(\phi_{tip})$. A definition sketch of the parameters is depicted in the figure below.

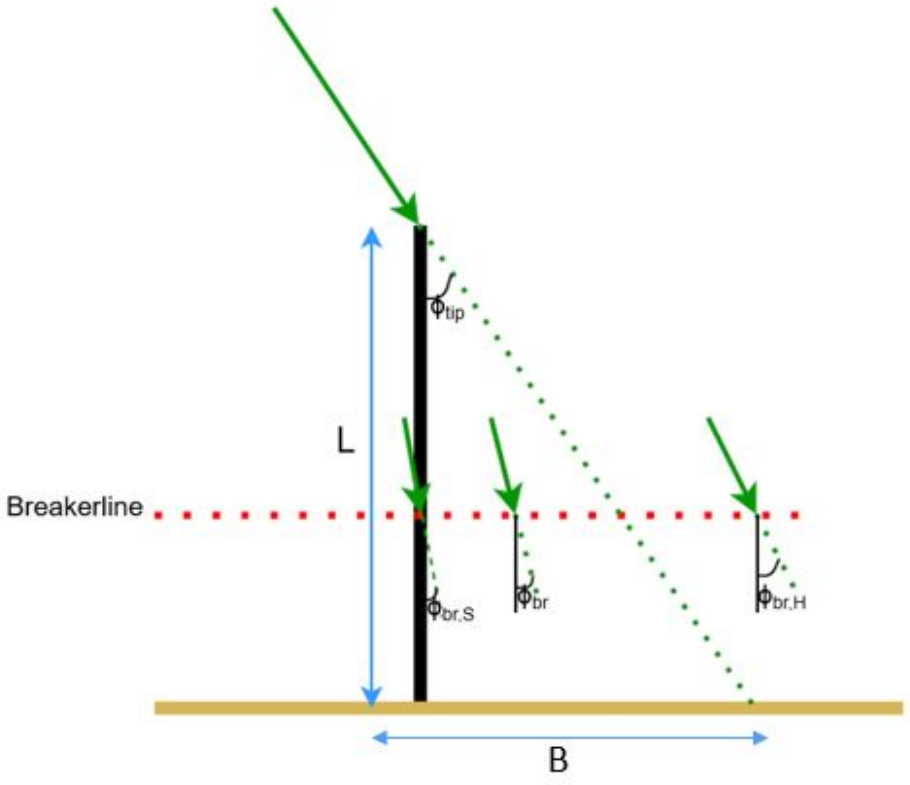

Figure 3.9: Definition of angles used in analytical solution of (Larson et al., 1987)

Larson et al. (1987) provided the analytical solution while assuming such a linear diffracted breaking wave angle. This solution consists of two parts, one being valid inside the shadow zone $\big(y_1(x_1,t)\big)$ and the other one outside the shadow zone $\big(y_2(x_2,t)\big)$.

$$\begin{aligned} y_1(x_1,t) &= \frac{(\phi_{br,H}-\phi_{br,V})st}{B}\left[2i^2\text{erfc}\Big(\frac{B-x}{2\sqrt{st}}\Big)+2i^2\text{erfc}\Big(\frac{B+x}{2\sqrt{st}}\Big)-1\right]-tan(\phi_{br,V})\left[2\sqrt{\frac{st}{\pi}}\exp^{\frac{-x^2}{4st}}-x\,\text{erfc}\Big(\frac{x}{2\sqrt{st}}\Big)\right] \\ y_2(x_2,t) &= \frac{(\phi_{br,H}-\phi_{br,V})st}{B}\left[2i^2\text{erfc}\Big(\frac{B+x}{2\sqrt{st}}\Big)-2i^2\text{erfc}\Big(\frac{B-x}{2\sqrt{st}}\Big)\right]-tan(\phi_{br,V})\left[2\sqrt{\frac{st}{\pi}}\exp^{\frac{-x^2}{4st}}-x\,\text{erfc}\Big(\frac{x}{2\sqrt{st}}\Big)\right] \end{aligned} \tag{3.18}$$

In which i^2erfc(x) is the *second integral of complementary error function.*

$$i^2\text{erfc(x)} = \frac{1}{4}\text{erfc(x)} - \frac{x}{2\sqrt{\pi}}\exp^{-x^2} + \frac{x^2}{2}\text{erfc(x)} \tag{3.19}$$

Figure 3.10 provides the analytical solution including the effect of wave diffraction in the case of a linear varying breaking wave angle inside the shadow zone. The analytical solution for the situation with the same input parameters but without the effect of diffraction is depicted in the same figure.

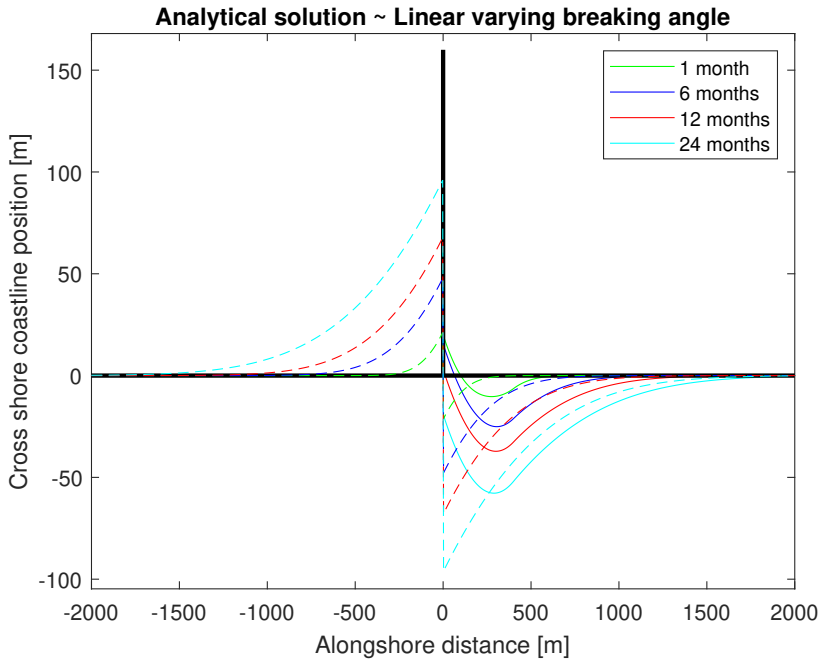

Figure 3.10: Analytical solution including diffraction (continuous lines) and excluding diffraction (interrupted lines)

In the previous analytical solution, the diffracted breaking wave angle is described using a linear function of x. An exponential formulation to describe the variation of the breaking angle inside the shadow zone could also be applied (Larson et al., 1987). Doing this, will also result in an easy analytical solution.

$$\phi_{br} = \phi_{br,H}\Big(1-e^{-\gamma x}\Big) \tag{3.20}$$

Here γ is a factor that denotes the rate at which the diffracted breaking wave angle approaches the un-diffracted breaking angle $\phi_{br,H}$. In this case, the analytical solution is not split into two parts (equation 3.21). The solution is valid for any value of x being located downdrift of the groyne, so for $x \geq 0$ in this situation.

$$\begin{aligned} y(x,t) = \frac{\phi_{br,H}\gamma}{2}\Bigg[&-\frac{4}{\gamma}\sqrt{\frac{st}{\pi}}e^{\frac{-x^2}{4st}}+2\frac{x}{\gamma}\text{erfc}\Big(\frac{x}{2\sqrt{st}}\Big)+\frac{1}{\gamma^2}e^{-\gamma x+st\gamma^2}\text{erfc}\Big(\frac{x}{2\sqrt{st}}-\gamma\sqrt{st}\Big) \\ &-\frac{1}{\gamma^2}e^{-\gamma x+st\gamma^2}\text{erfc}\Big(\frac{x}{2\sqrt{st}}+\gamma\sqrt{st}\Big)\Bigg]+\frac{\phi_{br,H}}{\gamma}e^{-\gamma x}\Big(1-e^{-\gamma^2 st}\Big) \end{aligned} \tag{3.21}$$

Figure 3.11 provides the analytical solution in the case of an exponentially varying breaking wave angle. Again, the solution without diffraction is also visualized in the same figure.

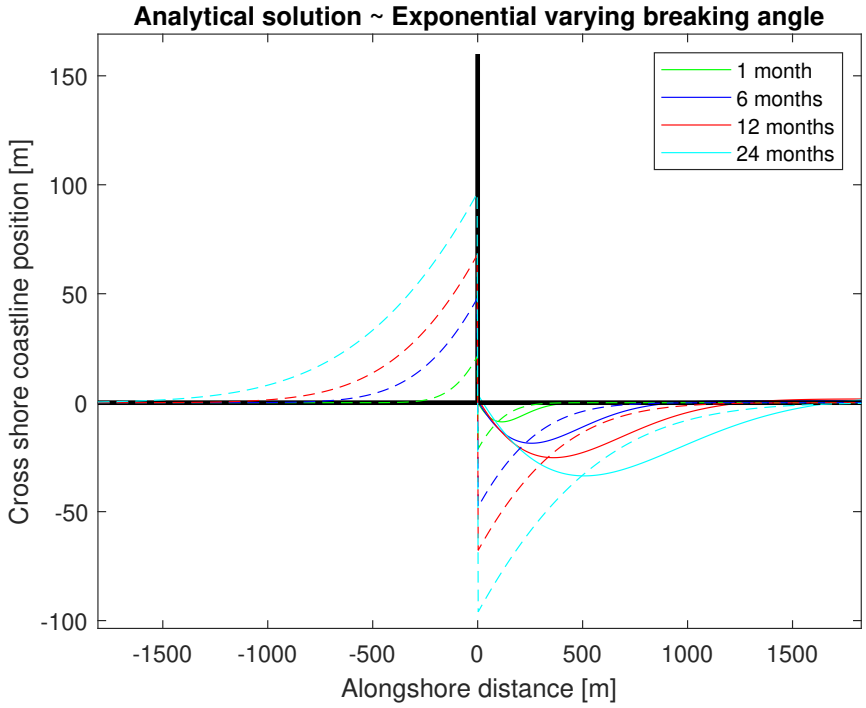

Figure 3.11: Analytical solution including diffraction (continuous lines) and excluding diffraction (interrupted lines)

Larson et al. (1987) concluded that both solutions overestimate the amount of diffraction downdrift of the groyne. This is because the alongshore sediment transport amplitude is assumed to be constant, while actually this parameter is reduced directly downdrift of the groyne. However, the solutions provide a much better shoreline evolution compared to the solution of Pelnard-Considere (1956). The input parameters $\phi_{br,S}$, $\phi_{br,H}$ and width B are concluded to have a significant amount of influence on the resulting coastline shape. Especially, the breaking wave angle at the structure in the linear varying breaking angle case ($\phi_{br,S}$) determines the amount of reduced erosion, or even sedimentation, directly downdrift of the structure a lot.

Analytical solution (Bakker et al., 1970)

Bakker et al. (1970) suggested to account for wave diffraction by splitting the effect of diffraction on the coastline evolution into two parts (figure 3.12). One part being the stationary effect, meaning that the wave height and angle are constant along the coastline. Therefore, the alongshore sediment transport will be constant as well, leading to a stable coastline. If the wave height and/or angle changes along the coastline, the alongshore transport will vary resulting in a coastline that adapts itself to retrieve a stable coastline again. This is called the instationary effect (Bakker et al., 1970). The coastline evolution as a function of x and t is now formulated using a stationary part $y_0(x)$ and instationary part $y'(x,t)$.

$$y(x,t) = y_0(x) + y'(x,t)' \tag{3.22}$$

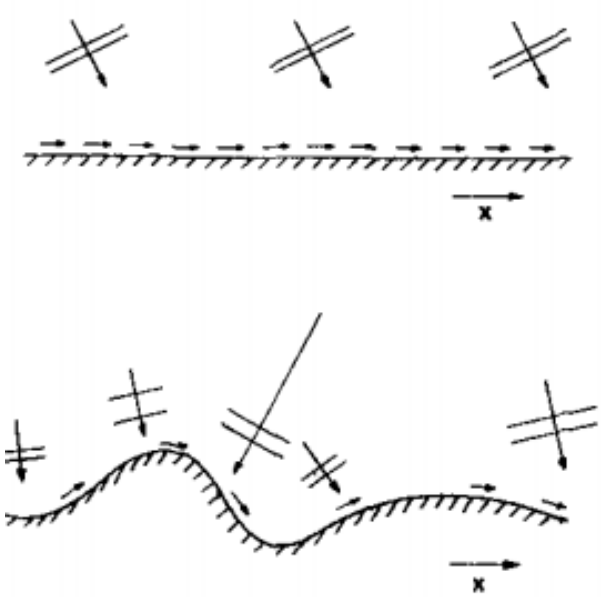

Figure 3.12: Stationary (top) and instationary (bottom) effect of diffraction (Bakker et al., 1970)

Bakker et al. (1970) used an expression for the alongshore sediment transport that includes they symbol *. This is done to denote that the particular parameter is a function of x.

$$Q = Q_0^* - q^* \frac{\delta y}{\delta x} \tag{3.23}$$

Using the sediment continuity equation, the above stated expression for alongshore sediment transport and applying the chain rule for differentiation resulted in an expression for the coastline evolution over time (equation 3.24).

$$\frac{\delta y}{\delta t} = \frac{1}{D}\left(q^* \frac{\delta^2 y}{\delta x^2} + \frac{\delta q^*}{\delta x}\frac{\delta y}{\delta x}\right) - \frac{1}{D}\frac{\delta Q_0^*}{\delta x} \tag{3.24}$$

To come up with an analytical solution, a more sophisticated expression for the sediment transport is needed. Bakker et al. (1970) used a formulation in which the transport is set proportional to the square of the wave height and to the angle of breaking wave incidence (equation 3.25). In this case, the incident wave angle ϕ_x is relative to the x-axis, instead of being relative to the local coastline orientation.

$$Q = Ah^{*2}\left(\phi_x^* - \frac{\delta y}{\delta x}\right) = q^*\left(\phi_x^* - \frac{\delta y}{\delta x}\right) \tag{3.25}$$

This expression is in fact a special case of formulation 3.23. In which A is a proportionality constant and h is the wave height at location x relative to the wave height at x=∞.

A solution for $y_0(x)$, the stable coastline, is first determined. Bakker et al. (1970) stated that based on continuity, Q should be constant for $y_0(x)$. Subsequently, a solution can be found using equation 3.25 while a point x at infinity is considered for which the following conditions hold: $h = 1$, $\phi_x = \phi_\infty$ and $\frac{\delta y}{\delta x} = 0$. Substituting these conditions into equation 3.25 gives the following result.

$$\begin{aligned} Q_x &= Q_\infty \\ Ah_x^2\left(\phi_x - [\frac{dy_0}{dx}]_x\right) &= Ah_\infty^2\left(\phi_\infty - [\frac{dy_0}{dx}]_\infty\right) \\ Ah_x^2\left(\phi_x - [\frac{dy_0}{dx}]_x\right) &= A\phi_\infty \end{aligned} \tag{3.26}$$

Dividing both sides of the above equation by A and rewriting, provides the following solution for $y_0(x)$.

$$\frac{dy_0}{dx} = \phi_x - \frac{\phi_\infty}{h^2} \tag{3.27}$$

If the wave height would not vary along the coast, the coastline orientation only depends on the term $\phi_x - \phi_\infty$, which represents the changing wave direction along the coast (equation 3.27). Here ϕ_∞ is a constant, being equal to the wave angle at a location far away from the groyne. Because the groyne blocks all the sediment transport, a gradient in the alongshore sediment transport will always be present. Hence, a stable coastline will never be reached. y_0 could be interpreted as the stable coastline that would develop if an imaginary nourishment Q_0 would be implemented at the lee side of the groyne.

Bakker et al. (1970) stated that an equation for the instationary part can be retrieved by substituting the solution for y_0 into equation 3.24 and subsequently subtracting this equation from equation 3.24.

$$\frac{\delta y'}{\delta t} = \frac{q^*}{D}\frac{\delta^2 y'}{\delta x^2} + \frac{1}{D}\frac{dq^*}{dx}\frac{\delta y'}{\delta x} = \frac{Ah^2}{D}\frac{\delta^2 y'}{\delta x^2} + \frac{1}{D}\frac{d\left(Ah^2\right)}{dx}\frac{\delta y'}{\delta x} \tag{3.28}$$

The same kind of solution was found by Pelnard-Considere (1956), however an additional term is present because q^* is a function of x now. So far, analytical solutions are provided for the stationary part (3.27) and the instationary part (3.28). Superposition of those according to equation 3.22, provides the shoreline evolution as a function of x and t. Hence, h and ϕ_x which are functions of x inside the diffraction area need to be determined. Bakker et al. (1970) used the simplified diffraction theory of Putnam and Arthur (1948) to obtain those parameters (equation 3.29).

$$\phi_x = \phi_\infty - \frac{\lambda}{2\pi}\frac{d\theta}{dx} \tag{3.29}$$

Here the wavelength of the diffracted wave is expressed as λ. The phase difference of the waves between point B (on the shoreline) for which y_0 is computed and imaginary point B' is represented by θ (figure 3.13).

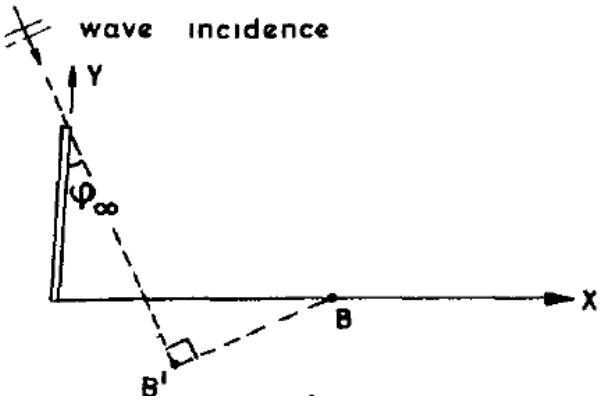

Figure 3.13: Definition of points B and B'. (Bakker et al., 1970)

After substituting equation 3.29 into equation 3.27 and applying integration, equation 3.30 is retrieved. It depicts the relation between y_0 and the diffracted parameters θ and h as a function of x. The first term on the right-hand side could be interpreted as the bending of waves around the tip and the second term as the affected wave height because of diffraction (Bakker et al., 1970).

$$y_0 = -\frac{\lambda}{2\pi}\theta + \phi_\infty \int \frac{h^2 - 1}{h}\,dx \tag{3.30}$$

The simplified diffraction theory presented by Putnam and Arthur (1948) defines a function *f(u)* which is used to solve the general diffraction problem in a simplified way. The modulus and argument of *f(u)* can be seen as the wave height ratio h and phase difference θ respectively (figure 3.14).

$$f(u) = \frac{1}{\sqrt{2}} \exp^{\frac{i\pi}{4}} \int_{-\infty}^{u} \exp^{\frac{-i\pi v^2}{2}}\,dv \tag{3.31}$$

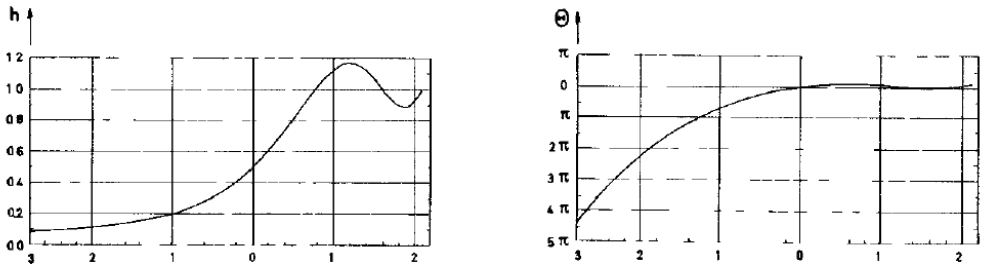

Figure 3.14: Wave height ratio h and phase difference θ as a function of u (Bakker et al., 1970)

The solution for the instationary part (equation 3.28), is retrieved by using numerical integration (Bakker et al., 1970). An explicit method is used to solve the differential equation, in doing so first q_{max} and Δt are defined as follows:

$$\begin{aligned} q_{max} &= A h_{max}^2 \\ \Delta t &= D \frac{(\Delta x)^2}{2 q_{max}} \end{aligned} \tag{3.32}$$

Here A is again a proportionality constant. After substituting both expressions into equation 3.28, a point on the curve at time = t+Δt could be retrieved from three adjacent points on a curve at time = t. In doing so, the boundary condition at the groyne should be taken into account. As explained at the beginning of this section, there will be zero sediment transport at the groyne for every moment in time. As a result, the incoming wave angle at the groyne (x=0) should be equal to the coastline orientation at the groyne (equation 3.33).

$$\frac{\delta y}{\delta x} = \frac{dy}{dx} + \frac{\delta y'}{\delta x} = [\phi_x]_{x=0} \tag{3.33}$$

Subsequently, the analytical solution of y_0 and the numerical solution of y' are added and the coastline evolution is determined (figure 3.15).

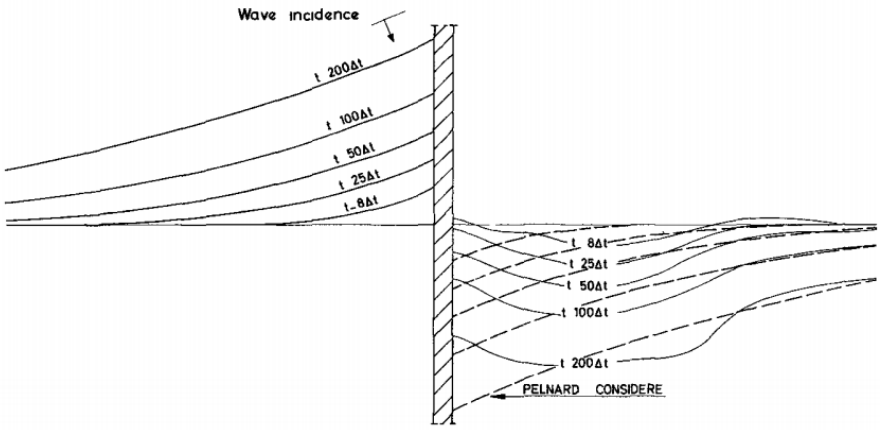

Figure 3.15: Solution of Bakker et al. (1970) compared to solution of Pelnard-Considere (1956)

3.4. Simplified methods to account for wave diffraction

Wave diffraction caused by a coastal structure alters the wave height and angle in the vicinity of the structure. The previous section contains analytical solutions from which the coastline evolution influenced by diffraction effects could be determined. These solutions make use of assumptions that simplify the trend of the diffracted wave height and angle. The breaking wave height could also be retrieved using the diagrams provided by USACE (1984a), as is discussed in section 3.2. However, accounting for irregular wave diffraction inside numerical modelling while using these diffraction diagrams is not computational effective. Nowadays, different methods are available to account for wave diffraction inside numerical models. Most of them are based on approximate equations which are retrieved by regression analysis of the irregular diffraction diagrams established by Goda (1985). This section describes methods that could be used inside coastline models to account for wave diffraction effects on the wave height and angle.

In general, the diffracted breaking wave height $H_{diff,br}$ is calculated using the wave height at the tip of the structure H_{tip} and the diffraction coefficient K_d (equation 3.34). Almost every method for calculating the K_d inside a numerical model use the same kind of parameter definitions. Figure 3.16 visualizes the schematic version of wave diffraction near a groyne. The red dotted line is the edge of the shadow zone and the blue dotted line represents the transition zone edge. Downdrift of the transition zone, diffraction effects do not influence the wave height and angle anymore. The horizontal black dotted line indicates the breaking depth contour. The wave energy reaching a particular point is in every method related to the angle θ, which is defined as the angle between the shadow line and the line between the structure tip and any random point, points B and C for example (figure 3.16). The sign and unit of the angle θ differ for each method.

$$H_{diff,br} = H_{tip} * K_d \tag{3.34}$$

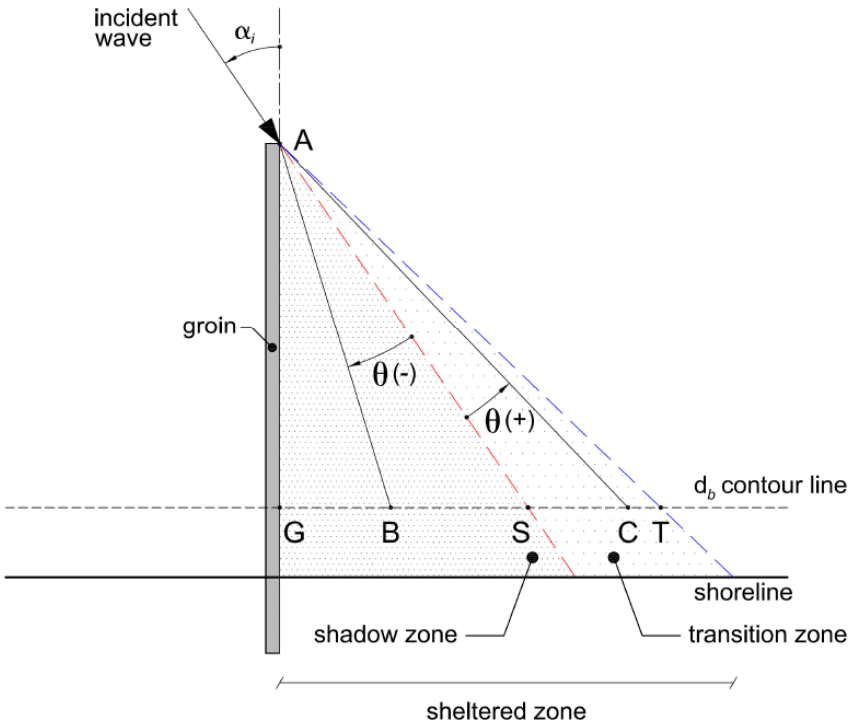

Figure 3.16: Definition sketch of wave diffraction near a groyne (Baykal, 2006).

3.4.1. Kamphuis

Kamphuis (1992) derived simple equations to calculate the diffraction coefficient in the shadowed area caused by a coastal structure (equation 3.35). Those equations are established by regression analysis on the work of Goda (1985). The angle θ is in degrees and has a negative value inside the shadow zone. In the transition, θ is positive.

$$\begin{aligned} K_d &= 0.69 + 0.008\theta \quad \text{for} \quad 0 \geq \theta > -90 \\ K_d &= 0.71 + 0.37\sin\theta \quad \text{for} \quad 40 \geq \theta > 0 \\ K_d &= 0.83 + 0.17\sin\theta \quad \text{for} \quad 90 \geq \theta > 40 \end{aligned} \tag{3.35}$$

The diffraction coefficient goes to a value of 1 if the angle θ approaches 90 °. In other words, the edge of the transition makes an angle of 90 degrees with the shadow line. In the case of a straight coastline, there is not a location landward of the groyne tip that makes such an angle with the shadow line. Meaning that theoretically, the edge of the transition zone lies infinitely down drift of the groyne. However, in reality, the effect of diffraction onto the wave heights and angles is restricted to a certain area. In section 4.3 more attention is paid to this 'problem'. At the shadow line itself, θ is equal to zero. Subsequently, K_d has a value of 0.7 (equation 3.35). This is in line with the theory described by Goda (1985). Kamphuis (1992) concluded that greater sophistication could be used in the diffraction calculations. However, this would lead to larger computation times and because of all the assumptions that are made to derive the one-line model, higher detail wave diffraction effect calculations would be pointless.

Furthermore, Kamphuis (1992) provided a method to determine the breaking angle by accounting for the following two different processes that will change the breaking wave angle in the vicinity of a groyne. Firstly, the diffraction around the groyne tip itself causes a change in the breaking angle. Secondly, additional refraction because of the reduced wave heights will affect the breaking angle. To examine the effect of diffraction onto the breaking angle, different tests were performed with varying parameters like groyne length, wave period, wave height, wave angle and breaking parameter. Kamphuis (1992) concluded that the breaking wave angle in the vicinity of the groyne was not affected by changes in the above mentioned parameters. Subsequently, a formulation was conducted that relate the undiffracted breaking angle $\phi_{br,undiff}$ to the diffracted breaking angle $\phi_{br,diff}$.

$$\phi_{br,diff} = \phi_{br,undiff} K_d^{0.375} \tag{3.36}$$

This formulation could be used to determine the diffracted breaking wave angles for points inside the shadow zone and transition zone. The diffracted breaking angle is related to the diffraction coefficient K_d at the same location. In this way, the effect of the reduced wave height and the subsequently additional refraction on the breaking angle is taken into account. Kamphuis (1992) established another relation to account for the decrease in breaking wave angle caused by diffraction itself. It was concluded that this effect was felt predominantly inside the shadow zone. Therefore, equation 3.36 is only valid for points inside the shadow zone.

$$\phi_{br,diff} = \phi_{br,undiff} K_d^{0.375} \frac{2(x_P - x_S)}{L_g(\tan(\phi_{tip}) + \tan(0.88\phi_{br,undiff})} \tag{3.37}$$

In the above equation x_S represents the location of the structure. x_P is the location of an arbitrary point P at the breaker line for which the breaking angle is calculated. The value 0.88 originates from the K_d value at the shadow zone edge (≈0.7) to the power 0.375.

3.4.2. Kraus

Kraus (1984) described a procedure for calculating the diffraction coefficient based on the cumulative relative wave energy reaching a point in the lee of a structure and the local directional concentration parameter S_{max} at the tip of the structure. Figure 3.6 visualizes the cumulative wave energy curves in the case of four different S_{max} values. Subsequently, the diffraction coefficient can be calculated as follows:

$$K_d(\theta) = \sqrt{\frac{P_E(\theta)}{100}} \tag{3.38}$$

Kraus (1984) established multiple best-fit interpolative equations describing the curves depicted in figure 3.6. To minimize the computational effort, those equations were simplified. Hence, being applicable inside numerical models. The curves in figure 3.6 concluded to be approximated good enough by these simplified equations (3.39,3.40 and 3.41). Kraus (1984) stated that the maximum error is 2% in the interval $10 \leq S_{max} \leq 75$. Again, θ is negative inside the shadow zone and positive in the transition zone. However, this time θ is in radians instead of degrees.

$$W = 5.31 + 0.270 S_{max} - 0.000103 S_{max}^2 \tag{3.39}$$

$$A = \frac{S_{max}}{W}\theta \tag{3.40}$$

$$P_E(\theta) = 50(\tanh(A) + 1) \tag{3.41}$$

Also in the method of Kraus, the value of K_d will only reach 1 if θ approaches 90°. For the case with a straight coastline, the complete shoreline downdrift of the groyne would therefore be affected by wave diffraction. Section 4.3 elaborates further on this. After applying the above procedure to different cases, Kraus (1984) concluded that the method could be implemented in a numerical model for simulating long-term coastline evolution while accounting for wave diffraction effects. Originally, the method was derived for an offshore parallel breakwater. However, Kraus (1984) stated that his approach is also applicable to a groyne.

3.4.3. Leont'yev

Leont'Yev (1999) derived a set of equations (3.42) to determine the diffraction coefficient based on the theory of Goda et al. (1978). It was concluded that a small variation of the directional concentration parameter in the interval 25-75 has a very small influence on the diffraction coefficient itself. Therefore, a uniform value of $S_{max} = 50$ was chosen to simplify the diffraction calculations.

$$\begin{aligned} K_d &= 1 \qquad \text{for} \quad \theta \leq -\pi/6 \\ K_d &= 0.1(\theta + \pi/6) + cos^3(\theta + \pi/6) \qquad \text{for} \quad -\pi/6 \leq \theta \leq \pi/2 \\ K_d &= 0.087(3 - 4\theta/\pi) \qquad \text{for} \quad \pi/2 \leq \theta \leq 3\pi/4 \\ K_d &= 0 \qquad \text{for} \quad 3\pi/4 \leq \theta \end{aligned} \tag{3.42}$$

In the above set of equations, θ is in radials and is positive inside the shadow zone. The edge of the transition zone makes an angle of $-\pi/6$ with the shadow line. At the shadow line, the diffraction coefficient is equal to 0.7. In doing so, corresponding to the observations of Goda et al. (1978).

3.4.4. Roelvink

A recently established method by D.J.A. Roelvink to account for wave diffraction inside a one-line model has been discussed in Elghandour et al. (2020). This method is tested for the offshore detached breaker water case, thereby showing promising results. Figure 3.17 visualizes the wave breaking angels affected by diffraction behind a detached breakwater, determined using the method of Roelvink. This method is also applicable to a groyne.

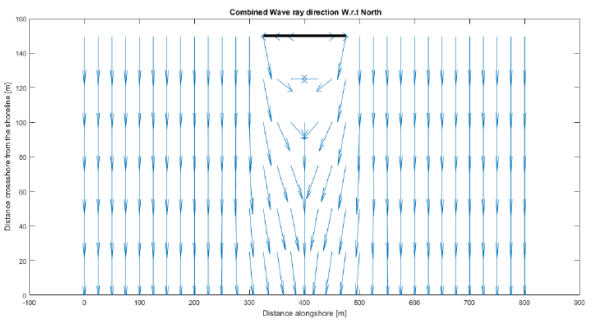

Figure 3.17: Breaking wave angles behind breakwater (Elghandour, 2018).

Instead of relating the diffracted wave angles to the K_d coefficient, the diffracted angles are calculated using a constant parameter δ (figure 3.18). For each point at the breakerline, situated inside the shadow or transition zone, the wave angle affected by diffraction $\alpha_{s,cor}$ is related to this δ (equation 3.43). The angle between the shadow line (black-dotted line) and transition line (blue line) is defined as δ. This angle could be seen as a correction factor to account for wave diffraction onto the breaking angle.

$$\alpha_{s,cor} = \alpha_s + \delta \tag{3.43}$$

α_s could be interpreted as the undiffracted wave angle relative to the x-axis. It is defined as the angle between the line connecting a certain point at the breakerline with the groyne tip and a line perpendicular to the groyne going through the same point (figure 3.18). The edge of the transition zone at the shoreline is determined by extending the shadow zone with a distance equal to 2.5 times the wavelength at the tip. In doing so, Dabees (2000) is followed in which the width of the transition zone was found to be 2 to 3 times the incoming wavelength in the case of a detached breakwater.

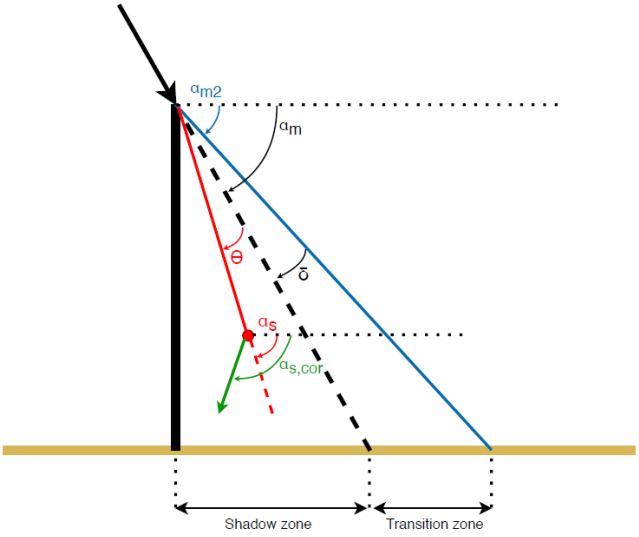

Figure 3.18: Definition sketch of Roelvinks method

3.4.5. Hurst

Hurst et al. (2015) explored the sensitivity of crenulate bay shorelines to different kinds of wave climates. A vector-based one-line model was used to simulate the shoreline evolution of sandy coastlines. Since a crenulate bay could cause shadow areas for particular wave directions, potential wave diffraction effects should be taken into account. Hurst et al. (2015) applied simple rules, based on Rea and Komar (1975), Kraus (1984) and Weesakul et al. (2010), to calculate the diffraction coefficient.

$$\begin{aligned} K_d &= 0.5 * \cos(\omega) \qquad \text{inside shadow zone} \\ K_d &= 0.5 * \left(1 + \sin(90\frac{x}{L_s})\right) \qquad \text{outside shadow zone} \end{aligned} \tag{3.44}$$

The angle between an arbitrary point at the breakerline and the shadow zone is defined as ω. L_s is the shoreline length inside the shadow zone and x is the alongshore position on the shoreline measured with respect to the edge of the shadow zone. In other words, at the shadow zone edge x is equal to zero. The edge of the transition zone is equal to $2 * L_s$. The diffraction coefficient at the shadow line is equal to 0.5, which is in line with the diffraction theory for monochromatic waves.

Besides these simple rules to calculate the diffraction coefficient, also a method to determine the diffracted wave angles is suggested by Hurst et al. (2015). A relation between the wave angle at the tip θ_0 and diffracted wave angle θ_s was established based on Kraus (1984) and Weesakul et al. (2010).

$$\theta_s = 1.5\Big(|\omega - \theta_0|\Big) \tag{3.45}$$

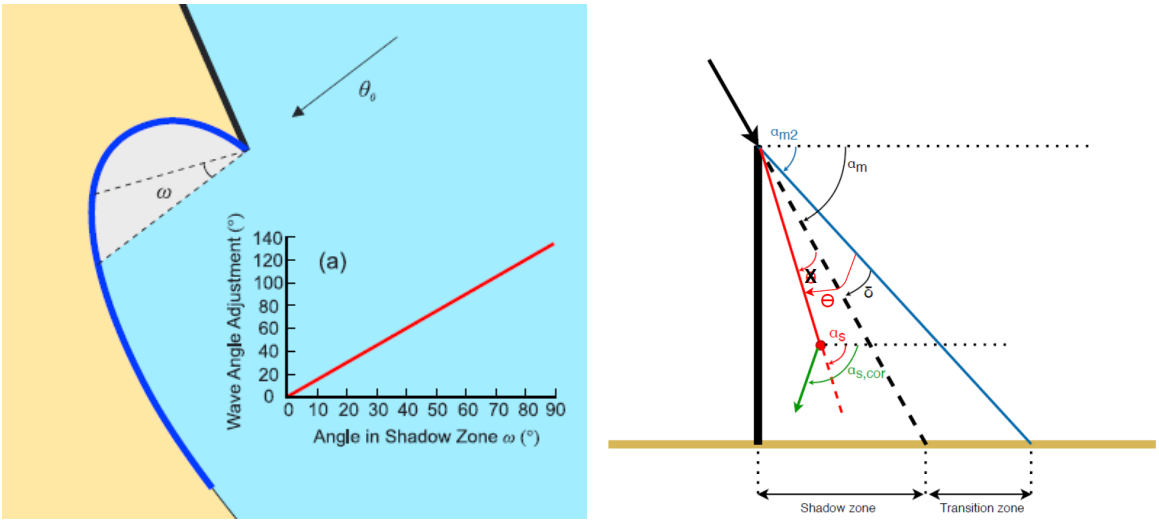

(a) Diffracted wave angle adjustment (Hurst et al., 2015)

(b) Different θ definition

Figure 3.19: Modified Hurst approach

Elghandour (2018) suggested to modify this method as follows. The breaking angle is equal to 1.5 times the angle between the point of interest and the transition zone edge instead of the shadow line. In equation form, this is written as follows:

$$\alpha_{s,cor} = 1.5 * \theta + \alpha_m \tag{3.46}$$

θ is defined in a different way compared to the approach of Roelvink, stressed with the black-cross in figure 3.19b. In the remainder of the thesis, the method of Hurst adapted by Elghandour (2018) is meant when the (modified) method of Hurst is stated.

4

Model development

To retrieve a representative coastline evolution in the vicinity of a groyne, a function is developed to be applied inside ShorelineS. The main purpose of this function is to account for wave diffraction effects onto the shoreline evolution. In doing so, a varying breaking wave height and angle at the lee side of the groyne are established. Prior to developing this function, an investigation is made on how to implement the boundary condition corresponding to a groyne.

Firstly, this chapter contains a description of the schematized coastline situation that is used to examine the shoreline evolution affected by diffraction. Subsequently, the applied method to account for the boundary condition of a groyne is explained. In doing so, the difference between the old and new approach regarding this boundary condition is provided. The old approach comprises the method that was available inside ShorelineS at the start of this thesis. The resulting shorelines using this method deviate from the analytical solution significantly as is explained in section 4.2.1. Therefore, a new approach is suggested. In section 4.3, details of the application of the simplified methods listed in section 3.4 are stated. Furthermore, a description of the wave diffraction function itself is provided. Finally, the model results belonging to the schematized situation are depicted in section 4.5.

4.1. Schematised situation

As an initial step, the model situation is made very simple. In doing so, it is easy to apply the wave diffraction function. The following assumptions are made regarding this simplified scenario:

- Initial infinitely straight coastline
- Constant wave forcing in time and space
- No sediment transmission and bypassing
- Water depth at groyne tip is larger than breaking water depth during the whole simulation
- Constant water depth and wave parameters at the groyne tip
- Refraction and shoaling from the groyne tip towards the breakerline are not taken into account
- Nearshore depth is equal to offshore depth
- Nearshore contour orientation is equal to the coastline orientation

Assuming that the water depth at the tip of the groyne is larger than the breaking water depth, implies that the groyne tip exceeds the surf zone. Therefore, alongshore sediment transport will only take place landward of the groyne tip. This is in line with neglecting potential sediment bypassing.

Besides the water depth being larger than the depth of breaking, it is also assumed that the water depth at the groyne tip is constant. This is in contradiction to the key aspects of a one-line model which states that the shape of the coastal profile stays constant. Assuming a constant water depth at the tip of the groyne while the shore is accreting or eroding, indirectly implies a change in the coastline profile as is explained as follows. After wave forcing, location A is shifted towards the direction of the sea (figure 4.1). Following the assumption of parallel depth contours, this coastline shift should take place for each depth contour inside the nearshore area. Going from location A to location A', the depth at the groyne tip should change from h_{tip} to $h_{tip'}$ because the coastal profile should be constant and the location of the groyne tip is fixed. Hence, assuming a constant water depth at the tip indirectly forces the shape of the coastal profile to change from the brown dotted line into the green dotted line.

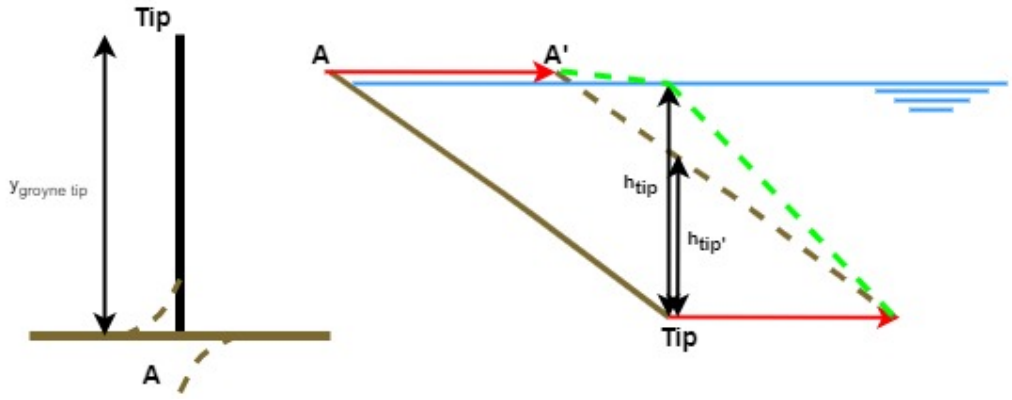

Figure 4.1: Constant water depth at the tip

The implementation of the dynamic boundary as is described by Mudde (2019), is initially turned off. This is achieved by setting the nearshore depth equal to the offshore depth and making the orientation of this nearshore depth contour equal to the coastline orientation. In this way, the offshore waves are directly transformed towards the breakerline (and groyne tip). Actually, the waves are transformed using an intermediate step towards the dynamic boundary. However, this does not affect the wave parameters since shoaling and refraction will not occur from the offshore location towards the dynamic boundary because of the corresponding depth and orientation values as described above. Mudde (2019) stated that the calculations of the breaking wave speed and breaking water depth are implicitly dependent on the values of the offshore and/or intermediate water depths inside ShorelineS. This is due to the assumptions that are made to rewrite equation A.10 into the explicit equation A.11. When not accounting for any other processes than shoaling and refraction inside the wave transformation, this dependency should not be present. Mudde (2019) concluded that in general, an intermediate water depth (water depth at the dynamic boundary) closer to the depth op breaking will lead to a better calculation result of the breaking depth itself. However, this breaking depth is not known beforehand. In the case of not using a dynamic boundary, setting the intermediate water depth equal to the offshore depth is concluded to be a safe choice (Mudde, 2019).

4.2. Boundary condition

This section elaborates on the implementation of the boundary condition that satisfies a zero transport condition at the groyne location. In doing so, the assumptions of no sediment transmission and bypassing are fulfilled. First, the resulting shorelines of the schematised situation using the current version of ShorelineS are examined. Subsequently, a new approach for the boundary condition is suggested and tested.

4.2.1. Old boundary approach

As stated before, the current version of ShorelineS does not account for wave diffraction effects onto the coastline evolution in the vicinity of a groyne. To establish an approach for incorporating these effects, first the resulting shoreline evolution of the schematised situation without diffraction effects is investigated. The effect of the groyne onto the coastline evolution is in the current model version taken into account by setting the alongshore sediment transport of the Q_s points located inside the shadow zone equal to zero.

The numerical and analytical shorelines after 1,6 and 12 months are compared to each other (figure 4.2). The offshore wave input is stated in table 4.1. The amplitude of the alongshore sediment transport, calculated by ShorelineS, is also provided. This parameter fulfills as input parameter in the analytical solution. The breaking wave angle with respect to the coastline orientation at the beginning of the simulation (straight coastline) is stated for convenience. Resulting shorelines belonging to different offshore wave angles are depicted in appendix B.

T_∞	H_∞	ϕ_∞	$\phi_{br,loc}$	Q_0
8 s	0.5 m	20°	4.27°	137359 $m^3/year$

Table 4.1: Input parameters ShorelineS and analytical solution

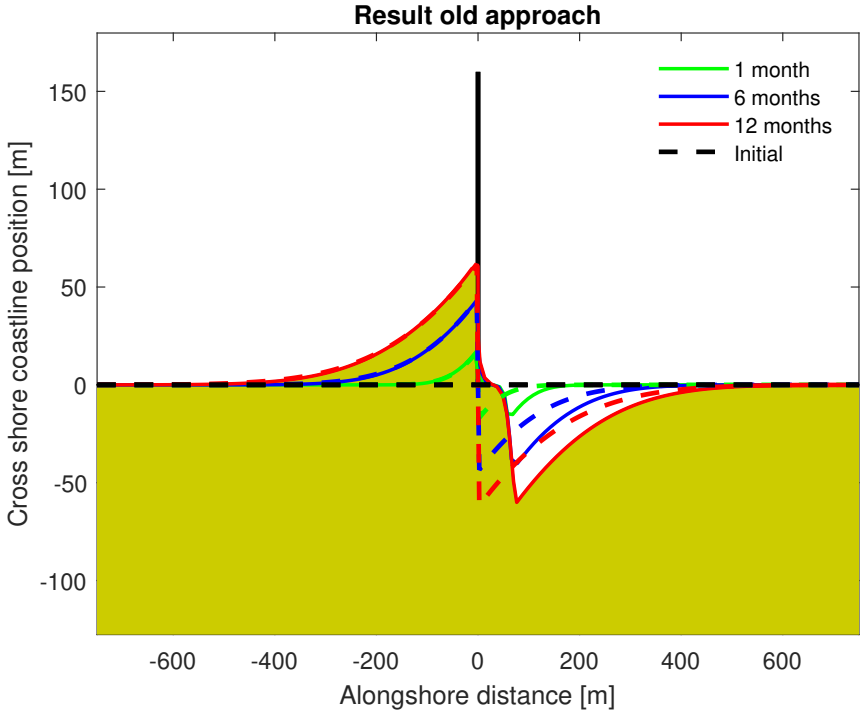

Figure 4.2: Comparison numerical and analytical (dotted-lines) result

The updrift sedimentation agrees very well with the analytical solution (dotted lines). The erosion directly downdrift of the groyne does not show a matching result. This is because the values of too many Q_s points are set equal to zero. Increasing the offshore wave angle results in a less matching shoreline evolution as could be seen in appendix B. Since wave diffraction predominantly will influence the coastline evolution directly downdrift of the groyne, first a new approach regarding the boundary condition of the groyne is established to obtain a better matching result. The next section will elaborate on this new approach, which is subsequently tested using different offshore wave input parameters.

4.2.2. New boundary approach

Accounting for wave diffraction should still satisfy an alongshore sediment transport at the groyne to be equal to zero. Different ways to incorporate such a condition are examined. As is described in section 2.2.3, consists the coastline of x, y grid points that can freely move around. The alongshore sediment transport is calculated in between two grid points. Initially, those so-called Q_s points lay exactly in the middle of two grid points. However, while the simulation is proceeding the position of the grid points is changing. Consequently, changing the location of the Q_s points.

First, the following procedure was suggested in order to apply the boundary condition of a groyne. Figure 4.3a provides a sketch of the suggested procedure.

- Initially define the structure at a Q_s point
- Apply Q_s=0 at that location
- Force adjacent x, y points to not move horizontally

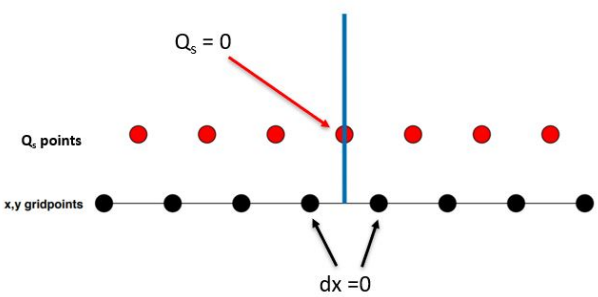

(a) Boundary condition sketch 1

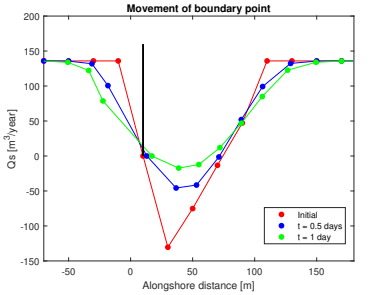

(b) Movement of the boundary point

Figure 4.3: Definition of the boundary condition

After applying this approach, it became clear that a solution was needed for the changing position of the boundary Q_s point (figure 4.3b). This Q_s point for which the boundary condition was specified was leaving the location of the structure. After 1 day of simulation time, the boundary point already moved 15 meters away from the original groyne location. In other words, the location for which the model thought the groyne was situated was changing significantly while the simulation was proceeding. This movement of the boundary point is mainly caused by the shoreline evolution itself since the location of the Q_s points depends on the adjacent x, y coastline points. The values of those coastline points change while the model is simulating the shoreline evolution. Furthermore, the x, y points are altered after each time step because of smoothing of the grid. Hence, affecting the position of the Q_s points. One of the core principles of ShorelineS is having a flexible grid to allow for the interaction and merging of different coastlines sections. Therefore, solving this movement of the boundary point should be applicable to a flexible coastline grid.

A solution was found for implementing a boundary condition that does not leave the structure by dividing the coastline into different sections. The first and last grid points of a coastal section are not affected by smoothing which is a great advantage. In this way, also the position of the adjacent Q_s points at the begin and end of a coastline section are not altered because of smoothing. The following procedure is suggested to apply the boundary condition at the groyne.

- Define the structure initially at an x, y gridpoint
- Divide the coastline into two sections; the location of the groyne is the first gridpoint of the downdrift section
- Insert an extra gridpoint to the updrift section

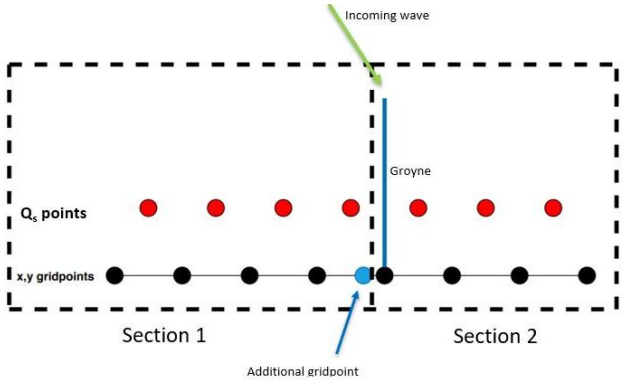

Figure 4.4: Boundary condition sketch 2

After applying the above procedure, still the effect of a zero alongshore sediment transport rate at the groyne needs to be incorporated. This is done by applying a boundary condition for the last gridpoint of section 1 and the first gridpoint of section 2. In this way, the effect of the groyne onto the shoreline evolution updrift (section 1) and downdrift (section 2) of the groyne is incorporated. Boundary conditions are established to force the grid points at the groyne to move along the structure.

$$\Delta y_{end} = \frac{Q_{s,end}}{0.5\sqrt{\left(x_{end} - x_{end-1}\right)^2 + \left(y_{end} - y_{end-1}\right)^2}} * \frac{1}{D} * \Delta t \qquad (4.1a)$$
$$\Delta x_{end} = 0$$

$$\Delta y_1 = \frac{Q_{s,1}}{0.5\sqrt{\left(x_2 - x_1\right)^2 + \left(y_2 - y_1\right)^2}} * \frac{1}{D} * \Delta t \qquad (4.1b)$$
$$\Delta x_1 = 0$$

Equation 4.1a belongs to coastline section 1 and equation 4.1b to section 2. Without implementing these conditions, there will be no shoreline evolution since initially there is no alongshore sediment transport gradient. Figure 4.5 visualizes the application of these conditions to section 1, the same holds for section 2. In the remainder of the simulation there will be a gradient in the alongshore sediment transport in the vicinity of the groyne. This gradient is caused by the initially forced movement of the grid points at the structure.

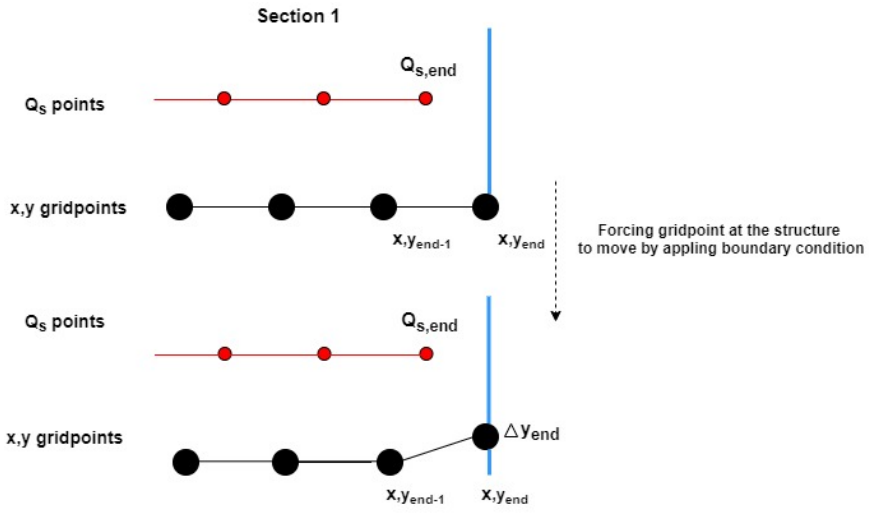

Figure 4.5: Boundary condition sketch 3

4.2.3. Testing new boundary approach

To examine whether the suggested boundary approach provides a good result of the shoreline evolution in the vicinity of a groyne, a comparison is made with the analytical solution of Pelnard-Considere (1956). Again, the resulting shorelines after 1,6 and 12 months are compared to each other (figure 4.6a). The same offshore wave input as applied in the case of the old boundary approach is used (table 4.2). The shoreline evolution in the case of offshore wave angles being equal to 10°, 30° and 40° can be found in appendix B.

T_∞	H_∞	ϕ_∞	$\phi_{br,loc}$	Q_0
8 s	0.5 m	20°	4.27°	137359 $m^3/year$

Table 4.2: Input parameters ShorelineS and analytical solution

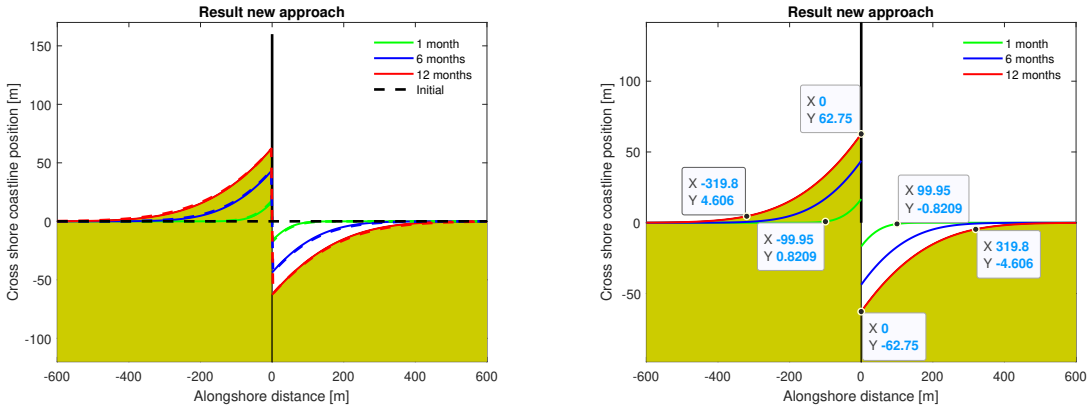

(a) Comparison numerical and analytical (dotted-lines) result

(b) Fully symmetric result

Figure 4.6: Shoreline evolution using the new boundary approach

Highlighting coastline points demonstrates the complete symmetric result (figure 4.6b).The updrift and downdrift points being equally extended from the groyne, have an equal cross-shore coastline position, only being opposite of sign. This behaviour agrees with the analytical solution of Pelnard-Considere (1956). To retrieve a fully symmetric result, the groyne should be located exactly in the middle of the model domain. Meaning that the total length and amount of grid points of section 1 is equal to section 2. In doing so, the resulting coastline of both sections is smoothed in the same way after each time step. The length and amount of grid points of a section influence this smoothing process. Therefore, they should be the same for both sections to retrieve a fully symmetrical result. If this is not the case, small differences in the cross-shore coastline position updrift and downdrift will arise. This difference is a couple of centimeters, relative to the total coastline shift having a magnitude of meters this is negligible.

From figure 4.6 and the results stated in appendix B it is concluded that the applied approach concerning the boundary condition works well. The numerical results are matching the analytical solution very properly. However, the result of scenario D stated in the appendix shows less agreement with the analytical solution. An explanation for this is that the analytical solution of Pelnard-Considere (1956) assumed small wave angles. In scenario D an angle of 40° is used which can not be identified as being small. Because of the better matching shoreline results in the case of the new boundary approach, it is chosen to apply this approach in the remainder of this thesis.

4.3. Application of simplified diffraction methods

Section 3.4 contains methods that can be used inside numerical models to account for wave diffraction effects. This section provides an elaboration of those methods and an explanation of how they should be incorporated inside a one-line model. Some of them need modifications as will be illustrated in this section. The same schematised model scenario as described in section 4.1 is applied. First, an issue concerning the transition zone edge is stated. Subsequently, required modifications to the diffracted breaking angles are explained.

4.3.1. Transition zone edge

Two key parameters in each method are the groyne tip wave angle and transition zone edge definition. Those two parameters together determine the size of the downdrift area that is influenced by diffraction effects. The transition zone definition is not very straightforward. A distinction between two approaches establishing this zone is made in this thesis as follows:

1. Transition zone edge is defined beforehand
2. Transition zone edge is established based on the calculated K_d values

For both cases should yield that the effect of wave diffraction is not felt anymore at the edge of the transition zone. Meaning that the breaking wave angle and height are equal to their undiffracted values. Hence, the corresponding K_d value at that location should be equal to 1. To demonstrate the difference between the above stated approaches, K_d values are calculated while using the wave parameters stated in table 4.3.

T_∞	H_∞	ϕ_∞	ϕ_{tip}	L_{tip}
8 s	0.5 m	45°	17°	42 m

Table 4.3: Wave parameters

1.Transition zone edge is defined beforehand

The different calculated K_d values using the predefined transition zone edge according to the method of Roelvink are compared (figure 4.7). This method applies a transition zone width being equal to 2.5 times the wavelength at the tip, as is suggested by Dabees (2000). In doing so, the edge of the transition zone depends on the location of the shadow zone edge and the wavelength at the groyne tip. The shadow zone edge depends on the wave angle at the tip. Hence, the tip wave angle and wavelength are responsible for the area size affected by diffraction. Both parameters are at their turn dependent on the offshore wave input. The wave characteristics at the tip are assumed to be constant during the simulation as is explained in section 4.1.

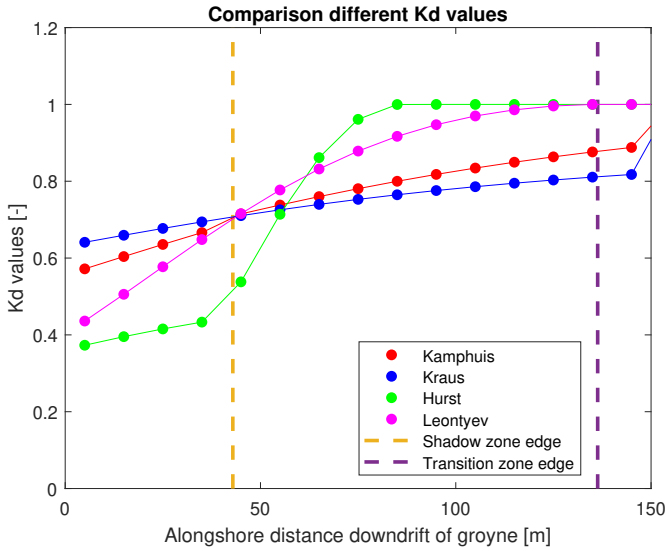

Figure 4.7: K_d values using a predefined transition zone

The methods of Kraus and Kamphuis do not result in a K_d value of 1 (figure 4.7). The length of the transition zone is so to say too small to reach a K_d value of 1 in this model scenario. Section 3.4 states that those two methods only provide a K_d of 1 in the case θ is equal to 90°. Measuring such an angle from the shadow line of the groyne in the situation of a straight beach is not possible (figure 4.8).

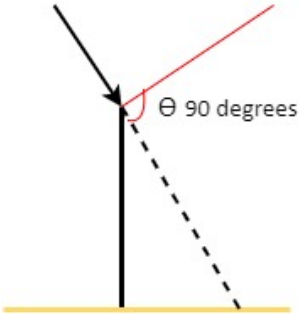

Figure 4.8: θ of 90 °

A suggestion is made to modify the K_d values retrieved using the Kamphuis and Kraus methods to reach a value of 1 at the predefined transition zone edge. This is done in two different ways. The first kind of modification is performed by extending the trend of the K_d values inside the shadow zone towards the transition zone end. In other words, the K_d value at the shadow zone edge is linearly interpolated towards the transition zone edge based on the increase of K_d inside the shadow zone. The trend of K_d inside the shadow zone is determined based on the K_d values at the structure and shadow zone end. Those values need to be determined beforehand and are depicted using light blue dots (figure 4.9). Written in equation form, K_d inside the transition zone is calculated as follows:

$$K_d(x) = K_{d,shadow} + \frac{K_{d,shadow} - K_{d,struct}}{x_{shadow}} * \left(x - x_{shadow}\right) \tag{4.2}$$

Here $K_{d,struct}$ and $K_{d,shadow}$ are the K_d values at the structure and shadow zone edge respectively. x_{shadow} is the distance from the shadow zone edge at the breakerline towards the structure and x is a location inside the transition zone.

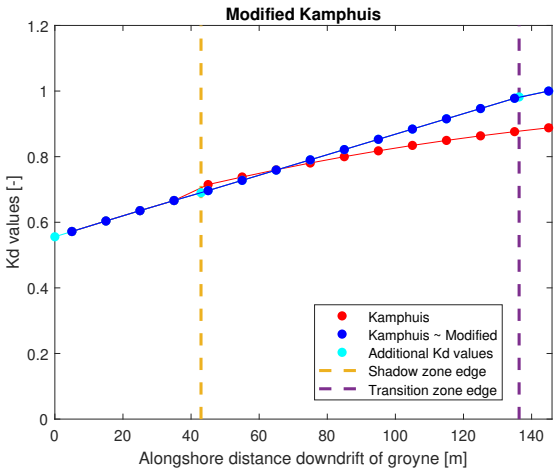

(a) Kamphuis Modified

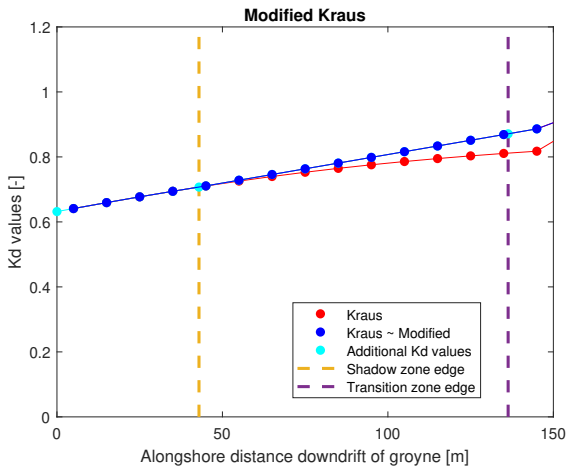

(b) Kraus Modified

Figure 4.9: Interpolation based on K_d trend inside the shadow zone area

The resulting K_d values at the transition zone end are closer to 1 than for the result of the non-modified methods (figure 4.9). However, it is still not exactly equal to 1. Especially for the Kraus Modified method, the K_d value at the transition zone edge is significantly smaller than 1. Apparently, the K_d trend inside the shadow zone is not sufficient or the transition zone width is too small to reach a value of 1. Therefore, a second interpolation method is suggested in which a K_d being equal to 1 at the transition zone edge is forced. For points lying inside the transition zone, the K_d values are calculated by linear interpolation based on the K_d value at the shadow zone edge, a K_d value of 1 at the transition zone edge and the width of the transition zone itself (equation 4.3)

$$K_d(x) = K_{d,shadow} + \frac{1 - K_{d,shadow}}{\text{transition zone width}} * \left(x - x_{shadow}\right) \tag{4.3}$$

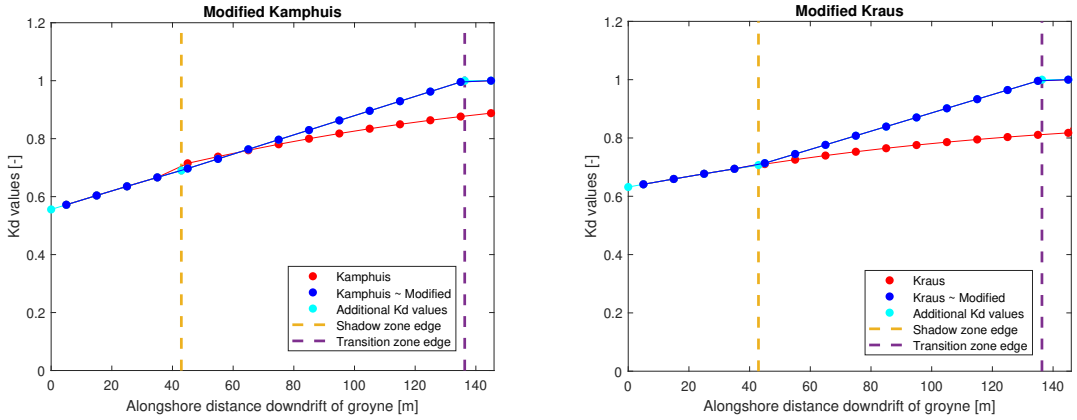

(a) Kamphuis Modified

(b) Kraus Modified

Figure 4.10: Interpolation with a forced K_d value of 1 at the transition edge

The resulting K_d values at the transition zone edge are equal to 1 (figure 4.10). Hence, satisfying the conditions that should be present there. While using different offshore wave input, also the K_d values at the transition zone edge calculated using Leont'yev and Hurst could be below 1. If that is the case, also modification of those K_d values is needed just like is done for the methods of Kraus and Kamphuis. Especially, the offshore wave period and the water depth at the groyne tip, which together determine the wavelength at the tip of the groyne, determine if interpolation of the K_d values is needed. Furthermore, the predefined definition of the transition zone edge has a significant role in this. If the edge is determined by adding 4 tip wavelengths to the shadow zone edge instead of 2.5 tip wavelengths, the transition zone width is larger. As a result, the calculated K_d values have more time to develop towards a value of 1 so to say.

2.Transition zone edge is established based on the calculated K_d values
In the previous section, it is explained that the K_d values in some cases need to be adjusted to reach a value of 1 at the predefined transition edge. Another way of looking at this issue is to follow the trend of the K_d values and define the transition zone edge at the location where K_d has reached a value of 1. When applying this approach, it becomes clear that the methods of Leont'yev and Hurst result in a K_d value equal to 1 before the predefined transition zone edge of Dabees (2000) is reached (figure 4.11). Hence, the area affected by diffraction according to those two methods is smaller than when using the transition zone edge definition of Dabees (2000). To come up with a transition zone edge based on the K_d trend retrieved using the methods of Kraus and Kamphuis, first interpolation is needed. This is necessary because applying those methods to a straight coastline will never result in a K_d value of 1 as is explained earlier (figure 4.8). The transition zone edge of those two methods could be determined by calculating the modified K_d values using equation 4.2 until a value of 1 is reached. Figure 4.11 visualizes the transition zone edges based on the K_d trend of each method.

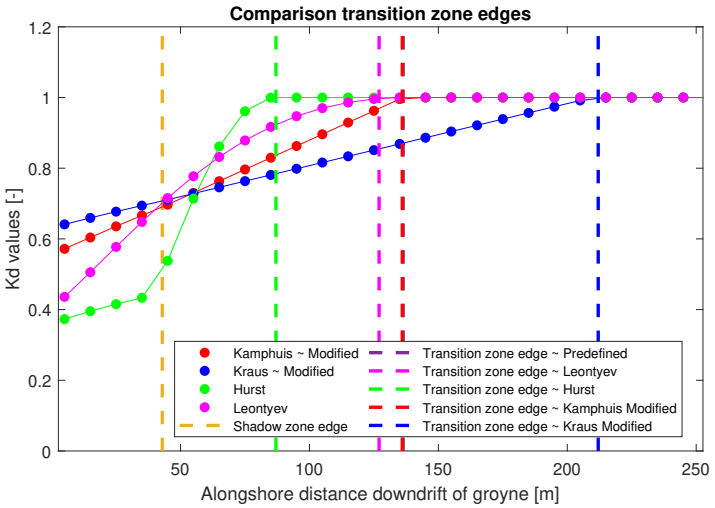

Figure 4.11: Transition zone edge definitions based on K_d trends

It becomes clear that not every combination of methods to determine the K_d values and breaking angles could be used without precaution because the transition zone edges are not matching (figure 4.11). For example, using the method of Roelvink for the breaking wave angles would lead to the calculation of diffracted breaking wave angles up to approximately 135 meters downdrift of the groyne (predefined transition zone edge in the above figures). Combining this method with the method of Hurst to calculate the K_d values, provides diffracted breaking wave heights up to roughly 85 meters downdrift of the groyne (green dotted line in 4.11 figure). In this way, the effect of diffraction onto the breaking angles is felt over a larger area compared to the effect of diffraction onto the breaking wave heights. From a physical point of view, this is not possible. To prevent this issue, the combination of methods that is going to be applied and in which way the transition zone edge will be defined should be examined beforehand. If necessary, interpolation of the K_d values should be performed.

In the current version of the wave diffraction function it could be that for the last couple of diffracted breaking wave angles the corresponding K_d values already reached a value of 1. Vice versa this is not possible; if a K_d value is not equal to 1, the corresponding breaking wave angle is always affected by diffraction. In this way, the effect of diffraction onto the angles is so to say the restricting factor. This approach is chosen because the wave angles are assumed to have a large influence on the final coastline shape. The K_d values, subsequently the breaking wave heights, are expected to only influence the speed at which the shoreline change is happening as will be stressed in section 4.5.1.

4.3.2. Breaking wave angles modification

After establishing the diffracted breaking angles using the method of Roelvink or Hurst, modification to the calculated values is needed. Since refraction from the groyne tip towards the breakerline is not considered while calculating the diffracted wave angle, it could be that the diffracted breaking angle exceeds the value of the corresponding undiffracted parameter. Therefore, a procedure is implemented that checks if the diffracted breaking wave angle is exceeding the undiffracted values for the same location. If that is the case, the diffracted values are set equal to their undiffracted values at the same location. The diffracted breaking angle could only have a larger magnitude than the undiffracted breaking angle if their sign is opposite. In other words, assuming that the undiffracted angle very close to the structure is 10° relative to the normal of the coastline, the diffracted angle could be -15° in the case of strongly diffracted waves. The implemented procedure approves in that situation a diffracted breaking angle magnitude being larger than the corresponding undiffracted one (figure 4.12). The diffracted angles calculated using the method of Kamphuis do not require any modifications. Equations used in this method are very simple, they relate the diffracted angles to the undiffracted angles and the K_d values. As a consequence, the diffracted angle will always have the same sign and smaller magnitude than the corresponding undiffracted angle. Therefore, modifications are not necessary. Section 4.5.1 elaborates further on the trend of diffracted breaking angles calculated using the method of Kamphuis.

The uncorrected breaking wave angle is equal to the incoming wave angle at the tip (red dots - figure 4.12). This is because the amount of diffraction is based on the wave characteristics at the tip. Neglecting shoaling and refraction results in wave characteristics at the transition zone edge being equal to the wave characteristics at the groyne tip. The last red dot belongs to a Q_s point that lies outside the transition zone edge at the breakerline. This point should not be included inside the diffraction calculations. Why this point initially is involved inside the diffraction calculations, is explained in the next section.

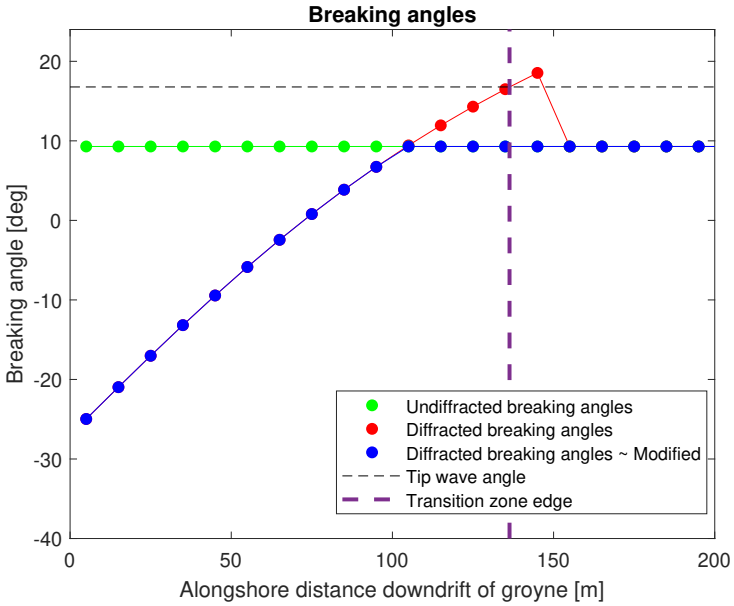

Figure 4.12: Correction of diffracted breaking angles

4.4. Wave diffraction function description

Taking into account the effect of wave diffraction in the vicinity of a groyne requires a new function to be implemented inside the ShorelineS model. The diffraction function is based on the method as applied in Hanson (1989) which first calculates the breaking parameters without the effect of diffraction, as if no structure is present. Subsequently, the diffracted wave heights are determined based on the wave tip characteristics. At the end refraction from the wave tip towards a point in the zone off diffraction is taken into account using Snell's law. As stated in section 4.1 the latter is not applied in this study. This section contains the general set-up of the established function.

The following summation provides the general set-up of the wave diffraction function.

1. Calculation of breaking parameters without diffraction
2. Calculation of the wave characteristics at the groyne tip
3. Establishing the shadow and transition zone
4. Identifying the Q_s points that are situated in those zones
5. Determining the K_d values and subsequently the diffracted breaking wave heights
6. Diffracted breaking wave angle calculation
7. Checking the diffracted breaking wave angles and heights
8. Alongshore sediment transport calculation

Step 1 and 2
The wave characteristics at the tip of the groyne are needed to calculate the breaking wave heights and angles affected by diffraction. As can be seen in section 3.4, the wave angle at the tip of the groyne is required in every simplified solution to account for diffraction effects. The calculation of the groyne tip wave parameters is only performed initially, so in the case of a completely straight coastline. Furthermore, these parameters are assumed to be constant during the entire simulation as is explained in section 4.1. The offshore waves are transformed towards the groyne tip while accounting for shoaling and refraction. While assuming a Dean coastal profile, the water depth at the groyne tip is known beforehand. Hence, the offshore wave transformation towards the groyne tip is very straightforward by using Snell's Law and solving the dispersion relation only.

Step 3 and 4
The shadow zone is established by extending the line representing the direction of the wave tip angle towards the shore. Section 4.3 provides an elaboration of establishing the transition zone edge. In the situation of figure 4.13a, the predefined transition edge approach is used. The definition as is described in the method of Roelvink is applied, therefore having a width equal to 2.5 times the wavelength at the tip.

Q_s points lying inside the area of diffraction are identified by first creating incoming waves rays with the same direction as ϕ_{tip} going true the Q_s points. Subsequently, it is checked if the intersection points with the shoreline lie in the area affected by diffraction. Figure 4.13a visualizes this process at the beginning of the simulation. The shadow and transition zone are the uninterrupted and interrupted green line respectively. Incoming wave rays are visualized with a red dotted line. The Q_s points in the area of diffraction and their corresponding intersection points with the shoreline are displayed with red and purple dots.

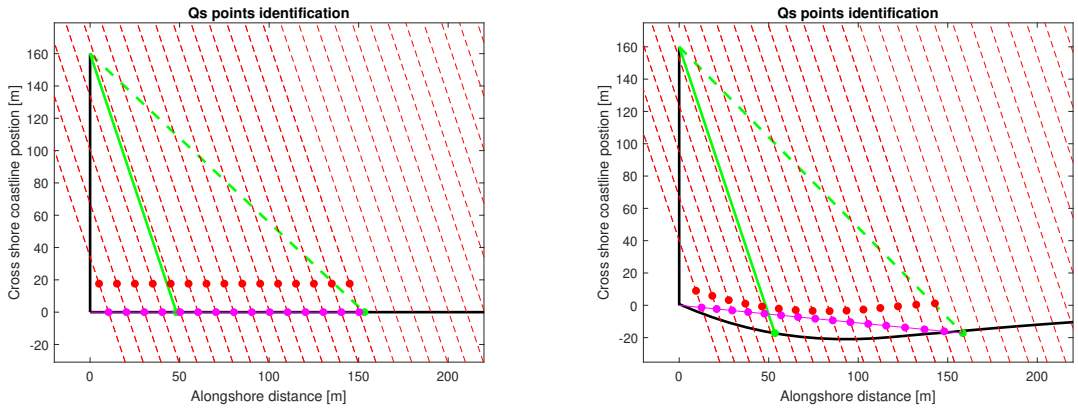

(a) Identifying Q_s points (red-dots) inside the diffraction area at the begin of the simulation

(b) Identifying Q_s points (red-dots) inside the diffraction area while shoreline is not straight anymore

Figure 4.13: Q_s points identification

As time proceeds, the shape of the shoreline evolves and will not be a straight line anymore. Because of a sharp gradient in the coastline shape immediately downdrift of the groyne, it could be the case that there is no intersection point with an incoming wave ray and the shoreline at that location. Especially, when the size of the grid cells is not small enough this could happen. In that case, the Q_s point at that location would not be affected by diffraction effects which makes no sense. Different approaches to solve this issue are examined. The one that is currently applied is the most computational effective and is visualized in figure 4.13b. Since Q_s points at the downdrift side very close to the groyne will always be subjected to diffraction it is chosen to look for an intersection point between an incoming wave ray and an imaginary line (purple line) drawn between the base of the groyne and the transition zone edge located on the *shoreline*. Shoreline is written in italics because this transition zone edge lies on the same depth contour as the shadow zone edge but could be different from the shoreline position at the location of the transition zone edge (green dot lies below shoreline figure 4.13b).

At the beginning of the simulation, the last identified Q_s point lies outside the transition zone at the breaker-line but inside the transition zone at the shoreline (figure 4.13a). Since the alongshore sediment transport is calculated at the breakerline, the edge of the transition zone at the breakerline should serve as the border of the area affected by diffraction. In step 7 the breaking wave angle and height are corrected for this Q_s point. Summarizing, Q_s points situated in the area of diffraction are identified based on the transition zone edge located at the same depth contour as the shadow zone edge at the shoreline. Diffracted breaking angles and wave heights of identified Q_s points lying outside the transition zone at the breaker line are corrected in step 7.

Step 5 and 6
If a Q_s point lies inside the shadow or transition zone, the diffracted breaking wave angle and wave height are calculated using one of the methods described in section 3.4. Some of the methods are modified to be applicable to the schematised situation described in 4.1.

Step 7
Before the alongshore sediment transport in the lee side of the groyne is calculated, an additional check regarding the diffracted wave parameters is performed. Since refraction and shoaling from the groyne tip towards the breakerline are not considered while calculating the diffracted breaking wave height and angle, it could be that those calculated values are not correct from a physical point of view. For example, the diffracted breaking wave height should never be larger than the undiffracted breaking wave height since diffraction does not result in adding energy or energy convergence. A procedure is implemented that checks if the local diffracted breaking wave height is exceeding the local undiffracted breaking wave height. If that is the case, the value of the diffracted breaking wave height is set equal to the undiffracted value. A same kind of procedure is applied to the breaking wave angles which is described at the end of section 4.3 .

Step 8
The alongshore sediment transport is calculated, using the diffracted breaking wave parameters for the Q_s points defined in step 4. Obviously, an alongshore sediment transport formulation that uses the breaking wave parameters should be activated inside ShorelineS to account for diffraction effects. Initially, a small abrupt step is visible in the alongshore sediment transport values going from the last point inside the diffraction area to the first point outside the diffraction area, so passing the transition zone edge at the breakerline. This is because inside the transition zone close to the edge, the K_d value is very close to 1. Subsequently, the resulting breaking wave height will be almost equal to the wave height at the tip (figure 4.14a). The first point outside the diffraction zone has a wave height being equal to the undiffracted breaking wave height. This wave height will be larger than the wave height at the tip because of the additional shoaling from the groyne tip towards breakerline (figure 4.14a). This results in a sharp gradient in the alongshore sediment transport (red line - figure 4.14b).

As the simulation proceeds, this abrupt transition in the alongshore sediment transport is smoothed out. The magnitude of this abrupt transition is in general very small. It depends on the difference between the wave height at the tip and the diffracted breaking wave height. In the case of a very long groyne leading to a large water depth at the tip compared to the breaking water depth, the difference between the two wave heights will be significant. However, even in that scenario the abrupt change in alongshore sediment transport at the transition zone edge is smoothed out while simulating and is not expected to influence the resulting coastline evolution. Especially, when looking to the shoreline evolution over a period of years this initial abrupt transition is irrelevant. The initial sharp gradient in alongshore sediment transport is already disappeared after 2 days of simulation time (100 time iterations) for the case depicted in figure 4.14b.

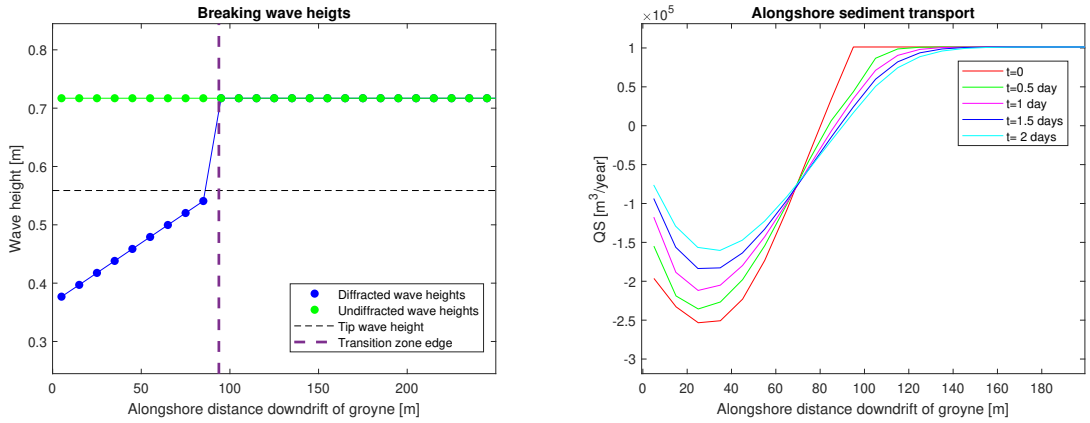

(a) Trend of breaking wave height

(b) Initial discrepancy in the alongshore sediment transport

Figure 4.14: Abrupt change from transition zone towards undiffracted area

4.5. Model results

This section contains model results concerning the coastline evolution of the schematised situation described in section 4.1. First, a comparison between the simplified methods to account for wave diffraction is made. Some conclusions are drawn regarding these methods and a suggestion is made on which method to use in the remaining of this thesis. Subsequently, a variety of model runs are performed to examine the influence of the offshore wave height and angle onto the shoreline evolution. Furthermore, the effect of the angle δ, angle between transition zone and shadow zone, onto the shoreline evolution is investigated by executing model runs in which δ is multiplied by a certain factor. Also, the sensitivity of the shoreline response to a varying transition zone width is examined.

The CERC3 alongshore sediment transport formulation is applied in every simulation. Mudde (2019) concluded that the inclusion of a dynamic boundary will result in more accurate alongshore sediment transport calculation because the wave transformation from offshore to breakerline is more precise. Therefore, the dynamic boundary will from now on be activated inside the model runs in which the diffraction effects are included. The depth of the dynamic boundary is set equal to the water depth at the groyne. To minimize the effect of refraction from groyne tip towards the breakerline, the orientation of the dynamic boundary is equalized to the coastline orientation. This is done because inside the diffraction calculations this additional refraction is not taken into account. Therefore, minimizing refraction from tip to breakerline will result in a better proportion between the diffracted and undiffracted breaking wave angles at the same location.

4.5.1. Comparison simplified diffraction methods

In the remaining of this study not, all methods to calculate the diffracted breaking wave angles and wave heights will be used individually to determine the coastline evolution in the vicinity of a groyne. In this section, first the methods to calculate the K_d values are compared. Subsequently, the method of Hurst, Roelvink and Kamphuis regarding the diffracted angles are related to each other. After both comparisons, it is chosen to use the method of Leont'yev and Roelvink to calculate the diffracted breaking wave heights and angles respectively. An argumentation of why those are selected is stated in this section.

Diffracted breaking wave heights

This section examines if a different method for determining the K_d values will provide a different coastline evolution. The breaking wave height is expected to only influence the rate of shoreline change and not the resulting shape. The earlier described methods to determine the diffracted wave heights are all based on the same kind of regression analysis. Therefore, the same resulting coastline shape is foreseen. Except the K_d values resulting from the method of Hurst, which lead to a K_d of 0.5 at the edge of the shadow zone. Hence, satisfying the diffraction theory based on monochromatic waves instead of random waves as described in section 3.1.

The results of the shoreline evolution using the methods of Kraus, Kamphuis, Leont'yev and Hurst to determine the diffracted wave heights are compared to each other (figure 4.15). The method of Roelvink is applied in each scenario, calculating the diffracted wave angles. Kraus and Kamphuis are modified based on the predefined transition zone edge described in the method of Roelvink. This modification is elaborated in section 4.3. The offshore wave input is kept the same and is listed in the table below. The tip of the groyne is located close to the breakerline to minimize the discrepancy in the alongshore sediment transport going from the last point inside the transition zone towards the first point outside the transition zone as is visualized in figures 4.14a and 4.14b.

H_∞	ϕ_∞	T_∞	h_{tip}	H_{tip}	L_{tip}	ϕ_{tip}	h_{br}	$\phi_{br,undiff}$	$H_{br,undiff}$
0.5 m	10 °	8 s	2.95 m	0.56 m	41.99 m	4.18 °	0.99 m	2.48 °	0.72 m

Table 4.4: Offshore, tip and breaking parameters

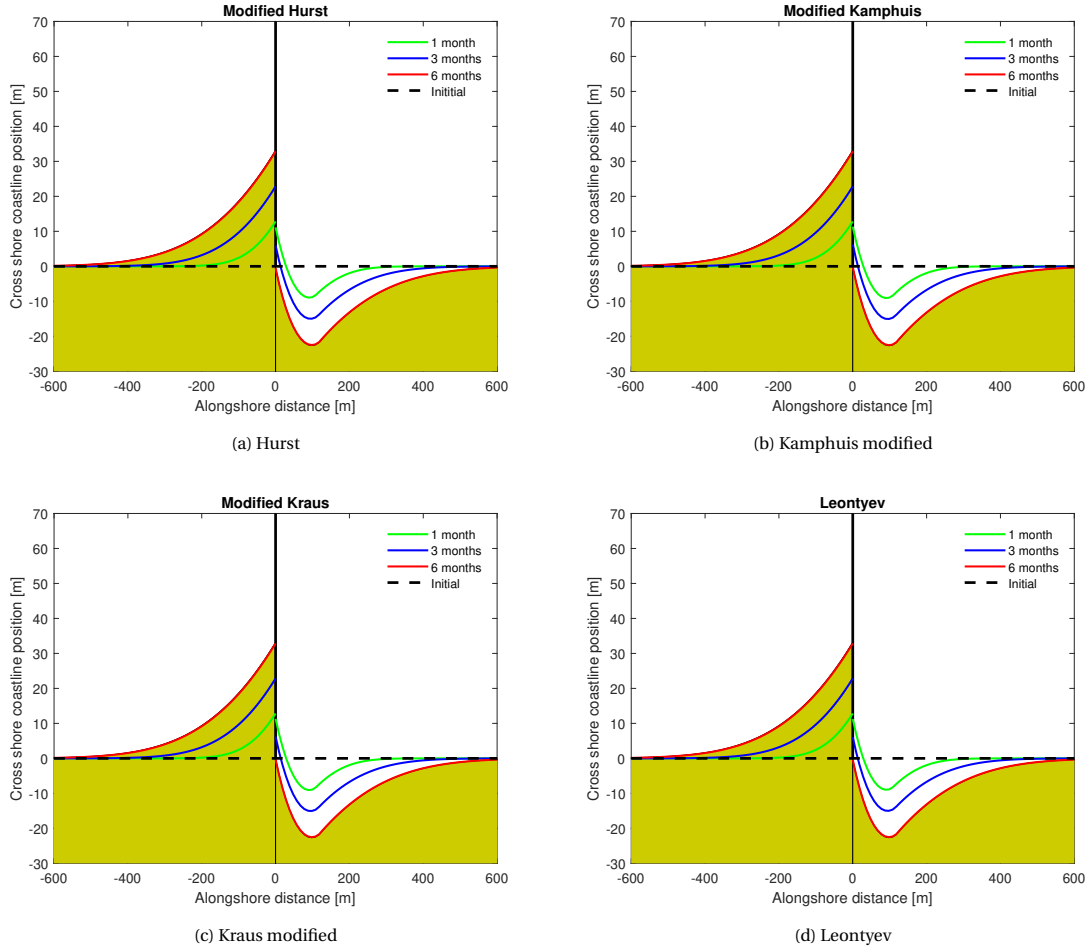

(a) Hurst

(b) Kamphuis modified

(c) Kraus modified

(d) Leontyev

Figure 4.15: Shoreline evolution using different approaches to calculate the K_d values

The resulting shorelines after 1,3 and 6 months hardly show any differences (figure 4.15). Using the methods of Kamphuis and Kraus, additional computations are required to interpolate the K_d values as is explained in section 4.3. Furthermore, the method of Hurst is based on the theory of monochromatic waves. In the remainder of this study, the method of Leont'yev is used to calculate the diffracted breaking wave heights. His method is chosen since it is based on regular wave diffraction theory and being more computational effective in this model scenario compared to the methods of Kamphuis and Kraus.

Diffracted breaking wave angles

Three different methods are stated in section 3.4 to determine the diffracted breaking angles. The equations describing the diffracted angle according to Kamphuis are simple and strongly correlated to the K_d values. From a first examination of equations 3.36 and 3.37, it is concluded that the diffracted breaking angle will always have the same sign as the undiffracted breaking angle because the K_d value is never below zero. Furthermore, the trend of the diffracted breaking angles inside the transition zone will be the same as the trend of the corresponding K_d values. In the shadow zone, additional refraction is taken into account as is explained in section 3.4.1 and determined using equation 3.37.

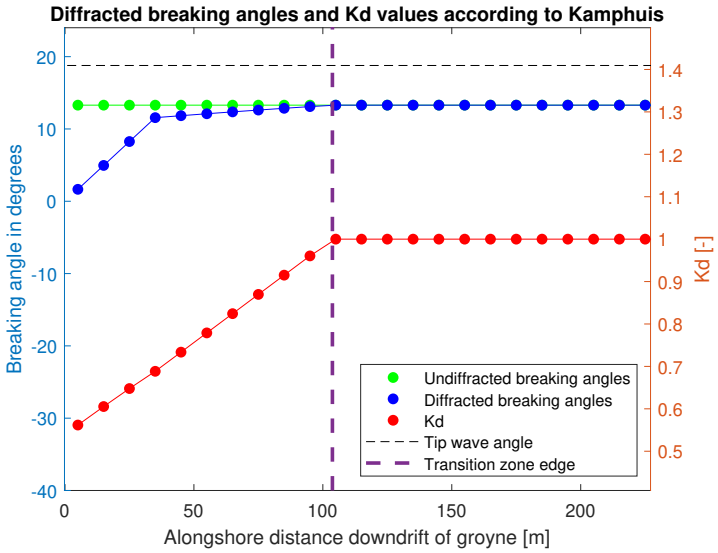

Figure 4.16: Relation between breaking angle and K_d according to Kamphuis

By observing the relation between the K_d values and breaking angles, both calculated using the approach of Kamphuis, it is concluded that sedimentation directly updrift of the groyne will never occur (figure 4.16). Assuming a positive alongshore sediment transport going from left to right, there will always be a positive gradient downdrift of the gronye following the trend of the breaking angle (and K_d values). Therefore, more sediment is flowing out than in for each section inside the area influenced by diffraction. Subsequently, resulting in erosion downdrift of the groyne. Since in real-world cases sedimentation downdrift of a groyne does appear, the model should be able to simulate this coastline behaviour. Because it is not possible to mimic this behaviour when applying the method of Kamphuis to the simplified model scenario, this method is not used in the remainder of this thesis.

Applying the method of Hurst or Roelvink, could lead to sedimentation downdrift of the groyne. The angles are stronger diffracted compared to the method of Kamphuis. For points lying close to the groyne, the diffracted angles could have an opposite sign to the undiffracted angles (figure 4.12). This means that the angles are diffracted so much that the local sediment transport is directed towards the groyne (figure 4.17). Hence, resulting in local sedimentation because of the negative gradient in along shore sediment transport. This negative gradient is caused by going from a negative alongshore sediment transport close to the groyne to a value of zero transport at the groyne.

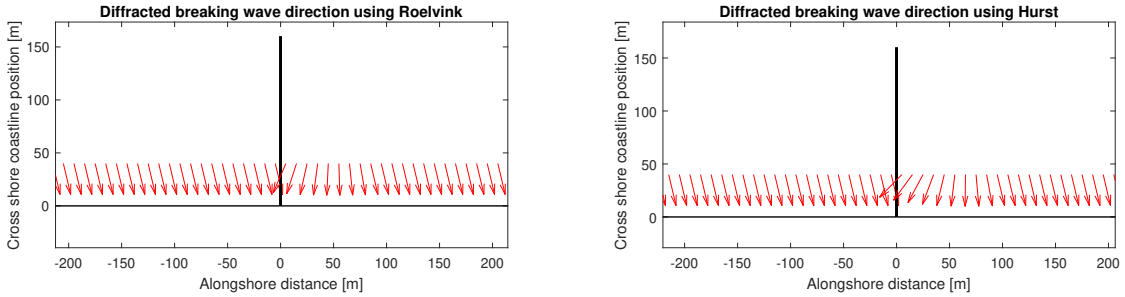

(a) Diffracted wave angles according to Roelvink

(b) Diffracted wave angles according to Hurst

Figure 4.17: Direction of diffracted breaking wave angles near the groyne

It is concluded that the method of Hurst results in stronger diffracted breaking waves compared to the method of Roelvink. Since the breaking wave angle determines the curvature of the resulting coastline evolution, the different influence of each method calculating the diffracted angles should be kept in mind.

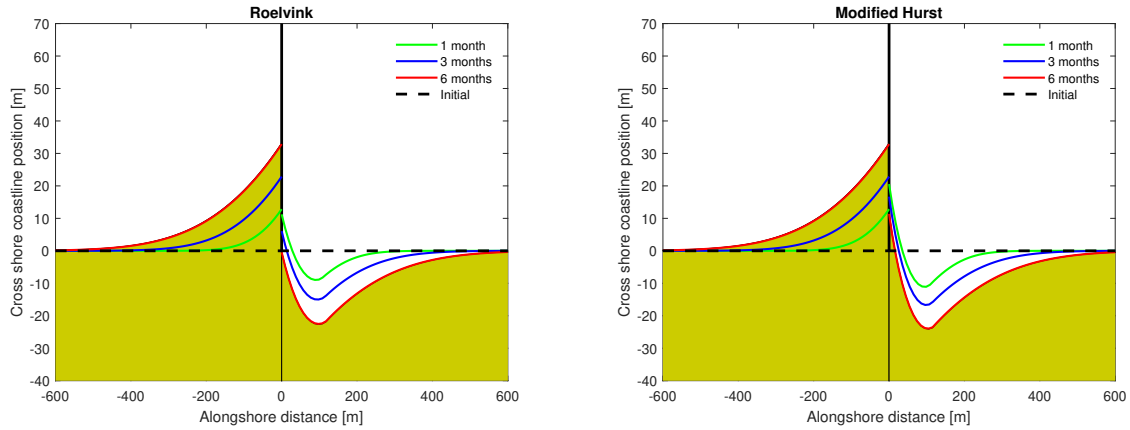

(a) Diffracted wave angles according to Roelvink

(b) Diffracted wave angles according to Hurst

Figure 4.18: Shoreline evolution

The shoreline responses of the methods of Hurst and Roelvink for calculating the diffracted angles are significantly different from each other (figure 4.18). The diffracted angles themselves, displayed as vectors, already showed that for Hurst his method the angels are more diffracted towards the groyne (figure 4.17). The amount of downdrift erosion directly near the groyne is reduced significantly while using Hurst. Furthermore, the angles are diffracted so much that even after 6 months there is sedimentation directly downdrift of the groyne. In the case of using Roelvink, after 6 months there is no sedimentation visible directly near the groyne. Erosion has replaced sedimentation and the shoreline is retreating over the total downdrift area. At this point, the approach of Roelvink is not concluded to be more correct, or vice versa. It is also not a goal to provide a recommendation concerning which method to use. The different resulting shorelines are depicted to stress the variation between them. Due to time constraints, in the remaining of this thesis only the method of Roelvink is used to calculate the diffracted breaking wave angles. This method makes use of a predefined transition zone edge like is described in section 4.3.

4.5.2. Influence offshore wave angle

To investigate the effect of the angle of incidence on the coastline evolution, model simulations are performed using different values for the offshore wave angle (figure 4.19). Since the CERC3 formulation is used, which assumes that the alongshore sediment transport is proportional to the sinus of the local breaking wave angle, a larger local breaking wave angle will result in a larger amplitude of the alongshore sediment transport. This is true for breaking wave angles from 0° to 45°, following the trend of a sinus function. However, such large breaking angles are not realistic in this simplified coastline situation because of refraction from offshore waves towards the coastline.

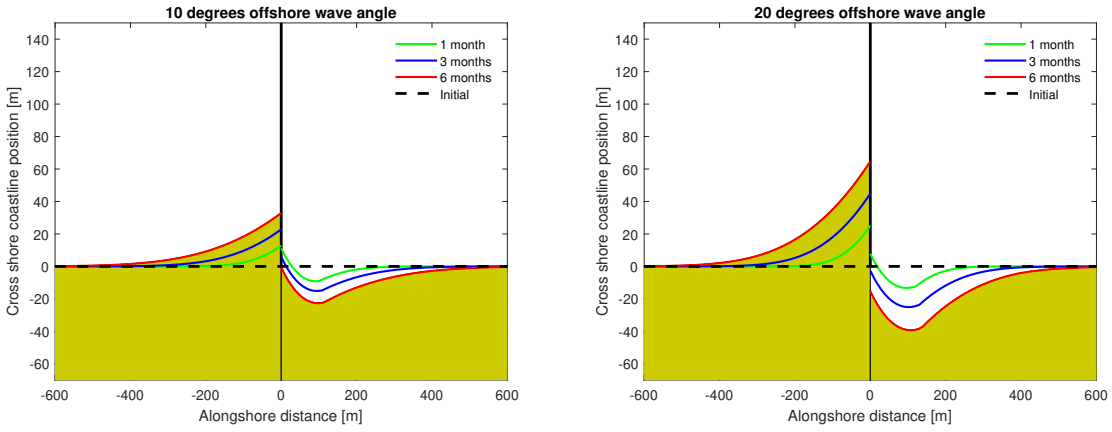

(a) $\phi_{\infty} = 10\,°$ (b) $\phi_{\infty} = 20\,°$

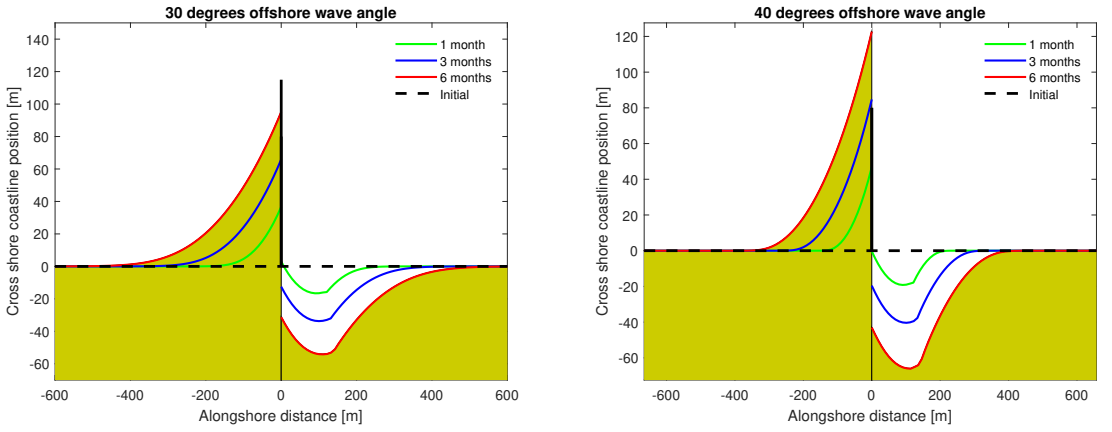

(c) $\phi_{\infty} = 30\,°$ (d) $\phi_{\infty} = 40\,°$

Figure 4.19: Shoreline evolution using different offshore wave angles

The axis of the scales in figures 4.19 are different, the coastline curvature and orientation are therefore a biased representation. A larger offshore wave angle demonstrated to result in a faster shoreline response at the updrift and downdrift part of the groyne. This is because the amplitude of the alongshore sediment transport is higher. The same was already concluded by Larson et al. (1987), as is stated in section 3.3.2.

A smaller difference between the wave height at the tip and undiffracted breaking wave height was needed to retrieve a smooth coastline development in the case of larger offshore wave angles. This is because the abrupt change in breaking wave height (figure 4.14a) together with a larger breaking wave angle results in a larger magnitude of discrepancy in alongshore sediment transport. Subsequently, the shoreline change is also showing an abrupt change. As time evolves, this abrupt change is smoothed out. However, taking much longer than in the case of a small offshore wave angle. This problem is solved by applying a shorter groyne, resulting in a smaller water depth at the groyne tip. The dynamic boundary is defined at the location of the tip of the groyne, therefore shifting landward.

In doing so, a smaller difference between the wave height at the tip and the breaking wave height is obtained. The water depth at the groyne reduced from 2.95 meters to 2.36 meters in the case of the 30° offshore wave angle, following the groyne length reduction from 160 meters to 115 meters and assuming a Dean profile. Considering the 40° offshore wave angle, a water depth of 1.86 meters at the tip was needed to prevent strange abrupt variations in the coastline development. In this last scenario, the seaward shift of the coastline position directly updrift of the groyne is exceeding the groyne tip. Meaning that sediment bypass definitely should have been incorporated there. Considering the 30° situation, bypass of sediment should have been incorporated as well because for the updrift section close to the groyne the cross-shore position of the breakerline will exceed the groyne tip location for sure.

The shoreline evolution for a 40° offshore wave angle while using the original water depth at the tip is showing unrealistic behaviour (figure 4.20a). It can be seen that while time proceeds, the abrupt coastline change at the edge of the transition zone is being reduced. However, still being significant even after 3 months of simulation time.

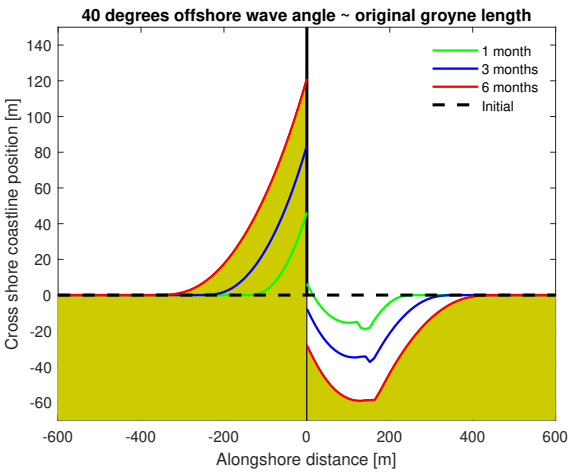

(a) Smoothing of abrupt shoreline change

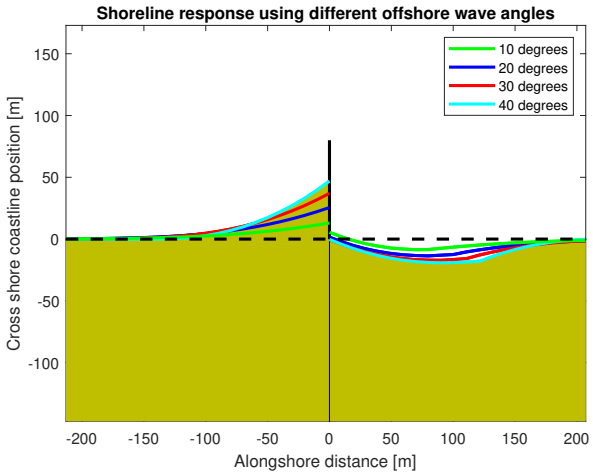

(b) Coastline response for different offshore wave angles

The shoreline evolution after 1 month concerning different incoming offshore wave angles is examined (figure 4.20b). In doing so, the groyne length is set equal to 80 meters, resulting in a groyne tip water depth of 1.86 meters. Subsequently, showing smooth coastline developments for each offshore wave angle that is used. The analytical solution of Pelnard-Considere (1956), described in section 3.3.1, stated that the coastline orientation at the groyne will develop in such away that it becomes parallel to the incoming wave crests. In other words, the local breaking wave angle becomes zero, providing zero sediment transport at the groyne. Each scenario shows a coastline orientation directly updrift at the groyne that evolves towards a new orientation. In doing so, the normal direction of the particular coastline section becomes equal to the offshore wave angle input. The axis of the figure 4.20b are set equal, therefore showing the coastline orientation correctly.

4.5.3. Influence offshore wave height

Changing the offshore wave height is expected to only influence the speed at which the shoreline evolves, thereby not affecting the curvature. To examine this, different model calculations are performed in which the offshore wave input is varying, all other parameters remain the same.

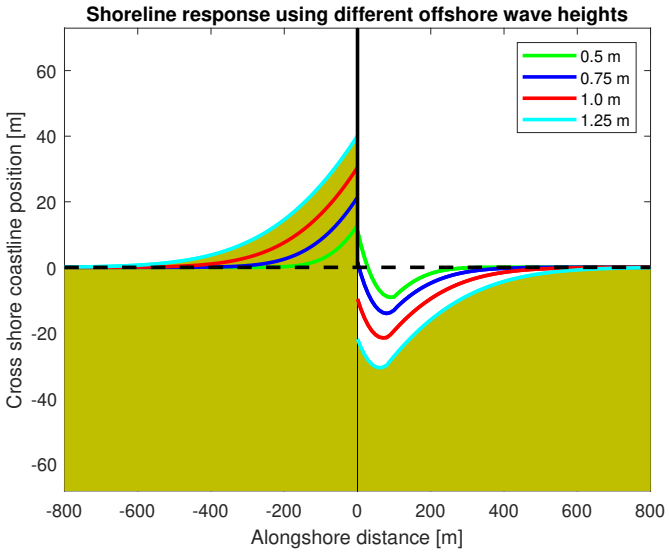

Figure 4.21: Coastline response after 1 month for different offshore wave heights

It is concluded that a larger offshore wave height indeed results in a faster shoreline response (figure 4.21). For the case of an offshore wave height of 0.5 meters, sedimentation downdrift of the groyne is still noticeable. Contradictory, the shoreline responses regarding the other three offshore wave heights show only erosion downdrift of the groyne. Furthermore, it could be seen that for the same downdrift alongshore coastline location the corresponding cross-shore position has retreated more when the offshore wave height is increased. The curve of the coastline is staying constant, being in line with the expectations.

4.5.4. Influence transition zone edge

Section 4.3 addresses on the definition of the transition zone edge. In this section, the results of the shoreline evolution using different variations of the predefined transition zone edge determined by the method of Roelvink are compared. The method of Roelvink establishes the transition zone edge based on a particular factor times the wavelength at the groyne tip, the original factor is 2.5 as suggested by Dabees (2000). Model runs are performed in which this factor is changed to 1, 3 and 5 respectively. The offshore wave angle, period and height are 10°, 8 seconds and 0.5 meters in each simulation.

The transition zone edge determines the area that is subjected to diffraction. Therefore, applying a larger transition zone width is expected to result in a larger downdrift area for which the breaking angles and wave heights are influenced by diffraction. However, that is not the only result of a larger transition zone width. Following the method of Roelvink, a larger transition zone will also affect the undiffracted angles heavier in terms of magnitude. In section 3.4.4, it is explained that the diffracted wave angles are calculated by adding a certain angle δ to the undiffracted angles. This δ is the angle between the shadow zone edge and transition zone edge (figure 3.18). A larger transition zone will result in a larger δ. Subsequently, more severe diffracted wave angles are obtained. Using a transition zone width equal to 5 times the tip wavelength, there is still a significant amount of sedimentation directly downdrift of the groyne visible (figure 4.22d). This is because δ is very large in that case, leading to diffracted wave angles being directed towards the groyne during a large part of the simulation.

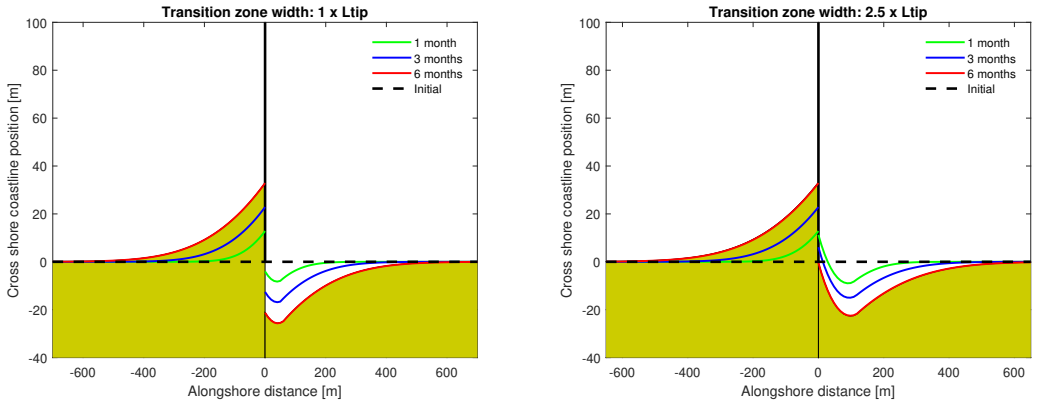

(a) Transition zone width : 1 x L_{tip}

(b) Transition zone width : 2.5 x L_{tip}

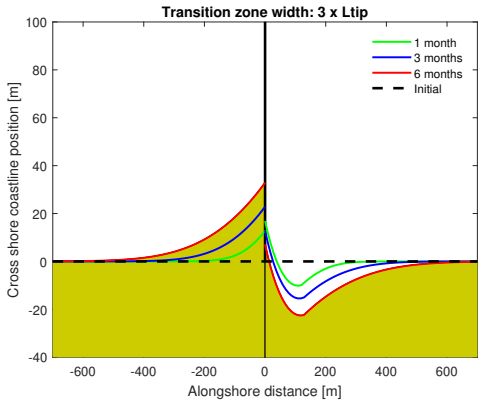

(c) Transition zone width : 3 x L_{tip}

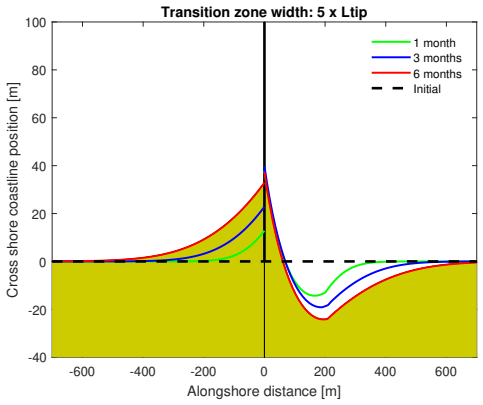

(d) Transition zone width : 5 x L_{tip}

Figure 4.22: Shoreline evolution using different transition zone widths

Increasing the transition zone width demonstrated to result in less erosion directly downdrift of the groyne (figure 4.22). Furthermore, the area that is subjected to erosion is shifted more downdrift of the groyne when the transition zone width is increased (figure 4.23). In the case of a transition zone width being equal to the wavelength at the groyne tip, (light blue line - figure 4.23), the effects of diffraction onto the shoreline shape are almost disappeared completely.

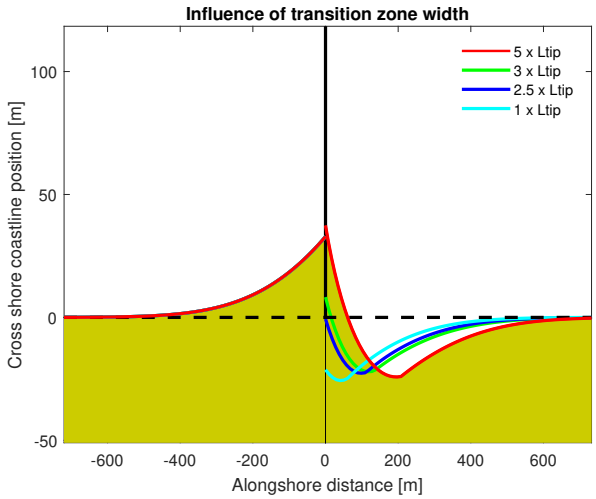

Figure 4.23: Coastline response after 6 months for different values of transition zone width

To elaborate on the influence of an increasing transition zone width, the breaking wave angles and heights are compared. The last point for which the angle is affected by diffraction is located more downstream when the width is increased. The location and value of this angle are depicted in figure 4.24. Furthermore, the angles are indeed heavier diffracted when a larger transition zone width is used. Here, a larger negative angle means that the waves are more diffracted towards the groyne. In each case, the diffracted wave angle at the transition zone edge is approaching the wave angle value at the groyne tip. In doing so, exceeding the undiffracted wave angle because of neglecting wave shoaling and refraction. Those angles are corrected as is described in section 4.3.2 (red dots change into green dots).

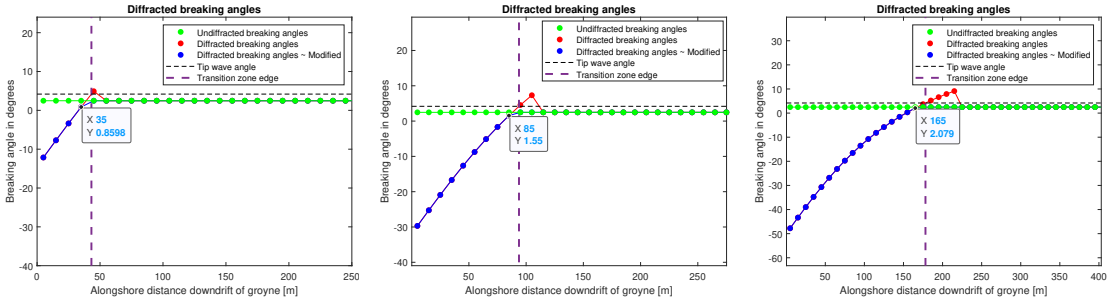

(a) Transition zone width: 1 x L_{tip} (b) Transition zone width: 2.5 x L_{tip} (c) Transition zone width: 5 x L_{tip}

Figure 4.24: Breaking wave angles for different transition zone widths

The diffracted wave heights are calculated using the method of Leont'yev (section 3.4.3). Following his equations, Q_s points having an angle θ (figure 3.18) larger than 30° will have a K_d value equal to 1. Increasing the transition zone width from 2.5 to 5 x L_{tip} does not result in different diffracted breaking wave heights (figure 4.25). The additional identified Q_s points have a θ value being large than 30°, hence resulting in a K_d value of 1 and subsequently result in diffracted breaking wave heights being equal to the wave height at the groyne tip. In other words, the additional identified Q_s points lie outside the transition zone edge that is implicitly described in the equations of Leont'yev (equation 3.42). For convenience, the difference between the last diffracted breaking wave height and undiffracted breaking wave height is because of neglecting wave refraction and shoaling from the groyne tip towards the breakerline.

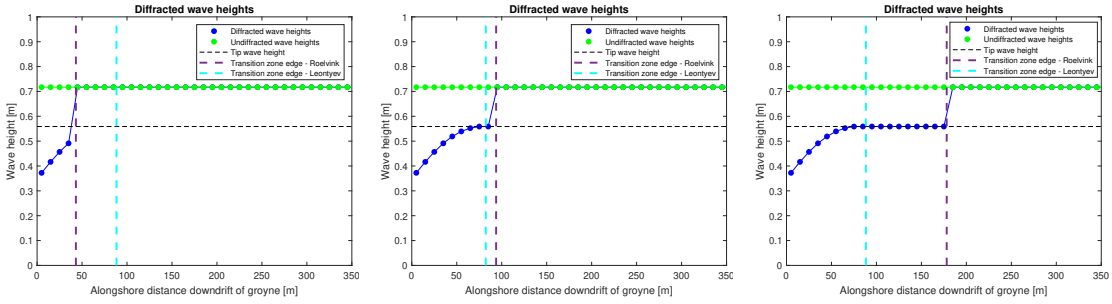

(a) Transition zone width: 1 x L_{tip} (b) Transition zone width: 2.5 x L_{tip} (c) Transition zone width: 5 x L_{tip}

Figure 4.25: Breaking wave heights for different transition zone widths

Applying a transition zone width equal to 2.5 x L_{tip}, the equations of Leont'yev result in a K_d that becomes 1 very close to the edge of this transition zone. Therefore, it could be conclude that applying Leont'yev in combination with the method of Roelvink while using a transition zone width equal to 2.5 x L_{tip} works well; the implicitly assumed transition zone edge according to Leont'yev is almost the same as the predefined transition zone edge calculated using the method of Roelvink (purple & light-blue lines figure 4.25b).

4.5.5. Influence angle δ

The angle between the shadow zone edge and transition zone edge is called δ (figure3.18). This angle δ is used to calculate the diffracted angles according to the relation stated in equation 3.43. Because δ is influencing the diffracted angle in a direct manner, it is expected that multiplying δ with a certain factor will influence the shoreline evolution significantly. The shoreline responses after 1,3 and 6 months while multiplying δ with different factors are examined (figure 4.26). All of the other input parameters remain constant.

Varying the factor in front of δ without changing the transition zone width is not logic from a physical point of view. This is because δ is determined based on the transition zone width itself. The method of Roelvink is established in such a way that the diffracted breaking angle at the transition zone edge is equal to the wave angle at the groyne tip. Applying a factor different than 1 in front of δ results in a diffracted angle being larger or smaller than the groyne tip wave angle at the transition zone edge (figure 4.28a and 4.28c). The sensitivity analysis of this factor in front of δ is performed to gain insight in the method of Roelvink.

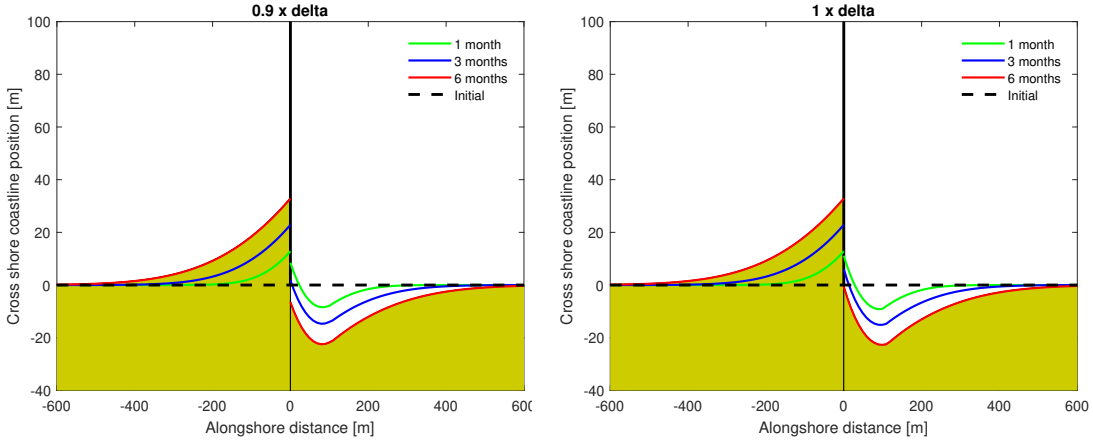

(a) 0.9 * δ

(b) 1 * δ

(c) 1.1 * δ

(d) 1.2 * δ

Figure 4.26: Shoreline evolution using different δ

Increasing δ demonstrated to result in less erosion or even more sedimentation directly downdrift of the groyne. A reason for this is that a larger δ value causes the diffracted angles to be more orientated towards the groyne. To highlight the effect of δ onto the shoreline response, the shorelines after 6 months are compared to each other (figure 4.27).

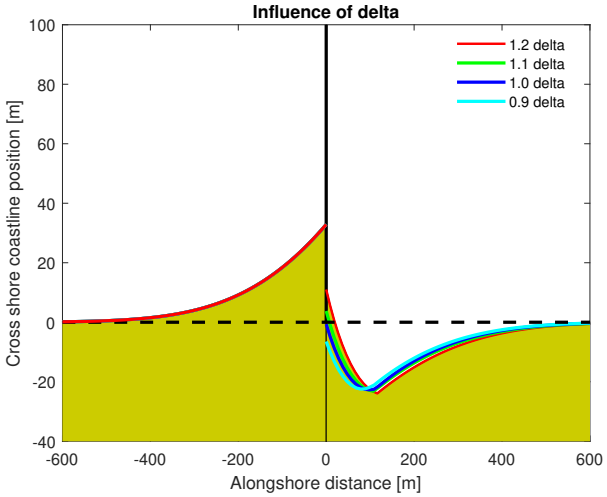

Figure 4.27: Coastline response after 6 months for different values of δ

The amount of downstream area affected by diffraction is concluded to remain constant while changing the factor in front of δ. This is contradictory to the effect of an increasing transition zone width (figure 4.23). Closely downdrift of the groyne, the influence of diffraction is increased significantly when increasing the factor in front of δ. This last observation was already concluded from figure 4.26.

The effect of δ onto the diffracted breaking angles is examined by calculating the angles while using different factors in front of δ inside the diffraction calculations (figure 4.28). The breaking wave height is not affected when changing this factor.

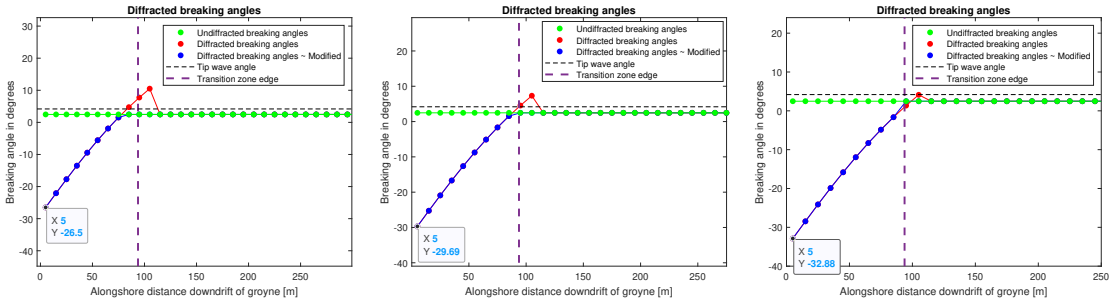

(a) 0.9 x δ (b) 1 x δ (c) 1.1 x δ

Figure 4.28: Diffracted breaking wave angles

Increasing the factor in front of δ indeed results in more strongly diffracted angles towards the groyne (displayed values in figure 4.28). Applying a factor smaller than 1 leads to a diffracted wave angle at the transition zone edge being larger than the tip wave angle (figure 4.28a). A diffracted angle smaller than the wave tip angle is obtained when using a factor larger than 1 (figure 4.28c). In each situation, modifications are performed; every point lying outside the transition zone has an undiffracted breaking angle. Besides that, the value of the first red-dot in figure 4.28a is set equal to the undiffracted value (green-dot) as is described in section 4.3.2.

5

Model validation

The validation of a new model, or in this case a new function, is a very important task. One should after all know if the results are reliable. Each numerical model is based on assumptions, therefore not being able to simulate a particular process with 100 % agreement to a real-world case. However, most of the time that is also not necessary. Especially, when modelling the coastline evolution for engineering purposes. Engineers are often interested in the development of the coastline shape over years to decades, therefore 100 % agreement to the truth coastline evolution is not crucial. The correctness of the established function described in chapter 4 is examined in this chapter. As a first check, the trend of breaking wave angle, breaking wave height and alongshore sediment transport are examined. Subsequently, the amount of sedimentation and erosion at the updrift and downdrift sides are investigated. Finally, the numerical shoreline is compared with the analytical solution described in section 3.3.2.

5.1. Evolution of wave height, angle and alongshore sediment transport

The main purpose of the improved shoreline model is visualizing a representative coastline evolution in the vicinity of a groyne. However, it is also interesting to see how wave parameters are being changed during the simulation. This section elaborates on the behaviour of the breaking wave height, wave angle and alongshore sediment transport while simulating the shoreline position. These parameters are investigated because they are established by the developed function for incorporating the effect of wave diffraction. Examination of these parameters fulfils as a first check regarding the correctness of the implemented procedure.

All of the figures in this section belong to the same shoreline simulation using an offshore wave height,angle and period of 0.5 meters, 20° and 8 seconds respectively (figure 5.1a). The red lines are the initial values and the black ones correspond to the final shoreline position after 2 years of simulation time. The other lines represent the intermediate values at different moments in time.

Breaking wave height

Updrift of the groyne a constant breaking wave height during the whole simulation is expected. This expectation is based on the the assumptions of a constant cross-shore profile and coastline parallel depth contours. In other words, the distance of a particular point of breaking to its corresponding coastline section remains constant while the shoreline is evolving. Assuming a simple dissipation model as is described in section 2.1.2, the breaking wave height is simply related to the breaking water depth via the constant breaker index γ. Consequently, implying a constant breaking wave height. However, very small variations in the updrift breaking wave heights are observed (figure 5.1b). These variations are caused by the assumptions that are made to retrieve equation A.11 for calculating the breaking water depth. If an iterative procedure is used instead of the calibration factor α to determine the unknown breaking parameters in equation A.11, the resulting breaking wave heights would be completely constant. However, this iterative procedure is not computational effective. Besides that, the variations are very small, in the order of millimeters, therefore not affecting the coastline response.

The breaking wave heights at the downdrift side of the groyne are following the trend of the K_d values (figure 5.1b). At the end of the transition zone, the breaking wave height shows an abrupt step towards the undiffracted wave height. This is caused by not taken into account the combined effect of wave refraction and shoaling from the groyne tip towards the breakerline. The value of the undiffracted breaking wave height is reached closer to the groyne in the beginning of the simulation: the red line is equal to the undiffracted breaking wave height at approximately 100 meters and the black line at 130 meters downstream. This is because the changing curvature of the coastline which affects the alongshore location of the shadow zone edge and therefore also the location of the transition zone edge. Consequently, after two years, more Q_s points are situated inside the influence area of diffraction compared to the situation at the beginning of the simulation.

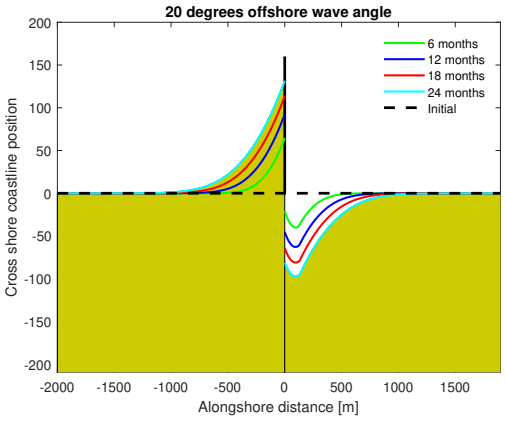

(a) Coastline evolution over two years

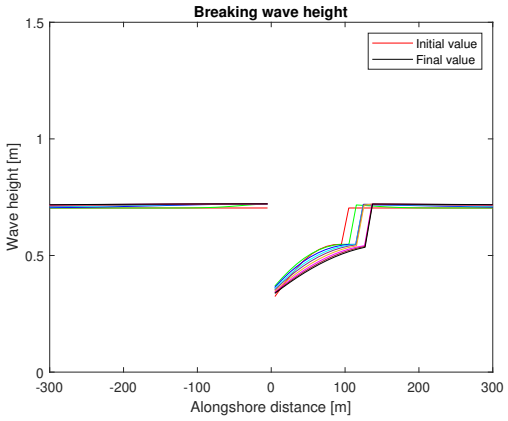

(b) Development of the breaking wave height as time proceeds

Figure 5.1: Evolution of shoreline and breaking wave height

Breaking wave angle

Initially, the coastline orientation relative to the North is everywhere equal to zero degrees. This means that the normal direction of a coastline gridsection is parallel to the North. The breaking angle with respect to the local coastline orientation is initially equal to roughly 5° along the whole coast, except in the area influenced by diffraction. Here the diffracted breaking wave angle is forced to a particular value, calculated using the approach of Roelvink. At the beginning of the simulation, the breaking angle relative to the coastline orientation is negative (red line - figure 5.2a). Because the incoming diffracted waves have initially a larger angle than the local coastline orientation, a negative local breaking angle is present. The shoreline directly downdrift of the groyne is rotating towards the incoming diffracted waves as time is proceeding. The difference between the local coastline orientation and angles of incoming diffracted waves is getting smaller. Therefore, reducing the local breaking wave angle (figure 5.2a).

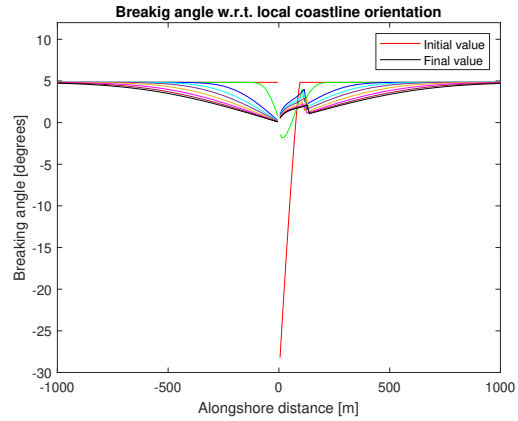

(a) Development of the breaking wave angle as time proceeds

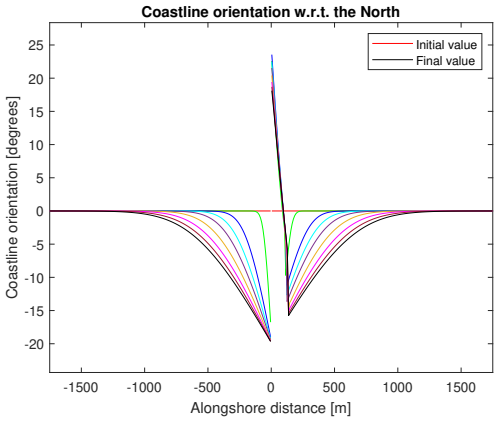

(b) Development of coastline orientation as time proceeds

Figure 5.2: Breaking wave angles and coastline orientation

Updrift of the groyne, the coastline is rotating towards the direction of the incoming waves, which is 20° from the North in this case (figure 5.2b). Directly downdrift of the groyne, the shore is rotating towards the direction of the diffracted angles. Moving more downstream, thereby leaving the area of diffraction, the coastline orientation is directed towards the offshore wave angels again. Going from the right boundary of the domain towards approximately 100 meters downdrift of the groyne it becomes clear that the coastline curvature wants to approach the angle of the incoming offshore waves but it is forced in an opposite direction because of diffraction (figure 5.2b).

Alongshore sediment transport
As explained before, the coastline evolution is dependent on gradients in the alongshore sediment transport. The presence of a groyne, blocking the entire transport, will create a gradient that lasts forever. Consequently, the coastline evolution will proceed infinitely, never reaching a stable shape. Initially, there is a stable coastline because the coastline is straight, wave forcing is constant and the groyne is not 'implemented' yet. At time t=0 the groyne is inserted, causing a sediment transport of zero at the location of the groyne (x=0). This affects the coastline positions of the two adjacent grid points, located directly downdrift and updrift. In the beginning of the simulation, the sediment transport is negative downdrift of the groyne (figure 5.3). This is caused by the trend of local breaking waves angles (figure5.2a). As time proceeds, going from the red to the black line, the effect of the groyne is felt over a larger area.

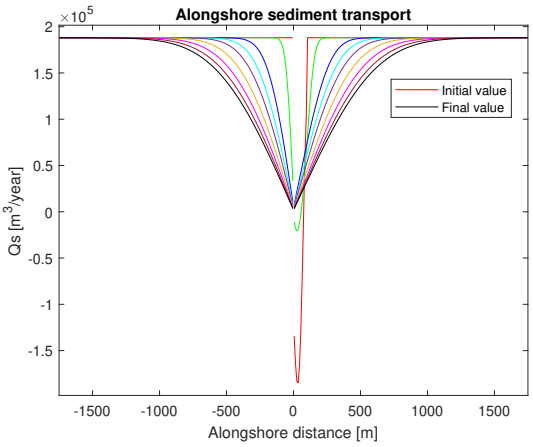

Figure 5.3: Development of the alongshore sediment transport as time proceeds

5.2. Conservation of sediment mass

To check whether the process of diffraction is implemented correctly, the amount of sediment mass inside the model domain is examined. It is known beforehand that the conservation of sediment mass should be hold during the whole simulation. In the case that wave diffraction is not taken into account, it is very simple to examine if the conservation of mass is valid. The amount of sedimentation updrift of the groyne should exactly be the same as the total erosion downdrift of the groyne. The boundaries of the model domain should not have any influence on the coastline evolution to achieve this conservation. This can be ensured by making the model domain sufficiently large enough. Meaning that the effects of the groyne are not felt at the begin and end boundaries of the model domain. The mass transport going into the model domain is than equal to the mass transport leaving the domain and therefore not affecting the mass volume inside the domain.

Firstly, the sediment mass conservation for the shoreline evolution without diffraction effects is investigated. In doing so, the shorelines retrieved using an offshore wave angle, height and period of 10°, 0.5 m and 8 s respectively are applied (figure 5.4a). Subsequently, the resulting shorelines for the same offshore wave input but with diffraction effects activated are used (figure 5.4b). In this way, it can be determined if the approach that is used to incorporate diffraction effects influences the conservation of sediment mass. The latter should not be the case of course.

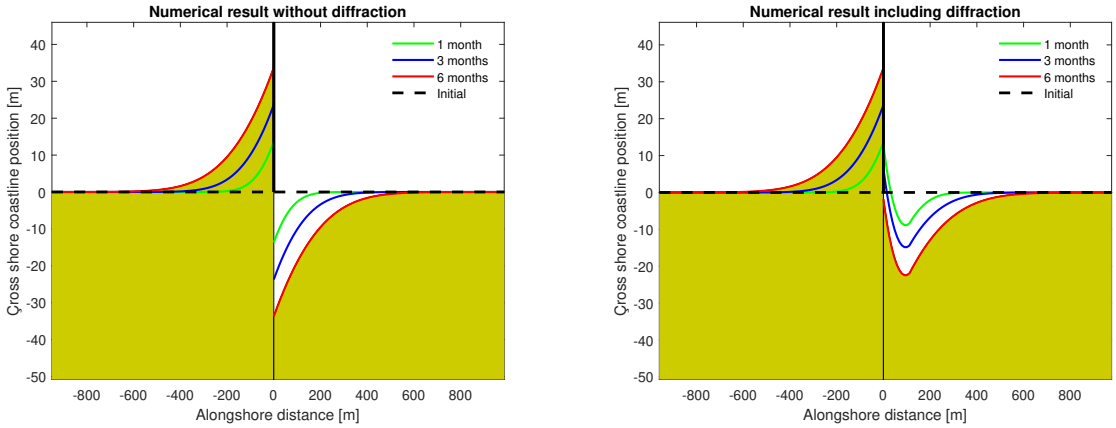

(a) Resulting shorelines without diffraction effects

(b) Resulting shorelines including diffraction effects

Figure 5.4: Resulting shorelines to be examined regarding the conservation of mass

Without diffraction effect, it is easy to check whether the amount of updrift sedimentation is equal to the downdrift erosion. Table 5.1 provides the calculated updrift and downdrift areas for the shorelines after 1,3 and 6 months (figure 5.5).

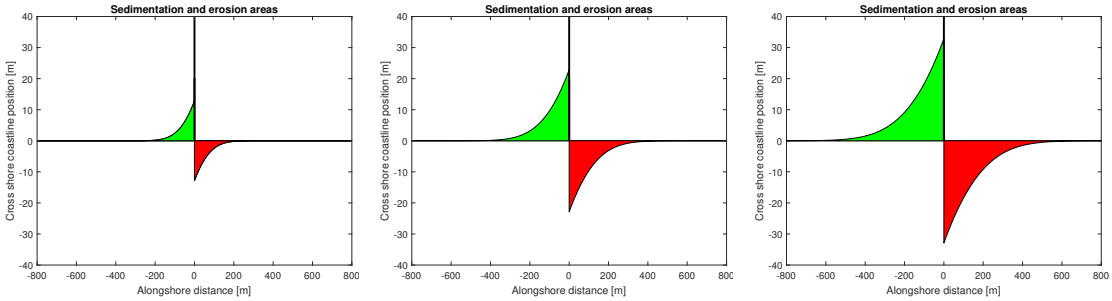

(a) 1 month

(b) 3 months

(c) 6 months

Figure 5.5: Conservation of mass without diffraction. Green: sedimentation. Red: erosion

	Updrift sedimentation	Downdrift erosion
1 month	831 m^2	831 m^2
3 months	2495 m^2	2495 m^2
6 months	5045 m^2	5045 m^2

Table 5.1: Sedimentation and erosion areas without the effect of diffraction

In the case of neglecting the effect of diffraction onto the coastline evolution, the conservation of sediment mass is concluded to remain valid as time proceeds (table 5.1). After applying the effect of diffraction onto the coastline evolution, sedimentation directly downdrift of the groyne could be present. The total amount of sediment mass should still be conserved, meaning that the amount of updrift sedimentation should equalize the *net* erosion downdrift (table 5.2). Net erosion depicts the eroded material reduced with the material that is accreted.

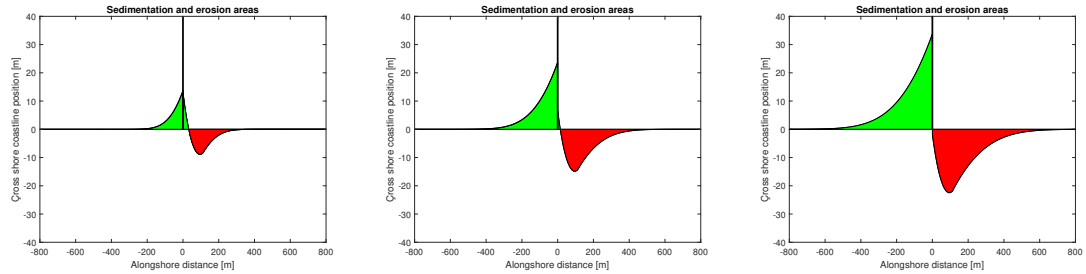

(a) 1 month (b) 3 months (c) 6 months

Figure 5.6: Conservation of mass including diffraction

	Updrift sedimentation	Downdrift sedimentation	Downdrift erosion	Net downwdrift erosion	Updrift & downdrift difference	Difference in %
1 month	831 m^2	189 m^2	1025 m^2	836 m^2	-5 m^2	0.6%
3 months	2495 m^2	46 m^2	2542 m^2	2496 m^2	-1 m^2	0.04%
6 months	5045 m^2	-	5044 m^2	5044 m^2	1 m^2	0.01%

Table 5.2: Sedimentation and erosion areas including the effect of diffraction

It is observed that a very small amount of mass is lost or added to the control volume while incorporating diffraction effects. However, the difference between the total updrift sedimentation and net downdrift erosion is so small that it is assumed to be insignificant. This small difference could be caused by the discretization of a strongly curved coastline. The updrift sedimentation is not affected when the effect of diffraction is incorporated This could be seen from the values of the first columns in tables 5.1 and 5.2.

5.3. Comparison with analytical solution

Section 3.3.2 contains analytical solutions regarding the shoreline change as a function of time (t) and location (x) including the effect of diffraction. This section utilizes the analytical solutions assuming a linear and exponential varying breaking wave angle inside the diffraction area which are retrieved from Larson et al. (1987). A detailed description can be found in the begin of section 3.3.2. The required parameter input of this solution is as follows:

- Q_0: Amplitude of the alongshore sediment transport
- $\phi_{br,undiff}$: Undiffracted breaking wave angle
- $\phi_{br,struct}$: Diffracted breaking wave angle at the structure
- D: Depth of closure
- B: Width of the shadow zone at the breakerline
- γ: Rate at which $\phi_{br,undiff}$ is reached

Q_0,$\phi_{br,undiff}$,D and B are simply retrieved from the ShorelineS model, their values are depicted in the table 5.3. This table provides an overview of the important parameters calculated using ShorelineS. Here $\phi_{br,undiff}$ is the undiffracted breaking wave angle for the initial straight coastline. A comparison is made between the analytical solutions and the numerical shorelines depicted in figure 4.19a.

5.3.1. Linear varying breaking wave angle

The breaking wave height at the structure, which is needed in the analytical solution, requires more attention because it is not directly calculated in the ShorelineS model. The diffracted angles are only determined for the Q_s points situated in the diffraction zone, as is described in section 4.4. A consequence of the applied boundary condition procedure, stated in section 4.2, is that there is no Q_s point located at the groyne. Therefore, the value of the diffracted breaking angle belonging to the first downdrift Q_s point is used in the analytical solution as being the diffracted angle at the structure. To establish an appropriate value for this breaking angle to be used in the analytical solution, first the development of the breaking angles downdrift of the groyne while simulating are examined (figure 5.7a). It is observed that the downdrift local diffracted breaking angles are initially strongly directed towards the groyne. While the model is simulating, the coastline is evolving in such away that it is adapting towards the direction of the diffracted angles. In other words, the diffracted breaking angle with respect to the normal of the local coastline orientation becomes smaller (figure 5.7a).

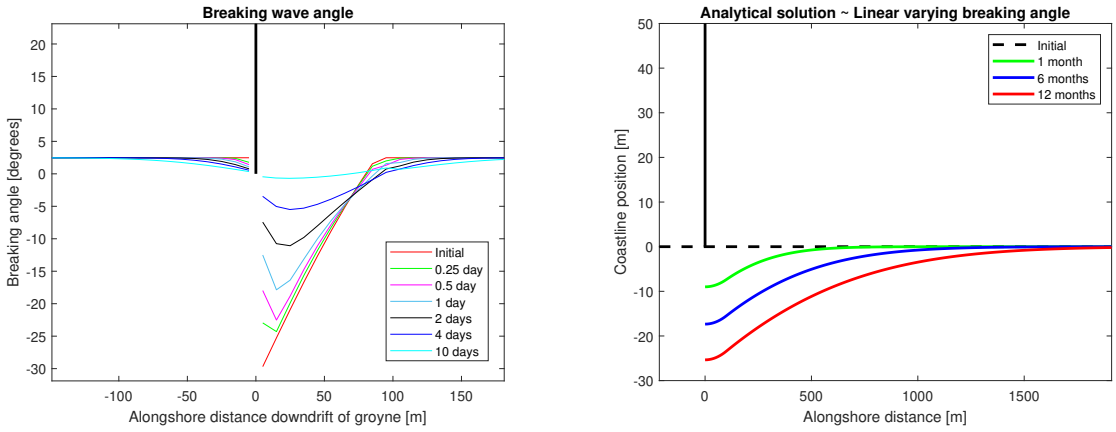

(a) Development of breaking wave angles

(b) Analytical soluting using $\phi_{br,struct}$=0

Figure 5.7: Shoreline evolution

After 10 days of simulation time, the local breaking angles near the groyne are already almost zero (figure 5.7a). Using a diffracted angle of zero at the structure inside the analytical solution, sedimentation downstream of the groyne is not observed (figure 5.7b). To realise sedimentation, thereby getting closer to the numerical result (figure 4.19a), the effect of the diffracted angle at the structure onto the resulting shoreline is examined.

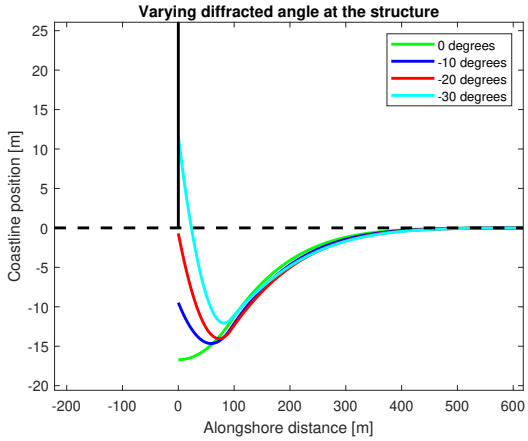

Figure 5.8: Shoreline response after 6 months for different values of the diffracted angle at the structure

When the angle at the structure becomes more negative, the amount of erosion directly downdrift of the structure is reduced. For a diffracted angle at the structure equal to -30°, even sedimentation is noticeable (figure 5.8).

The shape of the numerical and analytical results is quite similar (figure 5.9). However, it should be stressed that the diffracted breaking angle at the structure is chosen in such a way that the analytical result shows the most agreement to the numerical result. The values of the applied diffracted breaking angle are stated in table 5.3. Besides those angles, values of the other parameters needed inside the analytical solution are listed. Relevant parameters such as H_{tip} are provided in the same table for convenience. The maximum landward retreat of the coastline is approximately the same between the numerical and analytical results. However, this point of maximum retread is located further away from the groyne in the numerical results. Furthermore, the curvature of the more downdrift part is for both results exactly the same since this depends on the undiffracted breaking angles which are similar in both cases. The mentioned differences between the two results could be explained by the fact that the analytical solution assumes a linear varying diffracted breaking angle during the entire simulation, such behaviour is not present in the numerical results (figure 5.7a) Besides that, the analytical solution assumes a constant alongshore sediment transport. In doing so, the breaking wave height is implicitly assumed to be constant as well. The breaking wave heights in the numerical result are reduced using specific K_d values, therefore being far from constant.

ϕ_∞	H_∞	T_∞	D	h_{br}	$H_{br,undiff}$	$\phi_{br,undiff}$	Q_0	L_{groyne}	h_{tip}	H_{tip}	L_{tip}	ϕ_{tip}	B
10 °	0.5 m	8 s	10 m	0.99 m	0.72 m	2.48 °	295995 $\frac{m^3}{year}$	160 m	2.95 m	0.56 m	41.99 m	4.18 °	95 m
20 °	0.5 m	8 s	10 m	0.98 m	0.70 m	4.84 °	292504 $\frac{m^3}{year}$	160 m	2.95 m	0.55 m	41.99 m	8.26 °	104m
30 °	0.5 m	8 s	10 m	0.95 m	0.68 m	6.98 °	290904 $\frac{m^3}{year}$	115 m	2.36 m	0.55 m	37.83 m	10.91 °	103 m
40 °	0.5 m	8 s	10 m	0.91 m	0.65 m	8.79 °	286303 $\frac{m^3}{year}$	80 m	1.86 m	0.55 m	33.68 m	12.51 °	67 m

Table 5.3: Parameter values retrieved from ShorelineS model

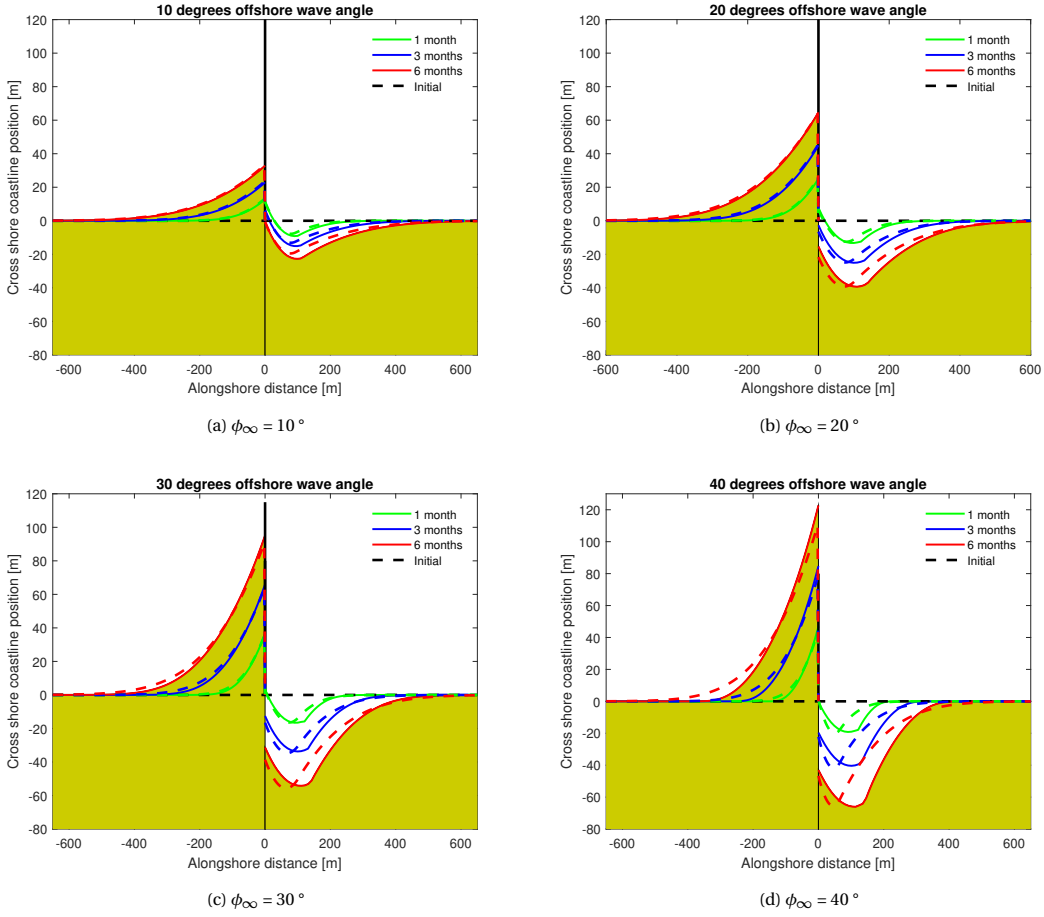

(a) $\phi_\infty = 10$ °

(b) $\phi_\infty = 20$ °

(c) $\phi_\infty = 30$ °

(d) $\phi_\infty = 40$ °

Figure 5.9: Comparison analytical (interrupted lines) and numerical solution, both including the effect of diffraction

The agreement between the numerical and analytical result is concluded to become worse when the offshore wave angle is increased. This is true for the updrift and downdrift side of the groyne. A reason for this is that the analytical solution described by Larson et al. (1987) assumes a small incident wave angle.

5.3.2. Exponential varying breaking wave angle

The analytical solution assuming an exponential varying breaking wave angle is only dependent on two parameters as is illustrated in equation 5.1. A coefficient γ, describing the rate at which the diffracted breaking wave angle approaches the undiffracted breaking wave angle, is used in this solution. First, the influence of this coefficient is examined since not much information concerning γ is provided by Larson et al. (1987). Using the parameters belonging to the scenario of an offshore wave angle of 10°, first row of table 5.3, the effect of different γ values is investigated. To do so, γ is expressed as a certain factor of the groin length (figure 5.10)

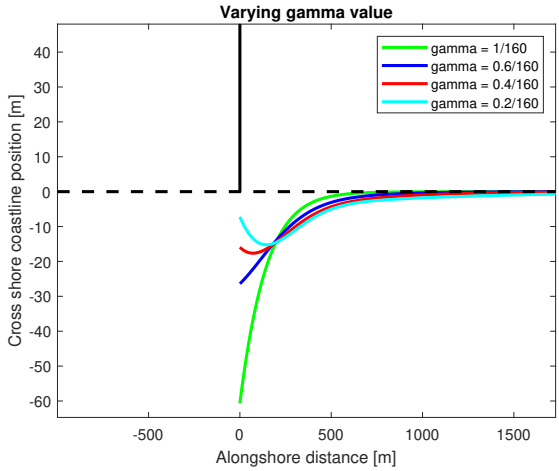

Figure 5.10: Shoreline response after 6 months for different values of γ

The resulting shorelines demonstrate that γ has a large influence on the coastline evolution (figure 5.10). Less erosion is visible for a decreasing γ value. Furthermore, a larger downstream area is affected by erosion when γ is decreased. The light blue line in figure 5.10 is staying below the initial coastline position, even at a downdrift distance of 1500 meters. Meaning that the coastline is eroding at that location. Using a value of 1/160, the green line, shows an eroded coastline until approximately 600 meters downstream of the groyne. Applying a γ value smaller than 0.2/160 would in this scenario lead to an unrealistic large downstream area affected by erosion and is therefore not visualized.

From equation 5.1, which is used in this analytical solution, it becomes clear that for a larger value of γ the diffracted breaking angle is approaching the undiffracted value at a location closer to the groyne. In other words, the area influenced by diffraction is decreased. The green line in figure 5.10 corresponds to a relative large γ value. Hence, the corresponding shoreline shape is hardly showing any effects of diffraction. It is concluded that a larger γ value, reduces the influence of diffraction effects onto the shoreline evolution.

$$\phi_{br,diff} = \phi_{br,undiff}\left(1 - e^{-\gamma x}\right) \tag{5.1}$$

According to this relation, the diffracted angle at the structure is equal to zero (x=0). Moving downstream from the groyne location, the diffracted angle will increase and approach the undiffracted breaking wave angle. While assuming a constant amplitude of the alongshore sediment transport Q_0, this trend of varying breaking angle will always result in a negative gradient of the alongshore sediment transport. Hence, when moving downstream of the groyne, more sediment is leaving than flowing into a particular area. Subsequently, only erosion effects are visible downstream of the groyne no mater what the value of γ is.

A comparison is made between the numerical and analytical results, this time assuming an exponential varying diffracted breaking wave angle (figure 5.11). In doing this, the particular γ values are used that resulted in the most matching shoreline responses.

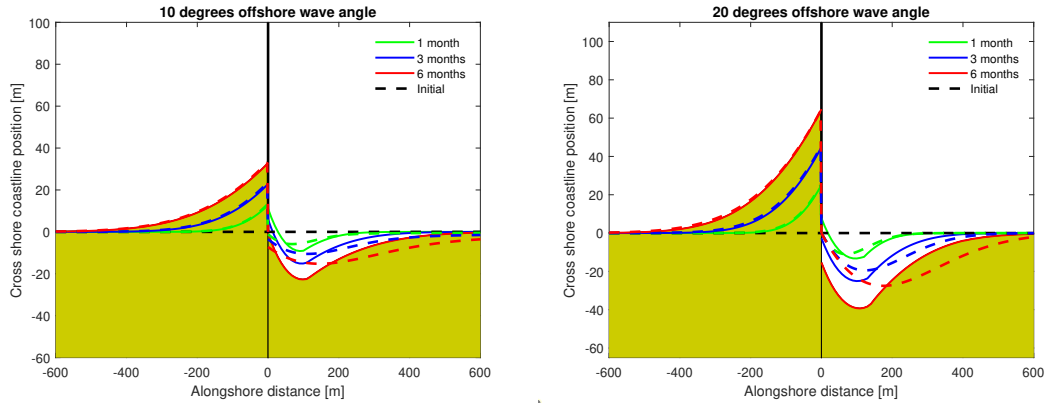

(a) $\phi_\infty = 10°$ & $\gamma = 0.2/160$

(b) $\phi_\infty = 20°$ & $\gamma = 0.001/160$

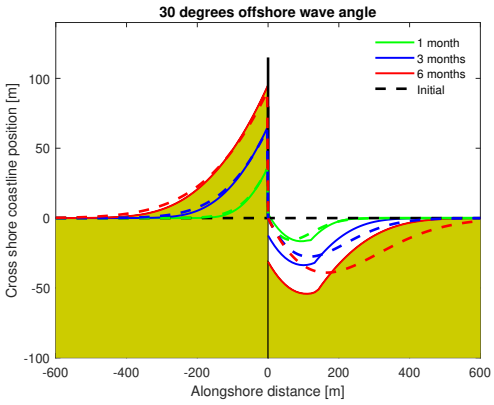

(c) $\phi_\infty = 30°$ & $\gamma = 0.001/160$

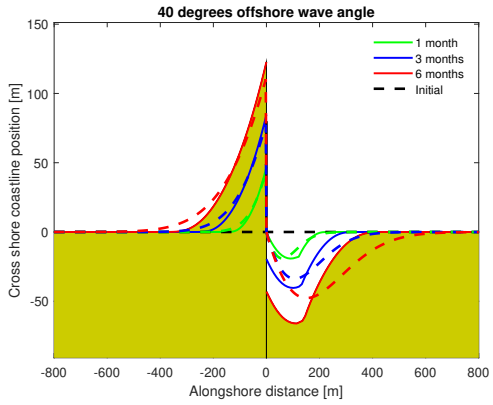

(d) $\phi_\infty = 40°$ & $\gamma = 0.001/160$

Figure 5.11: Comparison analytical (interrupted lines) and numerical solution, both including the effect of diffraction

It is demonstrated that the analytical solution assuming an exponential varying diffracted breaking wave angle does not match the numerical result. The curvature of the coastline and the amount of landward retread varies a lot between the numerical and analytical results (figure 5.11). Furthermore, sedimentation directly downdrift of the groyne could indeed not be modelled while using this analytical approach.

To conclude, it is shown that the breaking wave height, wave angle and alongshore sediment transport are evolving properly while simulating. No instabilities or numerical issues have been observed. Subsequently, the conservation of sediment mass is proven to remain valid while the effects of diffraction are taken into account. Finally, the numerical results are illustrated to be in line with the analytical solution using a linear varying diffracted breaking wave angle. From here on, the effects of diffraction onto the coastline evolution in the vicinity of a groyne are assumed to be implemented correctly inside ShorelineS. In the subsequent chapter, the improved model is applied to a real-world case.

6

Case study

The improved model is until this point only applied to a highly schematized situation. To be used for engineering purposes, the model should first be tested with real-world cases. In this chapter, the model results and field measurements of shoreline changes at Constanta, Romania are compared. First, a summary of the applied approach and an introduction to the case study is depicted. Subsequently, an overview of the most important model input and details of the application of the wave diffraction function are described. The model results are visualized in section 6.4. Finally, a discussion regarding the findings of this case study is provided.

6.1. Introduction

This section first contains the approach that is applied in this case study. Subsequently, background information of the Constanta case study is provided.

6.1.1. Approach

To apply and test the improved model onto the Constanta case study, the following approach is used:

1. Investigate wave data and bathymetry
2. Modify input wave data and establishing the boundary conditions
3. Perform model simulation without the effect of diffraction
4. Examine the calculated diffracted breaking wave heights and angles
5. Apply minor modifications to the model based on the test runs
6. Compare the numerical result and survey data
7. Calibrate the model to improve its performance

Section 6.2 contains relevant information regarding step 1 and 2. Intermediate results of the K_d values, breaking wave heights and breaking wave angles are depicted in section 6.3. Furthermore, this section elaborates on the application of the improved model regarding the coastline of Constanta. Finally, section 6.4 contains the resulting shorelines of Constanta while incorporating the effect of diffraction. Also, model calibration regarding the transition zone width is stated there.

6.1.2. Background

Constanta is a city situated in the South-East of Romania, lying at the coast of the Black Sea. It contains roughly 350.000 inhabitants and gives place to the biggest port of Romania. A large part of Romania's 240 km long coastline, adjacent to the Black Sea, is subjected to erosion. Therefore a project called *Protection and Rehabilitation of the Southern part of the Black Sea* exists which has the purpose to provide a coastal protection system to reduce the risks of erosion and potential floodings. Different works are involved in this project, for example, the construction of breakwaters, extension of existing groynes and the application of sand nourishments. In this thesis, the coastline section lying between two groynes and situated in the area labelled *Tomis South* is used as a case study. The shoreline position directly after finishing the construction works (figure 6.1b) will serve as the initial coastline position in the ShorelineS model. Section 6.2.2 elaborates further on this.

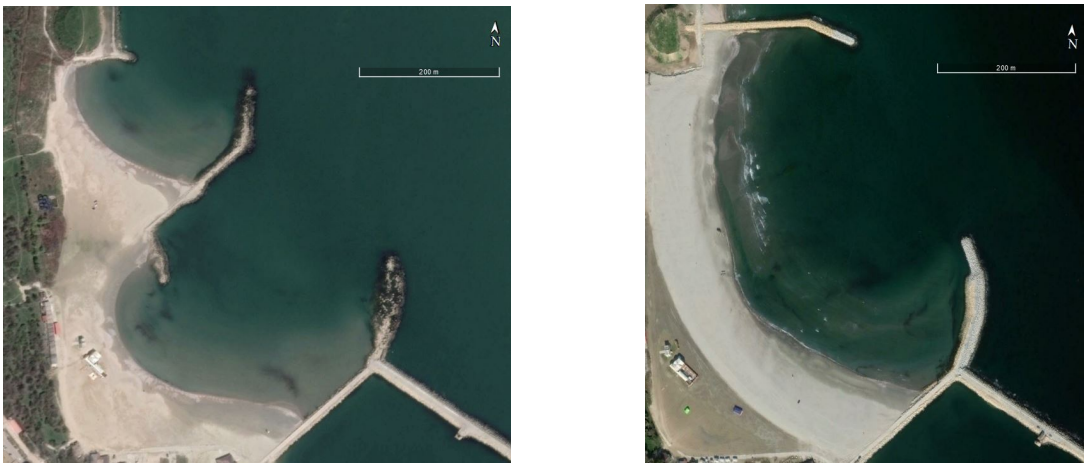

(a) Shoreline before the start of construction works (Google Earth, 11/2014)

(b) Shoreline after the removal of the old groynes ,the construction of new groynes and the artificial deposition of sand (Google Earth, 10/2015)

Figure 6.1: Coastline of Tomis South

This particular coastal cell is chosen because the observed coastline shape is not in line with the incoming wave direction (figure 6.2). Especially, the coastline area close to both groynes contradicts the expected shoreline shape based on the governing wave climate. Diffraction effects are suggested to be responsible for this. Section 6.2.1 addresses the wave data that is visualized in figure 6.2.1.

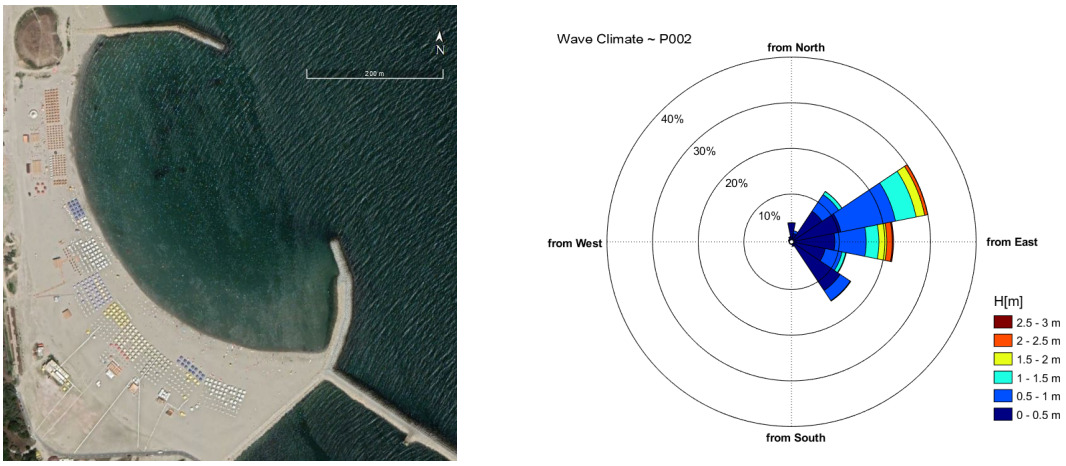

(a) Shoreline Tomis South (Google Earth, 11/2020)

(b) Wave heights and direction at location P002

Figure 6.2: Tomis South: Shoreline shape and wave climate

6.2. Model input

The following sections contain an elaboration of the wave input parameters and the bathymetry. Also, the schematization of the groyne structures is addressed. Furthermore, the influence of cross-shore processes to the coastline shape is briefly highlighted.

6.2.1. Wave data

To retrieve a realistic model result, the wave forcing should be in line with the actual incoming waves. The wave climate that will be used is established based on an offshore wave data set having data coverage from January 1990 till January 2020. First, discretization of the offshore data set has been performed. Subsequently, a limited number of representative offshore wave sets is established after investigation of the total data set. Those representative sets are used as boundary conditions inside the numerical wave model SWAN to transform the offshore waves towards the nearshore. The calculated nearshore wave parameters were validated against wave height measurements, obtained during the construction works from April 2013 until October 2015 (6.3b). Overall, the modelled and measured wave data showed good alignment, for higher waves the model slightly underestimates the incoming waves (Brandenburg, 2020).

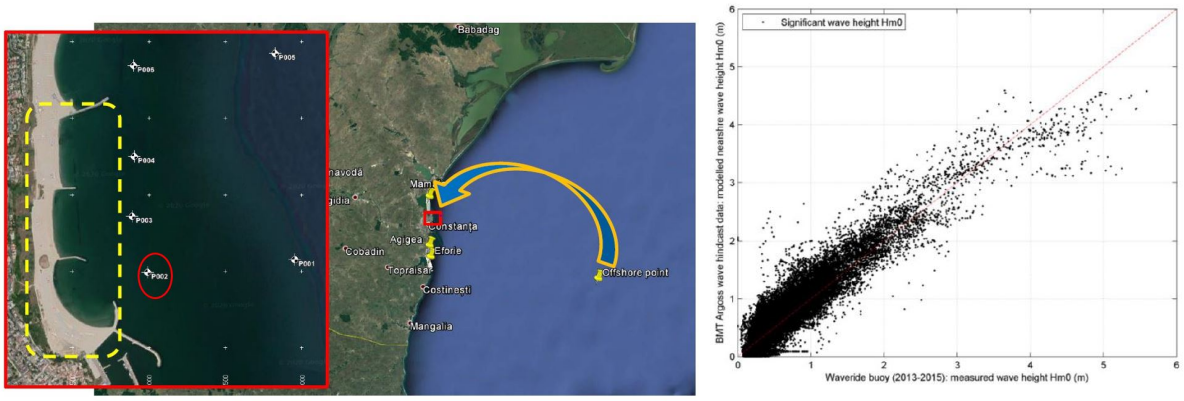

(a) Offshore wave buoy and nearshore location P002 (red circle)

(b) Relation between measured wave heights (x-axis) and modelled wave heights (y-axis)

Figure 6.3: Offshore wave transformation (Brandenburg, 2020)

This study uses the nearshore wave data set at location *P*002 (red-circle in figure 6.3a). It contains 12655 sets of wave data, consisting of values for the wave height, period and direction. Before the wave data is applied to the model, an investigation of the data is performed. Some data points are removed because they are believed to be the result of measurement errors. Moreover, zero values of data points are taken out. Wave conditions that are from a physical point of view not relevant for this case study are also removed. For instance, a wave with a direction equal to 280° with respect to the North has been removed because this wave would propagate away from the shore, causing difficulties while taking into account diffraction effects.

6.2.2. Bathymetry

Three bathymetric surveys are performed on 21th of September 2015, 23th of July 2016 and 29th of January 2020. Those moments are directly, 10 months and 4 years after completion of the construction works respectively. Each time a cross-shore single beam bathymetry survey was performed. The corresponding coastline contours were extracted from those bathymetric surveys. This thesis focuses only on the Southern beach cell of Tomis South (highlighted area - figure 6.4). The initial coastline input will be established based on the black contour line in figure 6.4. The data points of that contour line are modified due to numerical purposes. If necessary, points are added or removed, making the coastline more smooth to avoid numerical instabilities.

Figure 6.4: Coastlines in 2015 (black) ,2016 (blue) and 2020 (red). Red-highlighted coastline section: study area (Brandenburg, 2020)

The general trend of coastline evolution is an anti-clockwise rotation from 2015 to 2020 (figure 6.5). Furthermore, between the initial coastline and July 2015, the total shoreline is shifted in a seaward direction. Cross-shore processes are probably responsible for this behaviour. Section 6.2.4 elaborates further on this.

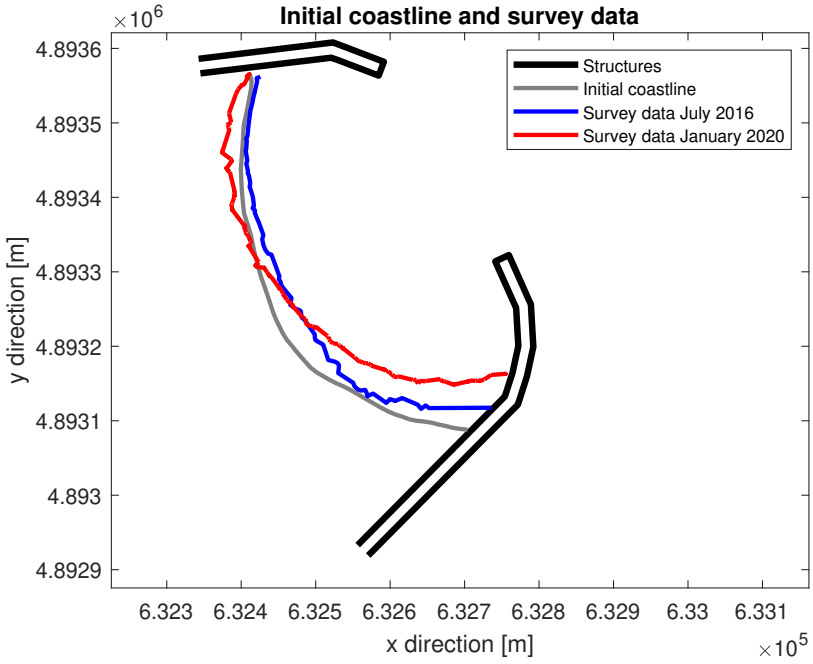

Figure 6.5: Initial coastline and survey data 2016 and 2020

6.2.3. Boundary conditions

The Southern beach cell of Tomis South consists of one coastline section being enclosed between two groynes. To satisfy the corresponding boundary conditions, the model grid points near the structures have been repositioned following the newly suggested approach (section 4.2.2). The shape of the two groynes is schematized into two straight lines (figure 6.6) while keeping the groyne tips at the same location. Therefore, the source terms from which the diffraction processes starts are positioned at the same locations as for the *real structures*.

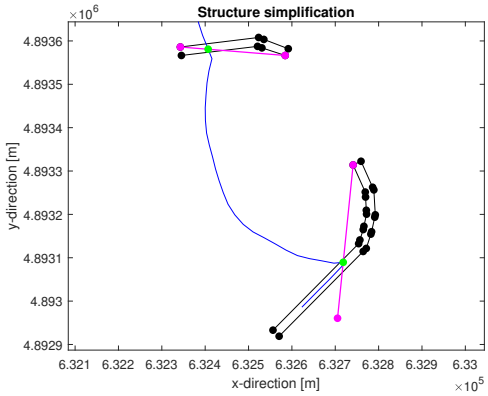

Figure 6.6: Simplification of structures. Purple line: groyne lay-out used inside the model. Green dot: First and last gridpoint

The boundary conditions belonging to a groyne should be forced upon the green dotted grid points. Section 4.2.2 contains the boundary conditions that are applied in this case study. The movement of the first and last grid points is determined by the value of the first and last Q_s point respectively. To make sure that the boundary grid points are not leaving the structure while simulating, special equations describing the movement of those grid points are developed. These equations are similar to those depicted in equations 4.1a and 4.1b. However, the coastline of Constanta is curved and the two groynes are not perfectly shore normal. Therefore, the displacement of the last and first grid point needs to be related to the geometry of the groynes with respect to the coastline orientation of the first and last coastline sections. Appendix C provides details about the grid point movement located at the Northern groyne. The same kinds of relations are also applied to the movement of the last grid point, which is situated at the groyne in the South.

6.2.4. Cross-shore processes

The bathymetry surveys from September 2015 and July 2016 suggest that the amount of sediment mass inside the control volume is not constant. The shoreline seems to evolve towards the sea along the whole coastline during that period. In other words, sediment is added to the control volume causing accretion along the coastline. After analyzing the cross-shore profiles in the beach cell, this was concluded to be due to cross-shore redistribution of sediment (Brandenburg, 2020). As this goes beyond the scope of this thesis, this is not further studied.

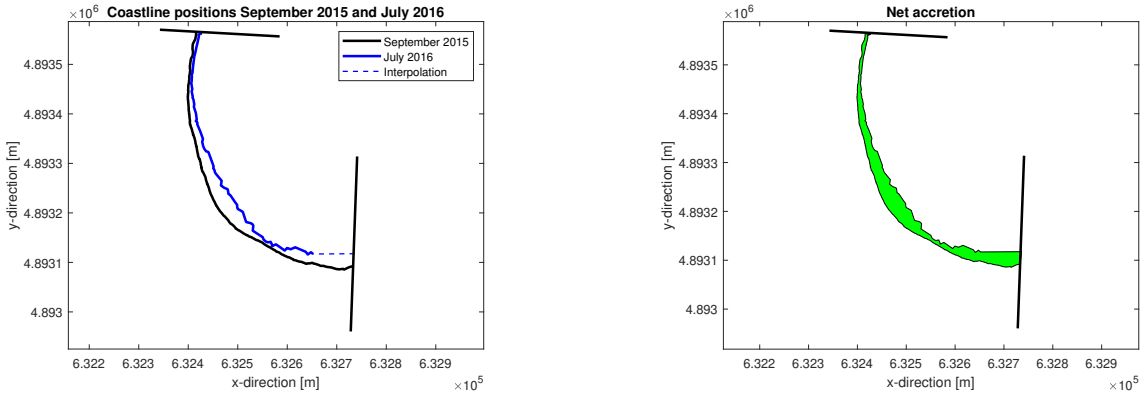

(a) Coastline in September 2015 and July 2016

(b) Added coastline area

Figure 6.7: Coastline accretion between September 2015 and July 2016

The coastline area highlighted in green, has a surface of 10.903 m^2 (figure 6.7b). This accretion has taken place during a time interval of approximately 10 months. The length of the coastline between the two groynes is equal to 348 meters. Using this length and time interval, results in a net accretion of 26 meter coastline per year. To compensate for the cross-shore redistribution in comparing shoreline positions, a nourishment rate of 26 m/year for the first 10 months is applied. Section C.3, stated in the appendix, provides the numerical result in the case of not applying artificial nourishment.

6.3. Diffraction

The diffraction of waves around the groyne tips is expected to influence the evolution of the considered coastal cell. This section contains additional information about the application of the diffraction function to the case study. First, the characteristics of the waves at the groyne tip are discussed. Subsequently, an elaboration regarding the transition zone width is provided. In the end, intermediate results of the calculated diffracted breaking waves and angles are highlighted.

6.3.1. Wave characteristics at the tip

The method of Roelvink is used to determine the diffracted breaking angles. Leontyev's method is applied for calculating the K_d values. Both methods are based on the wave characteristics at the groyne tip. A dynamic boundary is implemented at the same depth (i.e. 3.56 m) as the Northern groyne tip depth. The orientation of the dynamic boundary is set equal to the coastline orientation. A difficulty arose regarding the wave angle at the groyne tips. Because of the highly curved coastline shape, the local coastline orientation is varying significantly along the shoreline and so is the dynamic boundary. It was chosen to use the same wave data at location P002 as groyne tip wave characteristics of both groynes. In this way, it is not necessary to choose a specific coastline grid section for which its corresponding angle at the dynamic boundary contour is used as the angle at the groyne tip. In doing so, wave refraction and shoaling are neglected from location P002 to the points at the breakerline affected by diffraction. Wave heights and angles at points of wave breaking located outside the influence area of diffraction are calculated by incorporating wave refraction and shoaling effects. Those values are so to say the undiffracted values; values not being influenced by diffraction effects.

6.3.2. Identification Q_s points influenced by diffraction effects

To identify Q_s points that experience the effects of diffraction, first the shadow and transition zone are established. The determination of the transition zone edge required adaptations because of the curved coastline shape. In the schematized situation, the transition zone edge was established by a translation of the shadow zone edge in the alongshore direction. In this case study, the direction of this translation has been made variable for the two groynes, even though the wave angles at the groyne tips are the same. The transition zone edge of the groyne in the North is for each incoming wave angle larger than 20° determined using a translation in the y-direction. Smaller angels, which are only occurring a few moments in time, will enforce a translation in the x-direction. For the Southern groyne yields, if the incoming wave is smaller than 50° with respect to the North, the transition zone edge is calculated by translating the shadow zone edge in the x-direction (figure 6.8). In the case of angles larger than 50°, the translation is into the y-direction because the intersection of the shadow zone with the shoreline is then situated in the area of the coast being more parallel to the y-direction than to the x-direction.

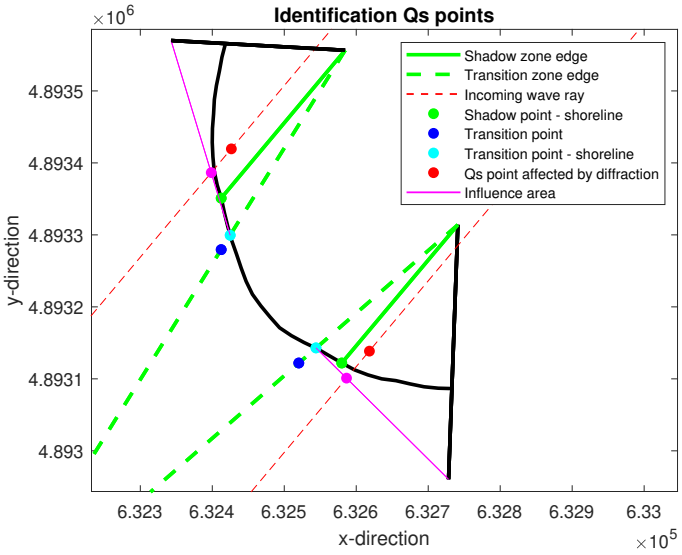

Figure 6.8: Identifying Q_s points (red-dots) affected by diffraction effects

Figure 6.8 visualizes the situation in which the transition zone of the Southern groyne is based on a translation in the x-direction (from green dot to dark-blue dot). For the same incoming wave angle, the edge of the transition zone in the North is based on a translation in the y-direction. If an incoming wave ray intersects one of the purple lines (figure 6.8), the corresponding Q_s point at the breakerline will be subjected to effects of diffraction. The light blue dot represents the intersection of the transition zone edge and the shoreline.

To check whether the process of identifying Q_s points situated in the area of diffraction is implemented correctly, test runs are performed for different wave angles at the tip (figure 6.9). The limits of the wave tip angles, which are from a physical point of view relevant in this case study, are 1° and 125° with respect to the North. In between those limits, different values of angles are chosen to test the procedure. For the 125° incoming wave, the transition point on the shoreline, a light blue dot, would be situated outside the model domain. If that is the case (figure 6.9d), the transition zone edge at the shoreline is set equal to the first coastline point, which is situated at the groyne. Besides the shadow zone and transition zone edges, also the breaker points lying inside those zones are depicted, using red dots. The purple dots are the intersections between the incoming wave rays and a line connected to the groyne and the edge of the transition zone at the shoreline.

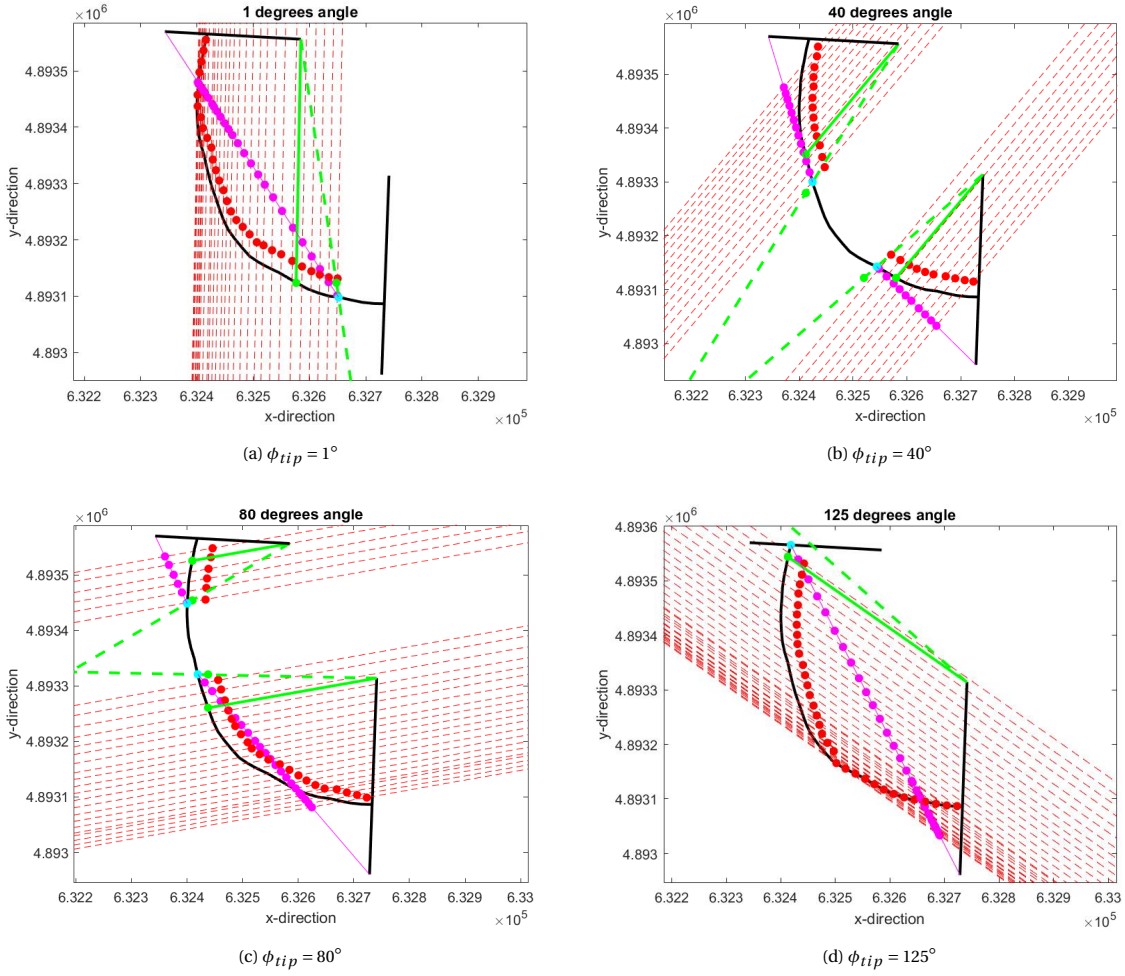

(a) $\phi_{tip} = 1°$

(b) $\phi_{tip} = 40°$

(c) $\phi_{tip} = 80°$

(d) $\phi_{tip} = 125°$

Figure 6.9: Identification of Q_s points (red-dots) inside diffraction area

6.3.3. Wave heights and angles

The following figures are depicted to elaborate on the calculation of the diffracted breaking wave heights and angles.

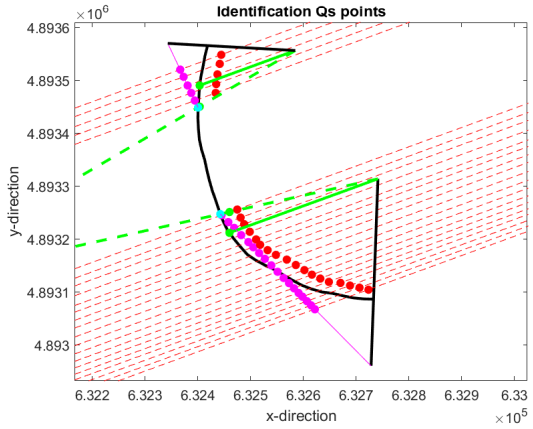

(a) Identification of Q_s points (red-dots)

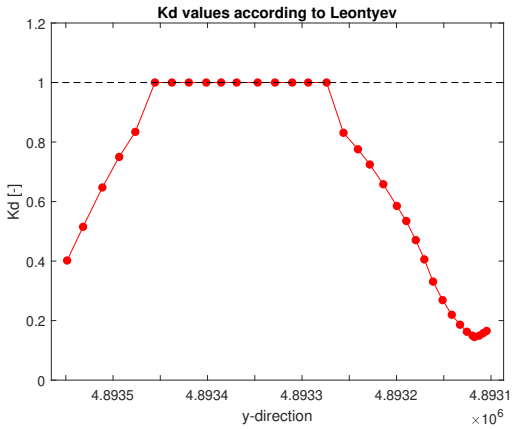

(b) Kd values

Figure 6.10: Identification of Q_s points and corresponding K_d values

The two groynes affect the breaking wave heights, with K_d values decreasing to approximately 0.4 and 0.2 for the Northern and Southern groyne respectively (6.10b). This results in reduced wave heights close to the groynes and unaltered wave heights in the middle of the coastline section (6.11a). Apparently, in this situation is the combination of the method of Roelvink and Leont'yev not resulting in a K_d value reaching the value of 1 at both transition zone edges. Therefore, showing a big step in the trend of K_d values when going from the last point inside the transition zone to the first point outside the transition zone. The transition zones, established by the method of Roelvink, are too small to reach a K_d of 1 at the edge. The existence of this problem was already addressed in chapter 4.3.

The diffracted wave heights demonstrated to properly follow the trend of the K_d values (figure 6.11a). When K_d is 1, the diffracted breaking wave heights are equal to the undiffracted breaking wave heights. The latter ones can be interpreted as the wave heights in the case there are no structures. Therefore, they are calculated without any shadowing or diffraction effects. The diffracted heights are established by multiplying the wave height at the tip with the K_d values. Hence, approaching the tip wave height at the edge of the transition zone (figure 6.11a). As mentioned before, wave refraction and shoaling from location P002 towards the breakerline are not incorporated inside the diffraction calculations. This produces the abrupt downward step, going from the last diffracted wave height to the first undiffracted wave height outside the transition zone (figure 6.11a).

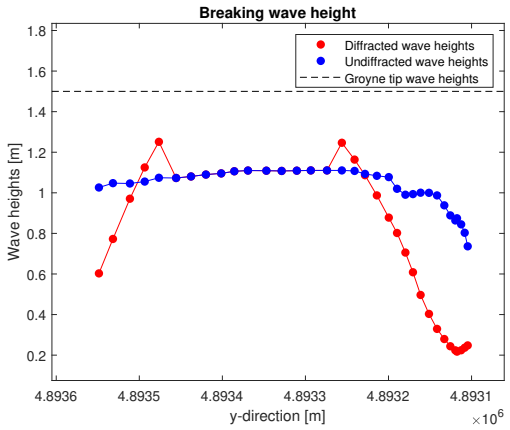

(a) Diffracted and undiffracted breaking wave heights

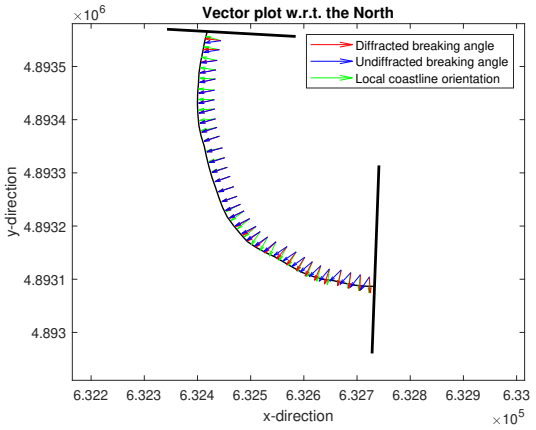

(b) Orientation of breaking wave angles and coastline orientation

Figure 6.11: Breaking wave heights and angles

Regarding the simplified scenario, described in chapter 4, this abrupt step was in the upward direction (figure 4.14a). This contrast between the two cases is caused as follows. For the simplified scenario, multiple test runs demonstrated that the combined effect of refraction and shoaling increases the wave height from the groyne tip towards the breakerline. Contradictory, model results showed that the combined effect of refraction and shoaling decreases the wave heights when waves propagate from location P002 towards the shore in the Constanta case study. This opposite effect is due to the completely different coastline shapes (straight vs curved).

After examining the shoreline response, it was concluded that the abrupt downward step in breaking wave heights was not causing instabilities in the shoreline evolution. Applying a realistic wave climate in the Constanta case study, caused a varying location and magnitude of this abrupt downward step during the simulation. In doing so, preventing instabilities in the coastline evolution. For the simplified case, the abrupt upward step was causing instabilities in the shoreline evolution (figure 4.20a). A constant wave forcing will lead to an abrupt step in breaking wave heights situated at the same location. Therefore, an initial small disturbance in coastline evolution will grow, causing instabilities in the shoreline.

From a physical point of view, diffracted wave heights exceeding their corresponding undiffracted values is incorrect. Wave heights in the lee of a groyne should not exceed the wave height that would be present at the same locations while pretending there is no structure. However, the breaking wave heights are expected to not influence the curvature of the coastline shape (results chapter 4). Furthermore, the coastline response demonstrated to develop smoothly. Therefore, it is concluded to make no adaptations to the diffracted wave heights, even though they are not completely in line with theory.

The diffracted breaking angles require modifications in particular cases. Those modifications are performed because the diffracted angles demonstrated to have a large influence on the resulting coastline shape (results chapter 4). Since wave diffraction results in the bending of waves into the lee side of a groyne, the diffracted breaking angle should always be more orientated towards the structure than the corresponding undiffracted breaking angle. The later one is calculated while pretending their is no structure, so established by accounting for shoaling and refraction of waves propagating from location P002 towards the breakerline. Since those two processes are not incorporated inside the diffraction calculations, it could be that the undiffracted angle is orientated more towards the groyne than the diffracted angle. If that is the case, it is chosen to use the undiffracted breaking angle inside the alongshore sediment transport calculation. Consequently, wave diffraction effects will only result in diffracted angles being equally or more orientated towards the groyne compared to their undiffracted values. In doing so, the effect of the bending of wave towards the groyne caused by diffraction is modelled. Figure 6.11b visualizes the orientation of the local coastline, the undiffracted breaking angle and diffracted breaking angle, all with respect to the North. If the diffracted angle is not visualized for a certain point while it is situated in the diffraction zone, it means that the undiffracted breaking angle is used in the sediment transport calculations. Appendix C contains the intermediate results of the K_d values, breaking wave heights and breaking angles corresponding to the situations depicted in figure 6.9.

6.4. Results

This section contains the model results of the coastline evolution. To stress the model improvement, first the resulting shorelines without the effect of diffraction effects are visualized. Subsequently, the numerical results incorporating diffraction effects in the vicinity of the groynes are shown. Multiple model results are performed in which the amount of wave diffraction influence onto the shoreline evolution is increased.

6.4.1. Excluding diffraction effects

The shoreline evolution without accounting for diffraction effects is investigated first (figure 6.12). The alongshore sediment transport of the coastline area inside the shadow zone is set equal to zero by the model. The artificial nourishment rate, described in section 6.2.4, is incorporated.

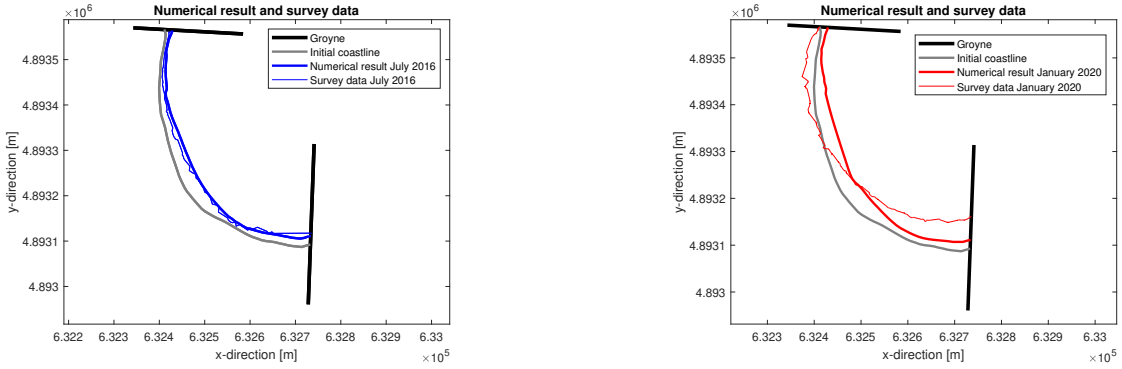

(a) Shoreline shape July 2016

(b) Shoreline shape January 2020

Figure 6.12: Comparison numerical result without diffraction and survey data

The behaviour of an overall anti-clockwise rotation of the coastal cell is not observed in the numerical data. However, the coastline change between September 2015 (initial coastline) and July 2016 is simulated properly (figure 6.12a). Incorporating diffraction effects seems not to be essential for simulating a representative shoreline evolution during this period.

6.4.2. Including diffraction effects

Subsequent to neglecting wave diffraction, the shoreline evolution while accounting for diffraction effects is investigated. The numerical and survey data of July 2016 demonstrated to almost match perfectly (figure 6.13). The data of January 2020 is showing less agreement. In the latter case, the survey data is showing a more pronounced anti-clockwise rotation of the shoreline position than the numerical result is visualizing. The next section contains a model calibration to retrieve a better matching result.

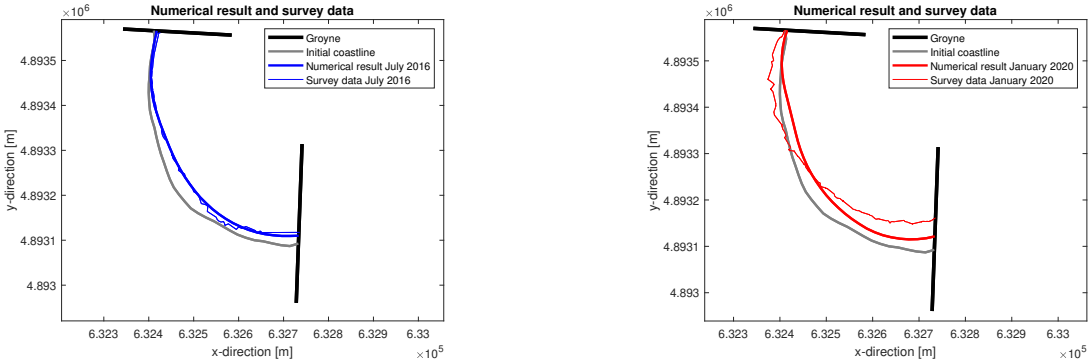

(a) Shoreline shape July 2016

(b) Shoreline shape January 2020

Figure 6.13: Comparison numerical result and survey data

6.4.3. Model calibration

Diffraction in ShorelineS is influenced by the width of the transition zone. For a larger transition zone width, the effects of diffraction are more pronounced (section 4.5.4). To examine if a larger influence of diffraction leads to a better matching result, model runs are performed in which the width of the transition zones is increased. This width could differ for each groyne separately.

	Northern groyne	Southern groyne
scenario A	3.25 x L_{tip}	2.75 x L_{tip}
scenario B	3.75 x L_{tip}	3 x L_{tip}
scenario C	4 x L_{tip}	3.25 x L_{tip}
scenario D	4.5 x L_{tip}	3.75 x L_{tip}

Table 6.1: Transition zone widths, represented as a factor of the wavelength at the groyne tip

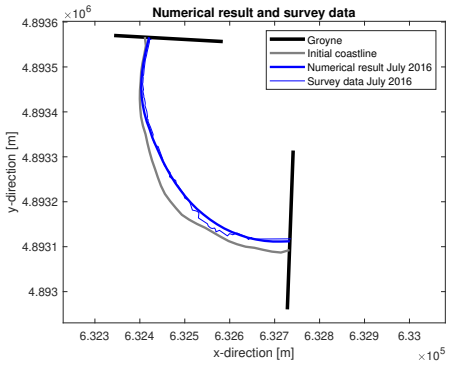

(a) Shoreline shape July 2016

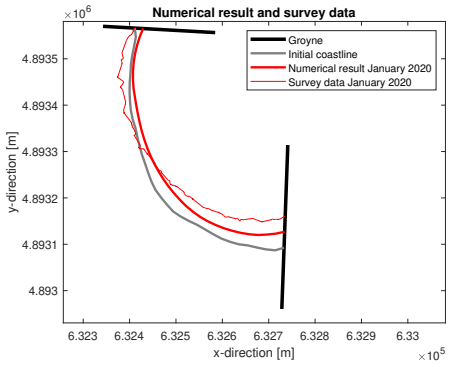

(b) Shoreline shape January 2020

Figure 6.14: Scenario A: Comparison numerical result and survey data

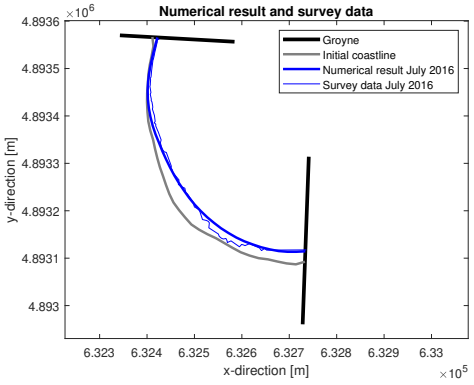

(a) Shoreline shape July 2016

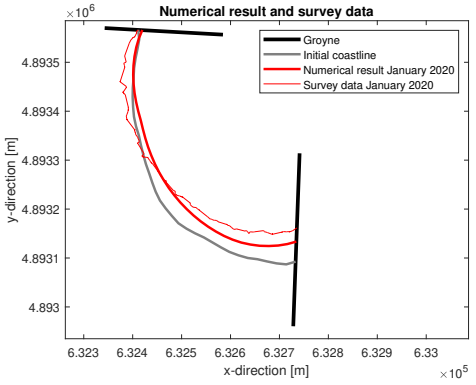

(b) Shoreline shape January 2020

Figure 6.15: Scenario B: Comparison numerical result and survey data

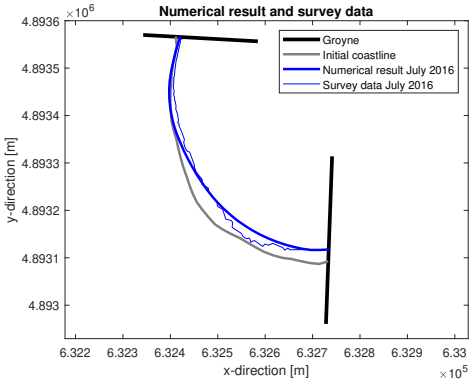

(a) Shoreline shape July 2016

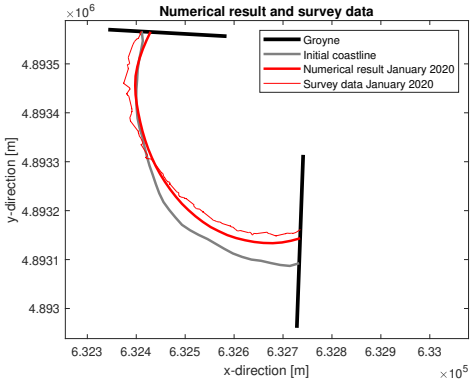

(b) Shoreline shape January 2020

Figure 6.16: Scenario C: Comparison numerical result and survey data

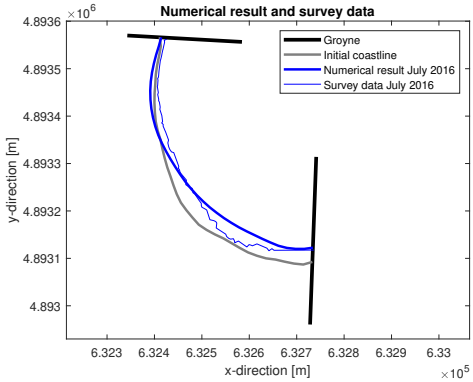

(a) Shoreline shape July 2016

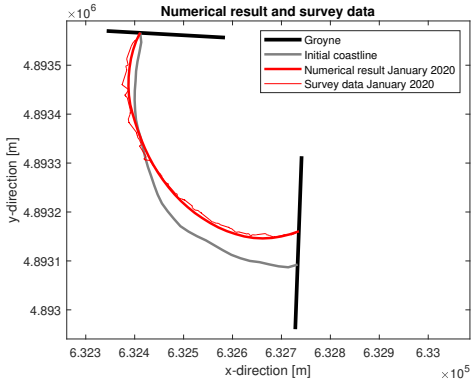

(b) Shoreline shape January 2020

Figure 6.17: Scenario D: Comparison numerical result and survey data

It is observed that increasing the transition zone width indeed leads to an increase of the influence of diffraction onto the shoreline evolution. A more anti-clockwise rotation is retrieved when the width of the transition zone is getting larger. This results in more agreement between the numerical and survey data of January 2020. However, the numerical result and survey data from July 2016 is showing less agreement when the transition zone width is increased. It was already stressed (section 6.2.4) that cross-shore process play a role during the period from September 2015 to July 2016. Those processes could have exceeded the diffraction effects, therefore counteracting the anti-clockwise rotation of the coastal cell.

The K_d values and breaking wave heights, before and after calibration are examined to provide more details regarding the effect of calibration (figure 6.18).

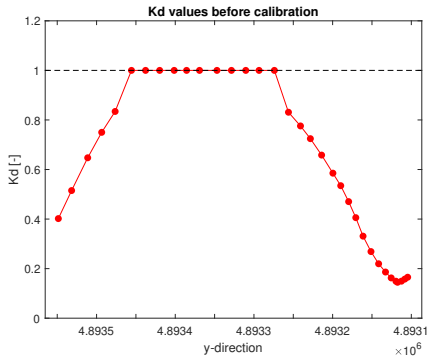

(a) K_d before calibration

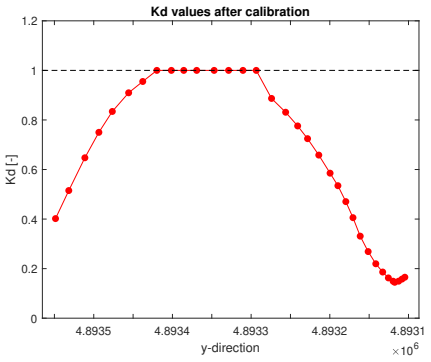

(b) K_d after calibration

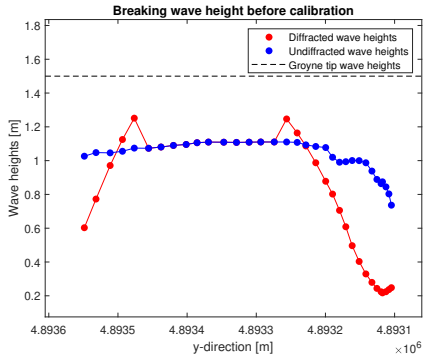

(c) Wave height before calibration

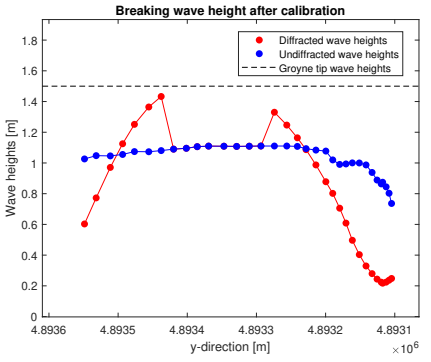

(d) Wave height after calibration

Figure 6.18: Effect of calibration onto the K_d values and diffracted breaking wave heights

For the Northern groyne, two additional K_d values being different from 1 are visible after calibration (figure 6.18b). In other words, two more Q_s points are identified to be influenced by diffraction effects. Regarding the Southern groyne, one extra Q_s point subjected to diffraction is established. After calibration, the development towards a K_d value of 1 is more smooth for both groynes, especially for the Northern groyne. Because the additional diffracted breaking wave heights, the wave height at the transition zone edge is getting closer to the wave height at the groyne tip (figure 6.18d).

Besides the calibration effect on the breaking wave heights, the effect on the breaking wave angles is also demonstrated. Each breaking angle situated in the transition or shadow zone of a groyne is diffracted more towards the particular groyne after calibration. This effect is clearly visible in the zoomed-in situation (figure 6.19b).

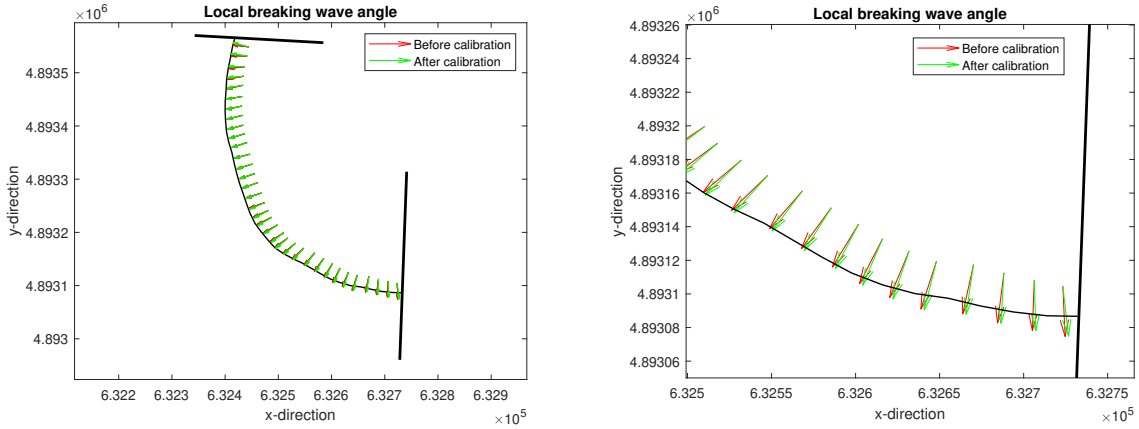

(a) Total coastline

(b) Southern groyne coastline section

Figure 6.19: Local breaking wave angle before and after calibration

To highlight the calibration effect, the coastline change observed in the survey data is compared to the numerical coastline change before and after calibration (scenario D) respectively (figure 6.20). The coastline change in the normal direction of each grid section between September 2015 and January 2020 is used.

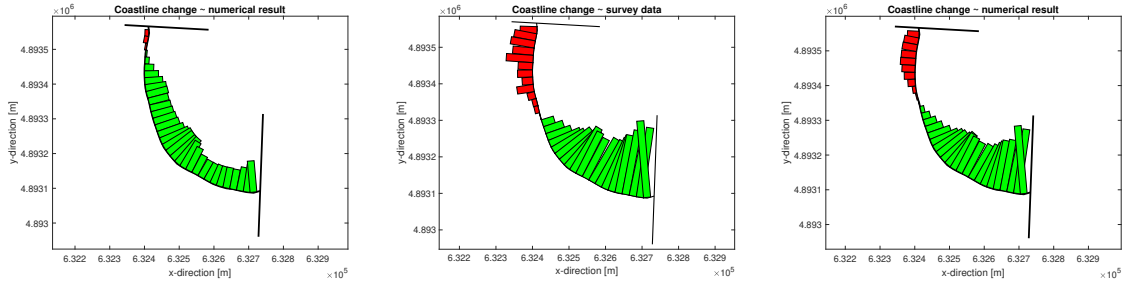

(a) Before calibration

(b) Survey data

(c) After calibration

Figure 6.20: Coastline change September 2015 - January 2020. Green bars: change in seaward direction. Red bars: change in landward direction

Calculation of the root mean square error (RMS error) and bias is performed to stress the calibration effect in a quantitative manner. The RMS error could in this case be interpreted as a measure of the amount of variation regarding the difference between the observed and modelled coastline change. A lower value means that this difference is more evenly distributed along the coastline. The bias is the mean value of the difference between the observed and modelled coastline change. Both parameters are significantly decreased after calibration (figure 6.21). Therefore, indicating that the numerical result and survey data are better matching when the transition zone width is increased.

An overview of the RMS error and bias belonging to different model simulations performed while calibrating the model, is provided in table 6.2 stated at the end of this chapter. The same kind of figures as 6.20 and 6.21, belonging to scenario A, B and C are stated in Appendix C.

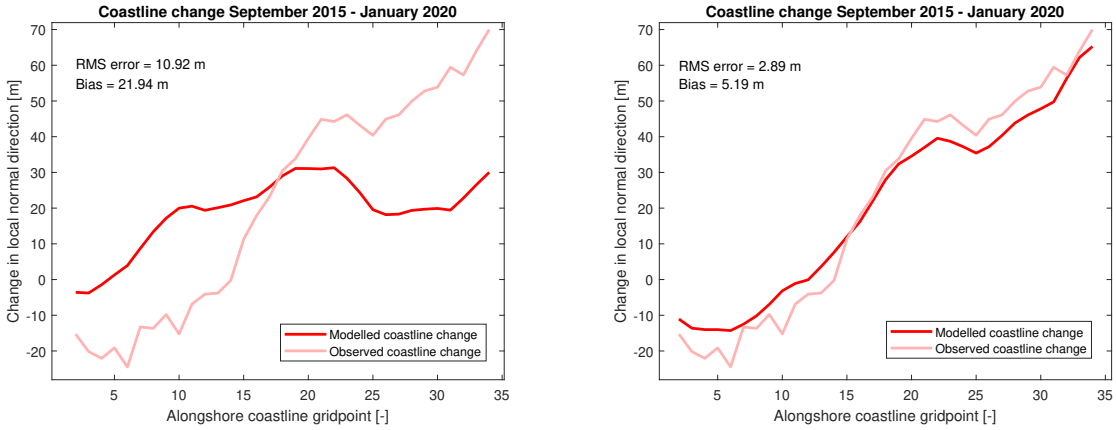

(a) Before calibration

(b) After calibration

Figure 6.21: Root mean square error and bias

The transition zone width is concluded to be an important parameter inside the diffraction calculations. After increasing this width of the Northern and Southern groyne by a factor of 1.8 and 1.5 respectively, the model performance increased significantly (figures 6.20 and 6.21). The initial value of the two zones was based on Dabees (2000), thereby following the method of Roelvink. Apparently, the suggested value of 2 to 3 times the wavelength at the tip is in this case study not sufficient. The long groynes provide shelter to a larger part of the shoreline than is suggested by Dabees (2000). In other words, the wavelength at the tip is not sufficient large enough to create a representative transition zone area when following the method of Dabees (2000) in this case study. To put this conclusion in a wider perspective, section 6.5 provides a discussion of the model results.

6.4.4. Comparison results excluding and including diffraction effects

To emphasize the effect of the improved model, a comparison is made between the numerical results excluding and including diffraction. The following figures contain the resulting shorelines, coastline change, the root mean square error and bias.

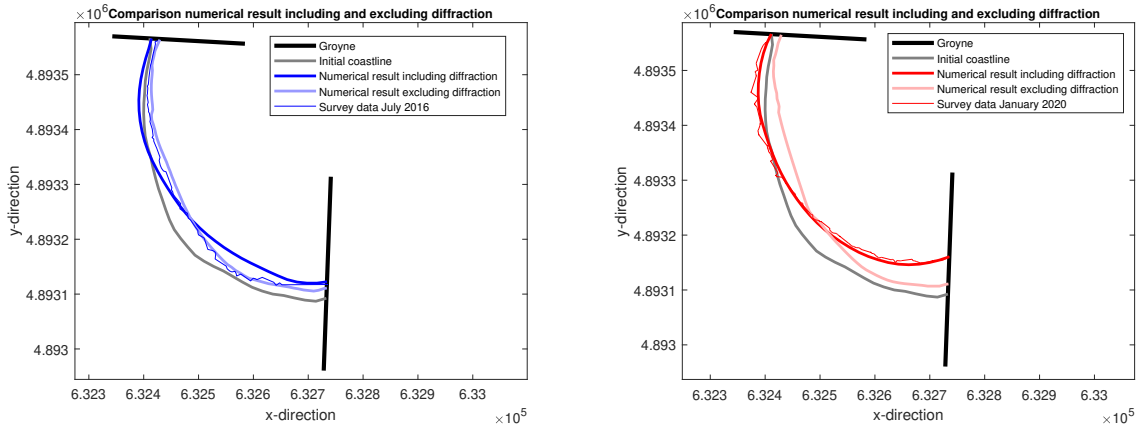

(a) Shoreline shape July 2016

(b) Shoreline shape January 2020

Figure 6.22: Numerical results including and excluding diffraction effects

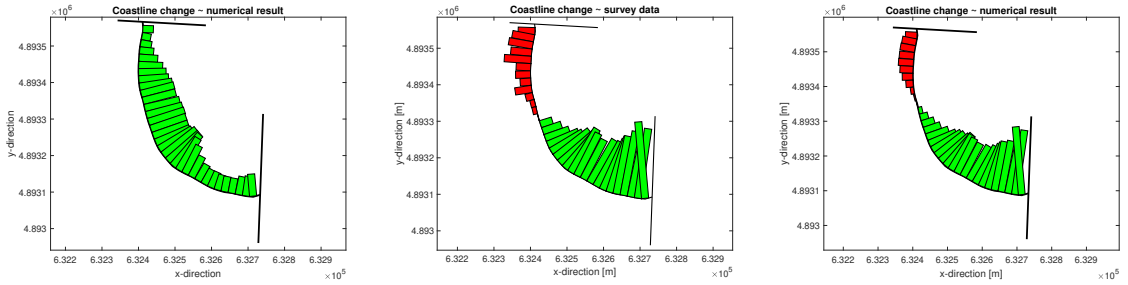

(a) Numerical result excluding diffraction (b) Survey data (c) Numerical result including diffraction

Figure 6.23: Coastline change September 2015 - January 2020. Green bars: change in seaward direction. Red bars: change in landward direction

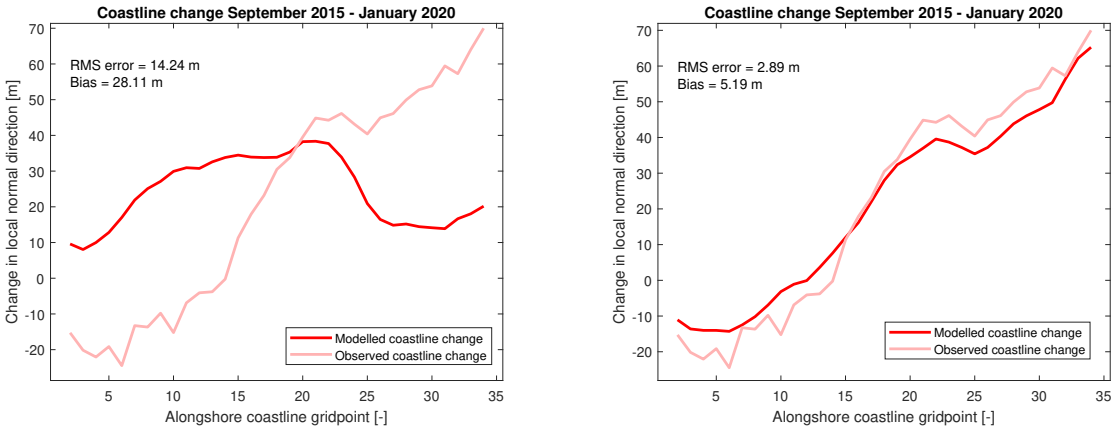

(a) Excluding diffraction (b) Including diffraction

Figure 6.24: Root mean square error and bias

	RMS error	Bias
Without diffraction	14.24 m	28.11 m
Before calibration	10.92 m	21.94 m
Scenario A	9.19 m	20.89 m
Scenario B	8.01 m	17.19 m
Scenario C	5.84 m	14.26 m
Scenario D	2.89 m	5.19 m

Table 6.2: Bias and RMS error

After incorporating the effects of wave diffraction onto the shoreline evolution, the agreement between the survey data and the numerical results is increased significantly. Especially, the erosion close to the Northern groyne is visible in the numerical result including diffraction while this behaviour is absent when diffraction effects are neglected. Likewise, the seaward movement in the vicinity of the Southern groyne is modelled more accurately while using the improved model. Furthermore, the bias decreases from 28.11 m to 5.19 m. Implying that the mean of the difference between the observed and modelled coastline change reduces by a factor of 5.6. Additionally, the spreading of this difference along the coastline scales down from 14.24 m to 2.89 m. Hence, denoting that the numerical result is more fitting the observed coastline change along the whole shoreline. To conclude, by accounting for the effects of wave diffraction it is accomplished to simulate the anti-clockwise rotation of the coastal cell. Without the model improvement, this could not be achieved.

6.5. Discussion

The influence of diffraction effects is increased to retrieve a better matching result with the survey data. In doing so, the transition zone width is calibrated. A larger width resulted in significant higher agreement between the numerical result and survey data. Hence, it was concluded that the transition width proposed by Dabees (2000) was not sufficient in this case study. However, the influence of two assumptions made in the model set-up needs to be examined in more detail before this conclusion can be confirmed as is explained as follows.

Firstly, neglecting wave shoaling and refraction effects inside the diffraction calculations resulted in diffracted breaking wave heights and angles that were not completely correct as is described in section 6.3.3 (figure 6.11). While taking into account these processes, it is expected to obtain more accurate diffracted breaking heights and angles, resulting in more influence of diffraction onto the shoreline evolution. Those diffracted breaking heights will be significant lower than the ones displayed in figure 6.11a. The breaking angles are predicted to be heavier diffracted towards the groyne while incorporating the wave refraction process towards the curved coastline shape. Secondly, assuming that the incoming wave angles at both groyne tips are the same is a large simplification of reality. Those angles will be different from each other because of the refraction of waves towards a varying alongshore coastline orientation. The later is briefly analyzed by investigation of the wave angles along the dynamic boundary. This boundary was applied while having a depth equal to the water depth (i.e 3.56 m) at the Northern groyne tip and an orientation being the same as the local coastline orientation. After the model was forced with an incoming wave from 40° to the North at the nearshore location P002, the resulted wave angles along the dynamic boundary were varying significantly between 64° at the Northern groyne to -39° at the Southern groyne. Hence, assuming two equal wave angles at the groyne tips is demonstrated to be a large simplification.

After establishing the required model adaptations, to allow for a different wave angle at both groyne tips and incorporating effects of shoaling and refraction, the numerical result is expected to be more in line with the survey data. However, if still more influence of diffraction effects is necessary, the transition zone width could be increased again to retrieve a better matching coastline response. Consequently, it would be more well-grounded to conclude that the transition zone definition of Dabees (2000) is arguable.

7

Conclusions and recommendations

7.1. Conclusions

The research objective of this thesis is to develop the existing wave diffraction routine in ShorelineS to incorporate the diffraction effect in the vicinity of a groyne field, to simulate the coastline evolution of the Constanta case study. To achieve this objective, five research questions were defined. In this section, the key findings for each question are summarized.

1. How to account for wave diffraction inside coastline modelling?
The process of wave diffraction will cause a reduced wave climate in the lee of the structure. Therefore, accounting for the influence of wave diffraction comprises the modelling of diffracted breaking wave heights and angles. Diagrams provided by Wiegel (1962), could be applied to determine the diffracted wave heights behind breakwaters. However, using these diagrams inside numerical models is not computational effective. By the means of a literature study, the following methods are found to be capable of incorporating the effect of wave diffraction onto the breaking wave height and angle inside a numerical model: Kraus (1984), Kamphuis (1992), Leont'Yev (1999), Hurst et al. (2015) and the method of Roelvink described in Elghandour et al. (2020).

The shoreline shape was found to be highly dependent on the method that was used to calculate the diffracted breaking angles. Kamphuis (1992) demonstrated to be incapable of reproducing erosion directly downdrift of the groyne. Therefore, this method is not applied in the remainder of this thesis. Using the modified method of Hurst et al. (2015), resulted in stronger diffracted breaking waves compared to the method of Roevlink. Consequently, the amount of erosion directly downdrift of the groyne is significantly more reduced while applying the modified method of Hurst et al. (2015). Both methods make use of a predefined location of the transition zone width, thereby following Dabees (2000). The term *predefined* indicates that the transition zone width is independent of the trend of K_d values. Due to time constraints, only Roelvink his method is applied in the remainder of this study to calculate the diffracted wave angles. The modified method of Hurst et al. (2015) is also implemented inside the model, however it has not been validated or applied in the case study.

For calculating the diffracted wave heights in the simplified diffraction scenario, it is concluded that the methods of Kraus (1984) and Kamphuis (1992) require modifications. By definition, the K_d value at the transition zone edge should be equal to 1 in such a simplified situation. Applying these methods to the case of a straight coastline, there is no point at the breakerline for which this condition holds. Therefore, modifications are made to make sure that a K_d value of 1 is obtained at the predefined transition zone edge. Using different methods to calculate the diffracted breaking wave heights, the shoreline response hardly showed any variation after 1,6, and 12 months of simulation time. Consequently, which method to use for determining the K_d value is concluded to be not so relevant. In the remaining model simulations, the method of Leont'Yev (1999) is applied since no modifications were needed when using this approach. The other methods are also incorporated inside the model. However, due to time constraints they are not validated and used in the case study.

2. How to correctly implement the boundary condition belonging to a groyne into the freely moving coastline model ShorelineS?
A new approach satisfying the condition of zero alongshore sediment transport through the groyne is established. The key aspect of this approach is to divide the shoreline into two sections, containing the total updrift and downdrift area respectively. Furthermore, the two grid points located at the groyne are forced to move along the structure only. Compared to the numerical results retrieved using the old boundary approach, the shoreline evolution obtained while using this new approach showed significant higher similarity to the analytical solution provided by Pelnard-Considere (1956). Therefore, it was chosen to use the new boundary approach while modelling the coastline evolution influenced by the effects of wave diffraction.

3. To what extent are certain model parameters, involved in the diffraction calculations, influencing the resulting coastline shape?
A variety of model runs is performed to examine the influence of the offshore wave height, the offshore wave angle and the transition zone width. It is concluded that a higher offshore wave angle results in a faster coastline response. The curvature of the coastline is stated to be highly dependent on the offshore wave angle. Furthermore, a larger offshore wave height demonstrated a faster shoreline response. However, the curvature of the coastline remained constant.

More interesting is the influences of the transition zone width since it is defined by the applied methods to incorporate diffraction effects. Using different transition zone widths, the wave diffraction effects onto the shoreline evolution are concluded to be more pronounced while increasing this width. More precisely, when using a larger transition zone width the total downstream area influenced by diffraction expanded. Besides that, the amount of erosion directly downdrift the groyne is reduced significantly or even sedimentation is caused when increasing the transition zone with. In the case of a very small width, the effect of diffraction onto the coastline evolution is reduced significantly. Hence, the shoreline shape becomes very close to the analytical solution of Pelnard-Considere (1956).

4. How does the model perform in modelling the shoreline evolution of a simplified diffraction scenario?
Before applying the improved model to the Constanta case study, a verification regarding the performance of the improved model to a simplified shoreline is made. As a first check, using details concerning the development of the breaking wave heights, angles and alongshore sediment transport, it is concluded that those three parameters properly evolve while modelling the shoreline evolution. To be more precise, the effect of the groyne and the corresponding diffraction was clearly visible in the development of these parameters. Subsequently, the conservation of sediment mass is demonstrated to remain valid when the effects of diffraction are taken into account. Finally, the numerical results showed to be in line with the analytical solutions provided by Larson et al. (1987). Based on these three findings, the effects of diffraction onto the coastline evolution in the vicinity of a groyne are concluded to be implemented correctly.

5. How does the model perform in modelling the shoreline evolution of the Constanta case study?
After incorporating the diffraction effects onto the shoreline evolution, the agreement between the survey data and numerical result increased. However, while simulating the shoreline evolution of Constanta under the stated assumptions, such as neglecting refraction and shoaling effects inside the diffraction calculations, it is concluded that the effect of diffraction onto the shoreline evolution needed to be increased to retrieve a more representative result. In doing so, multiple model runs with a varying transition zone width to increase the effects of diffraction were performed. Subsequent to the calibration of this parameter, the bias and root mean square error of the numerical result are 5.19 m and 2.89 m respectively. Those parameters reduced by factors of 5.5 and 5 compared to the numerical result excluding diffraction effects. All in all, by accounting for the effects of wave diffraction it is accomplished to simulate the anti-clockwise rotation of the coastal cell in agreement with the survey data. Without the developed model implementations, this result could not be produced.

7.2. Recommendations

This section contains recommendations for future development to improve the ShorelineS model performance regarding modelling the coastline evolution in the vicinity of a groyne. Most of them are built upon the assumptions and difficulties that arose while establishing the procedure to include wave diffraction effects.

1. Include refraction and shoaling from groyne tip towards breakerline
After analysis of the resulting breaking wave heights, it became clear that at the end of the transition zone the breaking wave height was showing an abrupt step towards the first undiffracted breaking wave height outside the transition zone. This could be caused by neglecting wave refraction and shoaling from the groyne tip towards the breaker points inside the influence area of diffraction. As a result, a sharp gradient inside the alongshore sediment transport distribution was observed which together with a large incoming wave angle resulted in an abrupt shoreline change in the simplified model scenario. A proper way to avoid this unrealistic shoreline evolution could be retrieved by incorporating wave refraction and shoaling from the groyne tip towards the breakerline.

2. Wave characteristics at the groyne tip should be dependent on local coastline evolution near the groyne
Regarding the simplified model scenario, the wave tip characteristics are forced to be constant in time. Therefore, only depending on the initial (straight) coastline orientation. However, the wave characteristics at the groyne tip are most likely affected by the local coastline evolution directly near the groyne. Especially regarding the updrift section. Because of sedimentation, the shoreline is becoming closer to the groyne tip at that location. In doing so, probably affecting the wave tip characteristics. A procedure should be established to calculate the wave tip characteristics related to the varying local coastline position and orientation close to the groyne, updrift and downdrift.

As stated in the discussion of the Constanta case study results, assuming two equally wave angles at the groyne tips is demonstrated to be a large simplification. To retrieve more representative wave angles, the same kind of procedure as mentioned above is recommended. In doing so, it is suggested to examine which local coastline orientation should be used inside the calculations of the wave parameters at the groyne tip. Since these orientations are varying significantly along the shoreline, using a different coastline orientation would result in different wave characteristics at the groyne tip, subsequently influencing the diffraction calculations. As a consequence, the effect of diffraction onto the shoreline evolution will be changed. Therefore, research is suggested regarding this procedure for calculating the wave characteristics at the groyne tip.

3. Further investigation of the transition zone width definition
After applying the improved model to the Constanta case study it was concluded that the transition zone definition of Dabees (2000) is not sufficient to retrieve a representative coastline evolution. To confirm this conclusion, the required model adaptations described in the above stated recommendations should be established. After implementing the required model adaptations, the numerical result is expected to be more in line with the survey data. However, if still more influence of diffraction effects is required, the transition zone width could be increased again to retrieve a better matching coastline response. Consequently, it would be more well-grounded to conclude that the transition zone definition of Dabees (2000) is doubtful. In that case, it is suggested to perform further research on the definition of the transition zone width. Multiple case studies should be performed to demonstrate that the definition of Dabees (2000) is not applicable in every situation. Furthermore, a sensitivity analysis of the transition zone width is suggested. While keeping this width constant and varying other parameters, such as the the structure length, or vice versa, the resulting shoreline evolutions should be compared. If based on this analysis the definition of Dabees (2000) is arguable, a new definition could be established by using a correction angle to the incoming wave angle at the tip. It is suggested to relate this correction angle to the amount of directional spreading of the input wave characteristics. In doing so, the varying behaviour of different kinds of sea states can be accounted for. Wind waves penetrating the transition and shadow zone will quickly decrease in height because the wave spreading is large. Swell waves will keep their height significantly longer while propagating into the shadow zone because of the more uni-directional waves. This behaviour could be incorporated by applying a smaller correction angle in the case of swell waves, consequently leading to a smaller transition zone width. Hence, decreasing the effect of diffraction onto the shoreline response. In the case of wind waves, with larger directional spreading, the influence of diffraction is expected to be bigger, therefore a larger correction angle should be applied.

4. Include bypassing and transmission of sediment
Currently, wave diffraction effects are incorporated while neglecting sediment bypass and transmission through the groyne. However, from the numerical results it became clear that updrift of the groyne the breakerline could exceed the groyne tip. Meaning sediment would bypass around the tip of the groyne because the water depth of breaking waves is larger than the depth at the groyne tip location. A suggestion is made to investigate the influence of sediment bypassing, transmission and wave diffraction onto the shoreline evolution together by activating the procedure implemented by Ghonim (2019) regarding the first two processes.

Bibliography

Ashton, A. D. and Murray, A. B. (2006a). High-angle wave instability and emergent shoreline shapes: 1. modeling of sand waves, flying spits, and capes. *Journal of Geophysical Research: Earth Surface*, 111(F4):1–19. https://doi.org/10.1029/2005JF000422.

Ashton, A. D. and Murray, A. B. (2006b). High-angle wave instability and emergent shoreline shapes: 2. wave climate analysis and comparisons to nature. *Journal of Geophysical Research: Earth Surface*, 111(F4):1–17. https://doi.org/10.1029/2005JF000423.

Ashton, A. D., Murray, A. B., and Arnoult, O. (2001). Formation of coastline features by large-scale instabilities induced by high-angle waves. *Nature*, 414(6861):296–300. https://doi.org/10.1038/35104541.

Bakker, W., Klein Breteler, E., and Roos, A. (1970). The dynamics of a coast with a groyne system. *Coastal Engineering Proceedings*, 1(12):66. https://doi.org/10.9753/icce.v12.64.

Baykal, C. (2006). Numerical modeling of wave diffraction in one-dimensional shoreline change model. Master's thesis, Middle East Technical University, Ankara, Turkey.

Blue Jr, F. and Johnson, J. (1949). Diffraction of water waves passing through a breakwater gap. *Eos, Transactions American Geophysical Union*, 30(5):705–718. https://doi.org/10.1029/TR030i005p00705.

Bosboom, J. and Stive, M. J. F. (2015). *Coastal Dynamics I: Lecture Notes CT4305*. VSSD.

Brandenburg, P. (2020). Calibration of morphological model. Technical report, Van Oord Dredging and Marine Contractors. Lot 5 - Protection and rehabilitation of the Romanian Black Sea Coast in Eforie Area.

Carruthers, E. A., Lane, D. P., Evans, R. L., Donnelly, J. P., and Ashton, A. D. (2013). Quantifying overwash flux in barrier systems: An example from martha's vineyard, massachusetts, usa. *Marine Geology*, 343:15–28. https://doi.org/10.1016/j.margeo.2013.05.013.

Creel, L. (2003). Ripple effects: Population and coastal regions. *Population Reference Bureau, Washington DC*.

Dabees, M. A. (2000). *Efficient modeling of beach evolution*. PhD thesis, Queen's University, Kingston, Ontario, Canada.

Dean, R. (1977). *Equilibrium beach profiles: US Atlantic and Gulf coasts*. Department of Civil Engineering and College of Marine Studies.

Dean, R. and Dalrymple, R. (2001). *Coastal processes with engineering applications*. Cambridge University Press, New York. https://doi.org/10.1017/CBO9780511754500.

Deltares (2011). *UNIBEST-CL+ Manual: Manual for version 7.1 of the shoreline model UNIBEST-CL+*.

Deltares (2020). *Delft3D Manual:3D/2D modelling suite for integral water solutions, version 3.05*.

DHI (2011). *LITLINE: Coastline Evolution (LITLINE user guide)*. MIKE by DHI.

Dunham, J. H. (1951). Refraction and diffraction diagrams. *Coastal Engineering Proceedings*, 1:2–2. https://doi.org/10.9753/icce.v1.4.

Elghandour, A. M. (2018). Efficient modelling of coastal evolution. development, verification and validation of shorelines model. Master's thesis, UNESCO-IHE Institute for Water Education, Delft, Netherlands.

Elghandour, A. M., Roelvink, D., Huisman, B. J. A., Reyns, J., Costas, S., and Nienhuis, J. (2020). Reduced complexity of shoreline response behind offshore breakwaters. *Coastal Engineering Proceedings*, (36v):34. https://doi.org/10.9753/icce.v36v.papers.34.

Ghonim, M. E. (2019). Recent developments in numerical modelling of coastline evolution. Master's thesis, UNESCO-IHE Institute for Water Education,, Delft, Netherlands.

Goda, Y. (1985). *Random Seas and Design of Maritime Structures*. World Scientific Publishing Company.

Goda, Y., Takayama, T., and Suzuki, Y. (1978). Diffraction diagrams for directional random waves. *Coastal Engineering Proceedings*, 1:628–650. https://doi.org/10.9753/icce.v16.35.

Gracia, A., Rangel-Buitrage, N., Oakley, J. A., and Williams, A. T. (2018). Use of ecosystems in coastal erosion management. *Ocean and Coastal Management*, 156(F4):277–289. https://doi.org/10.1016/j.ocecoaman.2017.07.009.

Hallermeier, R. J. (1980). A profile zonation for seasonal sand beaches from wave climate. *Coastal engineering*, 4:253–277. https://doi.org/10.1016/0378-3839(80)90022-8.

Hanson, H. (1989). Genesis: A generalized shoreline change numerical model. *Journal of Coastal research*, 5(1):1–27.

Hanson, H. and Kraus, N. C. (2011). Long-term evolution of a long-term evolution model. *Journal of Coastal Research*, 59:118–129. https://doi.org/10.2307/29783108.

Holthuijsen, L. H. (2010). *Waves in oceanic and coastal waters*. Cambridge University press, New York, 3 edition.

Huisman, B. J. A. (2012). Webinar large-scale long-term coastline modelling, using unibest and delft3d.

Huisman, B. J. A. (2014). Modelling coastline evolution. Deltares.

Hurst, M. D., Barkwith, A., Ellis, M. A., Thomas, C. W., and Murray, A. B. (2015). Exploring the sensitivities of crenulate bay shorelines to wave climates using a new vector-based one-line model. *Journal of Geophysical Research: Earth Surface*, 120(12):2586–2608. https://doi.org/10.1002/2015JF003704.

Johnson, J. W. (1951). Generalized wave diffraction diagrams. *Coastal Engineering Proceedings*, 1(2):2. https://doi.org/10.9753/icce.v2.2.

Kamphuis, J. (1992). Computation of coastal morphology. *Design and Reliability of Coastal Structures, short course during the 23rd ICCE in Venice*.

Kraus, N. C. (1984). Estimate of breaking wave height behind structures. *Journal of Waterway, Port, Coastal, and Ocean Engineering*, 110(2):276–282. https://doi.org/10.1061/(ASCE)0733-950X(1984)110:2(276).

Kraus, N. C., Larson, M., and Wise, A. (1998). Depth of closure in beach-fill design. Technical report, US Army Engineer Waterways Experiment Station; Coastal and Hydraulics Laboratory, Mississippi,USA.

Kristensen, S. E., Drönen, N., Deigaard, R., and Fredsoe, J. (2016). Impact of groyne fields on the littoral drift: A hybrid morphological modelling study. *Coastal engineering*, 111:13–22. https://doi.org/10.1016/j.coastaleng.2016.01.009.

Larson, M., Hanson, H., and Kraus, N. C. (1987). Analytical solutions of the one-line model of shoreline change. Technical report, US Army Engineer Waterways Experiment Station; Coastal and Hydraulics Laboratory, Washington DC, USA.

Larson, M., Palalane, J., Fredriksson, C., Marinho, B., Hanson, H., and Coelho, C. (2016). Simulating cross-shore material exchange at decadal scale. model application. *Coastal Engineering*, 116:26–41. https://doi.org/10.1016/j.coastaleng.2016.05.007.

Leatherman, S. (1979). Migration of assateague island, maryland, by inlet and overwash processes. *Geology*, 7(2):104–107.

Leont'Yev, I. O. (1999). Modelling of morphological changes due to coastal structures. *Coastal Engineering*, 38(3):143–166. https://doi.org/10.1016/S0378-3839(99)00045-9.

Longuet-Higgins, M. S. (1970). Longshore currents generated by obliquely incident sea waves. *Journal of geophysical research*, 75(33):6778–6789. https://doi.org/10.1029/JC075i033p06778.

Longuet-Higgins, M. S. and Stewart, R. W. (1964). Radiation stresses in water waves; a physical discussion, with applications. *Deep Sea Research and Oceanographic Abstracts*, 11(4):529–562. https://doi.org/10.1016/0011-7471(64)90001-4.

McCall, R. T. (2008). The longshore dimension in dune overwash modelling: development, verification and validation of xbeach. Master's thesis, Delft University of Technology, Delft, Netherlands.

McCormick, M. E. and Kraemer, D. R. B. (2002). Polynomial approximations for fresnel integrals in diffraction analysis. *Coastal Engineering*, 44(3):261–266. https://doi.org/10.1016/S0378-3839(01)00034-5.

Miche, R. (1944). Mouvements ondulatoires de l'océan pour une eau profonde constante et décroissante. *Annales. des Ponts et Chauss-sees*, 121:285–318.

Mil-Homens, J. (2016). Longshore sediment transport: Bulk formulas and process based models. Master's thesis, Delft University of Technology, Delft, Netherlands.

Mil-Homens, J., Ranasinghe, R., de Vries, J. S. M. v. T., and Stive, M. J. F. (2013). Re-evaluation and improvement of three commonly used bulk longshore sediment transport formulas. *Coastal Engineering*, 75:29–39. https://doi.org/10.1016/j.coastaleng.2013.01.004.

Mitsuyasu, H., Tasai, F., Suhara, T., Mizuno, S., Ohkusu, M., Honda, T., and Rikiishi, K. (1975). Observations of the directional spectrum of ocean wavesusing a cloverleaf buoy. *Journal of Physical Oceanography*, 5(4):750–760. https://doi.org/10.1175/1520-0485(1975)005<0750:OOTDSO>2.0.CO;2.

Mobarek, I. and Wiegel, R. (1967). Diffraction of wind generated water waves. In *Coastal Engineering 1966*, pages 185–206. https://doi.org/10.1061/9780872620087.013.

Mudde, C. (2019). Development and verification of shorelines on longshore sediment transport and spit formation. Master's thesis, Delft University of Technology, Delft, Netherlands.

Neumann, B., Vafeidi, A. T., Zimmermann, T., and Nicholls, R. J. (2015). Future coastal population growth and exposure to sea-level rise and coastal flooding - a global assessment. 10(3):1–34. https://doi.org/10.1371/journal.pone.0118571.

Pelnard-Considere, R. (1956). Essai de theorie de l'evolution des formes de rivage en plages de sable et de galets. *Les Energies de la Mer: Compte Rendu Des Quatriemes Journees de L'hydraulique, Paris 13, 14 and 15 Juin 1956; Question III, rapport 1, 74-1-10*.

Penney, W. G., Price, A. T., Martin, J. C., and Moyce, W. J. (1952). Part i. the diffraction theory of sea waves and the shelter afforded by breakwaters. *Philosophical Transactions of the Royal Society of London. Series A, Mathematical and Physical Sciences*, 244(882):236–253. https://doi.org/10.1098/rsta.1952.0003.

Penny, W. G. and Price, A. T. (1944). Diffraction of sea waves by breakwaters. *Directorate, Miscellaneous Weapons Development Technical History*, (Artificial Harbors, sec 3D).

Pierson, W. J. (1955). *Practical methods for observing and forecasting ocean waves by means of wave spectra and statistics*, volume 603. Hydrographic Office.

Putnam, J. A. and Arthur, R. S. (1948). Diffraction of water waves by breakwaters. *Eos, Transactions American Geophysical Union*, 29(4):481–490. https://doi.org/10.1029/TR029i004p00481.

Rea, C. C. and Komar, P. D. (1975). Computer simulation models of a hooked beach shoreline configuration. *Journal of Sedimentary Research*, 45(4):866–872. https://doi.org/10.1306/212F6E6A-2B24-11D7-8648000102C1865D.

Roelvink, D., Huisman, B. J. A., Elghandour, A. M., Ghonim, M. E., and Reyns, J. (2020). Efficient modelling of complex coastal evolution at monthly to century time scales. *Frontiers in Marine Science*, 7:535. https://doi.org/10.3389/fmars.2020.00535.

Roelvink, D. and Reiniers, A. (2011). *A guide to modelling coastal morphology*. World Scientific Publishing. https://doi.org/10.1142/7712.

Ruessink, B. G., Kuriyama, Y., Reniers, A. J. H. M., Roelvink, J. A., and Walstra, D. J. R. (2007). Modeling cross-shore sandbar behavior on the timescale of weeks. *Journal of Geophysical Research: Earth Surface*, 112(F3).

Sauermann, G., Kroy, K., and Herrmann, H. J. (2001). Continuum saltation model for sand dunes. *Physical Review E*, 64(3):031305. https://doi.org/10.1103/PhysRevE.64.031305.

Sommerfeld, A. (1896). Mathematische theorie der diffraction. *Mathematische Annalen*, 47(2-3):317–374.

Sorensen, R. M. (1993). *Basic wave mechanics: for coastal and ocean engineers*. John Wiley & Sons.

Thomas, R. C. and Frey, A. E. (2013). Shoreline change modeling using one-line models: General model comparison and literature review. Technical report, US Army Engineer Research and Development Center, Vicksburg, USA.

USACE (1984a). *Shore protection manual US Army Corps of Engineers Vol 1*. Coastal Engineering Research Center.

USACE (1984b). *Shore protection manual US Army Corps of Engineers Vol 2*. Coastal Engineering Research Center.

Van der Salm, G. L. S. (2013). Coastline modelling with unibest: areas close to structures. Master's thesis, Delft University of Technology, Delft, Netherlands.

van Rijn, L. (2014). A simple general expression for longshore transport of sand, gravel and shingle. *Coastal Engineering*, 90:23–39. https://doi.org/10.1016/j.coastaleng.2014.04.008.

van Rijn, L. C. (2002). Longshore sand transport. pages 2349–2451, Cardiff, UK. International Conference on Coastal Engineering.

Vitousek, S. and Barnard, P. L. (2015). *A nonlinear, implicit one-line model to predict long-term shoreline change*. World Scientific. https://doi.org/10.1142/97898146899770215.

Wang, J. D. and Mehaute, B. L. (1980). Criterion for stability of shoreline planform. *Coastal Engineering Proceedings*, 1:77. https://doi.org/10.9753/icce.v17.77.

Weesakul, S., Rasmeemasmuang, T., Tasaduak, S., and Thaicharoen, C. (2010). Numerical modeling of crenulate bay shapes. *Coastal Engineering*, 57(2):184–193. https://doi.org/10.1016/j.coastaleng.2009.10.005.

Wiegel, R. (1962). Diffraction of waves by semi-infinite breakwater. *Journal of the Hydraulics Division*, 88(1):27–44.

A

Appendix A

This appendix provides more details about the model improvements described in section 2.3. An extensive elaboration can be found in the associated studies of Elghandour (2018), Ghonim (2019) and Mudde (2019).

A.1. Adaptive time step

The computational time of coastline models is relative small compared to other kinds of models. Particularly, when the simulation time is in the order of decades, the computational time of coastline models is a big advantage. Because the freely moving polyline describing the grid in ShorelineS, temporal and spatial differences in the grid size could arise. A constant time step may be suitable in the beginning of the simulation but could result in instabilities as the simulation continues (Elghandour, 2018). To overcome this problem, an adaptive time step routine was implemented based on the automatic time step generator described by McCall (2008). The adaptive time step is a method to determine the biggest applicable time step for which all grid points in the model are still stable. By doing this, the computational time is kept as small as possible.

To come up with solutions of the governing differential equations, an explicit scheme for the discretisation to time is used inside ShorelineS (Roelvink et al., 2020). A characteristic of an explicit scheme is that the solution is conditionally stable. The Neumann Criterion is applied to fulfill this condition. At each gridpoint, the time step is calculated according to this criterion. Finally, the smallest time step is used to determine the solution of the governing equations (Elghandour, 2018).

$$\Delta t \leq \frac{1}{2}\frac{\Delta x^2}{\epsilon} \quad \text{Neumann Criterion} \tag{A.1}$$

The adaptive time step criteria, including the definitions of the diffusion coefficient ϵ, are determined for different alongshore sediment transport formulations by Elghandour (2018). In order to still be able to simulate given wave data sets with specific moments in time, the adaptive time step procedure makes sure that it does not miss a specific moment in time at which a particular wave forcing is defined.

A.2. Boundary conditions

One of the unique aspects of ShorelineS is that it can coop with different coastal sections that could interact with each other. There is a possibility that some of these sections reach outside the boundaries of the domain. In that case, the applied boundary conditions should mimic the situation outside the domain as good as possible. Since there are a lot of different coastal environments, multiple boundary conditions are implemented inside the model. An extensive elaboration of these conditions is stated in Elghandour (2018), here a summary is provided.

Neumann boundary: Coastline position remains constant
Applying this boundary condition prevents a change of sediment at the considered boundary. In the case of the first gridpoint, this yields the following condition: $Q_{s,1} = Q_{s,2}$. Hence, a gradient in the alongshore sediment transport will not exist, implying a fixed coastline for the particular gridpoint.

Constant Orientation boundary: Coastline angle remains constant
This condition should be chosen if the initial coastline orientation at a boundary should remain constant during the whole model simulation. Hence, the following condition should be implemented:$Q_{s,start} = Q_{s,1}$. In which $Q_{s,start}$ is the initial value of the sediment transport. Consequently, the transport through the boundary is equal to this initial value during the entire simulation.

Dirichlet boundary: Transport value is specified
When the alongshore sediment transport at a boundary is defined for a specific time interval, this definition could be implemented in the model using a constant value or a function of time. Such a boundary is applied in the case of a known sediment supply by a river for instance. Or, in the situation of an impermeable groyne, thereby setting the alongshore sediment transport value to 0. This kind of boundary is called the Dirichlet Wall boundary.

A.3. Wave diffraction around offshore breakwaters

Offshore breakwaters will cause a shadow zone directly behind the breakwater. Inside such a zone, the breaking wave height and wave angle will be different than in the adjacent areas. Elghandour (2018) studied three different methods to determine the wave angle behind breakwaters. Two of them are retrieved from literature, Dabees (2000) and Hurst et al. (2015). Also a new approach was developed in collaboration with D.J.A. Roelvink. The most important aspect of this new approach is to gradually change the incoming wave angle from the exposed area to the shadow area behind the breakwater. In this way, the effects of the diffraction process are simplified enough to prevent much computational effort (Elghandour, 2018). The breaking wave height behind the breakwater is calculated using a diffraction coefficient K_d. This coefficient accounts for the reduced wave energy. Besides the reduced energy inside the shadow zone, an area down drift also experiences the influence of the offshore breakwater onto the wave energy. This downdrift area has a length that has the same order of magnitude as the length of the coast inside the shadow zone. For both areas, a relation for K_d exist that is implemented by Elghandour (2018) to account for the diffraction effects behind an offshore breakwater.

A.4. Sediment transmission and bypassing

Ghonim (2019) improved the model application close to shore normal structures by implementing sand bypassing and transmission. Those two mechanisms change the alongshore transport in the vicinity of a structure, therefore influencing the shoreline response. In doing so, first, the definition of structures inside the model domain was upgraded. He stated that the definition of a structure, like a groyne, inside ShorelineS resulted in an incorrect shoreline response on both sides of the groyne. The main reason for this is that according to that definition, the groyne is usually located between two grid points (figure A.1).

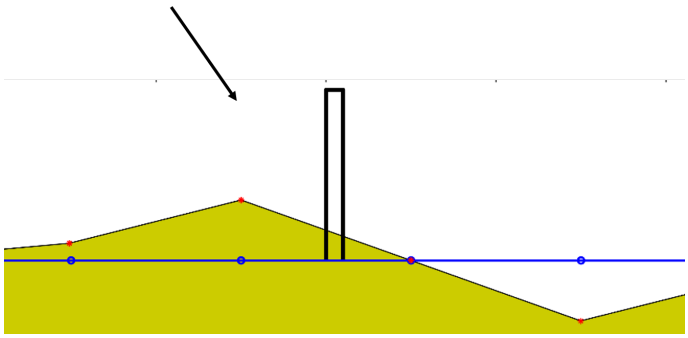

Figure A.1: Initial groyne definition in ShorelineS (Ghonim, 2019).

Based on field observations, the largest amount of sedimentation is expected to be located directly updrift of the groyne. However, the numerical results showed maximum sedimentation located somewhat further away from the groyne (figure A.1). This is because the grid points move perpendicular to the line connecting the two adjacent grid points (Ghonim, 2019). Another incorrect behaviour of the coastline determined by ShorelineS, is the accretion directly downdrift of the groyne. According to Bosboom and Stive (2015), in such a case as depicted in figure A.1, the shoreline usually retreats at that location. Ghonim (2019) proposed a new method of defining the structure (figure A.2). New grid points are added at locations where the groyne intersects the initial coastline. If one of the intersection points lies on top of a gridpoint, no extra point is added. Besides that, if there is a gridpoint that lies between the two intersection points, that gridpoint is removed.

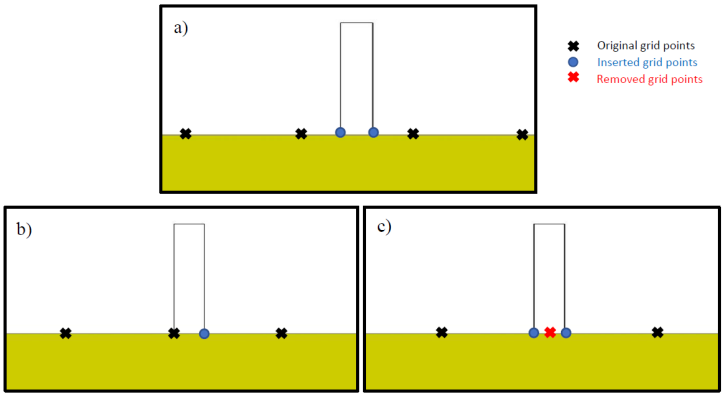

Figure A.2: New groyne definition in ShorelineS. a) adding 2 grid points b) adding 1 grid point c) remove grid point (Ghonim, 2019).

Besides this new structure definition, Ghonim (2019) examined the movement of the coastline at the groyne. In the initial ShorelineS model, grid points representing the coastline at the groyne could leave the structure. This should not be possible, therefore adjustments had to be made. A solution for this problem was to force grid points at the groyne to move only parallel to the structure. In doing so, Ghonim (2019) related the movement of grid points at the groyne to the angle between the groyne and the initial shoreline (figure A.3).

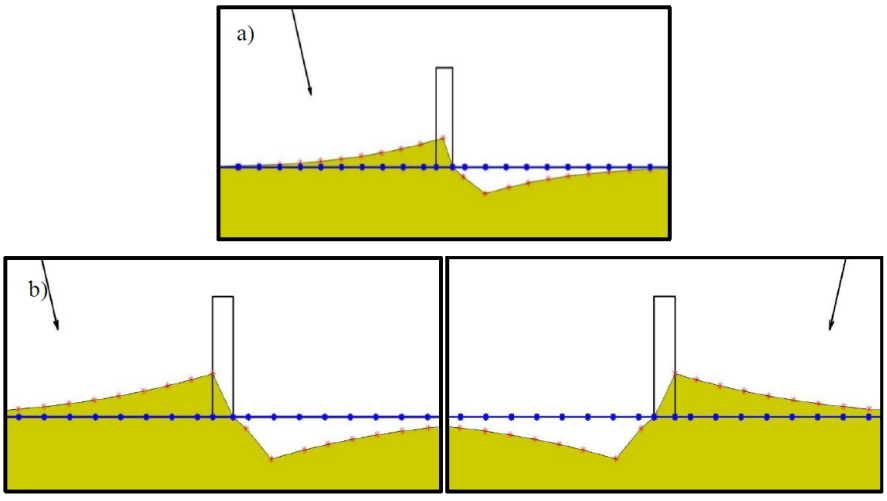

Figure A.3: Movement of grid points at the groyne, *a*; before model adjustment, *b*; after model adjustment (Ghonim, 2019).

This new definition of structures and the description of movement of grid points at the groyne made it easier to implement sand transmission and bypassing. Bypassing is the process of sand that moves past the seaward end of a groyne. Hanson and Kraus (2011) stated that bypassing occurs when the water depth at the seaward end of the groyne D_G is smaller than the water depth of the active alongshore transport D_{LT}.

This active depth could be interpreted a time dependent depth over which alongshore sediment transport takes place. Therefore being different than the depth of closure, mentioned in the beginning of chapter 2.2, which is a time-averaged depth over years to decades. Often, D_{LT} is established by taking the depth of the highest 1/10 waves at the seaward end of the groyne. Ghonim (2019) described that for engineering purposes, usually the follow relation is used to determine D_{LT}.

$$D_{LT} = \frac{A_w}{\gamma} H_{1/3,br} \tag{A.2}$$

Here $H_{1/3,br}$ is the significant wave height at the breaker line, γ the breaker index and A_w a factor that converts the highest 1/10 waves to the significant wave height. Ghonim (2019) followed a general method proposed by Hanson and Kraus (2011) to include sand bypassing and transmission inside ShorelineS. In doing so, a bypassing factor BYP is introduced.

$$\text{BYP} = 1 - \frac{D_G}{D_{LT}} \tag{A.3}$$

If D_G is larger than D_{LT}, it means that the groyne reaches beyond the greatest depth at which active longshore transport takes place. In that situation, bypassing will not occur and BYP is equal to 0. Based on an equilibrium cross-shore coastal profile presented by Dean (1977), the bottom profile is known and D_G can be determined. In analogy to the bypassing factor, a general transmission factor TMF is introduced by Hanson and Kraus (2011) to quantify the amount of sand transmission. A TMF value of 0 implies that no sand is transmitted over, through or landward of the groyne.

Ghonim (2019) combined the effects of sand bypassing and transmission, using a BPTM factor that is introduced by (Hanson, 1989).

$$\text{BPTM} = \text{BPF} + \text{TMF} - \text{BPF} * \text{TMF} \tag{A.4}$$

BPTM represents the percentage of sediment that transmits or bypasses from the updrift to the downdrift side of a structure. A low value means that the alongshore sediment transport is influenced significantly by the presence of the structure. Subsequently, leading to high accretion at the updrift side and large erosion at the downdrift side. Initially, the gridpoint updrift at the groyne was forced by the model to have an alongshore sediment transport value of 0. Ghonim (2019) adjusted the model in such a way that the amount of sediment that is bypassing and blocked by the structure is calculated using the BPTM factor. Two methods for doing this are elaborated in detail in Ghonim (2019). Only the main aspects are stated in this section.

The first method is based on Pelnard-Considere (1956) which assumed a fully impermeable structure while establishing a solution for the coastline evolution. Consequently, sediment will only bypass the structure when the whole structure is filled with sediment. To implement this consideration, the alongshore sediment transport and BPF are set to 0 at the beginning of the simulation. When sedimentation reaches the updrift tip of the groyne, it is assumed that all sediment bypasses the groyne, therefore implying a BPF value of 1. In doing so, the following lateral boundary condition is implemented:

$$Q_{s,i} = Q_{s,i-1} \tag{A.5}$$

Here $Q_{s,i}$ is the alongshore sediment transport at gridpoint i which is located at the groyne. Gridpoint $i-1$ lies updrift of the groyne. For distributing the sediment downdrift of the groyne, a method is chosen which ensures that the last sheltered gridpoint receives all bypassed sediment. Ghonim (2019) concluded that applying this method, the numerical results are in agreement with the analytical solution. The lateral boundary conditions forcing this distribution of bypassed sediment are stated in equation A.6. grid points $i+1, i+2$ and $i+3$ are downdrift of the groyne as visualized in figure A.4.

$$Q_{s,i+1} = Q_{s,i+2} = Q_{s,i+3} = Q_{s,i} \tag{A.6}$$

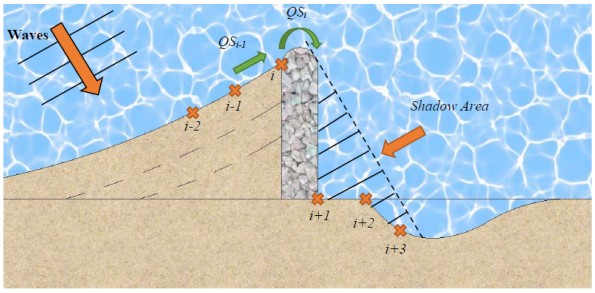

Figure A.4: Implementation of sediment bypassing a shore normal groyne (Ghonim, 2019).

Ghonim (2019) suggested a second method to calculate the amount of bypass and blockage of sediment using the BPTM factor. This method is based on the approach of Larson et al. (1987) which stated that bypassing may immediately take place after the construction of a groyne. Hence, being contradictory to the first method in which bypass starts when the groyne is completely filled with sediment. Larson et al. (1987) derived an equation which describes the rate at which the bypassing of sediment grows until the limited value is reached. Ghonim (2019) applied this approach and used equation A.3 to calculate the bypass factor until the groyne is completely filled with sand, implying a BYP of 1. The lateral boundary for the updrift gridpoint at the groyne is now as follows:

$$Q_{s,i} = \text{BPF} * Q_{s,i-1} \tag{A.7}$$

Regarding the downdrift gridproints, the same boundary conditions as in the first approach are used, those are stated in A.6.

A.5. Beach dune foot evolution

Dunes fulfil an important role in the protection of many coastlines around the world. Modelling the dune evolution and the effect that storm events have on the dunes is therefore essential for dealing with problems of coastal protection that may arise in the future. Ghonim (2019) studied the capabilities of ShorelineS to simulate the consequences of extreme storms on the long-term dune foot evolution. It was concluded that the most important processes that should take into account for modelling the dune foot evolution are the attack by waves and built up by aeolian transport. He implemented a method which determines the dune foot evolution over time based on the following equation:

$$\frac{\delta y_d}{\delta t} = \frac{1}{D_h}(q_{wind} - q_{wave}) \tag{A.8}$$

Here y_d is the position of the dune foot and D_h the dune height, which is the vertical distance between the dune foot and the surface of the dune. q_{wind} and q_{wave} are the aeolion transport rate and dune erosion rate as a consequence of wave attack. Both are determined using equations described in Larson et al. (2016) and Sauermann et al. (2001). Furthermore, the position of the dune foot along the considered coastline is described in the same manner as the coastline itself; a polyline consisting of freely moving grid points (figure A.5).

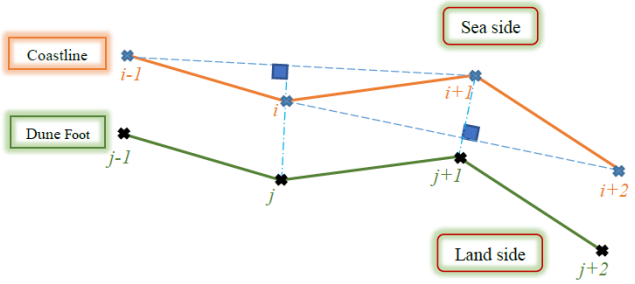

Figure A.5: Polylines describing the dune foot location and shoreline location (Ghonim, 2019).

Ghonim (2019) concluded that ShorelineS could not be used to model the evolution of the entire dune shape. However, ShorelineS demonstrated to be applicable for simulating the dune foot evolution over decades of years. Besides that, the impact of individual storm events onto the dune foot location could also be examined using the implemented procedure. A detailed description of the implemented model features and the accompanying numerical aspects can be found in Ghonim (2019).

A.6. Dynamic boundary

As stated in section 2.2.4, all depth contours inside a one-line model are assumed to be coastline parallel. Therefore, coastline evolution results in a similar rotation over the total depth profile. Mudde (2019) stated that this may result in a large simplification of the effect that a shoreline change has on the depth contours since sediment transport actually only affects the active nearshore part of the coastal profile. Depth contours lying outside this active area, are considered to be unaffected by the rotation of the shoreline. To take care of this problem, Mudde (2019) proposed to include the so-called dynamic boundary. In doing so, the approach applied in Deltares (2011) is followed. This boundary divides the cross-shore profile into a dynamic (active) part and a static part. Depth contours inside the dynamic part will follow the exact rotation of the shoreline orientation. The static part consists of depth contours that have a fixed orientation (figure A.6).

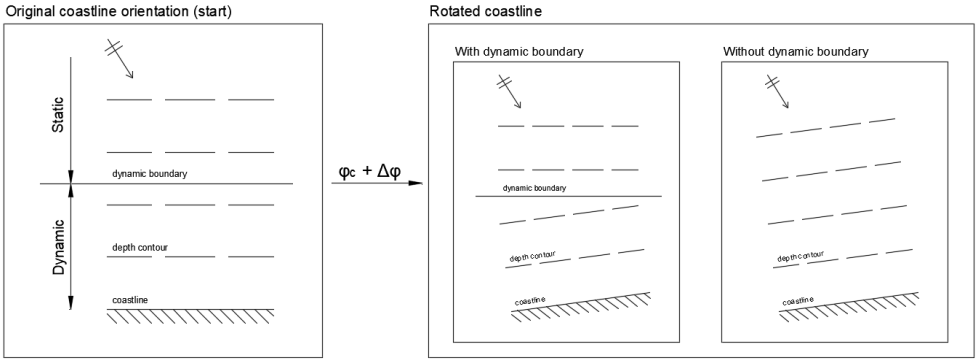

Figure A.6: Evolution of depth contours with and without the dynamic boundary (Mudde, 2019).

The wave transformation from an offshore location to the breakerline could now be performed using three steps as proposed in Mudde (2019). Each step is explained in the section below.

Offshore to dynamic boundary transformation
Generally, the offshore data is defined at the deep water depth contour. In the first step, the wave is transformed from deep water to the depth contour representing the dynamic boundary. To do so, first the deep water wave parameters need to be defined, $H_{s,0}$ is the significant offshore wave height and $\phi_{w,0}$ the offshore wave angle. The local offshore wave angle $\phi_{loc,0}$ is defined as the angle between $\phi_{w,0}$ and the orientation of the deep water depth contour ϕ_f. Both angles are with respect to the North. Subsequently, while accounting for refraction and shoaling, the wave height at the dynamic boundary $H_{s,db}$ is calculated (equation A.9).

$$H_{s,db} = K_r K_s H_{s,0} \tag{A.9}$$

Here K_r and K_s are the refraction and shoaling coefficient respectively. They are determined using the wave energy balance as described in section 2.1.1. After an offshore wave with a particular direction, height and period is forced onto the model domain, ShorelineS uses the wave dispersion relation to determine c_0 and c_{db}. Subsequently, equation A.9 is used to establish $H_{s,db}$. The wave angle at the dynamic boundary,$\phi_{loc,db}$, is determined by applying Snell's Law which is stated in section 2.1.1 .

At the dynamic boundary
Mudde (2019) implemented the dynamic boundary in such a way that only the orientation of this depth contour changes. All other parameters, like the water depth, stay the same. As a result, the local wave angle $\phi_{loc,db,B}$ differs from $\phi_{loc,db,A}$ (figure A.7). For convenience, location A and B are on the same depth contour. The new local wave angle is calculated using: $\phi_{loc,db,B} = \phi_{loc,db,A} + (\phi_c - \phi_f)$. The term between brackets is the relative rotation of the nearshore depth contour with respect to the deep water contour. This deep water contour has a fixed orientation.

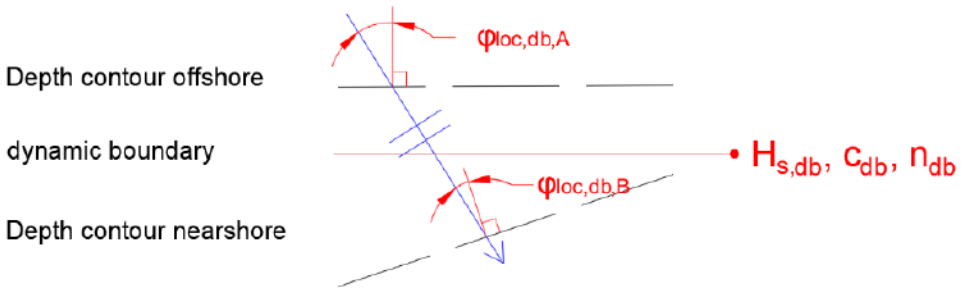

Figure A.7: Dynamic boundary schematisation (Mudde, 2019).

Dynamic boundary to breaker line transformation
The wave height and angle at the moment of breaking are determined by transforming the wave from the dynamic boundary to the depth contour at which wave breaking occurs. The same approach as applied in the transformation from offshore to the dynamic boundary is used. Here, the breaking wave height $H_{s,br}$ is determined by multiplying $H_{s,db}$ with the shoaling and refraction coefficients. The complete definitions of those coefficients are used in the equation below. A subscript br denotes the case of breaking waves.

$$H_{s,br} = \sqrt{\frac{n_{db}c_{db}}{n_{br}c_{br}}}\sqrt{\frac{cos(\phi_{loc,db,B})}{cos(\phi_{loc,br})}}H_{s,db} \tag{A.10}$$

To solve the above equation in a computational effective manner, assumptions need to be made since it contains to much unknown variables. These assumptions are retrieved from van Rijn (2014). Starting with the variables at the breaker line, the local breaking wave angle $\phi_{loc,br}$ is assumed to be very close to 0°. The underlying assumption is that the breaking waves are almost fully refracted and have the same orientation as the shore normal. n_{br} is suggested to be close to 1 because wave breaking takes place in shallow water. In shallow water yields that the individual wave phase speed is almost equal to the group wave speed, resulting in a ratio between them of almost 1. The product of n_{br} and $cos(\phi_{loc,br})$ is replaced by a calibration factor α (Mudde, 2019). The wave speed at breaking c_{br} is calculated using the shallow water assumption: $c_{br} = \sqrt{gh_{br}}$ in which h_{br} is the water depth at which breaking occurs. Finally, the breaker index γ is used to estimate at which water depth breaking occurs according the following relation: $\gamma = \frac{H_{s,br}}{h_{br}}$. After applying all the assumptions, h_{br} can be calculated in a computational effective manner.

$$h_{br} = \left(\frac{H_{s,db}^2\, c_{db}\, cos(\phi_{loc,db,B})}{\alpha\gamma^2 g^{0.5}}\right)^{0.4} \tag{A.11}$$

Finally, the ShorelineS model calculates the breaking wave height $H_{s,br}$ using γ and h_{br}. Subsequently, $\phi_{loc,br}$ is determined by appling Snell's Law in combination with the dispersion relation (same as in the static part). The wave parameters that are required in the alongshore sediment transport formulation are now established. Mudde (2019) showed by a model to model comparison that the implementation of a dynamic boundary resulted in more accurate wave transformation. Therefore, improving the subsequent sediment transport calculations.

A.7. Spit formation

Ashton and Murray (2006a) stated that the direction of spit formation is related to the critical angle. The upwind correction, described in section 2.2.6, determines the spit orientation inside the ShorelineS model. Elghandour (2018) presented the critical angles for each alongshore sediment transport formulation inside ShorelineS. Coastline parallel depth contours were assumed while establishing these angles. Implementing the dynamic boundary as is described in the section above, will be in contrast with the assumption of coastline parallel depth contours only. Mudde (2019) showed that the dynamic boundary causes a phase shift of the S,ϕ diagram, thereby also changing the critical angle. Therefore, this angle should not be a fixed value, but a parameter that is varying according to the wave conditions and the dynamic boundary characteristics.

Mudde (2019) presented a routine to calculate the critical angle including the effects of the dynamic boundary. This new routine establishes the S,ϕ diagram for each time step and determines the associated angle that maximizes the alongshore sediment transport. This angle is now varying instead of being a fixed value. Besides the spit orientation routine, also an adaption to the method determining the spit width is proposed by Mudde (2019). Inside the original routine, the width of the spit was directly related to the grid size. A non-physical parameter is in this way influencing a physical process which is often unwanted (Mudde, 2019). The proposed method is an improved version of the upwind scheme and is activated when the critical angle is exceeded. Subsequently, the linear decay of sediment transport over the head of the spit is established based on a user-defined spit width. As a result, the width of the spit is independent of the user-defined grid resolution.

B

Appendix B

The resulting shorelines after 1,6 and 12 months using the old and new approach of the boundary condition of a groyne are depicted in this appendix. The offshore wave height and period are 0.5 meters and 8 seconds in each scenario. Different values for the offshore angle are used (table B.1). Each figure also contains the corresponding analytical solution provided by Pelnard-Considere (1956). Scales of the x-axis and y-axis are different to visualize the comparison between the numerical and analytical result properly. In doing so, the shorelines could look a bit distorted. The important input parameters used in the analytical solution are listed in table B.1.

	Offshore wave angle from the North	Breaking wave angle relative to coastline orientation	Alongshore sediment transport amplitude
scenario A	-10°	2.18°	138924 $m^3/year$
scenario B	-20°	4.27°	137359 $m^3/year$
scenario C	-30°	6.14°	134757 $m^3/year$
scenario D	-40°	7.72°	131086 $m^3/year$

Table B.1: Input parameters ShorelineS and analytical solution

B.1. Old boundary approach

This section contains the resulting shorelines using the old approach concerning the boundary condition of a groyne (figures B.1 and B.2). In that case, the alongshore sediment transport of all Q_s points inside the shadow zone are made equal to zero.The analytical solution is depicted using dotted lines.

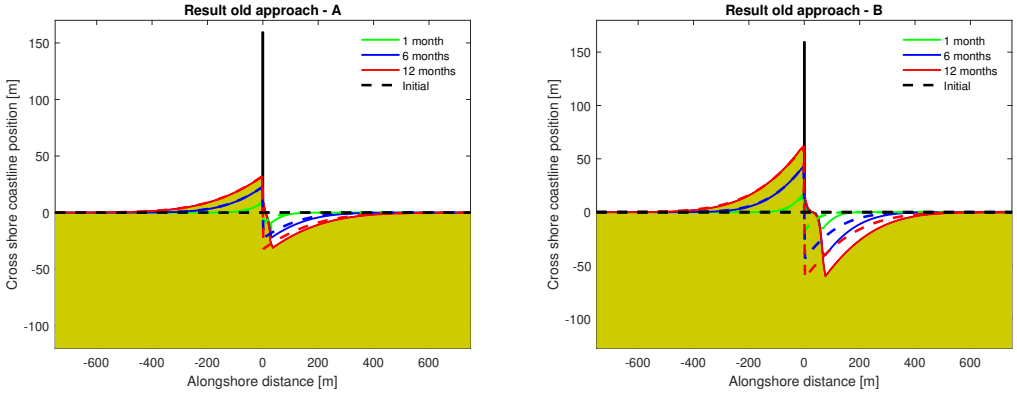

(a) $\phi_\infty = -10°$ (b) $\phi_\infty = -20°$

Figure B.1: Comparison analytical (dotted-lines) and numerical result using the old boundary approach

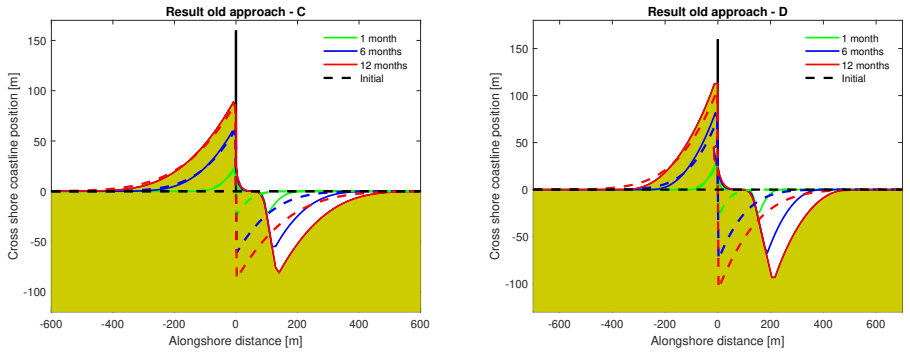

(a) $\phi_\infty = -30°$ (b) $\phi_\infty = -40°$

Figure B.2: Comparison analytical (dotted-lines) and numerical result using the old boundary approach

B.2. New boundary approach

To test the implemented boundary condition described in section 4.2, the same resulting shoreline evolutions of the scenarios depicted in table B.1 are compared with the analytical solution provided by Pelnard-Considere (1956).

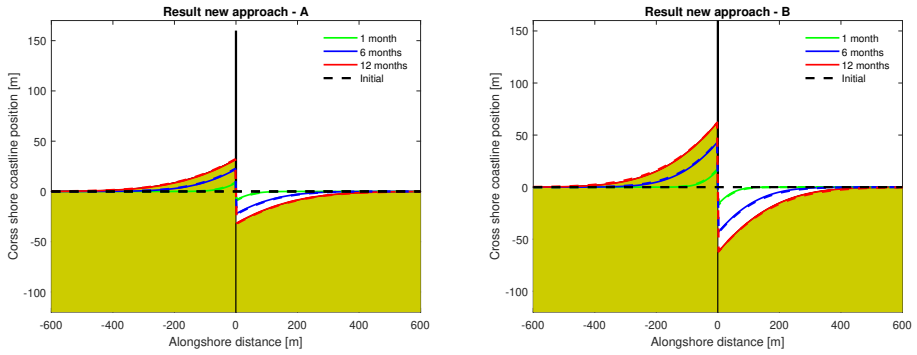

(a) $\phi_\infty = -10°$ (b) $\phi_\infty = -20°$

Figure B.3: Comparison analytical (dotted-lines) and numerical result using the old boundary approach

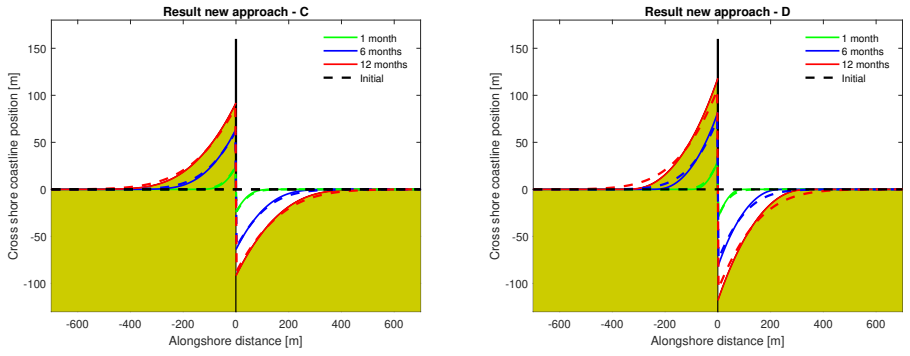

(a) $\phi_\infty = -30°$ (b) $\phi_\infty = -40°$

Figure B.4: Comparison analytical (dotted-lines) and numerical result using the old boundary approach

C

Appendix C

This appendix contains additional information concerning the Constanta case study. First, the applied boundary condition is explained in more detail. Furthermore, intermediate results of the K_d values, breaking wave heights and wave angels are depicted. Subsequently, the effect of the applied nourishment is highlighted. At the end, the coastline changes between September 2015 and January 2020 for scenarios A, B and C are visualized.

C.1. Boundary conditions

To make sure that the first and last gridpoint are not moving away from the structure while the shoreline is evolving, modifications to the equations describing these displacements need to be applied. Equation 4.1a and 4.1b are applicable in the case of a shore normal structure for an initially straight coastline. In such a situation is the x or y component of the displacement dn equal to zero, the other component is equal to dn. For clarification figure C.1 is depicted.

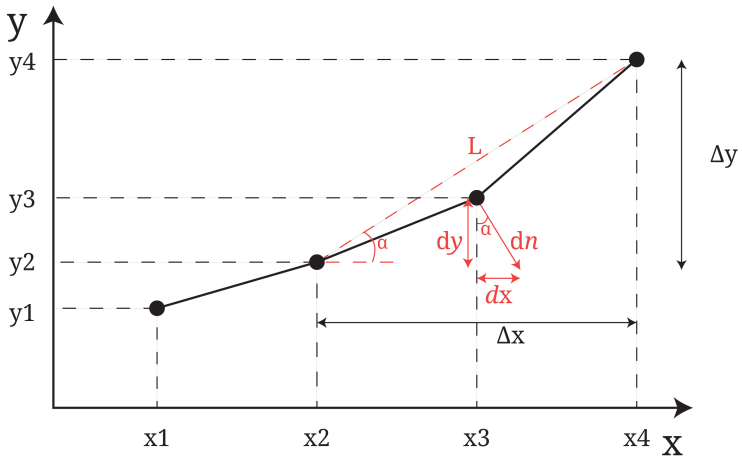

Figure C.1: Calculating new coastline position)

The displacement dn of a particular gridpoint consists of a displacement in the x-direction and y-direction. The displacement dn of the first and last gridpoint of the Constanta case is expressed in terms of groyne orientation to make sure that they are moving along the groyne. Figure C.2 visualizes the relations applicable to the groyne located in the North of the considered coastline section. For the Constanta case, the displacement of the first and last gridpoint has a x and y component. In the simplified case with an initial straight coastline, one of those components is zero.

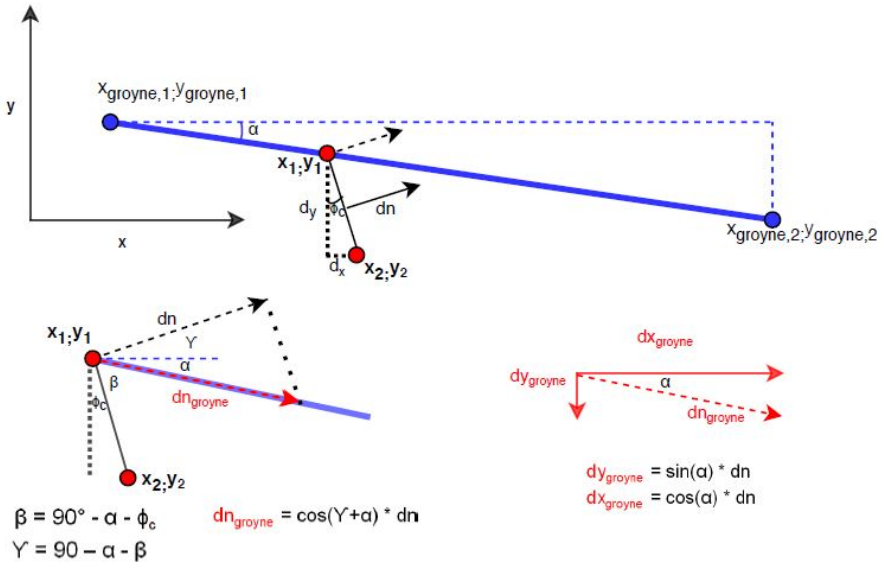

Figure C.2: Calculating new coastline position at the groyne

The blue line in figure C.2 represents the groyne. The coordinates of the gridpoint situated at the groyne are x_1 and y_1. α represents the orientation of the groyne and ϕ_c is the coastline orientation of the first gridsection. The displacement dn belonging to this gridsection is calculated based on the value of the first Q_s point only. This is because at the groyne a sediment transport being equal to zero prevails. Using the angles α, β, γ and ϕ_c, the coastline normal displacement dn is transformed into a displacement dn_{groyne}. Finally, the displacement in the x and y direction of the gridpoint located at the groyne are established based on geometry.

C.2. Intermediate results of breaking wave height and angles

The calculated K_d values, breaking wave heights and angles corresponding to wave groyne tip angles of 1°,40°,80° and 125° are visualized in the figures stated on the next pages. For convenience, figures displaying the identifycation of the Q_s points situated inside the area of diffraction are also depicted. Each scenario is stated on a separate page.

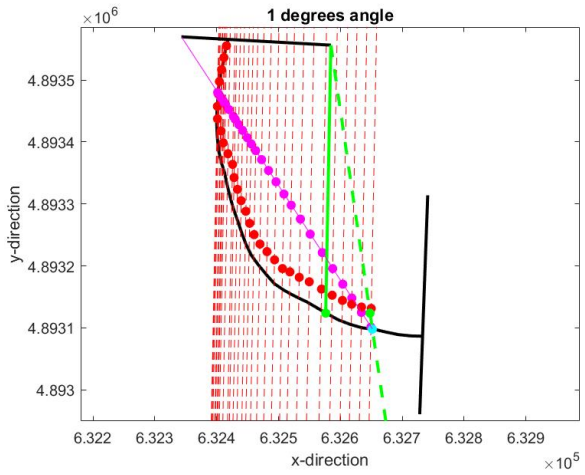

(a) Q_s points identification

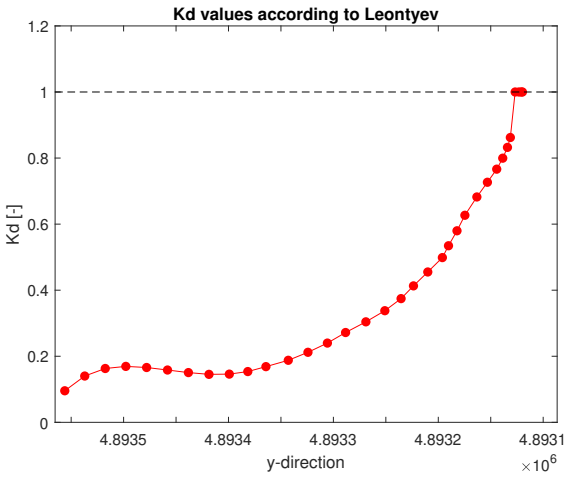

(b) K_d values

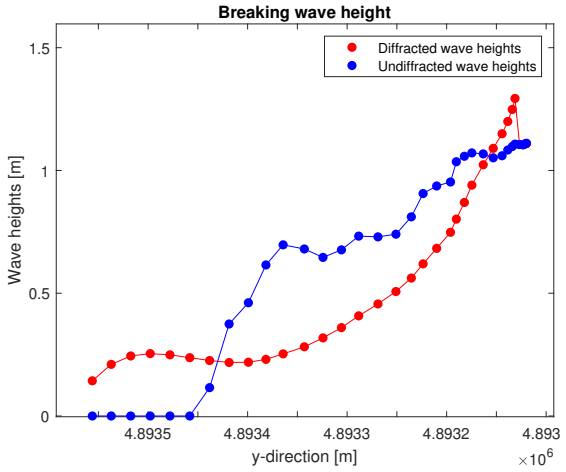

(c) Breaking wave heights

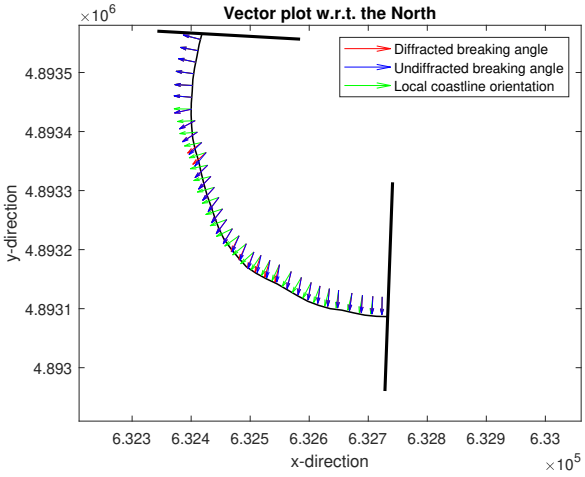

(d) Breaking wave angles

Figure C.3: Results corresponding to $\phi_{tip} = 1°$

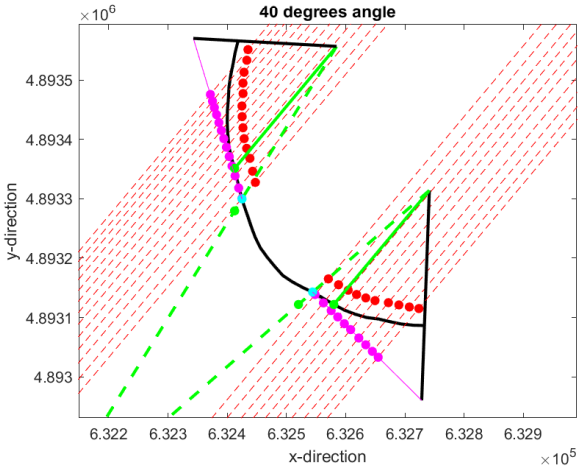

(a) Q_s points identification

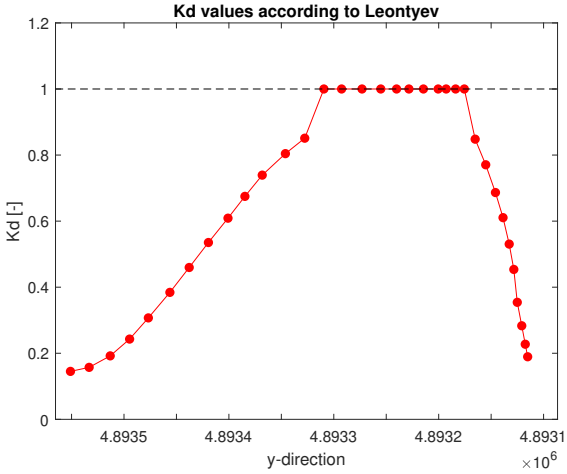

(b) K_d values

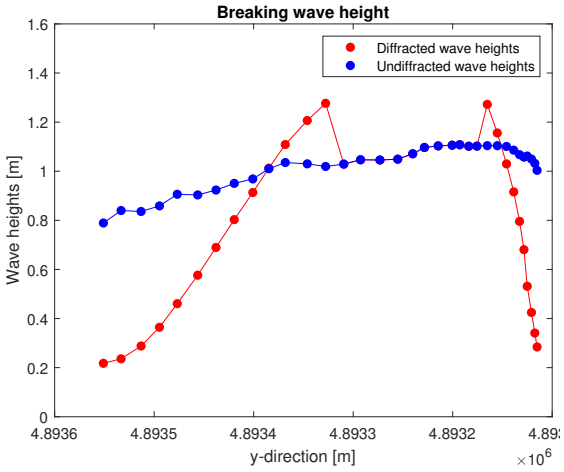

(c) Breaking wave heights

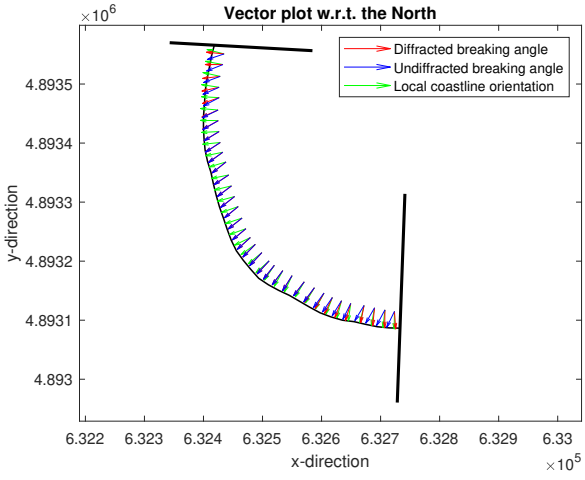

(d) Breaking wave angles

Figure C.4: Results corresponding to $\phi_{tip} = 40°$

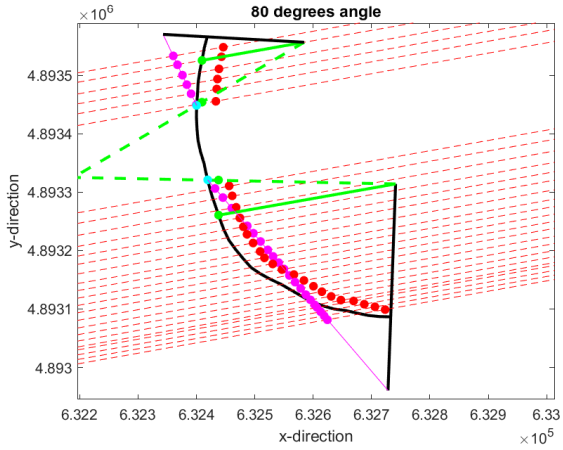

(a) Q_s points identification

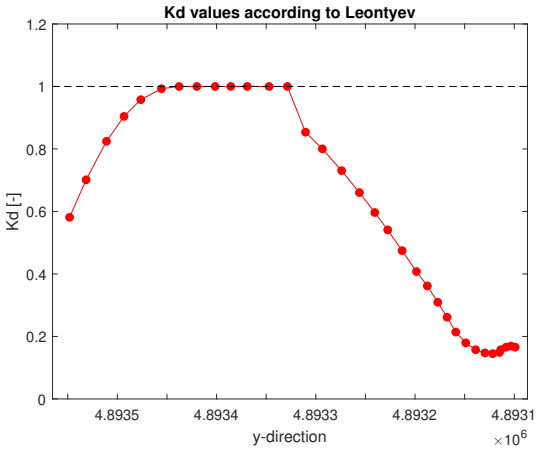

(b) K_d values

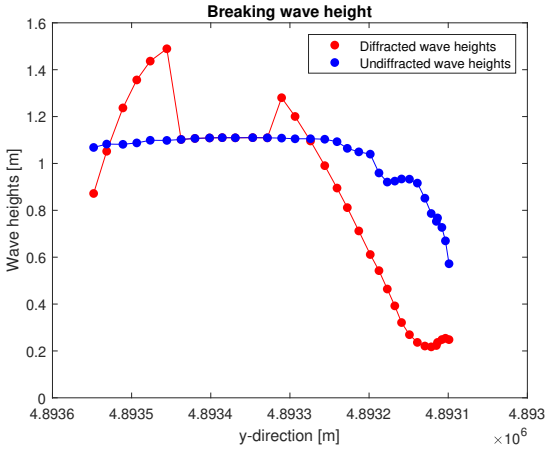

(c) Breaking wave heights

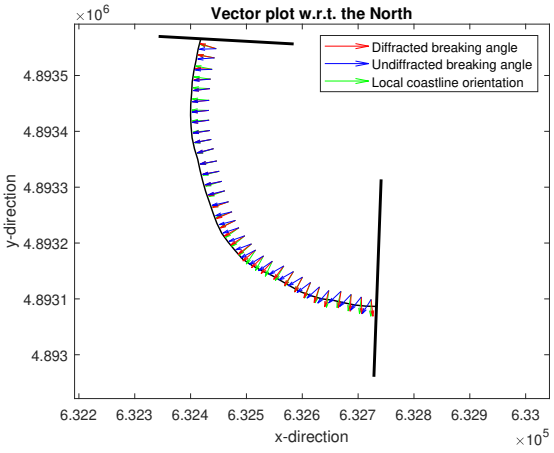

(d) Breaking wave angles

Figure C.5: Results corresponding to $\phi_{tip} = 80°$

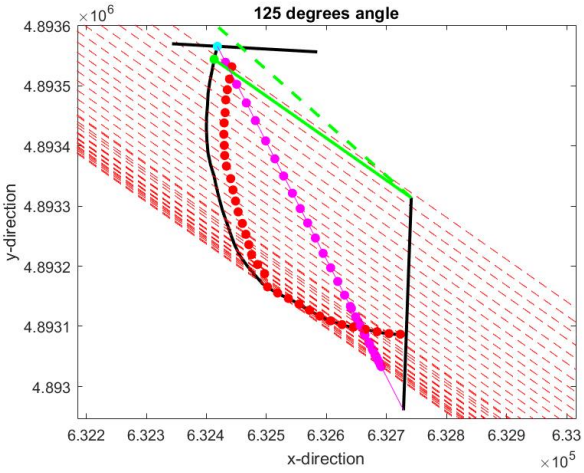

(a) Q_s points identification

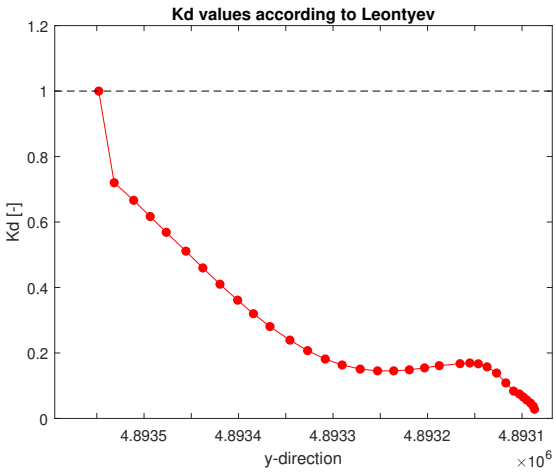

(b) K_d values

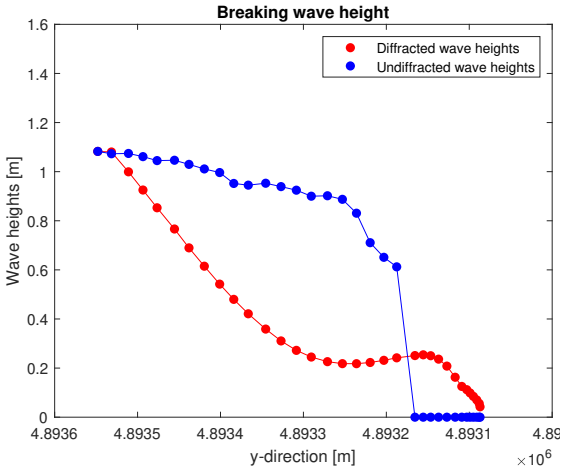

(c) Breaking wave heights

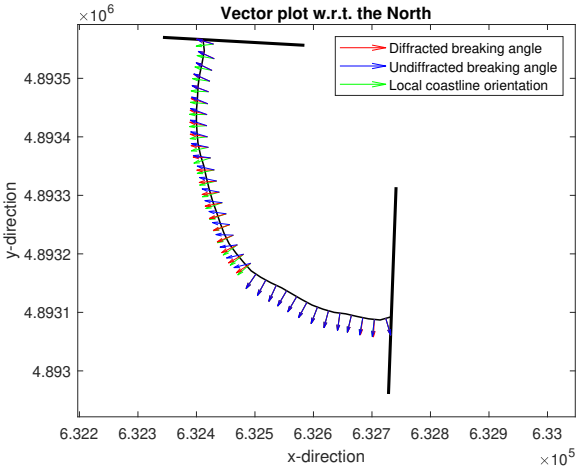

(d) Breaking wave angles

Figure C.6: Results corresponding to $\phi_{tip} = 125°$

C.3. Cross-shore processes

In section 6.2.4 it is stated that cross-shore processes are the cause of the total seaward displacement regarding the coastline position in the period between September 2015 to July 2016. Figure C.7 provides the numerical result of the calibrated model while including and excluding a nourishment rate. For convenience also the survey data is visualized.

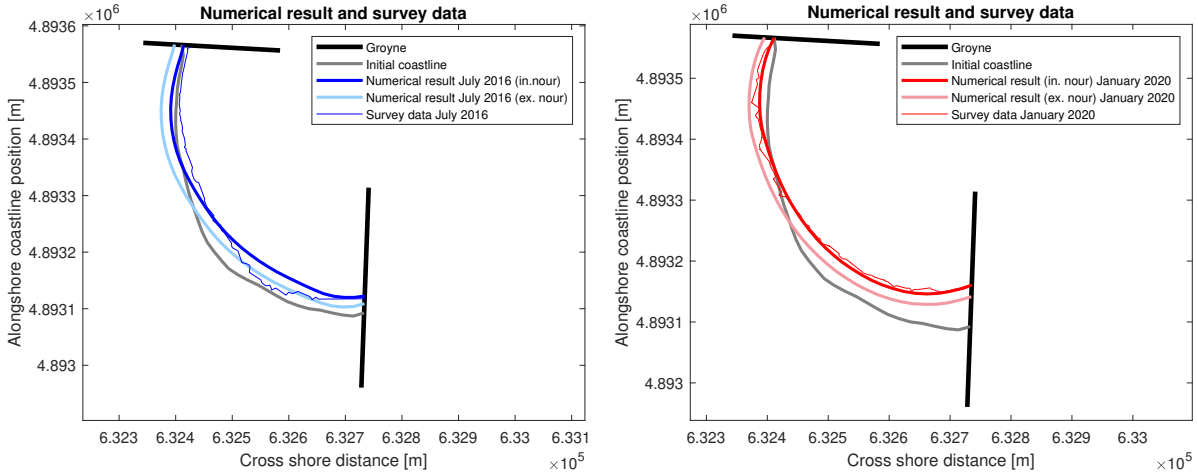

(a) Shoreline shape July 2016

(b) Shoreline shape January 2020

Figure C.7: Application of a nourishment rate

C.4. Bias and RMS error

To highlight and quantify the calibration effect, the coastline change observed in the survey data is compared to the numerical coastline change of scenario A, B and C. The coastline change in the normal direction of each grid section between September 2015 and January 2020 is used.

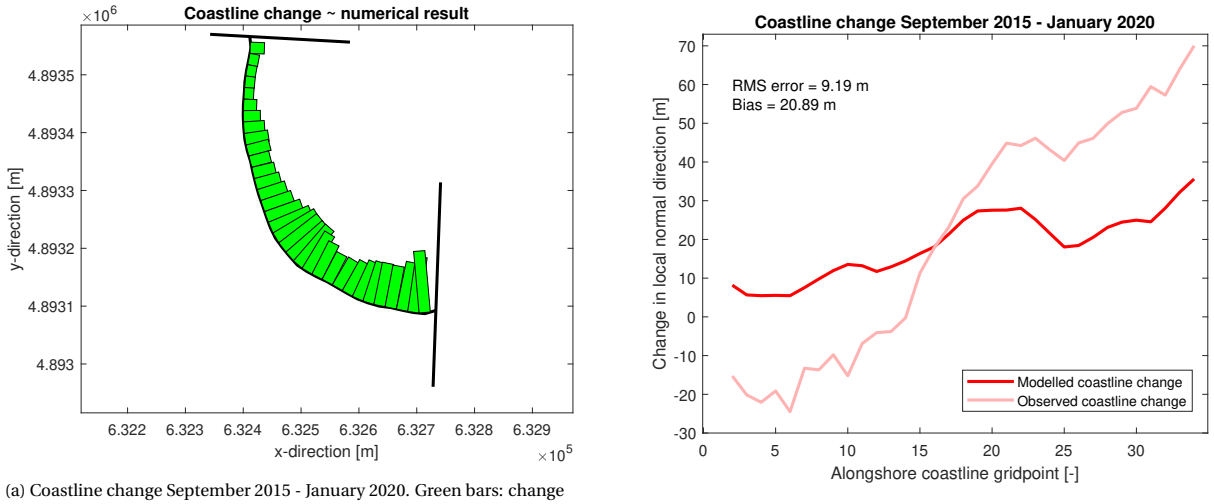

(a) Coastline change September 2015 - January 2020. Green bars: change in seaward direction. Red bars: change in landward direction

(b) Root mean square error and bias

Figure C.8: Coastline change scenario A

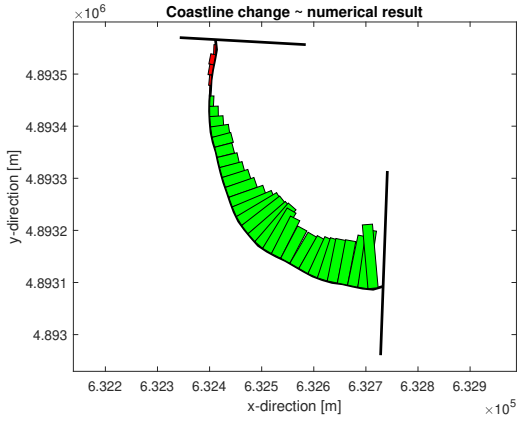

(a) Coastline change September 2015 - January 2020. Green bars: change in seaward direction. Red bars: change in landward direction

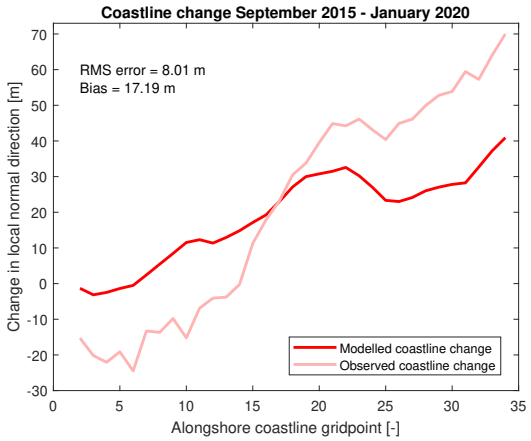

(b) Root mean square error and bias

Figure C.9: Coastline change scenario B

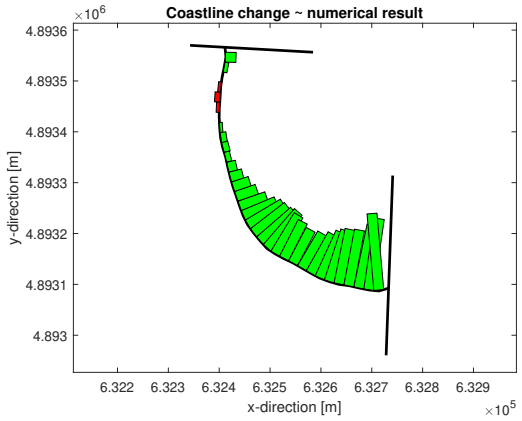

(a) Coastline change September 2015 - January 2020. Green bars: change in seaward direction. Red bars: change in landward direction

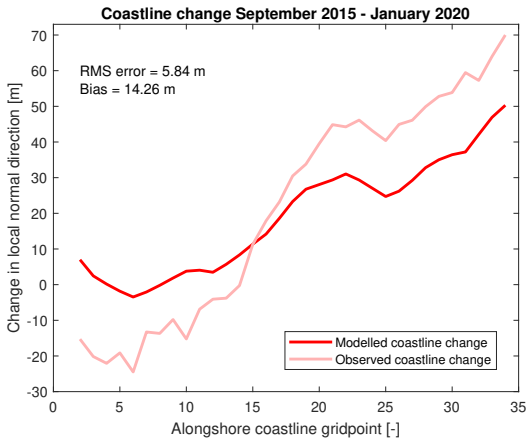

(b) Root mean square error and bias

Figure C.10: Coastline change scenario C